1-1-2010

Non-Destructive Assessment And Remedy Of Grouted Prestressed Cable Ducts In Post-Tensioned Decks

Hamidreza Khederzadeh
Ryerson University

NON-DESTRUCTIVE ASSESSMENT AND REMEDY OF GROUTED PRESTRESSED CABLE DUCTS IN POST-TENSIONED DECKS

By

Hamidreza Khederzadeh

B.Sc., Yasouj Azad University, Iran, 1999

A Thesis

Presented to Ryerson University

In partial fulfillment of the

Requirements for the degree of

Master of Applied Science

In the Program of

Civil Engineering

Toronto, Ontario, Canada, 2010

AUTHOR'S DECLARATION

I hereby declare that I am the sole author of this thesis.

I authorize Ryerson University to lend this thesis to other institutions or individuals for the purpose of scholarly research.

Author's Signature.. Date...........................

I further authorize Ryerson University to reproduce this thesis by photocopying or by other means, in total or in part, at the request of other institutions or individuals for the purpose of scholarly research.

Author's Signature.. Date...........................

BORROWER'S PAGE

Ryerson University requires the signatures of all persons using or photocopying this thesis.

Please sign below, and give address and date.

Name	Signature of Borrower	Address	Date

ABSTRACT

NON-DESTRUCTIVE ASSESSMENT AND REMEDY OF GROUTED PRESTRESSED CABLE DUCTS IN POST-TENSIONED DECKS

By

Hamidreza Khederzadeh

Master of Applied Science in Civil Engineering
Department of Civil Engineering, Ryerson University
Toronto, Ontario, Canada
2010

Post-tensioned concrete bridge decks have been in service in Ontario for more than 30 years. Many of such bridge deck have been operating without any waterproofing/asphalt protection from their initial construction. Concerns currently exist as to the condition of the prestressing cables in the grouted ducts, particularly in the negative moment regions where the cables are closest to the deck surface. Deterioration of post-tensioned bridge decks due to prestress cable corrosion is matter of considerable concern since the repair or replacement is proved to be a costly process. As Ontario bridge infrastructure enters the era of maintenance, rehabilitation and replacement, there is an urgent need for investigating non-destructive inspection methodologies or procedure to assess the conditions of the grouted ducts and cables inside without invasive concrete work involving major concrete removal to expose the ducts for visual inspection. As such, the main objectives of this research were to (i) conduct state-of-the-art and state-of-practice review on the available non-destructive testing (NDT) techniques; (ii) conduct laboratory testing on simulated bridge deck segments with grout-encased prestressing cables to evaluate promising candidate method identified from the literature review that may be applicable to detect voids in the ducts, cable fracture or corrosion in post-tensioned decks; and (iii) propose a remedial procedure to fill the detected voids with grouting materials. Eight concrete specimens were cast to investigate the applicability of selected NDT methods on locating the reinforcing steel bars, ducts, corrosion in cables and voids. These methods were (i) Ground Penetration Radar; (ii) Impact-Echo; and (iii) Half-cell Potential. Also, Remedial procedure using vacuum grouting was experienced to fill the detected voids.

TO MY FAMILY

TABLE OF CONTENTS

LIST OF TABLES

LIST OF FIGURES

ABBREVIATIONS

AASHTO	American Association of State Highway and Transportation Officials
ACI	American Concrete Institute
AE	Acoustic Emission
ASTM	American Society for Testing and Materials
CBD	Cable Break Detection
CHBDC	Canadian Highway Bridge Design Code
CSA	Cement Association of Canada
DOC	Degree Of Corrosion
HE	Hydrogen Embrittlement
FDTD	Finite Difference Time Domain
FFT	Fast Fourier Transform
FHWA	Federal Highway Administration
GPR	Ground Penetration Radar
IE	Impact-Echo
JCCBI	Jacques Cartier and Champlain Bridges Incorporated
LR	Linear Polarization
MTO	Ministry of Transportation of Ontario
NDT	Non- Destructive Test
PIES	Portable Impact-Echo System
PT	Post-Tension
RM	Remanent Magnetism
SAFT	Synthetic Aperture Focusing Technology
SASW	Spectral Analysis of Surface Waves
SCC	Stress Corrosion Cracking
UPV	Ultrasonic Pulse Velocity
UTI	Ultrasonic- Tomography Imaging

LIST OF SYMBOLS

A	Characteristic dimension
B	A constant in volt
C	Speed of electromagnetic wave
C_p	P-wave speed
C_0	Wave speed in air
D	Depth of reflecting interface
ΔE	Applied potential
f	Frequency
F	Faraday's constant, which is the amount of electrical charge in one mole of electron
Δi	Current Response
icorr	Corrosion rate
L	Path Length
M	Atomic weight
R	Reflection coefficient
Δt	Time
R_p	Polarization resistance
T	Depth of the concrete plate
T1	Transit time around the crack
T2	Transit time along the surface of concrete without cracking
X	Distance to the transducer from crack
Z	Ion charge
Z1	Acoustic impedance of material 1
Z_2	Acoustic impedance of Material 2
β	Shape Factor
ε	Dielectric constant
ε_0	Dielectric constant of free space (air)
εr	Relative dielectric constant
$\varepsilon r1$	Relative dielectric constant of material 1
$\varepsilon r2$	Relative dielectric constant of material 2
α	Signal attenuation
σ	Conductivity
$\rho 1, 2$	Reflection coefficients

CHAPTER I

INTRODUCTION

1.1 General

In 1949, pre-stressed (pre/post-tensioned) decks were built for the first time in the United State. The application of prestressing (pre/post-tensioning) systems to bridges has been growing rapidly since 1949. Today, they represent over 50% of all bridges built (Shivprakash et al. 2005). In pre-tensioning system, high tensile steel strands are pulled and anchored at both ends prior to casting of concrete. Once the concrete reaches its specified strength, the tendon strands are cut from ends causing to transfer stress from tendon strands to concrete due to the bond between them. As a result, when the strands are placed eccentrically into the concrete, concrete members tend to camber, and apply a compressive force to the concrete bottom face, which was primarily in the tension. Post-tensioned (PT) concrete combines efficient use of concrete and steel with durability and speed of construction. To fully understand the benefits of PT structures, it is worthwhile to understand the behaviour of reinforced concrete under applied loads. Concrete is very strong in compression but weak in tension. By applying vehicular loads on a bridge deck, it deflects resulting in elongation of concrete bottom face (tension side). Due to such elongation, concrete cracks at the positive moment as well as the negative moment locations when the applied load exceeds the member cracking load limit. Steel bars used in concrete do not carry any load until concrete starts cracking. Post-tensioning system, however, brings advantage to the structure in such a way that the prestressed tendon strands provide compression force to the concrete that counteract the tension force created by applying loads. This significantly increases the load-carrying capacity of concrete structures (Nawy, 1996).

There are two main types of post-tensioning systems; unbounded and bonded (grouted) systems. Unbounded tendon is a system in which steel strand is not bonded to the concrete, except at both ends anchorages. Unbounded tendon consists of mono-strand including seven wire strands that are used in beams for buildings or parking structures. On the other hand, in bonded system, two or more strands are used and placed into the metal or plastic ducts. The

tendon strands are stressed using multi-strand jack and anchored at both ends. The duct is then grouted with cementitious grout in which the grout acts as corrosion protection as well as bonding the strands to the concrete surrounding the duct.

PT structures are most durable if properly constructed and anchored. Prestressing wire strands used in civil engineering structures act as tensioning components in order to ensure the safety of the structure as well as bringing a high mechanical strength. These high tensile steel wires have many structural applications as single wires, or in the form of tendon bundles, cables or ropes. Examples of the application of PT system include numerous civil engineering structures such as; suspension and cable stayed bridges, parking garage and prestressed strands in concrete structures (bridges, dams, nuclear power plants, etc). It is essential to ensure the safety of such structures so that the safety of people and environment are guaranteed.

The current state-of-the-art in concrete bridge condition evaluation relies mainly on visual inspection. However, deterioration in prestressing tendon condition is not always reflected by distress visible on the concrete surface. Further, the effect of deterioration of prestressing steel is more disruptive than that of reinforcing steel bars. A strand, due to its high mechanical strength and metallurgical characteristics, is smaller in cross-section than conventional reinforcing steel bar and is proportionally more impaired by loss of section. The material is also susceptible to less common and less predictable forms of deterioration such as stress corrosion, hydrogen-assisted cracking, corrosion fatigue and fretting corrosion. Researchers have investigated diverse techniques such as magnetic, radiographic, acoustic/ultrasound, radar, thermographic, eddy current, electrochemical, and acoustic emission. A recent NCHRP research study (Ciolko and Tabatabai, 1999) has summarized advances in non-destructive testing (NDT). In addition, the technological horizon was assessed to identify candidate methods that would permit identification of loss of cross-sectional area in a strand attributable to corrosion and cracking.

As Ontario Bridge infrastructure enters the era of maintenance, rehabilitation and replacement, the need for investigating or developing non-destructive inspection methodology

or procedure has always been proposed to assess the conditions of the grouted prestressing ducts and cables inside without invasive concrete work involving major concrete removal to expose the ducts for visual inspection. As such, there is an urgent need to conduct a state-of-the-art and state-of-practice review on the available non-destructive testing techniques and procedure that may be applicable to detection of cracks or corrosion in post-tensioned decks.

1.2 The Dilemma

Post-tensioned concrete deck bridges have been in service in Ontario for more than 30 years. Many of them have been operating without any waterproofing/asphalt protection since their initial construction. Concerns currently exist as to the condition of the prestressing cables in the grouted ducts particularly in the negative moment regions where the cables are closest to the deck surface, as shown in Fig. 1.1.
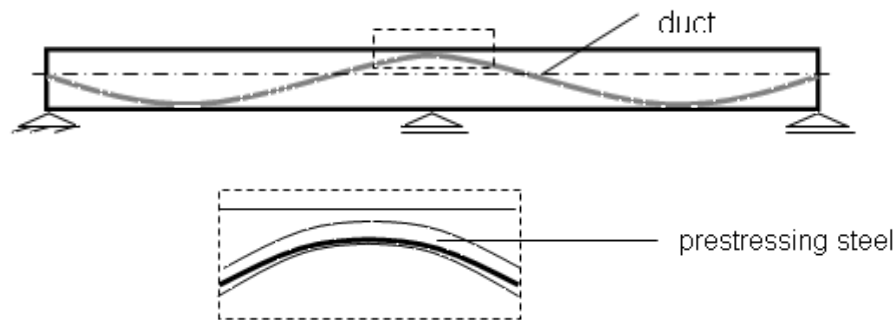
Fig. 1.1 Schematic diagram of the prestressing cable and duct in a continuous beam

Post-tensioning structures are complex due to several interfaces between concrete, wire-strands, grouting and duct. Such complexity makes it difficult to easily inspect inside conditions of PT structures. Wire strands placed into PT structures play an important role in durability of the structures. The loss or failure of strands may result in the failure of the entire structure and a considerable amount of repair cost. Generally, a post-tensioning system may be deteriorated due to wire breakage, voided duct and corrosion of wire strands. These failures are accelerated from original concrete placing as a result of the following reasons (see Fig. 2):

- Grouting procedure creates voids in the duct due to insufficient grout filling and/or grout settlement after hardening.

3

- Grouts susceptible to bleed-water evaporation produce voids.

- Voids also appear in the grout with air-entrapped inclusion.

- Duct with discontinuities or at seam connections allows direct ingress of water and corrosive agents to attack tendon strands.

- De-icing salt is the main factor for fracture of steel strands.
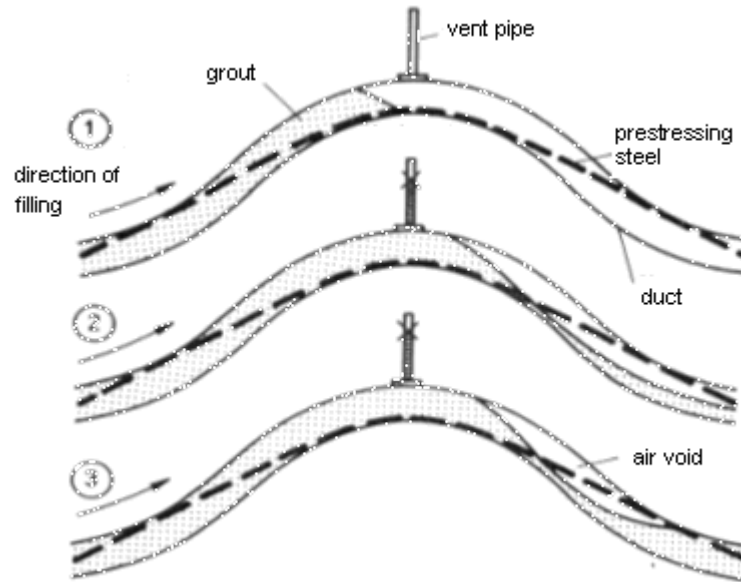
Fig. 1.2 Schematic diagram of the development of air void at the

high point of a PT cable duct in continuous span bridge decks

All prestressing strands are at risk of fracture if they are in contact with corrosive agents. In bonded post-tensioning bridge deck, if the deck is not properly waterproofed, chloride ions will reach the prestressing wires and cause fracture. In un-bonded PT systems, only water is required to cause corrosion and consequently wire fracture. Previous work showed that bleed water formation when the mix water and cement particles segregate (bleeding) during the grouting process is a key factor in the development of corrosion (Taveira et al., 2008). Corrosion can also occur at the region where the steel emerges from the grout into the void, either when the system is still wet from its original condition, or during later recharge events from external water intrusion into the voids at or near the anchorage. At the same time, high humidity environment inside the voids may induce atmospheric-like air space

corrosion on the bare steel. To increase the durability of such structures, a significant attention should be taken into account on protecting tendon strands against corrosion. Recently, most focus has been taken on corrosion problems in PT structures. Corrosion detection is vital for integrity of PT structures since loss of post-tensioning can result in the failure of the structure. Corrosion-related damage to the bridge structures is one the most important challenging issue for bridge owners.

1.3 Objectives

The main objectives of this research are:

(i)   conduct state-of-the-art and state-of-practice review on the available non-destructive testing (NDT) techniques;

(ii) conduct laboratory testing on simulated bridge deck segments with grout-encased prestressing cables to evaluate promising candidate NDT methods identified from the literature review that may be applicable to detect voids in the ducts, cable fracture or corrosion in post-tensioned decks; and

(iii) propose remedial procedure to fill the detected voids with grouting materials.

1.4 Scope of Research

The scope of this research includes the following:

1- A comprehensive literature review to identify and evaluate available and recently developed NDT techniques and technology-driven refinements of methods formerly shelved or rejected. Focus was mostly on the new advanced NDT methods developed to investigate their applications and effectiveness on the post-tensioning system.

2- Laboratory testing on eight bridge deck segments to evaluate promising candidate NDT methods identified from the literature review. Based on the results from the literature review, promising NDT candidate methods was considered for laboratory evaluation without concrete invasion. Inspection without invasion really removes the notion of making significant concrete removal which should definitely be avoided. Limited invasion was also considered in case of Half-Cell Potential method.

3- Investigation of vacuum grouting technology in the repair process of filling the detected voids in ducts.

5

1.5 Contents and Arrangement of the Thesis

Followed by the Introduction chapter, chapter II summarizes the literature review which is a general explanation of NDT history, application of NDT on concrete materials, various NDT methods and review of previous work performed on concrete post-tensioning systems using NDT methodologies. Chapter III explains the experimental work performed in this research including sample configurations and erection procedure. Chapter IV describes the outcomes of experimental investigation on selected NDT technologies without concrete invasion or with limited invasion. It also summarizes the experimental procedure for vacum grouting of voided ducts. Chapter V presents the conclusions of this research and recommendations for further research in the future. An appendix at the end of the thesis includes relevant figures for specimens' drawings and experiments' images.

Chapter II
LITERATURE REVIEW

2.1 General Concept of Non-destructive Testing

Non destructive test is a technique to determine the integrity of the structures by comparing the results derived from input and output data without damaging or destroying the structures. In other word, NDT methods do not sacrifice the structural systems by any internal or external effects. Hence, these methods are highly valuable methods that save time as well as the economic issue in the structure's evaluation and research. NDT methods for inspection and diagnosis of structural integrity have become dominating tools for maintenance and rehabilitation of structures in 21st century (Cartz et al.,1995). Common NDT methods include ultrasonic, magnetic-particle, liquid penetrant, radiographic, eddy-current and Ground Penetrating Radar (GPR) testing. NDT is a general method that can be used in many engineering fields such as forensic engineering, mechanical engineering, electrical engineering, civil engineering, systems engineering, as well as medicine, and art. Many other commonly used technologies such as radio astronomy, voltage, amperage measurement and rheometry (flow measurement) are also non-destructive but cannot be used to specifically evaluate material integrity. Generally, non-destructive tests focus more on the practical ways to evaluate the conditions inside the test samples - how long the sample is able to be used and when does it require to be rechecked?

2.2 Purposes of Non-destructive Testing

Since 1920s, non-destructive testing has developed from a laboratory curiosity to an indispensable tool of production. Non-destructive tests are used to detect structural changes, on time variation of surface finish and detection of cracks, flaws, delaminations in the structures as well as measuring materials thickness and other industrial products behaviour. Modern non-destructive tests are used by manufacturers to (i) ensure product integrity, and in turn, reliability; (ii) avoid failures, prevent accidents and save human life; (iii) make a profit for the user; (iv) ensure customer satisfaction and maintain the manufacturer's reputation; (v) aid in better product design; (vi) to control manufacturing processes; (vii) to lower

manufacturing cost; (viii) maintain uniform quality level; and (ix) ensure operational readiness.

2.3 NDT Classification

Non-destructive testing technology is generally divided into three categories:

1) To estimate in-situ strength of the materials.

2) To provide materials properties such as moisture, density, elastic wave velocity, elastic constant, thickness and temperature.

3) To detect and locate objects and problem areas within structures such as cracks, honeycombing, delamination, rebar, flaws and deterioration.

NDT methods developed to-date may classify into four levels according to their performance:

- Level 1, that only identifies if damage has occurred.

- Level 2, that identify if damage has occurred and determine the location of damage.

- Level 3, that identify if damage has occurred, determine the location of damage and estimate the severity of the damage.

- Level 4, that identify if damage has occurred, determine the location of damage, estimate the severity of damage and evaluate the impact of damage on structures.

2.4 History of Non-destructive Testing
2.4.1 Prior to World War II (Carino, 1994)

Early methods of evaluation of concrete in-place strength reply on the Brinell hardness method for metals, in which a high strength steel ball had been used to push into the test sample under a defined force and then measuring the area of indentation. In 1934, Prof. Gaede (Hanover, Germany) used a spring-driven impactor to produce the force to drive steel ball into the concrete (Malhotra, 1976). In 1936, Williams (England) stated the use of spring-loaded pistol-shaped device that is compressed by a screw with a 4 mm diameter steel ball attached to a plunger. A trigger had been used to release compressed spring and the plunger was shouted toward the concrete. In 1938, Skramtajev reported on 14 different techniques, 10 of which

were developed in the Soviet Union to measure in-place concrete strength. The reported methods comprise the following: mold placed in the structure to form in-place test specimens, pullout tests of embedded bars, an in-place punching shear test, an in-place fracture test using a pincer-device, penetration of a chisel by hammer blows, guns that fired indentors into the concrete and penetration of a ball by spring-driven apparatus. In 1938, Power (Portland Cement Association) announced the use of resonant frequency testing to measure the modulus of elasticity of concrete (Powers, 1938). This method was conformed quickly to evaluate deterioration during freezing and thawing cycles (Hornibrook, 1939) and became the first standardized NDT method by ASTM.

2.4.2 Post World War II

A great development has been made after World War II in NDT method technology, which some of the methods will be discussed in section 2.8 in this chapter. The following are notable events in early industrial NDT (Hellier, 2001):

- In 1854, Hartford, Connecticut: a boiler at the False and Gray Car Works exploded, killing 21 people and seriously injuring 50. Within a decade, the State of Connectiut passes a law requiring annual inspection (in this case visual) of boilers.
- In 1895, Wilhelm Conrad Rontgen discovers what are now known as X-rays. In his first paper he discussed the possibility of flaw detection.
- Between 1880 and 1920, The "Oil and Whiting" method of crack detection was used in the railroad industry to find cracks in heavy steel parts. A part was soaked in thinned oil, and then painted with a white coating that dries to a powder. Oil seeping out from cracks turned the white powder brown, allowing the cracks to be detected. This was the precursor to modern liquid penetrant tests.
- In 1920, Lester began the development of industrial radiography for metals. In 1924, Lester used radiography to examine castings to be installed in a Boston Edison Company steam pressure power plant.
- In 1926, the first electromagnetic eddy current instrument was available to measure material thickness.
- Between 1927 and 1928 Magnetic induction system to detect flaws in railroad track was developed by Elmer Sperry and H.C. Drake.

- In 1929, Magnetic particle methods and equipment were pioneered by DeForest and Doane.

- In 1930s, Robert F. Mehl demonstrated radiographic imaging using gamma radiation from Radium, which can examine thicker components than the low-energy X-ray machines available at the time.

- Between 1935 and 1940, liquid penetrant test was developed by Betz and DeForest.

- Between 1935 and 1940s, Eddy current instrument was developed by Knerr, Farrow, Zuschlag, and Foerster.

- Between 1940 and 1944, Ultrasonic test method was developed in USA by Floyd Firestone.

- In 1950, the Schmidt Hammer (also known as "Swiss Hammer") was invented.

- In 1950, Kaiser introduced acoustic emission as a NDT method.

2.5 NDT introduction to Concrete Structures

NDT methods were also developed in civil engineering field in many aspects to determine deficiency in the structures and evaluate or rehabilitate the integrity of the structures. In case of concrete structures, NDT method can be used to determine properties of existing concrete such as concrete strength, moisture content, density and temperature. The strength evaluation and quality of new concrete structures can be examined to determine deficiencies in the future life of the structure such as cracking, flaw and corrosion of rebars. NDT methods are applied to concrete construction for four primary reasons (ACI 228.2R): (i) quality control of new construction; (ii) troubleshooting of problems with new construction; (iii) condition evaluation of older concrete for rehabilitation purposes; and (iv) quality assurance of concrete repairs. Progress to date, non-destructive testing technologies are developing and researches carry on enhancing the existing methods and expanding the new methods in order to reach more accurate evaluation. ACI 228.2R is intended to provide the principles of various NDT methods being used in practice, and to summarize their applications and limitations. *The emphasis is placed on methods that have been applied to measure physical properties rather than the strength in post-tensioning systems, to detect wire fractures, voids, corrosion of wire strands, and to provide data for condition evaluation.*

Although there is lack of standard testing in NDT technologies to evaluate condition assessment of the new and existing constructions, the most suitable methods should be selected involving experienced operators to come up with the most precise evaluations. Generally, quality control of the concrete construction has been inspected mostly by visual inspection of the construction process by performing standard tests such as cylinder test to measure compressive strength of the concrete. However, visual inspection will not provide a true data collection of in-place concrete properties. NDT methods, on the other hand, non-destructively bring this advantage to the concrete construction in order to estimate the concrete in-place properties such as the elastic constants, density, strength, moisture content, and penetrability characteristics.

Most NDT's are indirect testing method providing that the concrete properties can be derived by measuring stimulus responses result from impact, sound propagation and electromagnetic radiation. For combination use of NDT methods, the test results might be acceptable and supplementary testing may not be necessary. However, in some cases the NDT results may not be acceptable and additional testing may be required. These additional tests can be another NDT method or any other non-effective method that can provide accessibility to observe internal condition of concrete such as drilling a small hole. Combination of NDT methods and the non-effective methods provide a true evaluation of concrete conditions.

2.6 Advantages of NDT

NDT methods have no physical or chemical damage to the structures. The tests are repeatable and can be done very fast. On economic issue, NDT methods are not expensive and can be repeated many times on a specific test object. Moreover, NDT equipments are portable, compact and can be used for several projects at the same time.

2.7 Disadvantages of NDT

Lack of awareness for using NDT methods and reliability are the factors concerning use of NDT methods. Since the test is being done by interpreting the results, there are no specific standards to compare the results. In addition, accessibility to critical section in the structures is an important problem that may reduce the use of NDT methods. Skilled and

experienced operators should be trained precisely to deal with these testing devices.

2.8 Non-Destructive Test Classification

 ACI 228.2R classifies 20 NDT methods to evaluate characteristics of concrete structures. Each method provides specific application in evaluation of concrete members. Brief description and application of recently developed NDT methods are summarized below.

2.8.1 Visual Inspection:

Normally, a visual inspection is one of the first steps in the evaluation of a concrete structure (Perenchio, 1989). By visual inspection, investigator can provide worthwhile information that may assist in recognising the causes of distress in concrete elements. Therefore, an expanded knowledge of structural engineering regarding concrete materials and construction tools is needed to truly derive information from visual inspection. Before starting visual inspection of the tested structure, an organized plan should be leaded to maximize the quality of the data collection. ACI 228.2R provides the following activities as a suitable approach:

- Cursory "walk-through" inspection to become familiar with the structure;
- Gathering background documents and information on the design, construction, ambient conditions, and operation of the structure;
- Planning the complete investigation;
- Laying out a control grid on the structure to serve as a basis for recording observations;
- Doing the visual inspection; and
- Performing necessary supplemental tests.

Visual inspection is one of the powerful methods in NDT technology. However, as stated above, this method requires strong knowledge to interpret the results. The method has also its limitation in which only the external surface of the tested object will be inspected. As a result, the method should be assisted with other NDT methods to enhance the power of visual inspection.

2.8.2 Ultrasonic Pulse Velocity (UPV) Method:

This method has been used successfully to evaluate the concrete quality over 60 years

(Malhotra 2004). UPV can be used to determine the quality of new and existing concrete structures. Some of the applications of the method include: detecting internal cracks as well as other concrete deteriorations due to aggressive chemical media, freezing and thawing. This method can also be used to determine concrete strength both at laboratory scale and in the field. The ultrasonic pulse velocity method applies mechanical wave that brings no damage to the concrete structures. The test is repeatable for several times at any location so that it can be used to check the concrete internal changes over period of time.

The advantages of this method are:

- It has high power of penetrating waves into the concrete object which allows detecting the deficiency in concrete such as flaw in deep part of the tested elements.

- The device is very sensitive and has capability to detect small flaws.

- Access to one side of the structure is needed.

- Provides more accurate results compared to other NDT methods in detecting cracks, flaws and element thickness.

- It is not dangerous to operators or nearby personnel and provides no deficiency on equipments and materials.

- The device is portable.

The disadvantages of this method are:

- Careful attention is needed for manual operation which in turn experienced operators are required.

- Rough, small or thin and non-homogeneous elements are difficult to inspect.

- Concrete surface should be cleaned with no dust or paint.

The Ultrasonic Pulse Velocity test instrument includes three major parts, namely: (i) wave pulse producer to produce and introduce pulse into the concrete elements (pulse generator and transmitter); (ii) a receiver amplifier to record the transmitted pulse from the transmitter; and (iii) a display device or oscilloscope which is connected to the instrument to

interpret the result from received pulse. The travelling time taken by pulse through the concrete should be accurately measured. A schematic diagram of the device is shown in Fig. 2.1, while Fig. 2.2 shows a photo of the device.
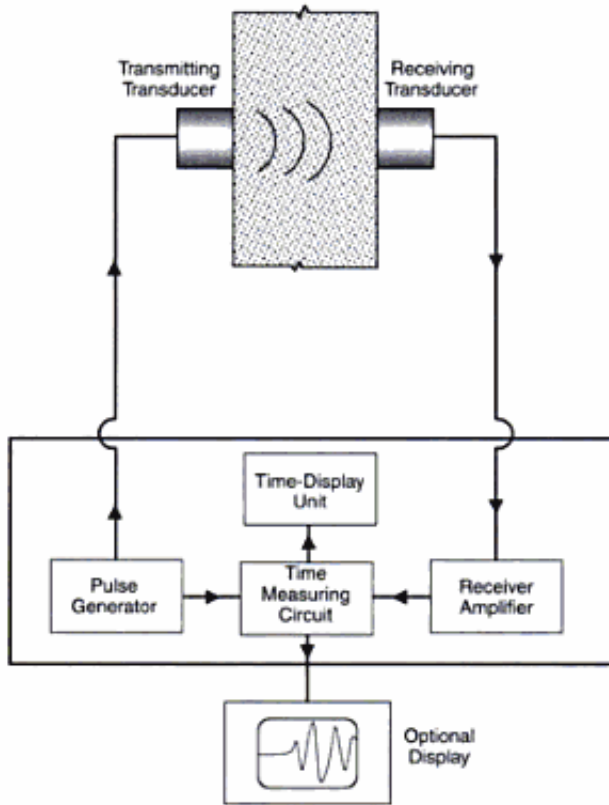
Fig. 2.1 Schematic diagram of pulse velocity test Circuit (Adapted from Malhotra, 2004)

Fig. 2.2 Pulse Velocity Instrument (Courtesy of James Instrument, Inc)

To perform the Ultrasonic Pulse Velocity test, a pulse is introduced to the tested element on the concrete surface by means of transmitter transducer (T); the receiver transducer (R) receives the pulse at second location after the pulse travels through the concrete. The time taken by the pulse, Δt, during the test can be recorded along with the path length, L (the distance between two transducers). The path length divided by the time is known as "pulse velocity", V:

$$V = L / \Delta t \tag{2.1}$$

There are three possible configurations of transducers' arrangement as shown in Fig.

2.3, namely: (i) direct transmission; (ii) semi-direct transmission and (iii) indirect or surface transmission. The direct transmission is the most satisfactory and desirable arrangement since it provides the maximum energy of the pulse transmitted and received.
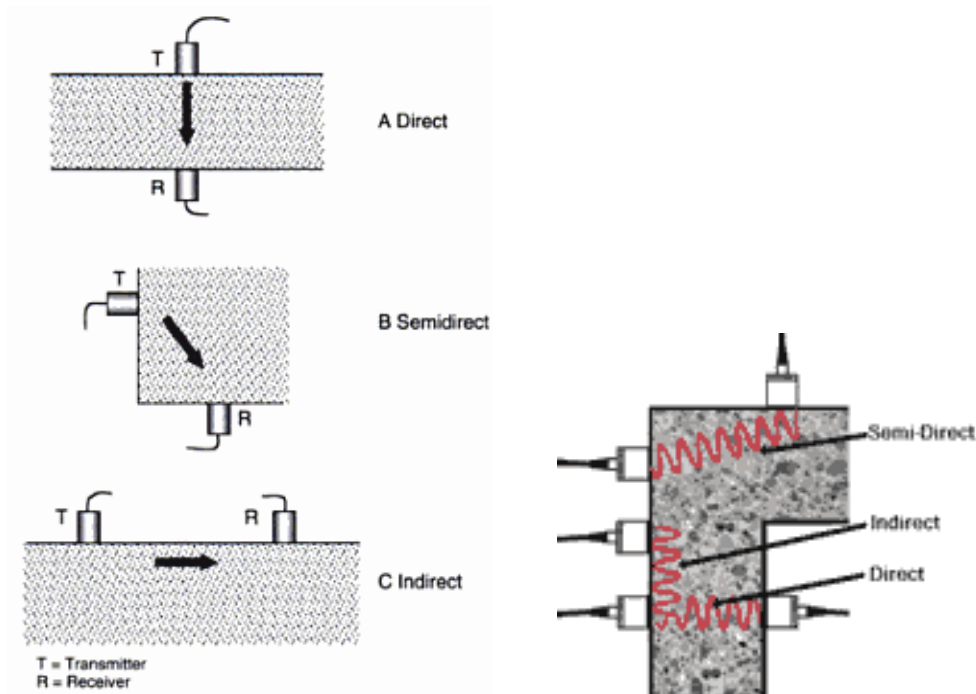
Fig. 2.3 Transducers arrangement in Ultrasonic Pulse Velocity test (Adapted from Malhotra, 2004)

The pulse transmitted into the concrete element encounters several aggregate and mortal boundaries at different elevation along the wave path. However, the pulse reaches the receiver transducer in a waveform format contains both compressional and shear waves. The compressional waves travel faster than shear waves and reach the receiver much sooner. To perform a true ultrasonic test, both transmitter and receiver must be in full contact with the tested element so that the air pocket between the test element and transmitter or receiver will not produce error in transiting time. Many couplants in the market can be used to eliminate the air pockets and assure a good contact (Malhotra, 2004). Petroleum jelly has proved to be one of superior couplants. Other couplants are grease, liquid soap, and kaolin-glycerol paste. Ordinary concrete has a pulse velocity of 3700-4200 m/s. For a short travel path (i.e. 300 mm), the travel time would be almost 70-85 µs. Therefore, the devices must possess a high level of accuracy to measure such a short travel path time.

There are several factors that may affect pulse velocity, namely: (i) aggregate size; (ii) cement type; (iii) water-cement ratio; (iv) admixture; (v) age of concrete; and (vi) transducer contact. In case of effect of aggregate size, it is found that the pulse velocity is affected significantly by aggregates size and shape. Pulse velocity in the cement paste is lower than that in aggregates. It was also found that for the same concrete mixture and compressive strength, rounded aggregates provide lowest pulse velocity, crushed limestone provides the highest pulse velocity and crushed granite had a pulse velocity between the above two. Moreover, it was found that higher aggregate content provides higher pulse velocity. In case of the effect of cement type, it was found that the type of cement has no significant effect on pulse velocity. However, since various cement types have different hydration rate, cements with higher rate of hydration provides higher pulse velocity. In case of the effect of water-cement ratio, it was reported that with the increase of water-cement ratio, the compressive and flexural strength of concrete decrease resulting in reducing pulse velocity. In case of admixture, it was found that calcium chloride reduces setting time of the concrete mixture, resulting in increasing the rate of cement hydration which in turn increases the pulse velocity. In case of transducer contact, as discussed earlier, the transducers must be in proper contact with concrete surface to provide the minor error in travelling time.
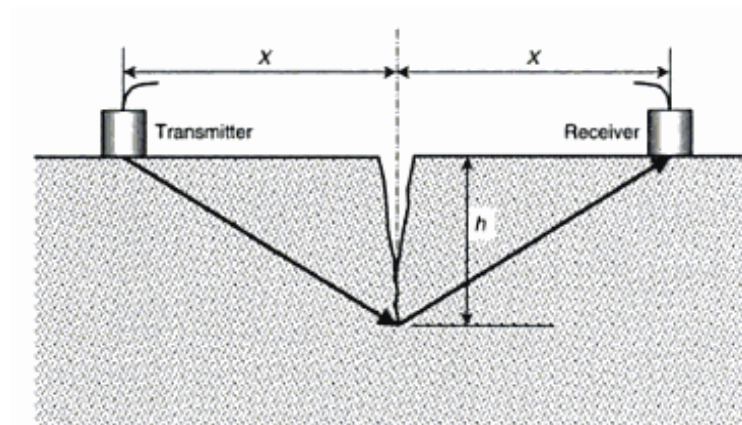
Fig. 2.4 Surface crack depth measurement using ultrasonic pulse velocity method (Adapted from Malhotra, 2004)

Surface crack depth can be measured by ultrasonic pulse velocity method by placing

transmitter and receiver transducers as indirect arrangement on both sides of the crack with equal distance X from crack as shown in Fig. 2.4. Transmitter transducer transmits a pulse to the test element in which it will be reflected by bottom side of the crack. The receiver transducer receives the pulse and transit time around the crack is recorded as T_1. The test has to be performed again for the same concrete properties but without crack inclusion. The transit time between transmitter and receiver without crack is recorded as T_2. Using equation 2.2, the depth of surface crack, h, in the concrete can be obtained:

$$h = \frac{X}{T2} \cdot \sqrt{T_1^2 - T_2^2} \qquad (2.2)$$

where: X= distance to the transducer from crack; T_1= transit time around the crack; and T_2= transit time along the surface of concrete without cracking.

2.8.3 Half Cell Potential Method to evaluate corrosion of reinforcement

Corrosion in concrete steel reinforcement is unavoidable. The reason is that steel in the concrete tend to return to its stable condition which is iron dioxide under atmospheric changes. Half cell potential method is a NDT method that has been widely used to determine the corrosion of steel reinforcement. Chloride ion from sea water or deicing salt is the main reason of corrosion in the reinforced concrete structures. High level of chloride in concrete results in depassivation of rebars in concrete and corrosion occurs in the presence of Oxygen and humidity around the rebar due to electro-chemical reactions. Half-cell potential is the potential of an electrochemical half-cell with respect to the standard hydrogen electrode. In other word, it is a cell consisting of an electrode immersed in electrolyte, designed to measure single electrode potentials. In concrete, dissolution zones are large (a centimeter or more), so electric field (current line) connects these zones to those where oxygen is reduced. The current lines are normal on equipotential surfaces for a given potential, which can be intersected by the concrete surface. The potential value can be measured by using a reference electrode placed on the concrete surface. Figure 2.7 depicts configuration of current and equipotential lines.
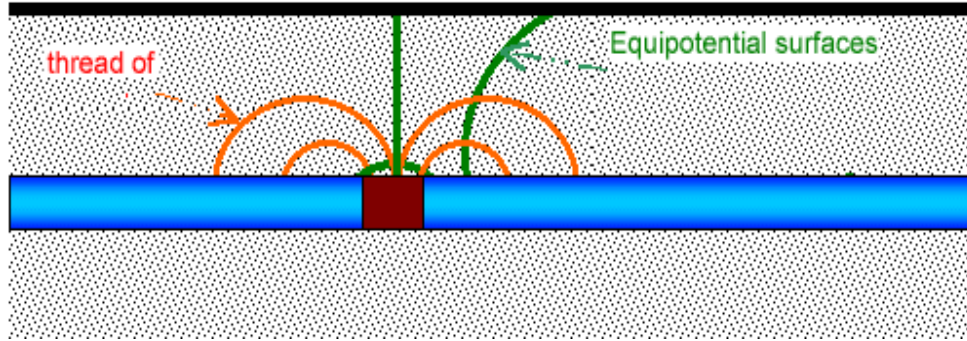
Fig. 2.5 Equipotential lines intersecting concrete surface (Concrete Corrosion)

The standard test method is given by ASTM C 876 and illustrated in Figs. 2.6 and 2.7 (Malhotra 2004). The half-cell potential instrument consists of a copper sulfate half cell, voltmeter and connecting wires. The half cell is composed of a copper bar which is sunk into the saturated copper sulfate solution. The half cell apparatus is used to measure electro-potential lines generated by the steel rebar. The positive side of the voltmeter is attached to the steel reinforcement and the negative side to the copper sulfate half cell. The copper sulfate half cell is also attached to the concrete by means of a porous plug and sponge that is moistened with a liquid detergent. Figure 2.7 shows a computerized base device that stores data taken from different points and display equipotential contours.
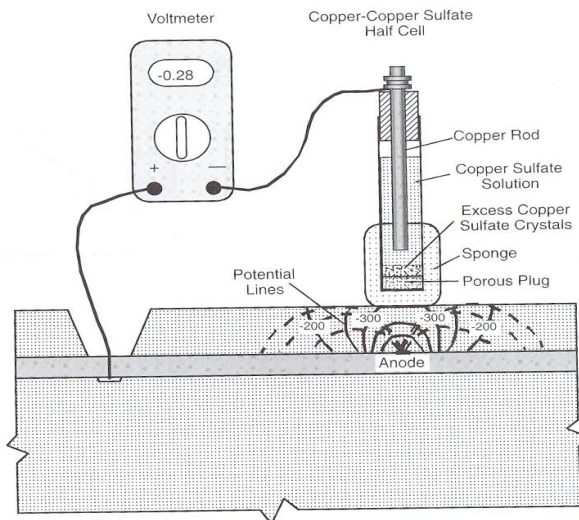
Fig. 2.6 Schematic diagram the Half- cell potential device
(Adapted from Malhotra, 2004)

Fig. 2.7 Computerized base
half-cell device

18

When concrete rebars are corroded, half cell potential device produce electro-potential lines around the corroded bars between cathodic and anodic sides of the rebar. Electro-potential lines intersect the concrete surface and potential line can be determined by half cell method. In case of corrosion of rebar, the excess electrons tend to transfer from the rebar to the half cell device, so the voltmeter shows negative voltage. By mapping the equipotential lines on the surface, the portions of the structure that have high likelihood of corrosion show high negative potentials (Malhota 2004). Two techniques can be used to interpret the results; namely: numeric technique and potential difference technique. In numeric technique, ASTM C 876 provides the following guidelines to interpret the results:

- If the potential is more positive than -200 mV, no corrosion is occurring at the time of measurement.
- If the potential is more negative than -350 mV, there is active corrosion
- Corrosion activity is uncertain if the voltage is in range of -200 to -350 mV.

However, ASTM C 876 suggested that for the following cases, the numeric technique may not be applicable:

- If carbonation extends to the level of the reinforcement.
- To evaluate indoor concrete that has not been subjected to frequent wetting.
- To compare corrosion activity in outdoor concrete with highly variable moisture or oxygen content.

In the second method of corrosion evaluation, potential difference technique, corroded steel locations are indicated by corrosion gradients. In equipotential line contour plots, the areas of high gradients indicate the location of corrosion activity. The advantages of half-cell potential method includes (i) the equipment is portable and of lightweight; and (ii) it indicates the corroded steel area at the time of testing. However, its disadvantages include (i) steel bars should be electrically connected to device; (ii) the method is not applicable to epoxy-coated bars; (iii) concrete has to be moist; (iv) the method requires professional personnel to interpret the results.

2.8.4 Linear Polarization (LR) Method

Because of major difficulty in Half-Cell Potential method in corrosion assessment, advances in research have led to the development of a new method, entitled "Linear Polarization Method", to measure rate of corrosion in concrete structures (Rodriguez et al. 1994; Flis et al. 1992, ACI 228.2R). The polarization refers to the change in the open-circuit potential as a result of the passage of current (ASTM G 15). In the Linear Polarization Resistance technique, a potential is applied to the corroding element and linear current response will be estimated. The Polarization resistance is the ratio between applied potential (change in voltage) and the resulting current response per unit area of bar as follows:

$$R_p = \frac{\Delta E}{\Delta i} \qquad (2.3)$$

The corrosion rate is therefore inversely related to the polarization resistance as follow:

$$\dot{i}_{corr} = \frac{B}{R_p} \qquad (2.4)$$

Where $\dot{i}_{corr}$= corrosion rate (ampere/cm²); B= a constant in volt (= 0.026 V commonly used for steel corrosion, Feliu et al. 1989); and Rp= polarization resistance (ohms. cm²)

The polarization resistance device consists of three electrode systems (3LP device) which include reference electrode, working electrode or reinforcement and counter electrode to introduce polarization current to reinforcement. Supplementary devices have been hired to measure voltage and current changes in different stages of the test. Since the current response should be determined per unit area of reinforcement bar where the area is perimeter of bar multiplied by the length below the counter electrode. It is found that this assumption is incorrect and current lines are not confined directly to the region below the counter electrode (Feliu et al. 1989; Flis et al. 1992). Thus, in order to better control the current lines below counter electrode, the forth electrode called guard or auxiliary electrode has been used that surrounds the counter electrode (Feliu et al. 1990 a; Feliu et al. 1990b). The guard electrode potential is kept the same as counter electrode so that the current flowing to the reinforcement is confined within the area below the counter electrode. The schematic image of both 3LP and 4LP instruments are shown in Figs. 2.8 and 2.9.
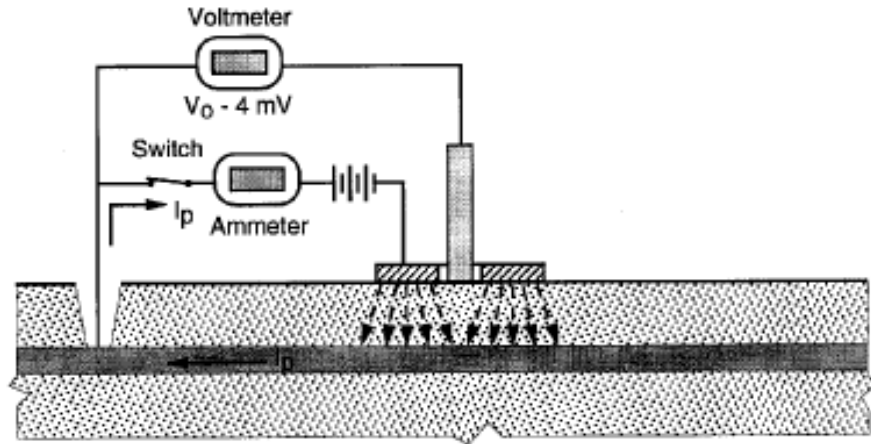
Fig. 2.8 3LP- measurement of current to produce small change in potential of working electrode (bar) (adapted from Feliu et al., 1990a).
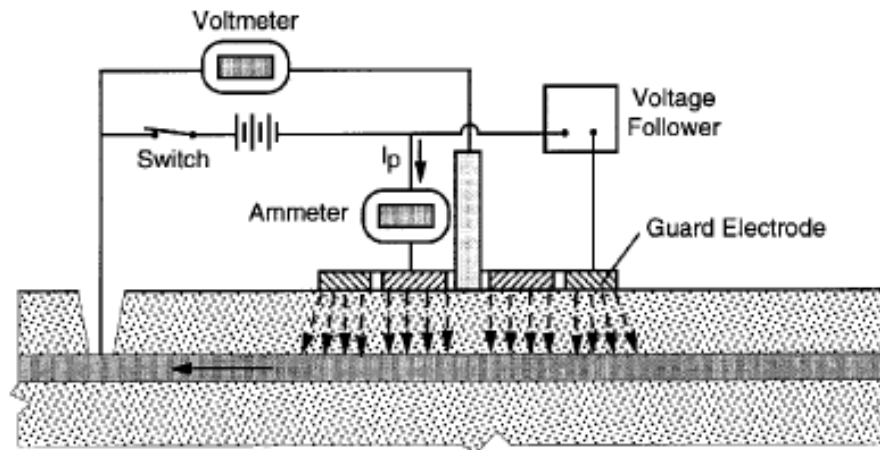
Fig. 2.9 4LP using guard electrode to confine current flow from counter electrode to reinforcement (adapted from Feliu et al., 1990a)

There is no standard specification to precisely measure corrosion rate of reinforcement steel in concrete structures. However, Clear (1989) revealed the following guidelines to assess the corrosion rate for 3LP device, presuming that corrosion rate is constant with time:

- If $\dot{i}$corr is less than 2 mA/m², no corrosion damage is expected.

- If $\dot{i}$corr is between 2 and 10 mA/m², corrosion damage is possible within 10 to 15 years.

- If $\dot{i}$corr is between 10 and 100 mA/m², corrosion damage is expected within 2 to 10 years.

21

The advantages of the Linear Polarization method are the same as those for the Half- cell Potential method stipulated above. However its disadvantages are (Cady and Gannon, 1992):

- Steel bars should be electrically connected to device.

- Not applicable to epoxy-coated bars or galvanized bars.

- Concrete surface has to be uncracked, free of moisture and smooth.

- Requires professional personnel to interpret the results.

- Cover depth should be less than 100mm.

To compare both methods, one may state that Half-cell potential method provides active corrosion of steel reinforcement in concrete structure. Linear polarization method, on the other hand, provides the rate of corrosion assessed in concrete reinforcement life. The data interpretation for both methods is not that simple because no standard method has been yet investigated to precisely indicate the corrosion of steel bars.

2.8.5 Stress Wave Propagation Method

Several stress wave methods can be used as non-destructive testing of the concrete reinforcement elements. The method includes: Pulse-echo, Impact-echo, Impulse-response and Spectral analysis of surface waves techniques in which only Pulse-echo and Impact-echo will be discussed. The stress wave is produced when a pressure such as impact is applied on the concrete surface. Due to impact effect, the stress propagates through the concrete with a speed depending on modulus of elasticity, passion's ratio, density and geometry of the elements. The dependence between concrete properties and stress wave propagation results allow interpreting the characteristics of concrete elements. The methods differ in various aspects such as stress wave, testing configuration, instrument and characteristics of the measured response. On the positive side, only access to one side of the structure is required to perform these types of NDT methods. These methods are applicable to thickness measurement, flaw detection and integrity testing of piles as well as thickness of pavements and elastic module of layered pavement systems.

By introducing impact to the concrete surface, the stress waves propagate through the concrete in three different waves as defined below:

- **P-Wave:** it is compression waves with which particle motion is parallel to the propagation direction.

- **S-Wave:** it is shear waves on which particle motion is perpendicular to the propagation direction.

- **R- Wave:** it is a Rayleigh or surface wave that propagates along the surface of a solid, on which particle motion is retrograde elliptical.

2.8.5.1 Pulse- echo Method

A schematic of the pulse- echo system is shown in Fig. 2.10. The instrument includes a transmitter and a receiver to introduce and receive pulse through the structure. The pulses are transferred to an oscilloscope or display device to determine the travelling time.
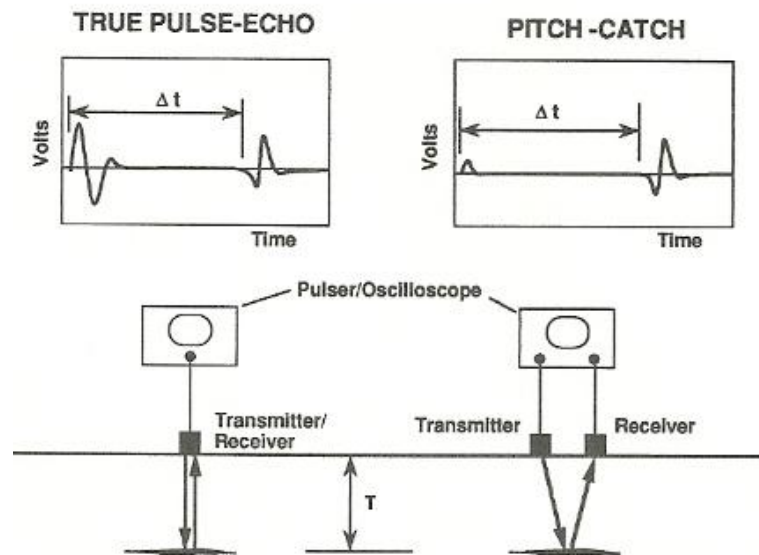
Fig. 2.10 Schematic of pulse-echo and pitch-catch techniques (Adapted from Malhotra, 2004)

The test starts when the transmitter introduces a pulse on the surface of the test element. The pulse propagates into the test element and is reflected by any defect in the elements. The reflected wave or echo at surface is monitored either by a transmitter acting as receiver (true

pulse-echo) or by a second transducer located near the transmitter (pitch-catch). The receiver output is displayed on a display device (Time Domain Waveform). The round-trip travel time of the pulse is determined by display device and if the wave speed in material is known, the depth of the reflecting interface can be determined using the following equation:

$$T= \frac{1}{2} \Delta t \cdot Cp \tag{2.5}$$

where: T = the depth; Δt= the round-trip travel time and Cp= the P-wave speed.

As an example, Fig. 2.11 shows a waveform obtained from a 235 mm concrete slab using pitch-catch system. The round-trip travel time between start of the transmitted pulse to arrival of the P-wave echo reflected from bottom of the slab determined is 106 μs. solving for Cp in equation 2.5, Cp= 2 x 0.235/(106x10^{-6}) = 4433 m/s.
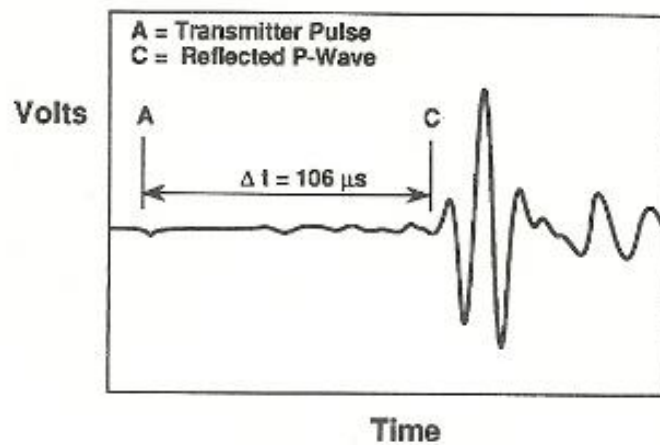
Fig. 2.11 Waveform taken on a 235 mm concrete slab using pitch-catch system (Adapted from Malhotra, 2004)

2.8.5.2 Impact-echo Method

A schematic of the impact-echo device is shown in Fig. 2.12. The instrument includes a mechanical impact pulse producer, a receiver to receive the wave pulse and a data acquisition system. To start the test, the impact-echo device is placed on the top of the test object and introduces an impact to the object. The impact wave propagates into the test sample as pulse or echo forms producing P and S waves. R waves will also be produced at the surface of the test sample running away from the impact point. Compression and shear waves (P and S waves) are reflected by any defect or external interface. The reflected waves at surface

24

produce displacement which can be determined by receiving transducer and recorded by data acquisition system. Two signal analysis methods can b used, namely: Time-domain analysis and frequency-domain analysis (Malhotra 2004).
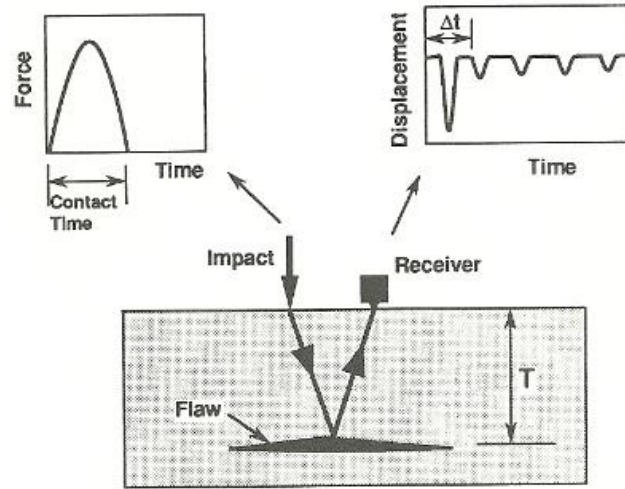
Fig. 2.12 Principle of the impact-echo method (Adapted from Malhotra, 2004)

Time domain analysis can be used for long slender structures such as piles and drilled shafts. In these types of structures, the geometry of structure acts to focus on propagating waves within narrowly defined boundaries. Equation 2.5 can be used to determine depth of the reflecting interface ($T= \frac{1}{2}\Delta t.C_p$). An example of the waveform tested on a pile due to impact is shown in Fig. 2.13. Once the impact introduced to the pile, the first set of peak is generated by R waves and the second lower peak represents bottom wave reflection. The total depth of the pile is measured 15.3 m. The travel time between zero time and bottom reflection is 7.5 ms. Solving for $C_p = 2 \times 15.3 / (7.5 \times 10^{-3}) = 4080$m/s.
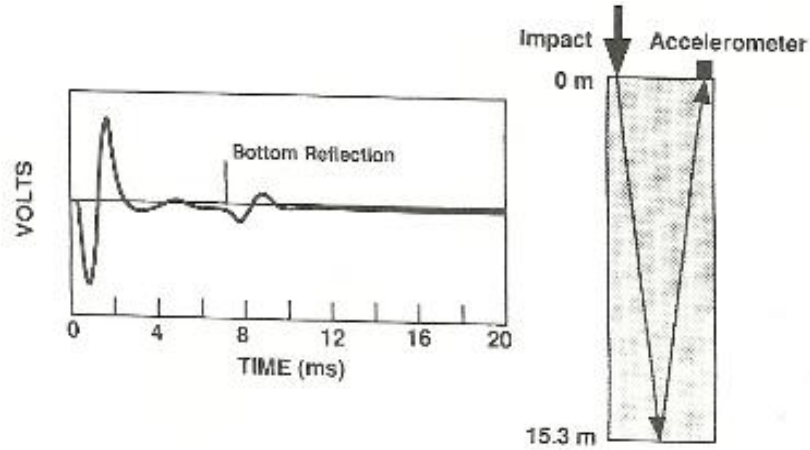
Fig. 2.13 Waveform from impact-echo test on a pile (Adapted from Malhotra, 2004)

Time domain analysis is possible for thin structures such as slab and walls; however, it might be sometimes difficult due to geometry of the structure. Frequency analysis, on the other hand, is an alternative way based on displacement waveform. By introducing impact to the test object, pulse propagates back and front between the defect and object surface producing a downward displacement at the top surface of the object. Thus, the waveform is periodic, and the period is equal to the travel path, 2T divided by the P-wave speed. Since frequency is the inverse of period, the frequency of the characteristic displacement is equal to:

$$f = \frac{C_{pp}}{2T} \tag{2.6}$$

where C_{pp} is the plate P-wave speed.

If the dominant frequency in a waveform is determined, the thickness of the plate or distance to a reflecting interface can be calculated as $T = \frac{C_{pp}}{2f}$.

As an example, an impact-echo test was performed on a solid concrete slab of depth 0.5 m (Figure 2.14-top). By introducing an impact to the concrete slab, a peak frequency of 3.42 KHz has been determined due to P-waves reflection between top and bottom of the slab. Solving for C_{pp}, the plate P-wave speed is calculated 3420 m/s. The same concrete configuration and properties has been chosen with a penny shape void at the depth 0.25 m from the top surface (Figure 2.14-bottom). Introducing impact to the second sample produces a peak frequency of 7.32 KHz between top surface and the void due to P-waves. Using the equation above to solve the depth of void: T= 3420/ (2x7320) = 0.23 m which is close to the

26

real location of the void in the sample (0.25 m).
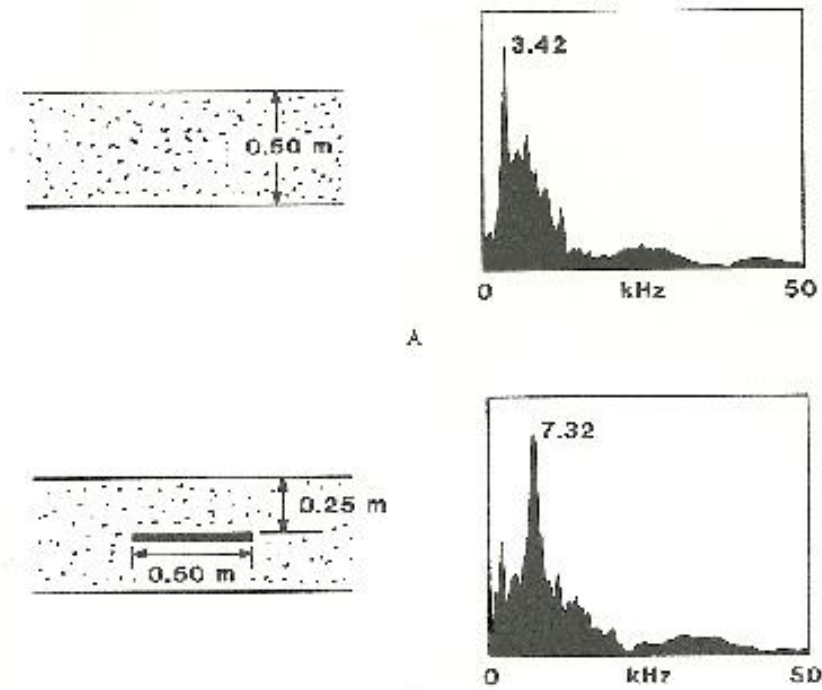
Fig. 2.14 examples of amplitude spectra (Adapted from Malhotra, 2004)

2.8.6 Infrared Thermographic Techniques:

This method is a remote sensing method and has been widely used in civil engineering structures. Some of the applications of the method are; determination of internal cracks, void, delamination in concrete structures such as bridge decks, highway pavements, garage floors, parking lot pavements and building walls (Malhotra et al., 2004). The method is proven to be accurate and efficient in determination of concrete subsurface deficiencies. Some of the most important qualities of this technique includes being (i) accurate; (ii) repeatable; (iii) not inconvenient the public; and (iv) economical.

Principle of the Infrared Thermographic method is based on heat emission from concrete surface. The subsurface deficiencies in concrete may affect the heat flow over the concrete surface. By using infrared thermography device and measuring temperature changes over the concrete structures, the subsurface deficiencies might be determined. ACI228.2R-98, specifies that heat-flow can occur naturally by solar heating (heat-flow into the concrete) and at night-time cooling (heat flow out from concrete), which the latter method is more

economical approach. The amount of radiation emitted by an object increases with temperature. Therefore, thermography allows the investigator to see variations in temperature. Thus, when viewed by thermographic camera, warm objects stand out well against cooler backgrounds. Thus, the environmental changes significantly affect the test result. To overcome environmental influences on testing, the following guidelines are suggested (ASTM D 4788):

- Remove debris from surface.
- Do not test when standing water, ice or snow are present; allow surface to dry at least 24 hrs before testing.
- Do not test if wind speeds exceed 25 km/h.
- The ground temperature should be above 0°C.
- Testing at night should be done under clear skies.

Infrared thermograph system has several advantages among other NDT methods as follows:

1) Only small calibration coring is need for the test to be fulfilled. This may result in saving in time, labor, equipments and traffic control.

2) It will not affect the structural aesthetician.

3) It does not affect the surrounding environment.

4) It is safe and only record thermal radiation from concrete and other objects.

5) The test is known to be area testing method compared to other NDT's, which are point or line testing method. So, the method is able to form two dimensional image of the test surface.

The main disadvantage of the method is that:

1) It is not capable of determining void depth or thickness. Other NDT method such as Ground Penetrating Radar (GPR) or Stress Wave Propagation methods should be used in this regard.

2)   Expensive equipment.

3)   The test requires proper environmental condition.

4)   Skilled operators are needed.

Generally, a high-resolution infrared thermographic camera, Fig. 1.15, is required to inspect a large area of concrete structure. The test instrument allows a large area of test object to be scanned and the resulting image to be displayed with areas of different temperature either by gray tones in black and white image or various colors in color image. A wide variety of equipment can be used to record or interpret the result data as follow:

1) Scanner and detector with interchangeable contact lens.

2) Black and white or color display monitor; cooler areas appear in darker gray tones, while warmer areas appear in lighter gray tones. Different temperature represents different colors in color display monitor.

3) Data acquisition system and analysis equipment composing of a computer with high resolution color monitor, data storage and analysis software.

4) Image recording system to record both visual and thermal images.

Fig. 2.15 Schematic of infrared camera device (Adapted from Malhotra, 2004)

Heat movement over the test object is required for infrared thermograph inspection. To properly perform the thermographic test, the following suggestion should be made (Malhotra et.al, 2004):

1) Begin inspection 2-3 hours after sunrise or after sunset (Times of rapid heat transfer).

2) Clear the test object from dust and debris.

3) Traffic control should be maintained to prevent accident or vehicle standing on the tested concrete object.

In case of large concrete area inspection such as bridge deck, once the above considerations are made, a mobile van is used along with scanner, recorder for data storage and a computer to analysis data. By moving the concrete deck establishes the sound concrete, scan and records the sound concrete image. Then, scan over the concrete deck containing defects such as void, delamination and make sure that equipment scan over both sound and defective areas plotting them in the same image for comparison. For black and white image, black tones represent defect in concrete and white represent sound concrete. For color image, three colors uses for defect, sound and intermediate concrete. Figures 2.16 and 2.17 show some typical examples of using infrared thermograph device in inspecting concrete structures.

Fig. 2.16 Visual and thermal images of powdery concrete, Martin Luther King Bridge- St. Louis (Malhotra et al., 2004)
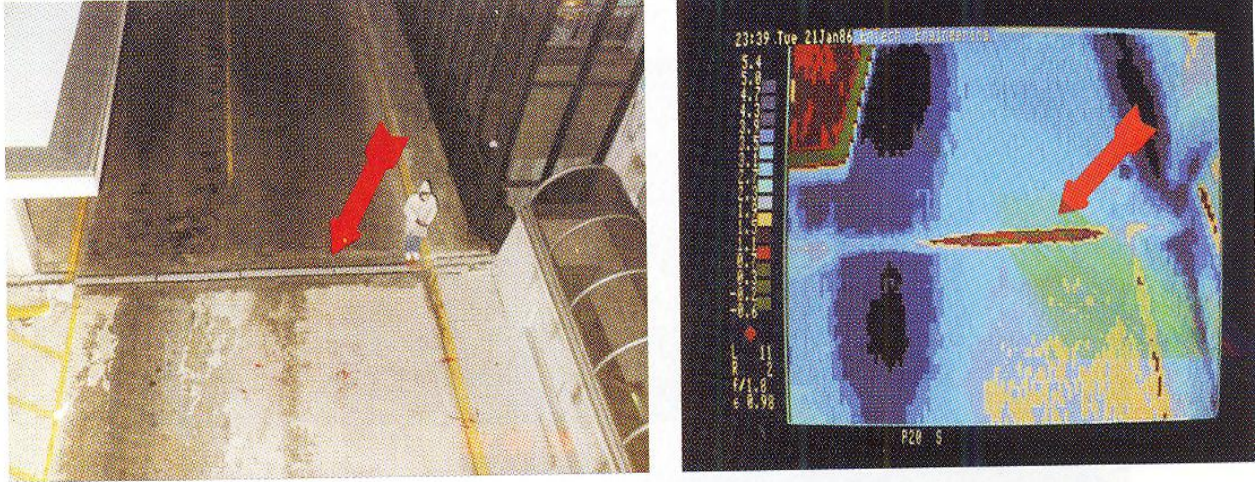
Fig. 2.17 : Visual and Thermal images of roadway expansion joint, Lambert St. Louis International Airport (Malhotra et al., 2004)

2.8.7 Acoustic Emission Method

Acoustic Emission (AE) is defined as transient elastic waves within a material caused by release of localized stress energy. In other word, once a structure is subjected to an external factor such as pressure, load or temperature, stress wave energy is generated in the materials propagating through the materials toward surface and is recorded by AE sensors. Generally, acoustic emission event is related to unalterable release of stress wave energy due to deficiencies in concrete such as crack, rebar or fiber breakage, voids and elastic deformation of rebars. AE cannot be generated from sources involving material failure such as friction, cavitation and impact.

Acoustic emission technique is primarily based on detection of elastic wave energy released through the concrete materials and interpreting the results as electrical signals. This can be performed by locating coupling piezoelectric transducers on the surface of the test object and applying load on the object. The output result is amplified by a low-noise preamplifier and further processed to remove any extraneous noise. AE can also predict early failure of the structure without any significant damage to the structure. The difference between AE method and other NDT methods is that AE detect activities within the materials, while other NDT methods can be done by sending and receiving pulse energy into the object and interpreting the results.

31

The signal arrived at piezoelectric transducer may be affected by stress waves energy released through the materials, geometry of the test object and characteristics of the receiving transducer. The arrival signals are classified as follow (Malhotra et.al 2004):

- *Continuous emission*: is a qualitative description of the sustained signal level produced by rapidly occurring acoustic emission events. In metal and alloys, this type of AE is generated by plastic deformation of the metals.

- *Burst emission*: is a qualitative description of the discrete signal related to an individual emission event occurring within the materials. This type of AE has short duration pulses and will be generated due to crack development, micro yielding and fracture of materials.

Some of the advantages of acoustic emission technique are listed below (Baldev Raj et al. 1997): (i) high sensitivity; (ii) early and rapid detection of defects such as flaw and cracks; (iii) cost reduction; (iv) no need for scanning the whole structural surface; and (v) minor disturbance of insulation. AE disadvantages include (i) plant environment are usually very noisy; (ii) AE signals are usually weak; and (iii) AE requires stimulus.

2.8.8 Ground Penetrating Radar (GPR) Method

Ground penetrating method is a method similar to pulse-echo technique but the electromagnetic waves or microwaves are used in lieu of stress waves. The technique is primarily used to detect cavities in airfield pavements and research continued to use of the technique in more broad areas such as concrete thickness, locating voids and reinforcing bars, identifying deterioration as well as strength development in concrete and water content assessment. Some of the features of the method are (ACI 228-2R); ability to penetrate into subsurface and detect unseen conditions; scan large surface area in short period of time and its high sensitivity to subsurface moisture and embedded metal. In case of civil engineering structures, the short pulse radar should be introduced to the structure since the structure being test is shallow. The technique, therefore, is called Short-Pulse radar or ground-penetrating (probing) radar (GPR).

The schematic of GPR device is illustrated in the Fig. 2.18. As shown, an antenna

introduces short pulse electromagnetic waves in the test element. The electromagnetic waves travel through the materials and are reflected by receiving antenna while facing materials with different dielectric characteristic. The antenna, then produces an output signal corresponds to existing material behavior.
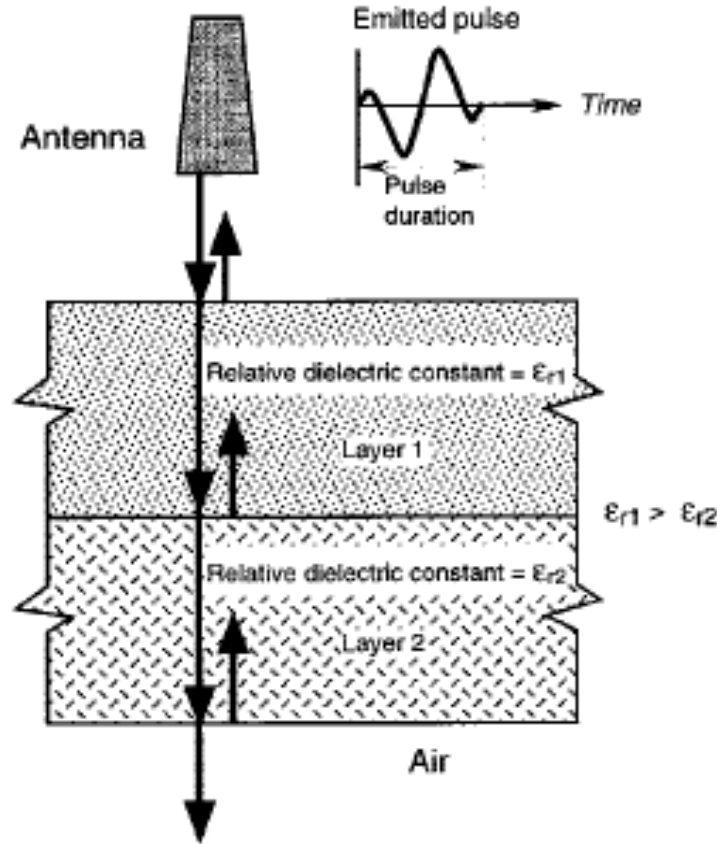
Fig. 2.18 Propagation of EM energy through dielectric boundaries (Adapted from Carino, 1994)

The theory of electromagnetic waves propagation is a complicated one. Daneials et al. (1988) and Halabe et al. (1993, 1995) introduced more detailed treatment for civil engineering applications. Concrete material properties that affect the transmitted and reflected energy are dielectric constant and conductive. The material's dielectric constant is the amount of electrostatic energy stored per unit volume for a unit potential gradient. The ratio between material's dielectric constant to that of free space is known as relative dielectric constant ε_r;

$$\varepsilon_r = \frac{\varepsilon}{\varepsilon 0} \qquad (2.7)$$

Where: ε = dielectric constant (farad/meter); ε_0 = dielectric constant of free space (air) equal

33

to 8.85 x 10^{-12}.

The speed of electromagnetic waves C can be then determined using the following equation;

$$C = \frac{C0}{\sqrt{\varepsilon r}} \tag{2.8}$$

Where: $C0$ = speed in air (3×10^8 m/s); εr = relative dielectric constant.

The depth of reflecting interface can be determined by measuring the round trip travel time (t) and using the equation below;

$$D = \frac{C.t}{2} \tag{2.9}$$

Reflection coefficient at interface for dissimilar materials is given by the following equation (Clemena, 1991; Bungey and Millard, 1997).

$$\rho 1, 2 = \frac{\sqrt{\varepsilon r}1 - \sqrt{\varepsilon r}2}{\sqrt{\varepsilon r}1 + \sqrt{\varepsilon r}2} \tag{2.10}$$

where: $\rho 1, 2$ = reflection coefficient; $\varepsilon r1$ = relative dielectric constant of material 1; and $\varepsilon r2$ = relative dielectric constant of material 2.

From the above equation, one can conclude that when the dielectric constant of material 2 is greater than material 1, reflection coefficient will become negative. This is due to change in polarity of the reflected waves in material 2 which appears as a negative dielectric constant in equation above. For instance, at reinforcement steel interface, there is complete reflection of radar resulting in reversing polarity of the reflected waves at steel reinforcement. This aspect in turn makes GPR as an effective way to locate reinforcement steel in concrete structures. However, since there is complete radar reflection at steel interface, GPR may block out other weaker reflected waves from greater depth of the tested element.

Signal attenuation due to energy loss of materials is given by Bungey and Millard (1993);

$$\alpha = 1.69 \times 10^3 . \frac{\sigma}{\sqrt{\varepsilon r}} \tag{2.11}$$

Where: α = signal attenuation (dB/m); σ = conductivity ($\Omega^{-1} m^{-1}$).

The equation shows that frequency of the emitted signal has direct relationship with concrete conductivity. By increasing frequency, concrete conductivity also increases. It is also observed that electromagnetic waves propagated through materials are affected by dielectric changes. Therefore, variation in concrete structure materials give various dielectric signals resulting in detecting concrete conditions such as void, delamination, ,moisture content and chloride content. As it is given in Table 2.1; relative dielectric constant of water is relatively higher than other materials. As a result, it can be concluded that electromagnetic radar is very sensitive to water consequently to moisture content of the concrete properties.

Table 2.1 Relative dielectric constant of the materials (ASTM D 4748)

Material	Relative dielectric constant (εr)
Air	1
Portland Cement Concrete	6 to 11
Bituminous Concrete	3 to 5
Gravel	5 to 9
Sand	2 to 6
Rock	6 to 12
Water	80

Typical GPR device consists of the following main equipment:

1) An antenna unit; to introduce electromagnetic waves to the structure and receive the reflections.
2) The control unit; to control frequency of pulse introduced and amplifies the received signals and interprets the output result to display device.
3) Storage device; a recorder or digital storage device is used to store data for later analysis and interpretation.
4) Display device; can be an oscillograph to plot the resulting waveform (topographic or waterfall plot) to detect variation in the waveform patterns.

By means of antenna, electromagnetic pulse waves are introduced into the test object. The reflected pulses generate a large amount of data determined by control unit. Several

techniques including computer processing can be used to interpret the results.

1) Cluster analysis is a technique that compares the recorded waveforms or signals with the previous ones. Similar signals are recorded and assigned as analogous cluster signals. Different signals represent dissimilar cluster or a new cluster signals. The clusters then are correlated to a known conditions determined through visual inspection, coring or excavation (Cantor, 1984).

2) Topographic plotting is one the techniques that displays radar traces with a fixed distance from previous ones. When a series of traces are plotted from radar analysis, the appearance of the total plot is similar to the topographic drawing (Cantor, 1984, see also Fig. 2.19). Radar traces with parallel drawing with respect to one another represent a uniform material. However, if the traces overlap or change with respect to one another, variation in the material properties such as deterioration, delamination, joints and varying thickness may be determined.
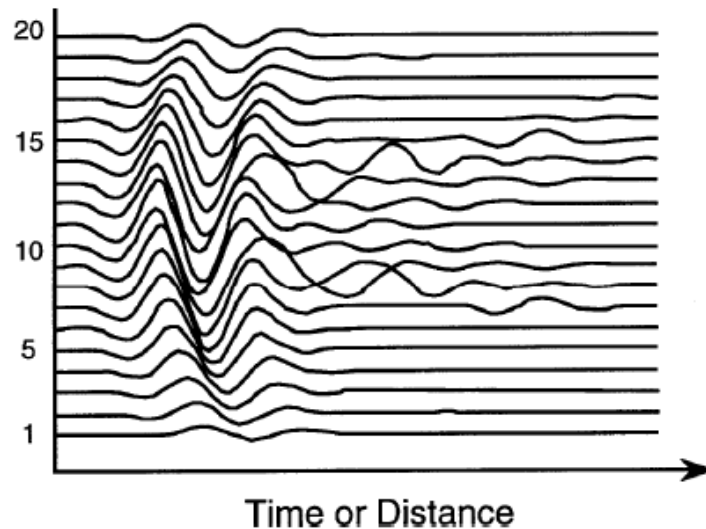
Fig. 2.19 Illustration of topographic technique by GPR (Adapted from Cantor, 1984)

3) Quantitative peak tracking is a technique that uses signal processing to determine amplitudes and travel times of peak reflection signals. Therefore, concrete properties as depth profile or area contour maps can be displayed (Ulriksen et al. 1983). Peak plotting can generally be used in the field for real-time display of GPR data and can introduce GPR data in form of graphic recorder or video display. Figure 2.20(a) shows a dipole antenna introducing a pulse into the test object

36

containing void. The time history of emitted pulse is shown above the antenna. Figure 2.20(b) plots the received signals by the antenna. The vertical axis represents the travel time. Reflected signal at surface is received directly from antenna as the first peak. The second peak is due to void interface reflection. And, the third peak is reflected from bottom face of the test object. To interpret the result, the operator may select threshold voltage lines. If the signals exceed the lines of threshold, a peak representing signal echo associated with dash lines is recorded on the graphic recorder. As the antenna moves along the test object surface, changes in the received signals are recorded on the graphic recorder. The paper on the recorder moves at a constant speed to record the arrived signals to the antenna. The resulting plot represents cross section of the test object showing top and bottom interface along with location of void as shown in the Figure 2.20(c).
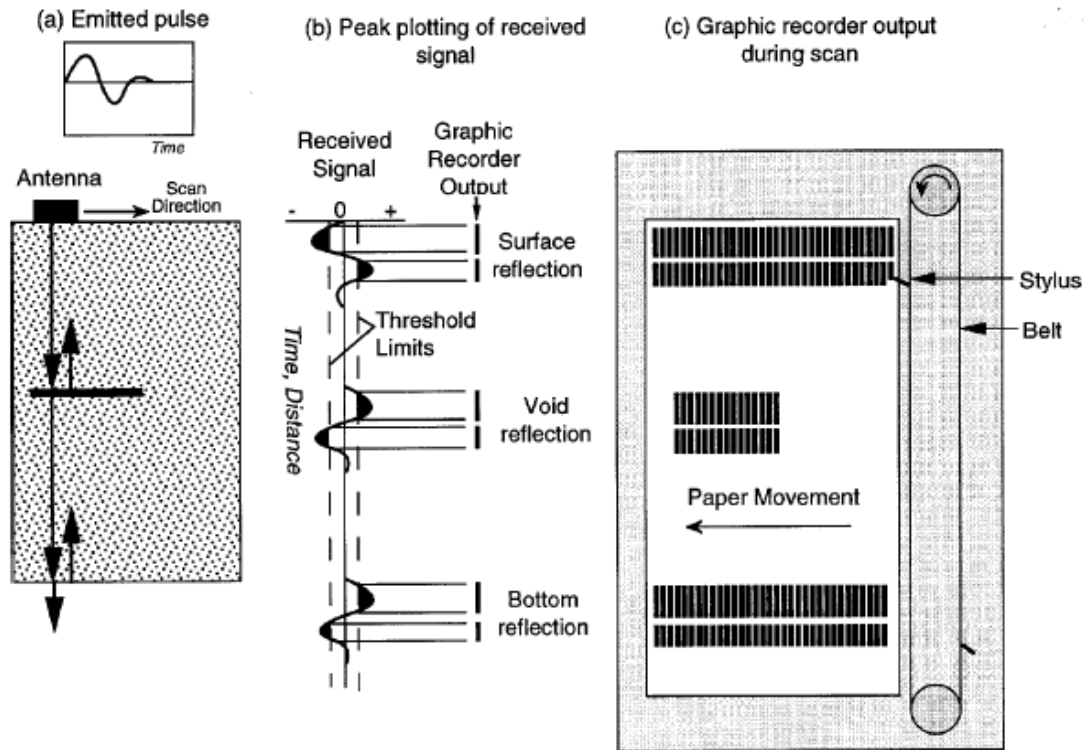
Fig. 2.20 Quantitative peak tracking technique in GPR testing (Adapted from Carino, 1994)

The advantages of GPR method include (ACI 228.2R) (i) fast scanning due to non-contact antennas; (ii) sensitive to presence of rebars and moisture in concrete structures; and (iii)

ability to penetrate in greater depth and across concrete-air interface. On the other hand, the disadvantages of GPR (ACI 228.2R) are (i) congested reinforcement can prevent penetration beyond the reinforcement; (ii) cracks and delamination cannot be easily detected by GPR unless those deficiencies are filled by moisture; (iii) high resolution pulses have limited depth of penetration (400 to 750 mm); (iv) the behavior of electromagnetic pulses propagating through reinforced concrete is not completely known; (v) experienced operators are required to operate the equipments and interpret the results.

2.8.9 Eddy Current Method (Carino, 1992):

Eddy current is one of the NDT techniques discovered by French Physicist Francois Arago in 1824 and then introduced by Michael Faraday's discovery of electromagnetic induction in 1831. It uses electromagnetic current as the basis of conducting examination. The method is induced by electric current that flow in a circular path. It is caused when a conductor is exposed to electromagnetic field due to field source motion and conductor or due to variation of field by time. This causes circular flow of electromagnetic current around the body of the conductor. Electromagnetic current may be affected by severity of the magnetic field and electrical conductivity of the conductor. The name originated from "eddies" that are formed when a liquid or gas flows in a circular path. Eddy current techniques are commonly used for the nondestructive examination (NDE) and condition monitoring of a large variety of metallic structures, including heat exchanger tubes, aircraft fuselage, and aircraft structural components. Some other applications of the method are as follow: (i) crack detection; (ii) material thickness measurements; (iii) coating thickness measurements; and (iv) conductivity measurements for material identification, heat damage detection; case depth determination, and heat treatment monitoring. Eddy current instruments are available in variety of configuration such as analog and digital instruments (i.e Fig. 2.21). Instruments are commonly classified by the type of display used to present the data. The common display types are analog meter, digital readout, impedance plane and time versus signal amplitude. Some instruments are capable of presenting data in several display formats.

Fig. 2.21 Eddy Current instrument   Fig. 2.22 Schematic of eddy-current test performance
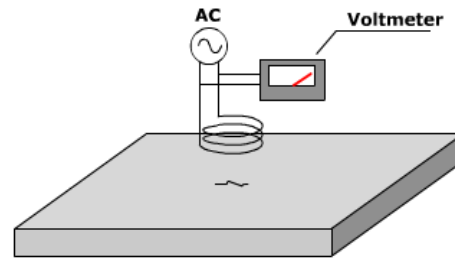
(Adapted from Carino, 1992)

Basic eddy current testing instrument consists of an alternating current source, a coil which is connected to this source by a wire, and a voltmeter to measure the voltage change across the coil (Fig. 2.22). An ammeter could also be used to measure the current change in the circuit in lieu of using the voltmeter. As mentioned, eddy current testing is based on electromagnetic induction. In the test format, a current flows through the coils and generates an oscillating magnetic field (Fig. 2.23). If the probe and electromagnetic field are placed close to the test object such as metal test object, an electric circular flow known as eddy current transfers to the metal test object generating its own magnetic field. Variation in metal thickness or defects such as surface cracks disturbs amplitude of eddy current and resulting magnetic field. This in turn changes electrical impedance of the coil resulting in change in the movement of electromagnetic currents in the coil. The changes in the impedance amplitude are plotted by eddy current instrument and an experienced operator is employed to interpret the changes in the test object.
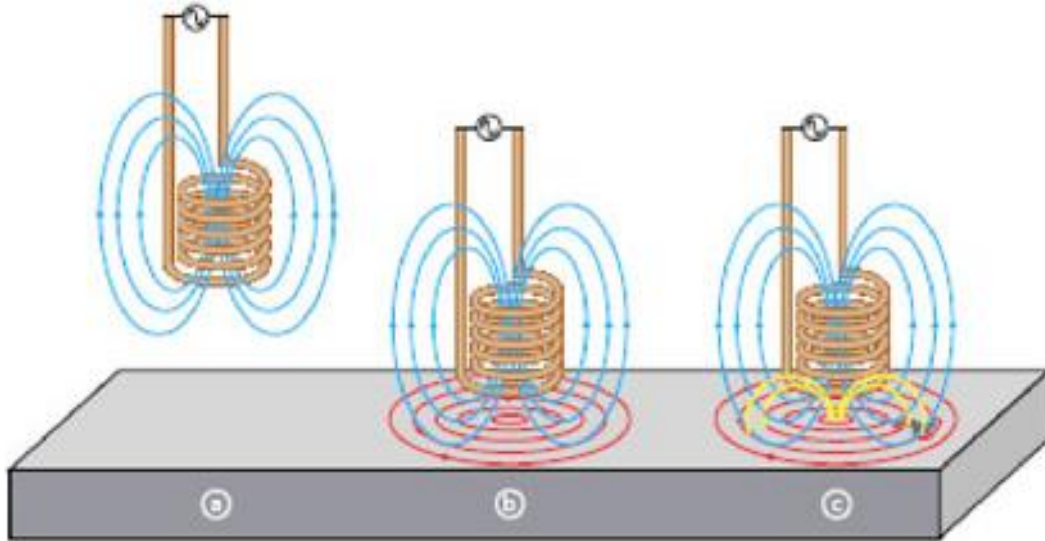
a- The alternating current flowing through the coil at a chosen frequency generates a magnetic field around the coil.

b- When the coil is placed close to an electrically conductive material, eddy current is induced in the material.

c- If a flaw in the conductive material disturbs the eddy current circulation, the magnetic coupling with the probe is changes and a defect signal can be read by measuring the coil impedance variation.

Fig. 2.23 characteristic of eddy-current instrument (Adapted from Tom N., et al., 2010)

There are many factors affecting the capabilities of an eddy current inspection. Eddy currents traveling into the materials with higher conductivity values are more sensitive to surface defects. However, they penetrate less into the material in which penetration depends on the test element's frequency. Higher test frequencies increase near surface resolution but limit the depth of penetration, while lower test frequencies increase penetration. Larger coils inspect a greater volume of the materials since the magnetic field flows deeper into the test piece, while, smaller coils are more sensitive to small defects.

Some of the advantages of eddy current NDT method are (i) sensitive to small cracks and other defects; (ii) detects surface and near surface defects; (iii) portable equipment; (iv) minimum part preparation is required; (v) test probe does not need to contact the part; and (vi) inspects complex shapes and sizes of conductive materials. On the other hand, its disadvantages are (i) only conductive materials can be inspected; (ii) surface must be accessible to the probe; (iii) skill and training requirement is more extensive than other

techniques; (iv) surface finish and roughness may interfere the results; (v) depth of penetration is limited.

2.8.10 Magnetic and Electric Methods

Magnetic and electric methods have wide applicability in evaluation of concrete structures. The methods are used to (Lauer, 1991): (i) locate reinforcement and measure member thickness by inductance; (ii) measure moisture content of concrete by means of its electrical properties; (iii) measure the corrosion potential of reinforcement; (iv) determine pavement thickness by electrical resistivity; and (v) locate defect and corrosion in reinforcement by measuring magnetic flux leakage. To evaluate strength in reinforced concrete, specific information regarding quantity and location of reinforcement is required. Thus, magnetic and electric methods can be used to acquire information regarding layout and location of reinforcement bars (Malhotra 1976, Bungey 1989, Lauer 1991). The device to locate reinforcement bars and assess the depth of concrete cover is called "covermeters".

Covermeters can be used to assess depth of concrete cover by investigating the interaction between reinforcement bars and a low-frequency electromagnetic field. Commercial covermeters can be divided into two classes: those based on the principle of magnetic reluctance, and those based on eddy currents. The description of each class is summarized below (Carino, 1992) as (i) Magnetic reluctance meters and (ii) Eddy current meters (ACI 228.2R-98).

2.8.10.1 Magnetic reluctance meters

Current in the electric coil creates a magnetic field in which the magnetic flux transfers between the magnetic poles. This leads to a magnetic circuit, in which the flow of magnetic flux between poles is analogous to the flow of current in an electrical circuit (Fitzgerald et al., 1967). The resistance to flow of magnetic flux is called reluctance, which is analogous to the resistance to flow of current in an electrical circuit. Figure 2.24 shows a schematic of magnetic reluctant covermeter with or without embedded reinforced bar. The covermeter (search head) placed on the top of the test object composed of; yoke (ferromagnetic core), excitation coil and a sensing coil. By applying alternation current to the excitation coil,

alternation magnetic flux generates flow between poles of yoke. In case of no embedment bar, high reluctance is generated between yoke and concrete contact locations (magnetic circuit) resulting in small alternating magnetic flux between poles, Fig. 2.24(a). Consequently, a small alternating magnetic flux is introduced into the sensing coil. Once reinforced bar is presented, Fig. 2.24(b), reluctance decreases and magnetic flux between poles increases resulting in increase of magnetic flux in the sensing coil. Therefore, it can be concluded that the presence of bar causes significant changes in sensing coil output data. Reluctance of magnetic circuit also depends on the depth of the concrete cover as well as size of the bar and its magnetic properties. By increasing concrete cover, reluctance increases and current decreases in the sensing coil.

2.8.10.2 Eddy Current meters

Once a coil with alternating current is placed near the electrical conductor (test object), the change in magnetic flux occurs resulting in appearance of circulating currents known as eddy current in the conductor. Eddy current raises a secondary magnetic field that interacts with field of coil. The effect of eddy current on the reinforced bar can be monitored either by continuous excitation of the coil using alternating coil or by pulsed excitation. Output of eddy current covermeter depends mainly on the electrical conductivity of the bar. Figure 2.25 shows a schematic of continuous eddy current covermeter. In case of no reinforced bar, Figure 2.25 (a), the alternating current in coil produces characteristic current amplitude which mainly depends on coil impedance. By presence of reinforcement bar in concrete, Figure 2.25(b), alternating eddy current is generated within surface of the bar. The secondary alternation current produced by eddy current also induces a secondary current in the coil. The secondary current, based on Lenz's Law (Sreway, 1983) opposes the primary current resulting in reduction of net current flow through the coil and increase of apparent impedance of the coil. Thus, the presence of bar can be determined by changes in current flow of the coil.
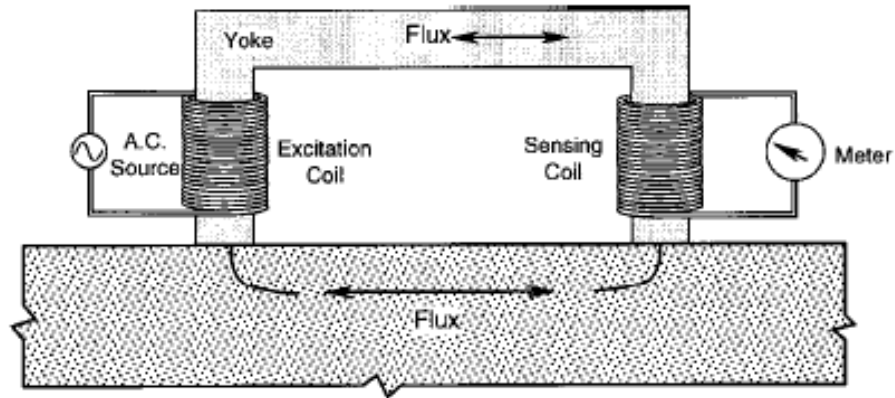
(a) Small current induced in sensing coil when no bar is present
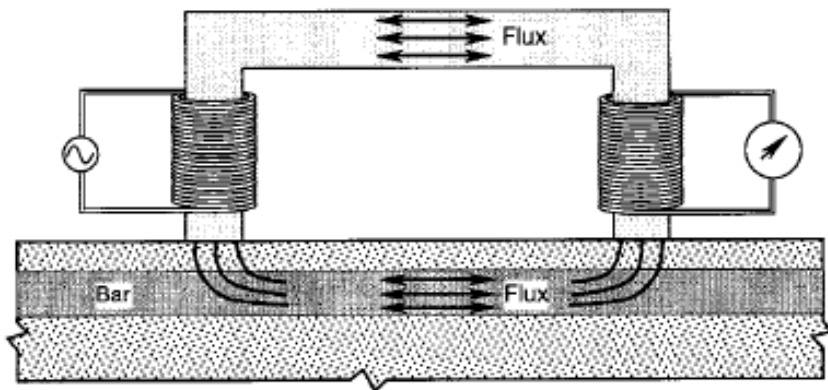
(b) Presence of bar increases flux and increase current in sensing coil

Fig. 2.24 Covermeter based on principle of magnetic reluctance (Adapted from Carino, 1992): (a) Small current induced in sensing coil when no bar is present, and (b) presence of bar increases flux and increase current in sensing coil
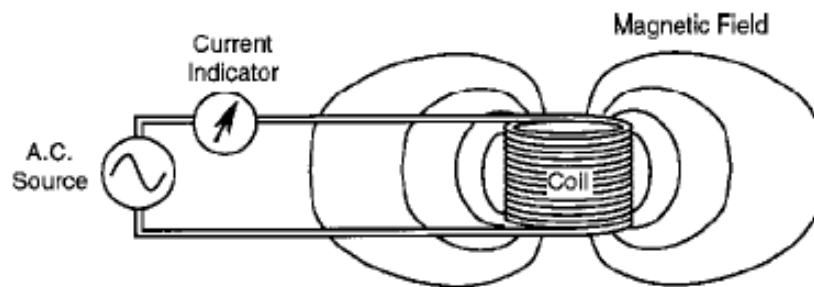
(a) Coil in air results in characteristic current amplitude
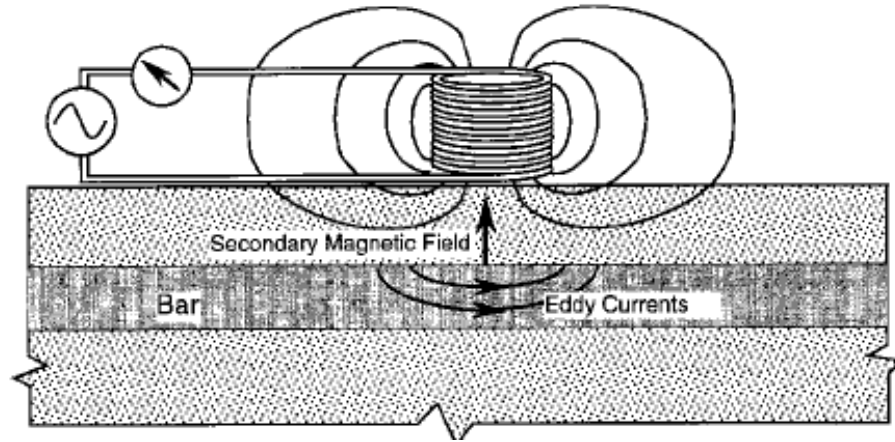
43

(b) Interaction with reinforcing bar causes changes in coil impedance and current amplitude

Fig. 2.25 Covermeter based on eddy current principle (adapted from Carino, 1992): (a) Coil in air results in characteristic current amplitude, and (b) interaction with reinforcing bar causes changes in coil impedance and current amplitude

To explain the limitation of this method, Figure 2.26 represents that bar's location can be determined when the bar is placed within the influence zone of the search head. When the search head is placed directly on the top of the reinforcing bar, the maximum response can be assumed. However, for a horizontal offset between center of search head and center of bar, an important characteristic of covermeter is supposed between amplitude and the horizontal offset. Figure 2.26(a) shows variation in amplitude with horizontal offset of magnetic reluctance covermter with a depth of cover equal to 21mm. Width of the curve in Fig 2.26(b) is defined as influence zone of the search head. Figure 2.26(c) shows amplitude and horizontal offset relationship of eddy current covermeter with variable covers (probe 1 &2). Probe 1 with smaller curvature width in which search head has smaller influence zone can detect closely spaced bars compared to probe 2 with larger influence zone. This type of covermeter, on the other hand, is not capable of detecting bars with deeper concrete cover (compared to the search head with larger influence zone).
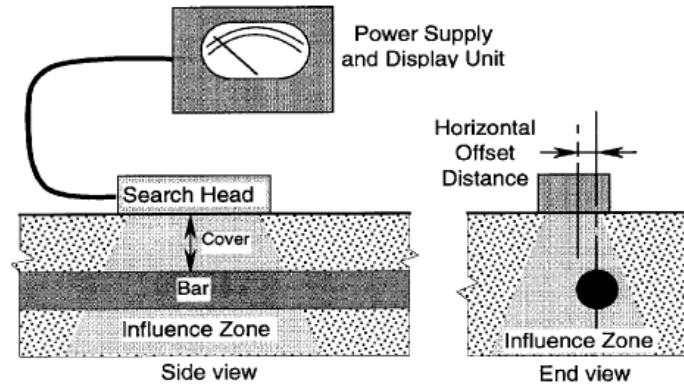
Fig. 2.26 (a) Zone of influence of covermeter search head; variation of amplitude with horizontal offset for: (b) magnetic reluctance covermeter, and (c) eddy current covermeter (adapted from Carino, 1992)

The advantages of covermeter are listed as (i) determination of the location of embedded bars; (ii) determination of the depth of concrete cover; (iii) lightweight equipment; and (iv) easy to use and fast installation. On the other hand, the disadvantages of covermeter are (i) maximum penetration of influence zone is limited; (ii) magnetic reluctance meters can only detect ferromagnetic objects; (iii) only first layer of reinforcement can be determined; (iv) depth of cover estimation is affected by bar size and spacing; and (v) distinction of single bars is affected by depth of cover, bar size and type of covermeter.

2.8.11 Nuclear (Radioactive) Methods

Nuclear method is classified into two main groups; *radiometric and radiographic methods.* The principle of both groups is based on estimation of interaction between test

materials and high-energy electromagnetic radiations (ACI 228.2R-98).

2.8.11.1 Radiometric Methods:

The method measures density of both fresh and hardened concrete based on electromagnetic radiations or gamma rays passing through the concrete test object. Radiometric method is further divided into two classifications, namely: (i) *The Direct transmission radiometry; and (ii) Backscatter radiometry.*

The Direct transmission radiometry method can be used to determine density of fresh and hardened concrete as well as location of reinforcing bars in the concrete. The principle of the method is based on measuring electromagnetic radiations after transmitting through concrete. Direct transmission method is similar to ultrasonic pulse velocity method in performance. To perform the test, access to both sides of the structure is required. Schematic diagrams of the device are shown in figures below. Figure 2.28 shows that radiometry source and detector are placed on both sides of the concrete element. As radiation passes through the concrete, a portion is scattered by free concrete (Compton scattering) and a small amount is absorbed by atoms. The amount of Compton scattering depends on the density of the concrete, while the amount of absorption depends on chemical composition (Mitchell, 1991). If the source- detection spacing is kept constant, a decrease or increase in concrete density leads to a change in the intensity of the detected radiations. Figure 2.29 illustrates schematic of direct transmission method using a drilled hole in the concrete so that the source can moved up and down to determine variation in density of concrete with depth.
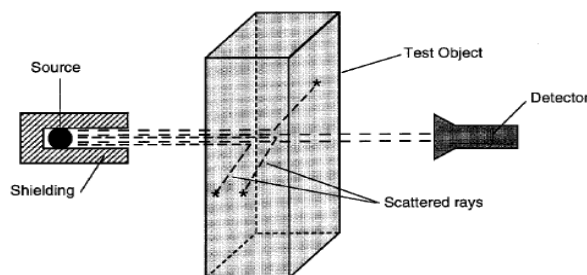
Fig. 2.27 Direct transmission radiometry with source and detector external to test object (ACI 228-2R-98)
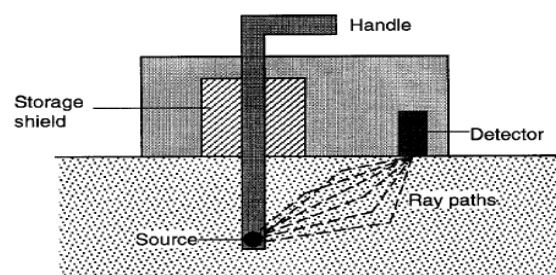
Fig. 2.28 Schematic of direct transmission nuclear gage

(ACI 228-2R-98)

The Backscatter radiometry method is suitable for in-situ measurement of density. The principle of method is based on measuring reflection or backscattering of electromagnetic radiations within the concrete test object which mainly occur at concrete top surface zones. The method is therefore very effective for monitoring density of bridge deck overlays. Figure 2.29 shows schematic diagram of the device. As illustrated in the figure, the source and detector are placed on the same side of the structure. The detector receives radiation within the concrete rather than those passing through concrete. This makes the difference between direct transmission and backscatter radiometry methods. Since the electromagnetic radiations travel within top surface of structure, the scattered rays provide lower energy than those with transmission method.
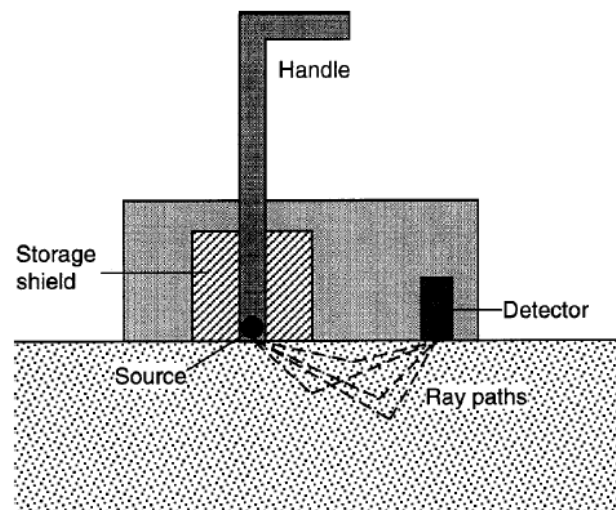
Fig. 2.29 Schematic of backscatter nuclear density gage (ACI 228.2R-98)

2.8.11.2 Radiography Method

Radiography method involves passing radiation through the concrete structure and recording the internal photographic images of the structure. From the recorded photograph, voids in concrete, location of reinforcement and voids in post-tensioned ducts can be determined. Figure 2.30 illustrates an image of the device. As shown, a radioactive source is placed to one side of the structure and the photograph film to the opposite side. The intensity of radiation is determined by passing radiation through concrete and recorded by photograph film. When the film is developed, a two dimensional visualization of the interior structure is obtained to identify location of reinforcement and voids in the structure.
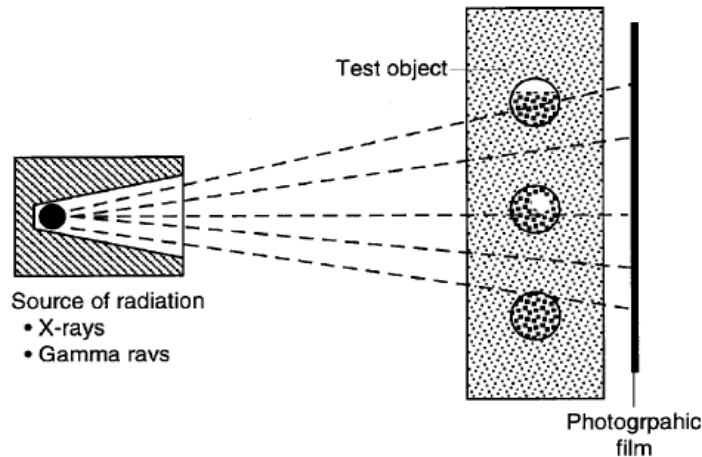
Fig. 2.30 Schematic of radiographic method (ACI 228.2R-98)

The advantages of nuclear methods are (ACI 228.2R): (i) equipments are potable; (ii) fast and rapid testing; (iii) access to one side of structure is required when using backscatter radiometry; and (iv) internal images of the structure can be displayed by using photographic method. On the other hand, the disadvantages of these methods are (i) access to both sides of structure is needed when using direct transmission or radiographic methods; (ii) X-ray travel path is limited to 300mm in direct transmission method and 500mm in radiographic method; (iii) operators must be licensed and require experienced operators while using radiographic method (iv) in backscatter method, measurement is affected by surface materials as well as chemical composition; and (v) it is difficult to determine crack perpendicular to the direction of radiation beam.

2.8.12 Penetrability Method

Generally, concrete structures might be susceptible to aggressive agents such as sulfates, carbon dioxide and chloride ions resulting in degradation of concrete materials. These aggressive agents may travel through the concrete elements from surface zones. Therefore, a proper performance of surface finishing may help durability of concrete structures. The ability of concrete against environmental attacks depends mainly on concrete mixture, curing and degree of consolidation. As a result, specific care should be taken into account to limit passage of such aggressive agents into concrete that may cause significant deterioration of concrete materials as well as corrosion of reinforcement bars. Various

penetrability test methods have been used to assess durability of a concrete surface;

- Water absorption tests
- Water permeability tests
- Air permeability tests

2.8.12.1 Water Absorption Test

Water permeability test is the amount of water absorbed into the concrete under low pressure head. The absorption rate is a function of capillary porosity which in turn depends on water/cement ratio and curing history (ACI 228.2R-98). The test can be done by either surface absorption techniques or by absorption with a drilled hole into the concrete structure.

2.8.12.2 Water Permeability Test

Water permeability test is classified into two groups; CLAM and Steinert methods. Both methods produce an empirical permeability index for concrete. However, absolute property measurement is preferable because of relationships between coefficient of permeability and other durability related factors (Whiting, 1987). Water permeability test is seriously affected by moisture content of concrete. Long testing time and the need for gluing or clamping the test equipment to the concrete surface are drawbacks of water permeability methods.

2.8.12.3 Air Permeability Test

The test is fast and simple to perform. Air permeability test is not affected by moisture content compared to water permeability tests. Therefore, the test is repeatable and can be done several times on a specific sample. The test is classified in the following test group;

- Figg air-permeability test
- Schonlin test, and
- Surface air flow (SAF) test.

The surface test such as SAF and schonlin test are affected by the top 15 mm of concrete cover and cannot provide penetrability properties of entire concrete cover zones. The Figg air-permeability method also requires drill hole in the concrete structure and cannot measure the top surface penetrability properties.

The advantages of the Penetrability Method are (i) simple and inexpensive testing equipments; (ii) equipments are portable; (iii) sensitive to changes in concrete quality; (iv) air-permeability tests are not sensitive to moisture content than water permeability tests. On the other hand, its disadvantages are (i) test methods are affected by surface coating and moisture content; (ii) it measures absorption of outer concrete surface only; (iii) it provides permeability index but not the coefficient of permeability; and (iv) some of the test methods require drilling hole which may affect concrete under the test.

2.8.13 Resonant Frequency Method

Resonant frequency method is based on estimating natural frequency of vibration in concrete materials in order to assess dynamic modulus of elasticity and density of concrete. This method first developed by Powers in U.S in 1938 (Malhotra and Sivasudaram 1991). The method was then refined by Hornibrook in 1939 to measure resonant frequency by using electronic materials. Later on, resonant frequency method was further developed in 1940 by Thomson, 1941 by Obert & Duvel and 1944 by Stanton. Figure 2.31 shows a schematic of ASTM C 215-02 test equipment named as "*Standard Test Method for Fundamental Transverse, Longitudinal, and Torsional Frequencies of Concrete Specimens*". The test display device is known as sonometer. One of the commercially sonometer available is shown in Fig. 2.32. The test equipment consists of (i) mechanical vibrator and (ii) vibration sensors.
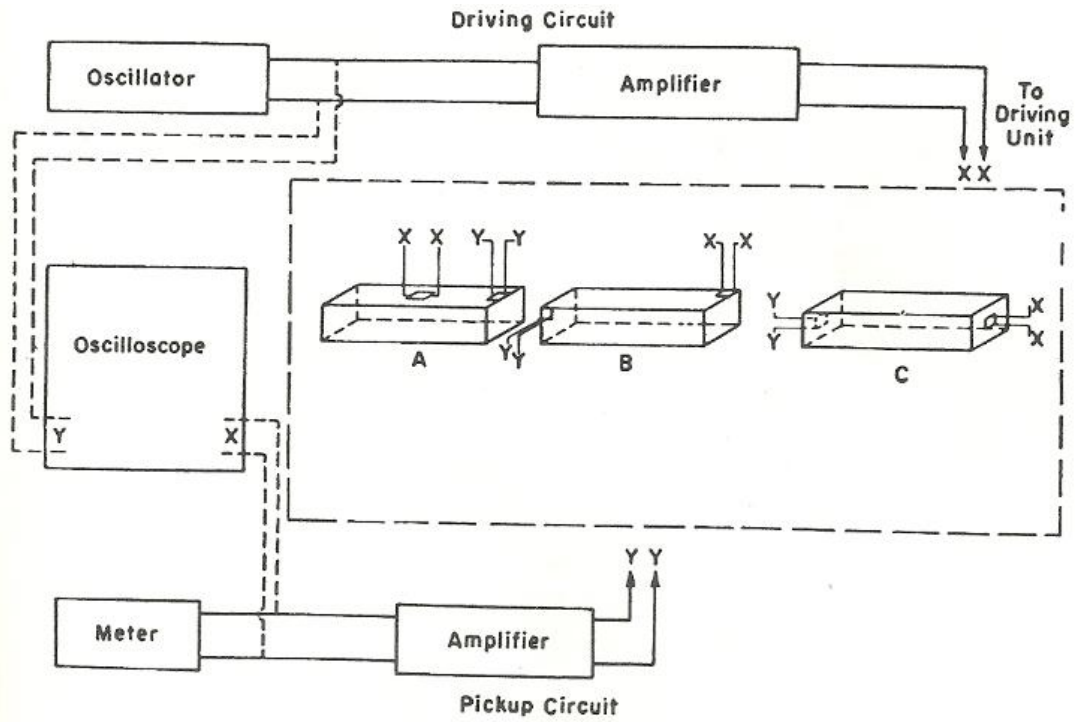
Fig. 2.31 Schematic diagram of a typical apparatus showing driver and pick up positions
(Adapted from ASTM C 215-85)
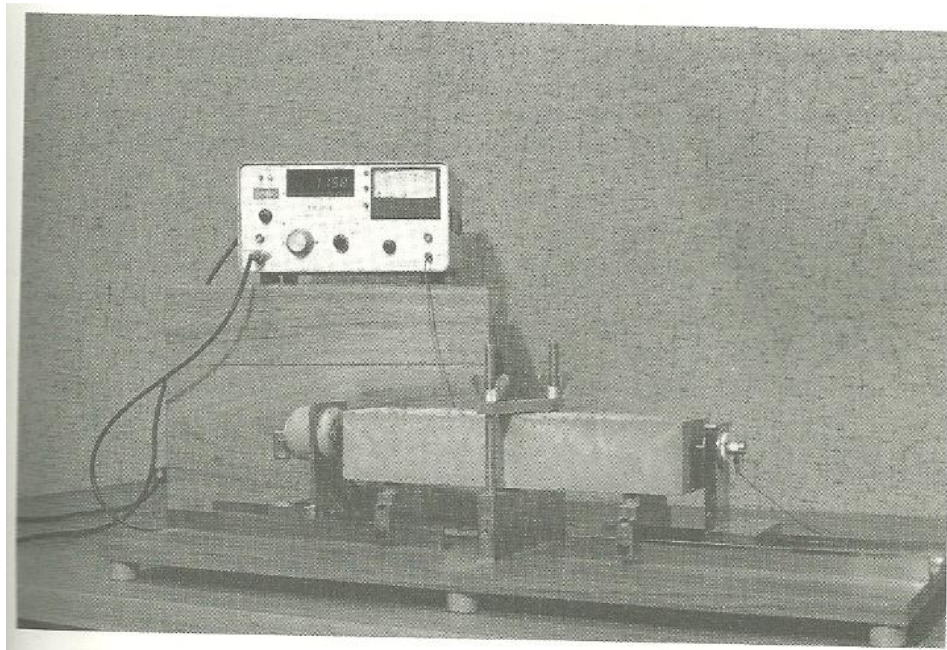
Fig. 2.32 Longitudinal resonance testing of a 76x102x406 mm

concrete Prism by sonometer (Adapted from ASTM C 215-85)

The significance and use statement of the test method given in ASTM C215-02 is as

51

follows (Malhotra 2004):

- This test method is intended primarily for detecting significant changes in the dynamic modulus of elasticity of laboratory or field test specimens that are undergoing exposure to weathering or other types of potentially deteriorating influences.

- The value of the dynamic modulus of elasticity obtained by this test method is generally greater than the static modulus of elasticity obtained by using Test Method C 469. The difference depends mainly on the strength level of the concrete.

- The conditions of manufacture, the moisture content, and other characteristics of the test specimens materially influence the results obtained.

- Different computed values for the dynamic modulus of elasticity may result from widely different resonant frequencies of specimens of different sizes and shapes of the same concrete. Therefore, it is not advisable to compare results from specimens of different sizes or shapes.

        The advantage of the resonant frequency method are (i) measures dynamic modulus of elasticity of concrete; (ii) provides an excellent means of studying for concrete deteriorations due to freezing and thawing and aggressive agents; and (iii) can be used to determine fire damage and deterioration by alkali- aggregate reaction. (Chefdeville, 1953; Swamy and Al-Asali 1988). On the other hand, its disadvantages are (i) resonant frequency is affected by concrete boundary conditions and concrete properties; (ii) the test is limited for small size specimens. 152x305 mm cylinders and 76x76x305 mm prisms; and (iii) dynamic elastic modulus equation is based on cylinder's or prism's shape factors. The change in shape of specimens may affect the results.

2.8 Pre-stressed Concrete

2.9.1 Introduction:

        In general, Concrete is weaker in tension than in compression. The tensile strength of concrete is about 10% of compressive strength. Therefore, by applying load on the plain concrete, concrete may cracks under loading especially in the tension zones (see Fig. 2.33). To resist the tensile stresses, reinforcements are placed in the tension zones assuming that tensile stresses resisted by tensile force in the reinforcement bars and plain concrete resists no load.

Therefore, the concrete member may cracks under loads and the reinforcement bars resist the design loads.

Reinforced concrete Beam under loading

Post-tensioning Beam before loading

Post-tensioning Beam after loading

Simply Supported Beam   Cantilever Beam
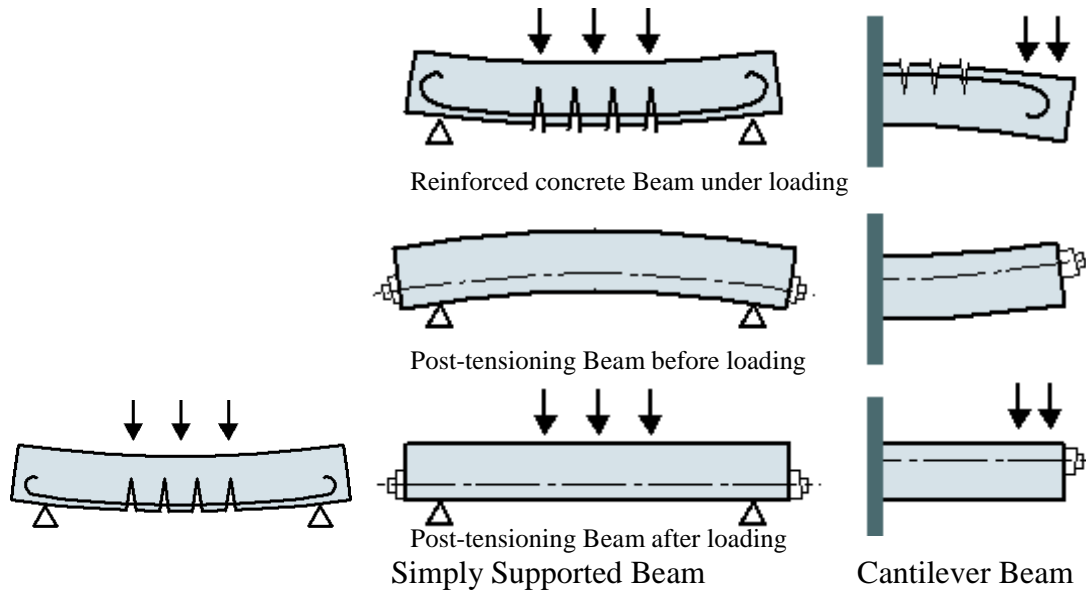
Fig. 2.33 Reinforced concrete   Fig. 2.34 Comparison of reinforced and pre-stressed
beam under load   concrete beam

The principle of pre-stressing system is to place concrete structure under compression in the tensile stress zones in a way that the tension stress caused by the load is cancelled by compression force due to prestressing before concrete cracks. Figure 2.34 shows the applicability of pre-stressing system in the concrete beams which is compared to the reinforced concrete. Pre-stressing can be accomplished in three ways; pre-tensioned concrete, bonded and unbounded post-tensioned concrete. Pre-stressing concrete combines the use of high strength concrete and steel strands in a structure. This combination makes a very strong structural material that is used in the building of bridge girders.

2.9.1.1 Pre-tensioned Concrete

In the pre-tensioning system, the pre-stressing strands are first tensioned (stretched in the mold) before casting concrete. After hardening of concrete, the cable strands are released from ends and compressive force is transferred from strands to the concrete as the cable strands shrink back to its original length. The compressive force counteracts the tensile stresses of an applied load. This method produces a good bond between the tendon and

concrete in which both protects the tendon from corrosion as well as allowing direct transfer of tensioned strands as compressive force to concrete member.

2.9.1.2 Bonded Post-Tensioned Concrete

Generally, prestressing by post-tensioning system involves installation and insertion of tendon strands into the metal/plastic ducts and pouring of concrete. Once the concrete get hardened, the tendon strands are tensioned by means of hydraulic jacks until reaching design specification (Hooke's Law). The tendons are wedged in the position and maintain tension after jacks are removed and transfer pressure to the concrete. The duct is then grouted to protect tendon strands against corrosion. The advantages of this system over unbonded post-tensioning are (Edward, 1989): (i) large reduction in traditional reinforcement requirements as tendons cannot distress in accidents; (ii) tendons can be easily 'weaved' allowing a more efficient design approach; (iii) higher ultimate strength due to bond generated between the strand and concrete; and (iv) no long term issues with maintaining the integrity of the anchor/dead end.

2.9.1.3 Unbonded Post-Tensioned Concrete

Unbounded post-tensioning system differs from bonded post tensioning system in a way that each individual tendon strands are free of movement relative to concrete. The main disadvantage of this method over bonded post tensioning system is that each individual strands can break itself and burst out of the concrete slab if damaged. The advantages of this method over bonded post-tensioning are (Edward, 1989): (i) the ability to individually adjust cables based in poor field conditions (For example: shifting a group of 4 cables around an opening by placing 2 to either side); (ii) the procedure of post-stress grouting is eliminated; (iii) the ability to de-stress the tendon before attempting repair work.

2.8 Review of Relevant Literature

Besides the NDT methods, numerous papers have been published regarding the effectiveness of non-destructive testing methods in civil engineering structures. The following literatures extracted from application of NDT technology on post-tensioned bridge decks are used to a great value during this thesis. The articles summarized below, not only provide an

insight into better understanding of non-destructive testing methods, but they also provide some of the works previously done on similar applications that might be of great interest.

2.10.1 Ultrasonic Imaging Methods for Investigation of Post-tensioned Concrete Structures (Krause et al., 2008)

Krause et. al. described results from three different PVC tendon ducts used in a large concrete slab named as D1, D2 and D3 with diameter of 40 mm each. D1 and D2 included 12 mm diameter strands compared to D3 with 35 mm strands. Using Ultrasonic Pulse Echo method, four variant characteristic results were compared. The - γ- radiograph was used to verify location of voided ducts in each D1, D2 and D3 tendon. The Ultrasonic- 3D SAFT (B-scan) image used to scan S-wave echoes. This method is used to determine depth of voided-duct (concrete cover). The Ultrasonic waves using phase sensitive mode. Red color represents positive sign that corresponds to strand's location. Green color represents negative sign corresponding to the location of duct. The Phase value of reflecting pulses around maximum of each reflector. Phase values of voided- duct and strand locations are recorded and the results are compared to a table color.

A schematic test result of tendon D1 is shown in Fig. 2.35. Figure 2.35(a) shows a sketch of the specimen with desired grouting faults, and Fig. 2.35(b) shows the verification of grouting faults with γ- radiography. The ungrouted areas show higher blackening than grouted areas. Figure 2.35(c) shows the results of scanning with 55 KHz shear waves; magnitude representations in a B- scan of 3D-SAFT reconstruction. At voids and areas without strand, ultrasonic waves backscattered at depth of 120mm representing concrete cover of the duct. At tendon strands location, the ultrasonic waves were backscattered at 140 mm due to reflection of the waves by strands. Figure 2.35(d) shows the depth profiles showing the pulse shape for typical points in Fig. 2.35(e). Figure 2.35(e) shows the pulse shape representation of the same area. Phase sensitive mode representing red sign as location of strands and green sign as duct location. Figure 2.35(f) shows phase value of reflecting pulses around the maximum of each reflectors calculated from FT- SAFT reconstruction. The phase value differentiates grouted and ungrouted areas in reflecting pulses at each reflector. It is around $50°$-$70°$ for ungrouted tendon and $70°$ for grouted ones.
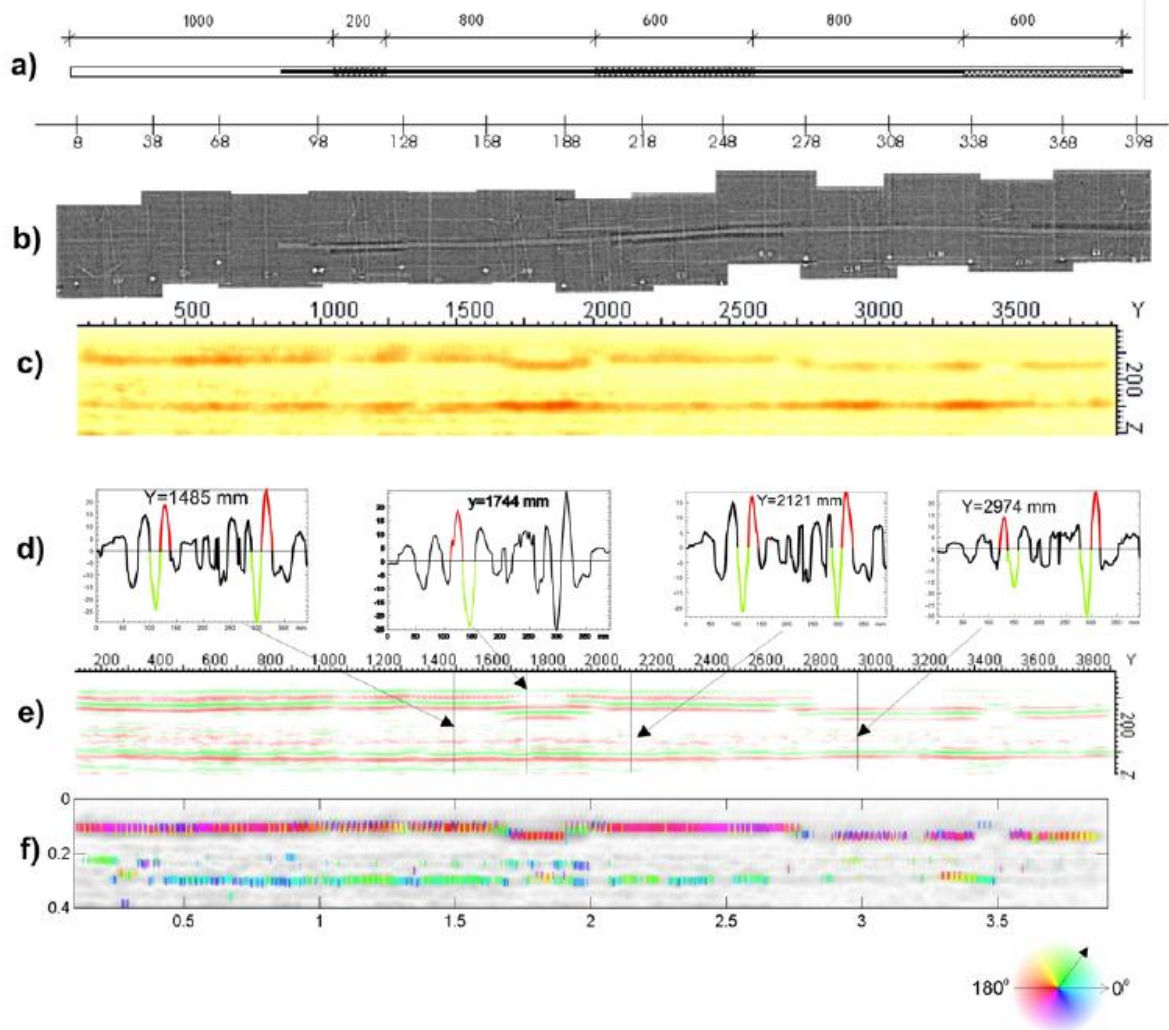
Fig. 2.35 Test results of tendon duct D1 in large concrete slab (Krause et al, 2008)

2.10.2 Application of Impulse-thermography for Non-destructive Assessment of Concrete Structures (Maiehofer et al., 2006)

Impulse- thermography is an effective NDT method to detect near surface deficiency in concrete structures. Themography uses internal/ external heat propagation into the test object and the transient heat flux can be observed by recording changes in the temperature at surface as a function of time. This method is very effective in detecting void and honeycomb in concrete structures up to concrete cover of 10 cm. To examine applicability of impulse-thermography for detection of grouting faults inside post-tensioned duct, a 3.5 m long sample was constructed including two tendon ducts and tendon wires. Based on experience, larger grouting faults are usually located at higher parts of the tendon, where the concrete cover of

duct is smaller than 5 cm. Therefore, the tendon ducts had a concrete cover of 5cm on one side and 8cm on the other side.

To detect grouting faults in the test sample, transient temperature was introduced to the test sample and grouting faults were found using the following methods;

1) Using heat generated from hydration of cement paste. A few minutes after grouting of the sample the location of duct at surface can be observed by using infrared camera.

2) The pre-stressed sample was heated up to 15 min from outside surface by infrared radiators and a total electrical load of 5200 W. The grouting faults were only detected from the side with 5cm concrete cover on the duct.

3) The wires inside the duct were heated up by using heat impulse. A current of 15A with the duration of 15 min was applied to the wires. The thermogram taken 40 min after beginning of heating showed warm and cold areas correspond to grouted and non-grouted areas as shown in Fig. 2.36.
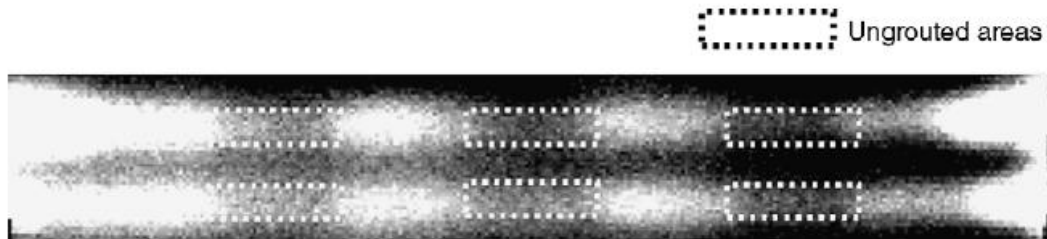
Fig. 2.36 Thermogram 40min after heating of sample: the six Ungrouted areas are colder than the grouted areas (Maiehofer et al., 2006)

2.10.3 Evaluating Non-Destructive Testing Techniques to detect voids in Bonded Post-Tensioned Ducts (Muszynski et al., 2003)

In this paper, the comparison between plastic and steel ducts by using Impact Echo (IE) scanning test, Spectral Analysis of Surface Waves (SASW) test and Ultrasonic-Tomography Imaging (UTI) test are presented. IE tests conducted the most guaranties in assessing the internal conditions of the steel ducts rather than plastic ducts since plastic ducts provides partial debonding between the duct and concrete wall. In this method, internal conditions of grouted ducts were successfully evaluated using IE thickness results along with a shift in the peak frequency and impact-echogram. The Impact- echogram was very useful for internal grout conditions of fully grouted plastic ducts when multiple fundamental frequencies

occurred.

The Spectral Analysis of Surface Waves (SASW) also presented the most promise in evaluating internal grout conditions of steel ducts. In this method, surface wave velocity taken from fully grouted ducts showed highest velocity in contrary with empty steel duct showing lowest velocity. The plastic ducts, on the other hand, did not release the same results. Ultrasonic Tomography Imaging (UTI) test showed only the location of grouting ducts rather than internal conditions of the ducts. This occurred because transducer frequency of 54 KHz was used for the conventional concrete. This range of frequency provides a wavelength longer than diameter of the duct. Thus, higher frequency resulting in shorter wavelength transducers should be used to investigate the internal conditions of the ducts. As a result, only IE scanning can be used to evaluate internal conditions of steel and plastic ducts as a function of time. Four days after introducing grout into the duct, the first comparison between true voids and fully grouted zones can be observed. After 24 days, scanning along the steel ducts provided significant differences between voided and non-voided parts of the ducts. But, scanning from plastic ducts concluded to be resultless due to debonding between plastic ducts and concrete wall.

2.10.4 Fast Location of Pre-stressing Steel Fractures in Bridge Decks and Parking Lots (Hillemeier et al., 2003)

Recently, concerns have been taken on the fracture of pre-stressed steel wires especially in bridge structures and parking lots. This occurs in pre-stressing wires mostly due to de-icing salt attack or contacting pre-stressing steels with corrosive agent (chloride ions). To identify the location of fractures in the tendon strands, Remanent Magnetism Method (RM- Method) is presented. RM- Method identifies unsafe conditions in pre-tensioned, post-tensioned structures by locating fracture of single wire even if they are bundled in an intact bonded-post tensioning system. Once the tendon wires are magnetized with an electromagnetic, the magnetic field resulting from magnetized wires is comparable with magnetic field of a bar magnet. In vicinity of fracture a magnetic dipole is produced resulting in magnetic leakage field in the surrounding regions. The magnetic field of tendon is then measured at concrete surface. Fractures produce characteristic magnetic leakage fields, which can be determined by using proper sensors at concrete surface (Fig. 2.37).
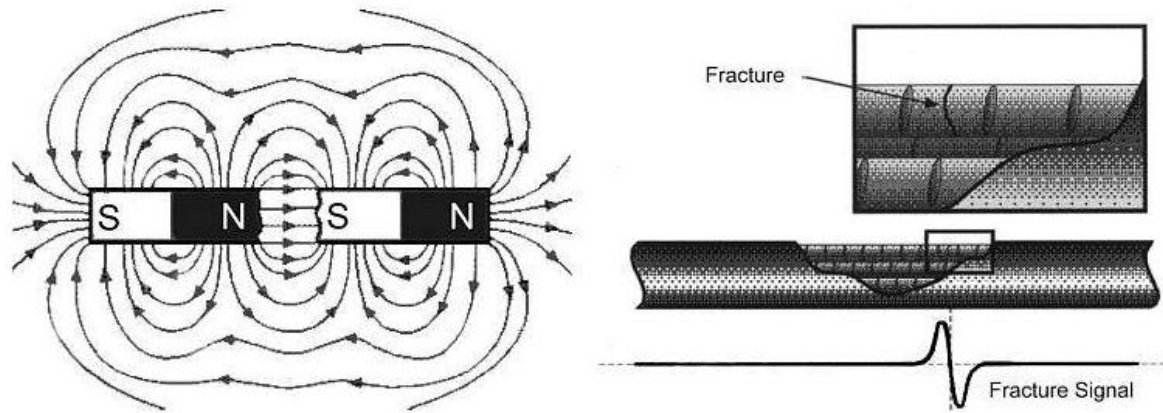
Fig. 2.37 A magnetized steel wire showing fracture of wire (Hillemeier et al., 2003)

In case of bridge deck evaluation using RM method, the application of RM on detection of wire fractures in PT systems may not be well-performed due to traffic disturbance involved. As a result, a high speed measuring mobile device (large yoke-shaped magnet with 3.5 m length) was developed to magnetize the tendons in one step and scan the magnetic flux density on the entire surface of the bridge deck.

2.10.5 Detection of Grout Voids in Post-Tensioning Ducts with Sonic/ Ultrasonic Impact Echo Testing (NDT Corporation, 2008)

NDT Corporation has successfully performed Sonic/ Ultrasonic Impact-echo testing to measure the voided duct characteristics as well as concrete thickness over the tendon duct in the post- tensioned structures. The Pulse- echo wave is a function of compressional wave velocity and element thickness. In case of no deficiencies in the concrete structures such as void or poor concrete, the concrete thickness and compressional velocity are normal. However, by presenting such anomalies, the sonic wave is delayed due to presence of low velocity air voids resulting in deflecting the wave length around the void which in turn increases the sonic path length time and the apparent thickness of the element as shown in Fig. 2.38. Once the location of void is determined, by drilling a small hole and inserting a small diameter borescopes, the in internal conditions of void can be video documented. An air pressure device can also be used to evaluate the void size approximately.

Sonic / ultrasonic Impact echo Testing to

Evaluate Post Tensioning Duct Grout

Grouted Duct
wave passes
through grout

Voided Duct
wave passes around
void / tendon duct
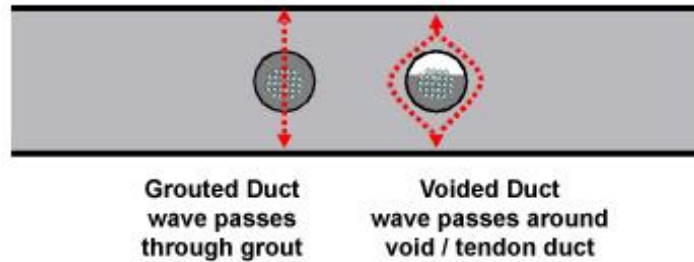
Fig. 2.38 Configuration of Sonic path wave around the voided duct

2.10.6 Development and Combined Application of NDT Echo Methods for Investigation of Post-tensioned Concrete Bridges (Streicher, et al., 2006)

In this paper, three echo methods, namely: impulse radar, ultrasonic echo and impact echo, are presented in order to detect materials with different interfaces, voids, honeycombing and reinforcement. In this contribution, results of bridge evaluation are presented using combination and data fusion of the three echo methods. This may concern the followings;

- Reinforcing bar and tendon ducts can be detected near surface using combination of radar data recorded with different polarization.
- Internal conditions of tendon ducts can be investigated using acoustic methods.
- Tendon ducts at deeper layers can be detected using ultrasonic- echo method.

The tendons in a post-tensioned concrete structure can be localized by using ultrasonic-echo device up to a depth of 40 cm. The ultrasonic waves are reflected by fully grouted tendons. Thus, tendon ducts can be localized by means of reflection of the waves from tendon ducts and shadowing the back wall behind them. If the reflection of the tendon ducts is more intense than concrete noise texture, concrete cover of the tendon ducts can then be estimated.

In case of combined and data fusion, radar and ultrasonic echo methods were performed on the web in a box girder bridge in Germany. Radar was more effective than ultrasonic echo method for near surface investigations due to multiple reflections of rebar and tendon ducts located near the surface. This was because of enhanced resolution or radar effectiveness

60

especially for the detection of metallic reflectors. Ultrasonic echo method, on the other hand, was more suitable to identify back wall reflections and rebar signals that are located above the back wall for a depth of 40-60 cm. By the combination of radar and ultrasonic echo, it is possible to compress information in one data set.

2.10.7 Continuous Acoustic Monitoring of Steel Tendons and Cables in Bridges (Cullington et al., 2000)

This papers presents installation of an acoustic monitoring device to detect wire fracture in the tendons which was carried out by Transport Research Laboratory (TRL) in Canada. Wire fracture of tendons release energy that can be monitored by acoustic sensors placed on the concrete surface. Steel wires have many applications as individual wires or in form of tendons that can be used in pre-tensioned or post-tensioned concrete bridge structures. Wires are generally difficult to inspect since they are either inaccessible or deep in the structures (such as post-tensioned bridges). Wire failure can occur in service due to corrosion, stress corrosion and fatigue. The Transport Research Laboratory has performed a trial evaluation of the SoundPrint acoustic monitoring system by continuously listening to the acoustic events to detect fracture characteristics of steel tendons.

2.10.7.1 The SoundPrint Acoustic Monitoring System

The system has been described elsewhere (Halsall et al, 1996; Paulson, 1999). This system can be used to detect fracture of steel in unbounded (ungrouted) tendons as well as the structures in which integrity of steel wires are difficult to inspect. Generally, when the steel wires break, there is a release of energy that transmits through to the materials. The sensors placed on the concrete surface are able to detect these acoustic events and transfer them to a data acquisition system. The system monitors continuously but collect no data until an acoustic event is introduced. Software filters are also used to filter the event of no further interest. Therefore, the acoustic events passed by the software would most likely to be wire fractures. The position and classification of the events were then determined by Pure Technologies in Canada. Pure Technologies have proved that the SoundPrint system is able to detect wire breakage in the office buildings with unbonded (ungrouted) tendons. However, in case of grouted tendons in bridge structures it was found to be more difficult to detect wire

breakage by SoundPrint system due to less energy released by grouted tendons compared to unbonded and non- break events and background noise were likely to be more dominant.

2.10.7.2 Trials on Post-Tensioned Tendons

Non destructive test has proven to be of limited value in detecting the presence of broken wires (Cullington et al, 1996). The SounPrint system was used by TRL to detect trial wire breakage in the two post-tensioned concrete elements; a 30m long Bank Lane Unit including fully grouted ducts and a 10m long beam built by TRL containing combination of well grouted and poorly grouted tendon ducts. Acoustic events were introduced to the trial tests by cutting, grinding or corroding of wires. The initial trial revealed that the SoundPrint system is capable of detecting ungrouted and partially grouted wire breaks as well as some fully grouted wire breaks. It was also capable of rejecting small sharp impact events in which some of them incorrectly reported as wire breaks. The system was able to reject non- wire break events. With the data problem supplied by TRL, Pure Technologies reconfigured the system using new sensors with high density and new software. The new system reliably detected fully grouted wire breaks and rejected the events of small sharp impact.

2.10.8 Testing/ Evaluation and Grout Remediation of Post-tensioning Tendons for Bridges (Nour, 2006)

In this paper the solution to the problem with corrosion of steel wires and re-grouting of the voided duct in post-tensioning system has been considered in the following four steps:

(i) Non-Destructive Testing (NDT) and Evaluation of Post-Tensioning Tendons with Voids: To evaluate the post-tensioning ducts containing voids, Ground Penetrating Radar (GPR) and Impact-Echo (IE) are of efficient methods. GPR can be used to locate metal ducts and mild reinforcements. Plastic ducts can also be located by experienced operators analyzing internal characteristics of bundled strands rather than plastic duct itself. The Impact- Echo can then be used to locate sections of the duct with voids.

(ii) Limited Invasive Inspection of Post-Tensioning Tendons: This method verifies the results taken from Non- destructive testing methods. The Limited Invasive Inspection employs using special drilling device with Automatic Shut- off system in contact with metal for metal ducts or in contact with strands for plastic ducts.

(iii) Visual Inspection and Void Volume Measurement of Tendon Voids: The same small hole used for Limited Invasive Inspection can be used to insert a flexible videoscope into the duct to detect presence of void and corrosion of strands. Pictures and video clips can be recorded along with audio report of the findings. Void volume of the tendon ducts can be then determined using Volumeter capable of compensating for leaks.

(iv) Vacuum Grouting of Post- Tensioning Tendons with Voids: The final step is filling the voided duct with grout. Vacuum Grouting technique can be used to develop vacuuming inside the void. Vacuum Grouting requires only one port to completely fill the void with grout as negative pressure created by vacuum inside the void. In case where an acceptable level of vacuum inside the void cannot be reached, a combination of vacuum and positive pressure can be used to fill the void. A flow meter will then be used to determine the volume of grout injected into the voided ducts. Comparing Void Volume size from step 3 and volume of injected grout presents whether the void is completely filled with grout or more grouting is required.

2.10.9 Detecting Wire Breaks in a Pre-stressed Concrete Road Bridge with Continuous Acoustic Monitoring (Fricker and Vogel, 2006)

Continuous monitoring of flat slab buildings and cable stayed bridges has become practical; however, less experience has gained in monitoring of post-tensioning system with fully or partially grouted tendons due to complexity of the structure. It is found that fully or partially grouted tendons (bonded tendons) release less energy compared to ungrouted (unbonded) tendons. Therefore, these events are more difficult to inspect. To examine continuous acoustic monitoring of grouted tendons, the SoundPrint monitoring has been performed on Ponte Moesa Bridge in Switzerland.

In the SoundPrint system developed in Canada, sensors are attached to the structure and acoustical waves induced by wire break are transferred through the structure, localized and detected by the sensors. The signal from each sensor is recorded while passing pre-defined threshold. Signals of no further interests are filtered out. Then, the software filters store and transfer data to the analysis center in Velizy/ Paris via internet. During the calibration phase, the software is tuned to give a corresponding and predetermined response.

Using calibration impact, the actual location (measured on site) and calculated location (from signal) are compared to get the accuracy of the set up.

Blind testing of the fully grouted tendons was performed by Institute of Structural Engineering of ETH Zurich. In this test method, artificial wire breaks were created using electrolytic corrosion- cell. The blind test was conducted on Ponte Moesa Bridge and the time required to corrode the wires up to failure was 22 to 29 hours. All detected and located wire breaks were listed by date. From visual inspection results, it was expected that wire breaks occur in the region of bad or poor concrete surface, while, the wire breaks occurred in the areas of proper concrete surface. The results from half-cell potential measurement also confirmed the wire breaks occurred in the region of high-likelihood of corrosion.

The paper concluded that continuous acoustic monitoring SoundPrint system in detecting fully or partially grouted tendons was examined by Blind Test. The system was able to detect and locate wire breaks even in a noisy environment. Invasive inspection also confirmed the location of wire breaks during monitoring. Moreover, the result of half-cell potential measurement revealed the location of wire breaks in the region of high-likelihood of corrosion. Based on the data obtained, it was concluded that continuous acoustic monitoring is capable of locating, analyzing and classifying the wire breaks in grouted or partially grouted tendons as well as capable of filtering out of the signals with no further interest.

2.10.10 Detection and Evaluation of Voids in Tendon Ducts by Sonic Resonance and Tomography Techniques (Fisk et al., 2004)

The application of non-destructive testing technology using sonic/ultrasonic in detection of voided ducts attributable to post-tensioning system is presented. The paper describes the use of sonic reflection at voids interface and tomography techniques to detect voids in the post-tensioning ducts in bridges. Generally, the amount of reflected energy so called "Impedance" is dependent upon the velocity and density of the boundaries between two different materials. Concrete has higher impedance (14000 ft/sec) than air (1000 ft/sec); therefore, there will be a high reflection at concrete-air interfaces. Two ducts in one of the bridge segments were examined with the following configurations; placing sensors on the

tendon and energizing the wall, sensors on the wall and energizing the tendon and sensors on the wall and energizing the wall. When the tests were performed with three mentioned sensor configurations, placing sensors and energizing source on the wall showed the most suitable results by presenting missed resonant frequency at the location of the voided ducts. However, exciting tendon with sensors on the wall or exciting wall with sensors on the tendon are not as definitive with the grouting conditions as the exciting the wall with sensors on the wall. The presence and size of the voids can be measured using either reflection data at voids interface, polarity and the area of the missed frequency or by using tomography (sonic) imaging.

2.10.11. Non Destructive Detection of Fractures in Prestressed and Post-tensioned Cables (Fallis et al., 2008)

In this paper, the use of Post-Tech Cable Break Detection (CBD) system as a non-destructive testing method to investigate fracture of wire strands in both bonded and unbounded post-tensioning system is presented. This method was developed first in Germany in 1990's and has been recently used in North America and Europe. The method relies on the Peak-Peak Amplitude principle of fracture characteristics in pre-stressing wire strands on the clarity of the signals received by the sensors as shown in Fig. 2.39. It is stated that at the location of fractures, there is a dip toward less positive flux and an abrupt raise toward the more positive flux. This reversal polarity change represents the location of fractures. Figures 2.40 and 2.41 show a bar magnet containing fracture at mid-length with its corresponding magnetic flux at fracture location.
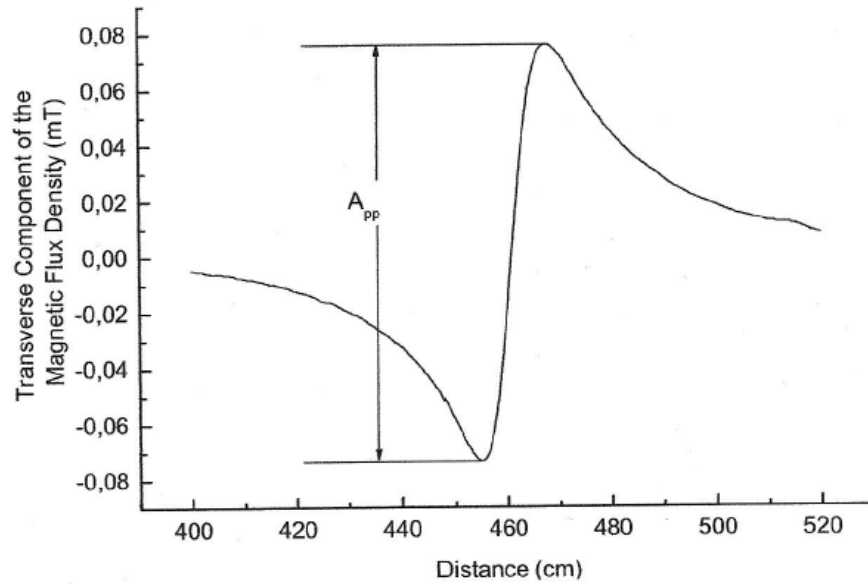
Fig. 2.39 Peak-Peak Amplitude at fracture (Fallis et al., 2008)
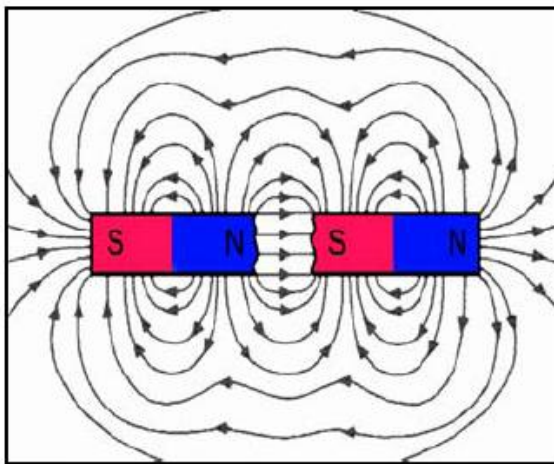
Fig. 2.40 Bar magnet with fracture at mid-length   Fig. 2.41 Magnetic flux at fracture
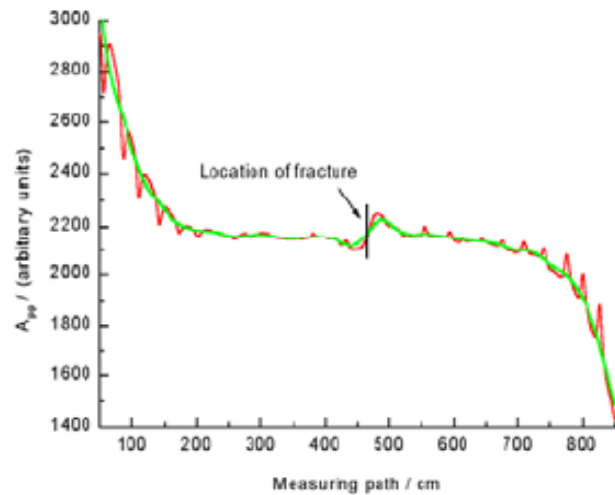
(Fallis et al., 2008)   (Fallis et al., 2008)

Two Post-Tech CBD methods were introduced for evaluation of the structures. Line Scan method which is used to evaluate single or bunched cables at a time in longitudinal direction, while Rotating Scan method is used to evaluate many cables transversely located to the direction of travel path in a short period of time.

2.10.11.1 Line Scan Method

In Line Scan Method, the unit is passed over the cable along its length in order to magnetize the cable. Then, the unit is passed again over the cable with sensors switched on to collect the data. Several passes may be required in case of presenting mild-reinforcement to distinguish the possible location of wire fractures in pre-stressing systems. This method is applicable to investigate cable fractures in the slab by scanning from top or bottom surfaces as well as scanning girder in bridges from sides.

2.10.11.2 Rotating Scan Method

Rotating Scan Method is used to investigate cable fractures in the direction perpendicular to the travel path. The unit consists of a vehicle running over the tendons to magnetize them and a rotating bar housing sensors along with an advanced software system to record and interpret the results from magnetic flux density. This method is applicable for post-tensioned bridge deck and parking garage investigations.

A study was performed using both Line and Rotating scan Methods by Vector corrosion Technology and Technische Universität Berlin in conjunction with Jacques Cartier and Champlain Bridges Incorporated (JCCBI) in September 2008 on Champlain Bridge in Montreal, Canada. By applying the Line and Rotating Scan methods on longitudinal girders and transverse post-tensioned bars on the deck respectively, two possible locations of fracture were found in a portion of the deck which were clearly visible from underside as shown in Figs. 2.42 and 2.43.

Fig. 2.42 Underside location of detected fracture (Adapted from Fallis et al., 2008)

Fig. 2.43 Close-up location of detected fracture (Fallis et al., 2008)

67

2.10.12 GPR detection of voids in post-tensioned concrete bridge beams (Giannopoulos et al., 2002)

This paper compares results from application of GPR to detect voids in post-tensioning concrete beams. Both experimental and numerical modeling were carried out and compared. The numerical models were based on the finite-difference time domain method (FDTD), which has been proved to be very effective in modeling GPR (Giannopoulos, 1997). In this paper, GPR responses from fully grouted and voided ducts on the 2D and 3D models using FDTD were investigated. To perform the test, long span beams with 2000x450x400 mm dimensions were built. In experimental study, several GPR scans were obtained from the beam using 900 MHz GSSI antennas. Results from 900 MHz scan showed that it was almost impossible to distinguish the voided section from the fully grouted duct when the orientation of GPR antennas was parallel to the long axis of the duct. However, the voided section of the duct was clearly identified once the orientation of GPR antennas was set perpendicular to the long axis of the duct.

In the numerical study, the results from two-dimensional (2D) model found it difficult to distinguish various degrees of grouting (different size of void) inside the plastic ducts once 900 MHz GPR antenna scan was used in the direction of tendon ducts. Moreover, the results from 3D model with parallel orientation of GPR antennas showed similar results as 2D model in such a way that the responses from voided and fully grouted ducts were not significantly different. However, performing 3D model with vertical orientation of GPR to the long axis of tendon ducts was analogous to the vertical scan of GPR in experimental study. In both cases, voided region in plastic ducts were clearly identified.

CHAPTER III

EXPERIMENTAL STUDY

3.1 General

To conduct non-destructive technology validation testing, eight actual size concrete were constructed. The specimens simulate portions of post-tensioned bridge decks and pre-tensioned beams. The experimental program was undertaken to investigate corrosion-related wire strands, voids and grout defaults attributable to post-tensioning system in bridge superstructure. In experimental study, three NDT methods were investigated, namely: Ground Penetration Radar, Impact-Echo and Half-Cell Potential. Results from this investigation were recorded and analyzed. In this chapter, detailed description of the simulated bridge deck specimens is presented, in addition to brief description of the NDT equipment used in this study.

3.2 Bridge Deck Models

The experimental study was performed on eight bridge deck and beam specimens. The first three models combine the effect of variable post-tensioning tendon duct placement along the bridge deck depth. These specimens included simulated break, notch or corrosion in the prestressing cables in addition to duct voids simulating improper grouting. Specimens No. 4 and 5 were cast with both metal and plastic ducts to investigate whether the duct material affects the results. Specimens No. 6 and 7 represent beams or girders incorporating pre-tensioning steel strands. All these specimens were built in the Structures laboratory of Ryerson University. However, specimen No. 8 was built at the MTO site at Arrow Road, Toronto, Ontario, due to its larger size (4m by 4 m in plan). This specimen was built to apply Remanent Magnetism (RM) technology. However, efforts to get the RM equipment did not succeed till the time or writing this thesis. On the other hand, specimens No. 8 was used to demonstrate the use of vacuum grouting technology in duct grouting to fill existing voids. It should be noted that vacumm grouting has been used in USA by DSI International Inc. for duct grouting at the construction stage only. Non-destructive test methods on specimen eight were performed in two phases. In the first phase, NDT methods were carried out on the top and bottom surfaces of laboratory specimens. In the second phase, Specimen No. 8

experienced the use of GPR to locate the ducts and vacuum grouting technology to fill the detected voids in the duct. Table 3.1 shows a summary of the tested specimens. It should be noted that the prestressing cables and strands were not post- or pre-tensioned as in reality since this research is concerned only with the existence of the duct, cables and strands irrespective of the imposed stresses or the loading level.

Table 3.1 Summary of the Tested Specimens

Group	Deterioration type	Comments
Specimen No.1	-Cable fracture at mid-length. - Notch at quarter point.	Including straight and curved tendons with metal ducts.
Specimen No.2	Simulated voids of 20, 60 and 100 mm lengths at length of 0.17, 0.5 and 0.83 of the length of the specimen, respectively.	Including straight and curved tendons with metal ducts.
Specimen No.3	Corrosion of the prestressing cable and steel bars along its length in addition to simulated voids in the duct	Including straight and curved tendons with metal ducts.
Specimen No.4	Fully grouted, partial grout and empty duct portions along the length of prestressing cables	Including straight tendons with variable metal and plastic ducts diameters
Specimen No. 5	Fully grout, partial grout and empty duct portions along the length of prestressing cables in addition to corrosion of the prestressing cables and steel rebars at middle third portion of the specimen.	Including straight tendons with metal and plastic ducts. 100 and 50 mm diameter ducts were used.
Specimen No. 6	Pre-tensioned beam including simulated wire break and a notch.	-
Specimen No. 7	Pre-tensioned beam including limited corrosion in the strands.	-
Specimen No.8	Simulated voids, simulation of prestressing cable break. Simulated voids of 400, 100, and 25 mm length located at 0.25, 0.375, 0.5 and 0.75 of the specimen length, respectively.	Including straight tendon with metal ducts only.

3.2.1 Description of Specimen No. 1

The first bridge deck specimen simulated fracture of the prestressing cables and notch at selected locations in both the straight and curved tendons. The specimen consisted of three, 100-mm diameter, ducts embedded into 1200x1200x400 mm concrete bridge deck as shown in Fig. 3.1. Each duct is filled with prestressing cable made of 19/15 tendon, representing 19-seven wire strands with 15-mm nominal diameter (0.6 inch) and 140 mm² effective areas per strand. Curved tendon with the height point located 150 mm from the top surface of the specimen and 120 mm apart from bottom face of the specimen at its ends as shown in Fig. 3.2. Two straight tendons were placed with 50 and 150 mm concrete cover from the top surface as shown in Figs. 3.3 and 3.4, respectively. The tendon's strands have been intentionally broken at their mid-length in addition to a small U-shape notch located at their quarter point as shown in Figs. 3.2 to 3.4. The middle tendon in specimen No.1 (with 50 mm concrete cover) represents those closest to the top concrete surface at the negative bending moment region over piers or interior supports. Limited mesh reinforcement was placed along a portion of concrete specimen to investigate their interaction with the prestrsssing cable and the metal duct when applying the NDT technology. Figures 3.5 to 3.9 show the specimen formwork, duct and reinforcement placement, notch and breaks in the prestressing cables. It should be noted that the gaps created by the presence of cable break over 50 mm length and the notch over 25 mm length were filled with styrofoam.
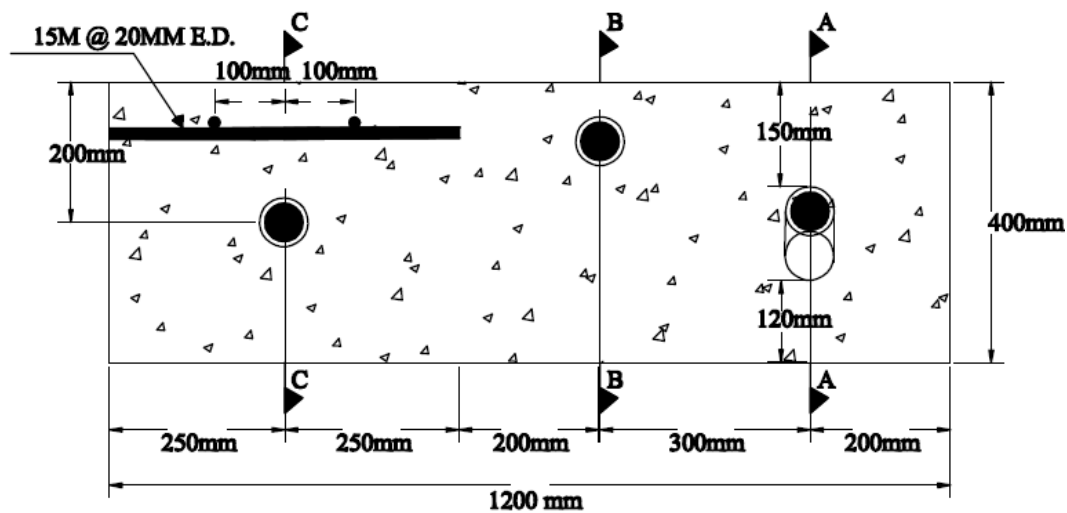
Fig. 3.1 Cross-Section in specimen No. 1
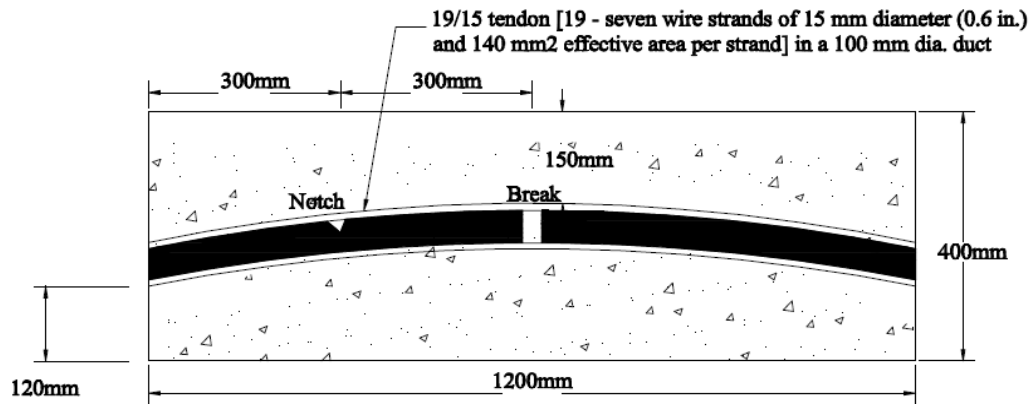
Fig. 3.2 Section A-A of specimen No. 1 showing curved tendon including

tendon notch and break
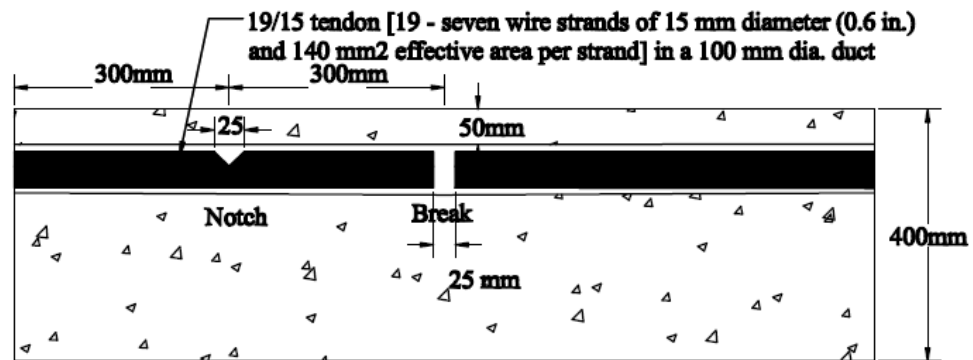
Fig. 3.3 Section B-B of specimen No. 1 showing straight tendon including tendon notch and
beak
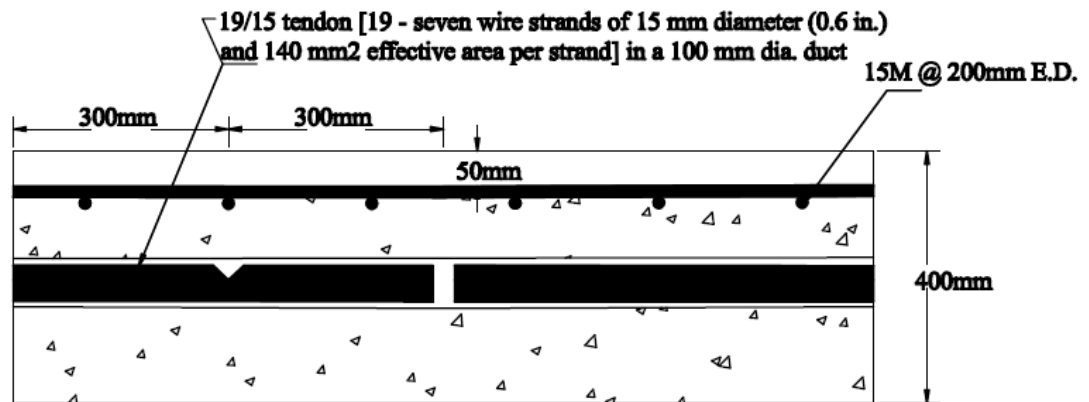
Fig. 3.4 Section C-C of specimen No. 1 showing straight tendon including notch and break As
well as top reinforcing steel layer

Fig. 3.5 View of the prestressing cable
showing a U-shape Notch

Fig. 3.6 View of the prestressing cable showing
simulated break at its mid-length

Fig. 3.7 Fracture in the prestressing cable
reinforcement simulated with styrofoam infill

Fig. 3.8 View of the ducts and steel
of specimen No.1 before concrete casting

Fig. 3.9 View of specimen No.1 after concrete casting

3.2.2 Specimen No. 2

The second specimen simulated the presence of voids in the duct due to improper grouting. The size and configuration of the second specimen were identical to the first specimens except the cable breaks and notch were replaced with simulated voids, as shown in Figs. 3.10 to 3.13. Voids with 20, 60 and 100 mm length were introduced at 0.17, 0.50 and 0.83 of the specimen length. Styrofoam was used to simulate such voids in a way that it was taped around the prestressing cable with a small gap to allow flow of the grout under gravity as shown in Fig. 3.14. The purpose of providing different voids size was to investigate the power of the NDT methods in locating small and large void sizes. Figures 3.15 to 3.16 show specimen No. 2 before and after concrete casting, respectively.
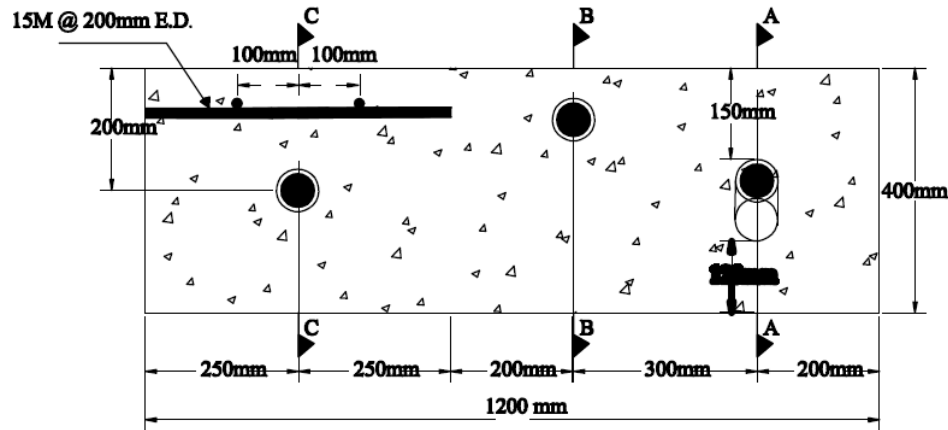
Fig. 3.10 Cross-section of specimen No. 2
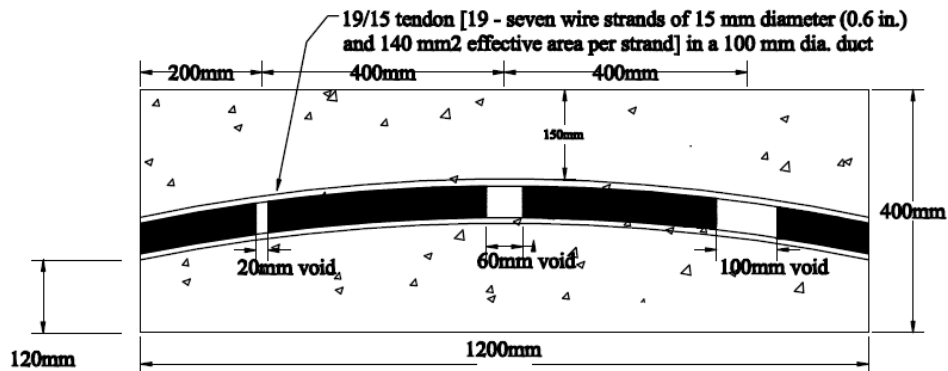
Fig. 3.11 Section A-A of specimen No. 2 with curved tendon and simulated voids in the duct
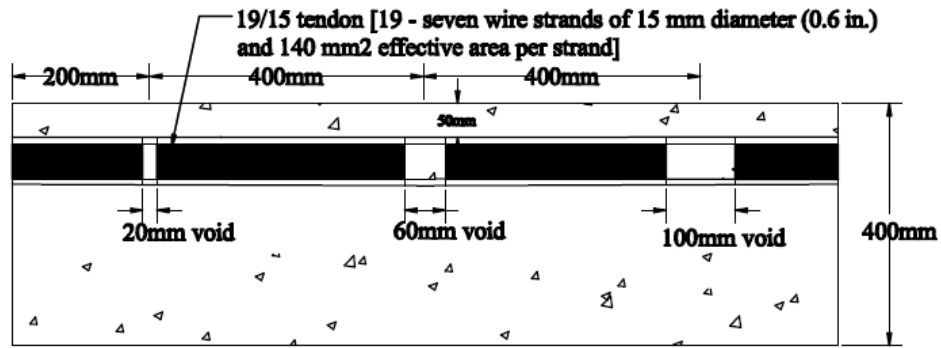
Fig. 3.12 Section B-B of specimen No.2 with straight tendon and simulated voids in the duct
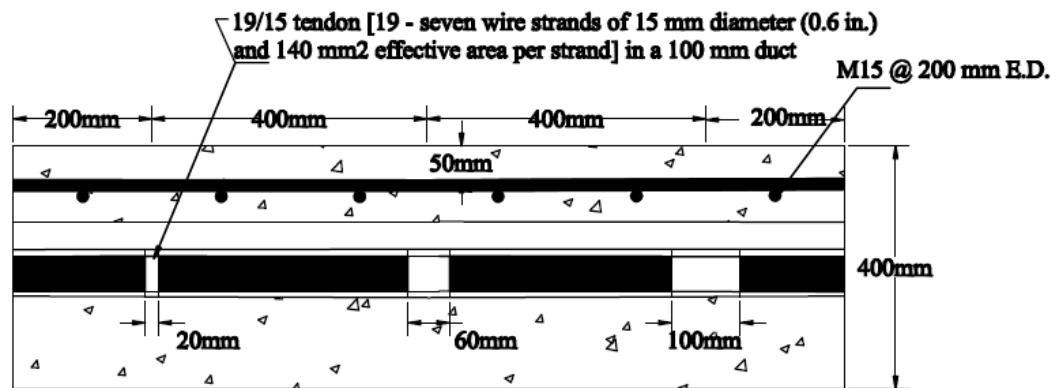
Fig. 3.13 Section C-C of specimen No. 2 with straight tendon, simulated voids

in the duct and top reinforcement layer

Fig. 3.14 View of simulated voids inside the duct by wrapping the prestressing cable with styrofoam

Fig. 3.15 View of specimen No. 2 before concrete casting

Fig. 3.16 View of specimen No. 2 after concrete casting

3.2.3 Specimen No. 3

The third specimen size and tendon duct layout were identical to specimen No. 2 except that the simulated voids were replaced with corroded portions in the presstressing cable and simulated void at the mid-length of the corroded portion. Figure 3.17 shows the cross-section details of the specimens, while Fig. 3.18 shows that 300 mm length of the middle portion of the curved tendon was artificially corroded and a 60 mm length void was introduced at the mid-length of the corroded portion. In the straight tendons, Fig. 3.19, artificial corrosion was introduced over 300 mm length at both ends of the straight tendons. However, simulated void of 60 mm length was introduced at the mid-length of one of the corroded cable segments as shown in Fig. 3.19. To establish artificial void in the curved tendon, the duct was cut at its mid-length and filled with styrofoam for a length of 60 mm. All other parts of the duct were then fully grouted. Then, the two halves of the duct were jointed together using mechanical tape. Figure 3.21 through 3.23 show views of the corroded portion of the prestressing cables and simulated voids in the metal duct. Along the straight duct at the edge of the specimen, shown in Fig. 3.17, top mesh of reinforcing steel bars were placed over the edge duct area to investigate its presence on detecting the location of the duct, corroded cables and simulated voids. It should be noted that artificial corrosion was introduced in the steel rebar along the corroded portion of the prestressing cable (i.e. 300 mm at each end as shown in Fig. 3.20). Figures 3.24 and 3.25 show views of specimens No. 3 before and after concrete casting, respectively.
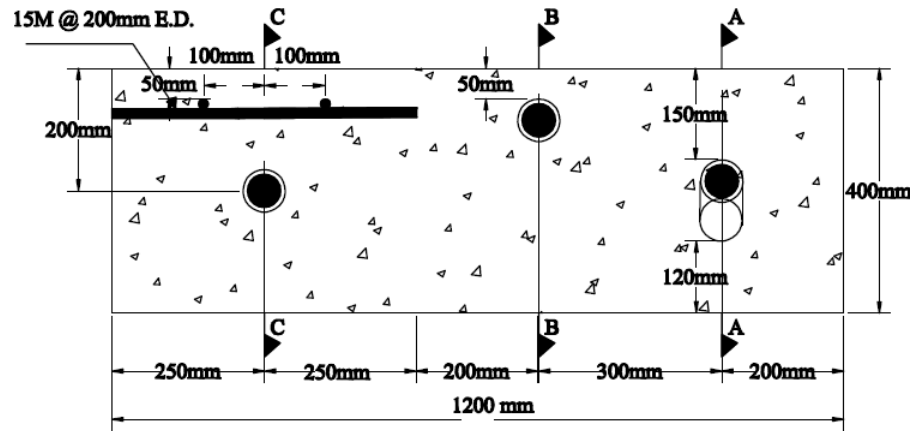
Fig. 3.17 Cross-section of specimen No. 3
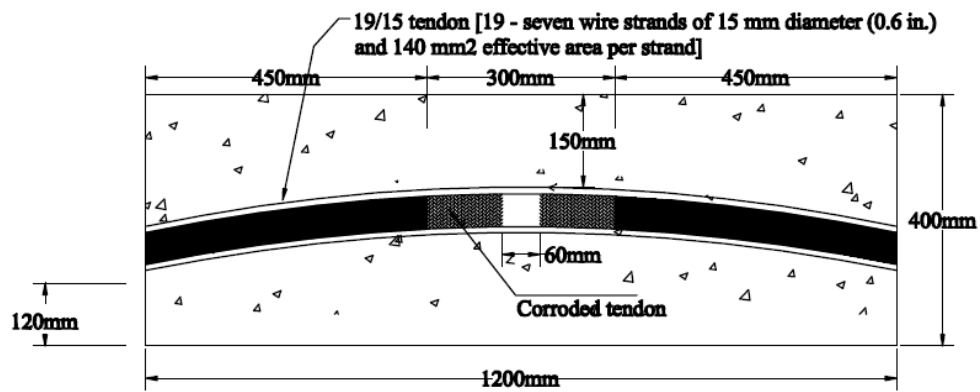
Fig. 3.18 Section A-A of specimen No. 3 with curved tendon and simulated void in the duct in addition to limited corrosion in the tendon
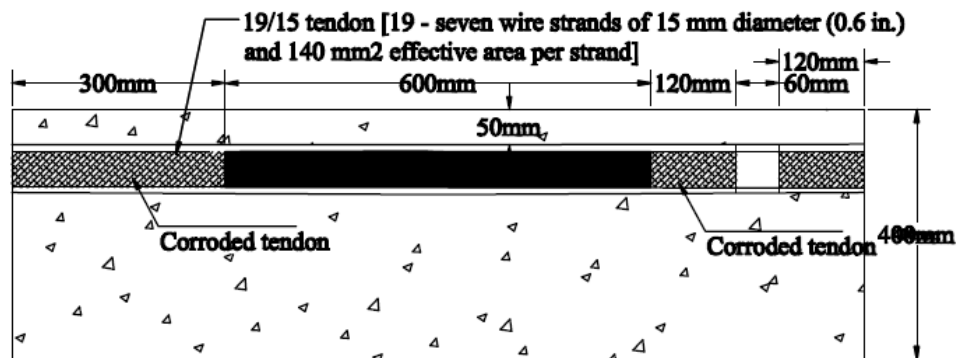
Fig. 3.19 Section B-B of specimen No. 3 with straight tendon and simulated voids in the duct in addition to limited corrosion in the tendon

77
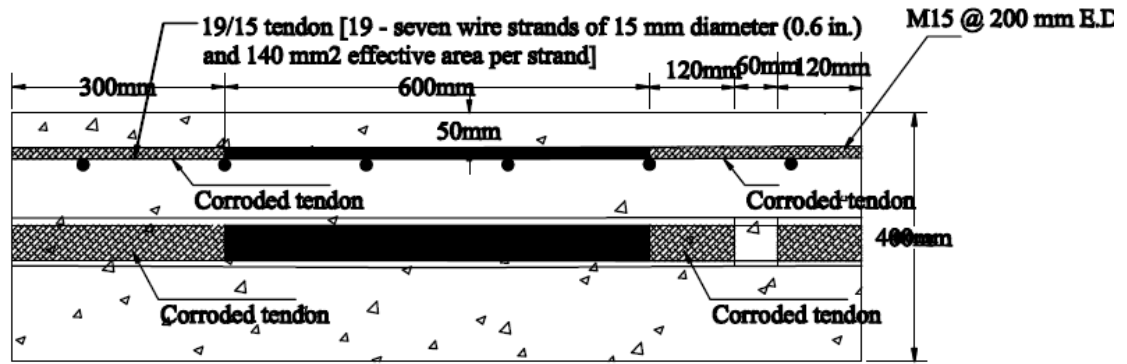
Fig. 3.20 Section C-C of specimen No. 3 with straight tendon, simulated void in the duct and top reinforcement layer in addition to limited corrosion in the tendon

Fig. 3.21 View of the corroded cable over 300 mm length

Fig. 3.22 Introducing simulated void of 60 mm length in the curved tendon using Styrofoam infill

Fig. 3.23 Introducing simulated void of 60 mm length in the straight tendon near its end

Fig. 3.24 View of specimen No. 3 before concrete casting

Fig. 3.25 View of specimen No. 3 after concrete casting

3.2.4 Specimen No. 4

Specimen No. 4 was intended to investigate the difference between plastic and metal ducts in NDT application. The specimen was of 1200 length and 300 mm thickness. It had two plastic ducts and two metal ducts located at its mid-thickness. The 100-mm diameter duct contained 19/15 strands, representing 19-seven wire strands with 15-mm nominal diameter (0.6 inch) and 140 mm² effective areas per strand. While the 50-mm diameter duct contained 3-15 strands, representing 3-seven wire strands with 15-mm nominal diameter (0.6 inch) and 140 mm² effective areas per strand. Three types of grouting were introduced in each duct, namely: (i) fully-grouted; (ii) partially-grouted; and (iii) no grout. Figure 4.26 shows layout of the locations of these grouting types in each duct. While Fig. 3.27 shows view of the prestressing cable showing its middle portions with simulated void at its mid-length and partially grouted duct at its end. Figures 3.28 and 3.29 show views of partial grouting of the 100 mm and 50 mm ducts. Two mesh reinforcements, made of 15M bars placed at 200mm c/c each direction, were placed on each face of the specimen with concrete cover of 40 mm, as shown in Fig. 3.26. Figures 3.30 and 3.31 show views of specimens No. 4 before and after concrete casting, respectively.
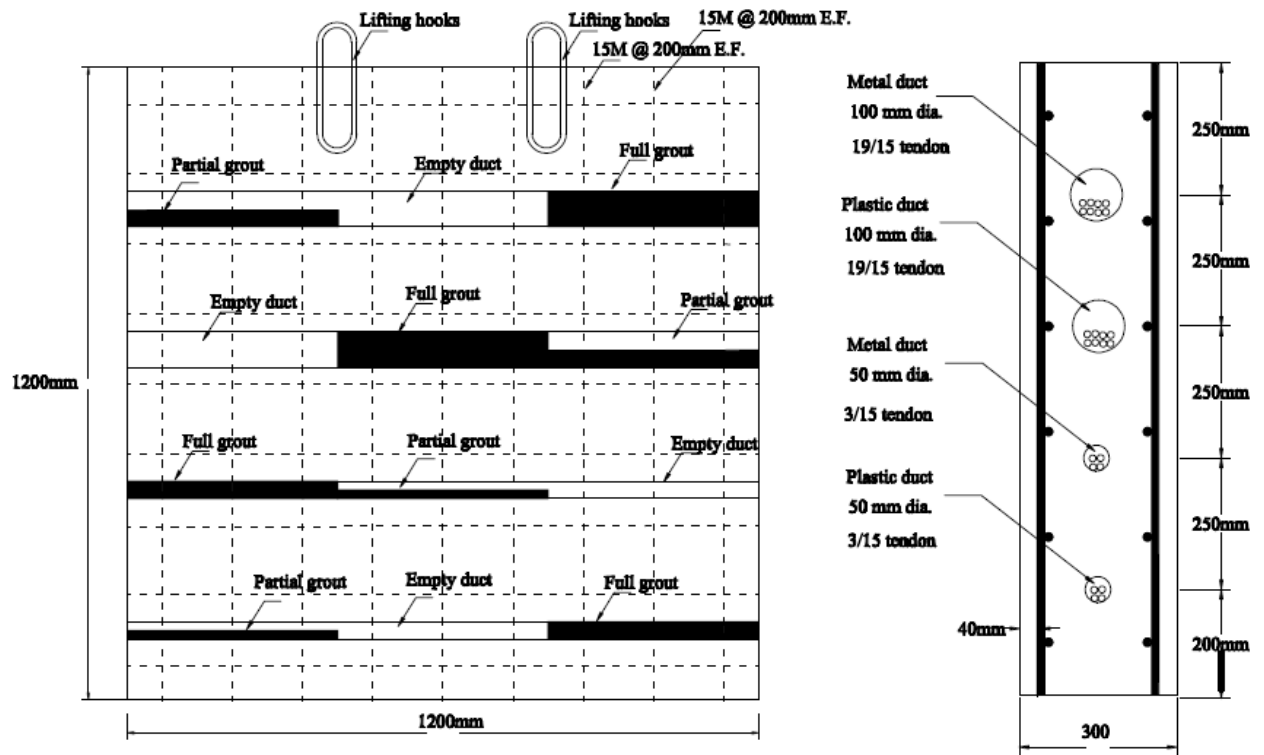
Fig. 3.26 Cross-section (right) and layout of specimen No. 4 showing duct and reinforcement details (left)

Fig. 3.27 View of the prestressing cable showing its middle portions with simulated void at its mid-length and partially grouted duct at its end

Fig. 3.28 View of the duct and the
prestressing cable during grouting

Fig. 3.29 Views of partial grouting of
100 mm and 50 mm plastic ducts

Fig. 3.30 View of specimen No. 4 before
concrete casting
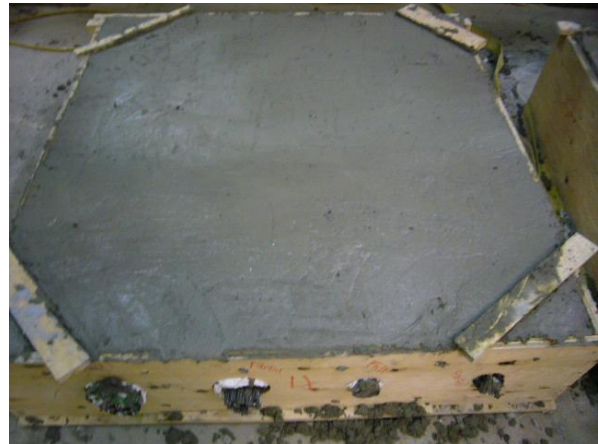
Fig. 3.31 View of specimen No. 4 after
concrete casting

3.2.5 Specimen No. 5

Specimen No. 5 was identical to specimen No. 4 in all aspects including overall dimension, cross-section, tendon and reinforcement arrangement except that the middle portion of the prestressing cables and reinforcing steel bars were artificially corroded over 400 mm length. It should be noted that corrosion of the steel bars and the prestressing tendons were artificially imposed on them. Then, they were placed in the formwork before concrete casting. In the region of corroded tendons and rebars, the ducts were fully grouted, partially

grouted and left empty for dual purpose of evaluating the degree of corrosion of cables with associate problem in grouting. Figure 3.32 shows layout and cross-section of the specimen showing reinforcement and duct details as well as grouting details. While Figures 3.33 to 3.35 show views of the corroded tendons and duct grouting. Figures 3.36 and 3.37 show views of specimens No. 5 before and after concrete casting, respectively.
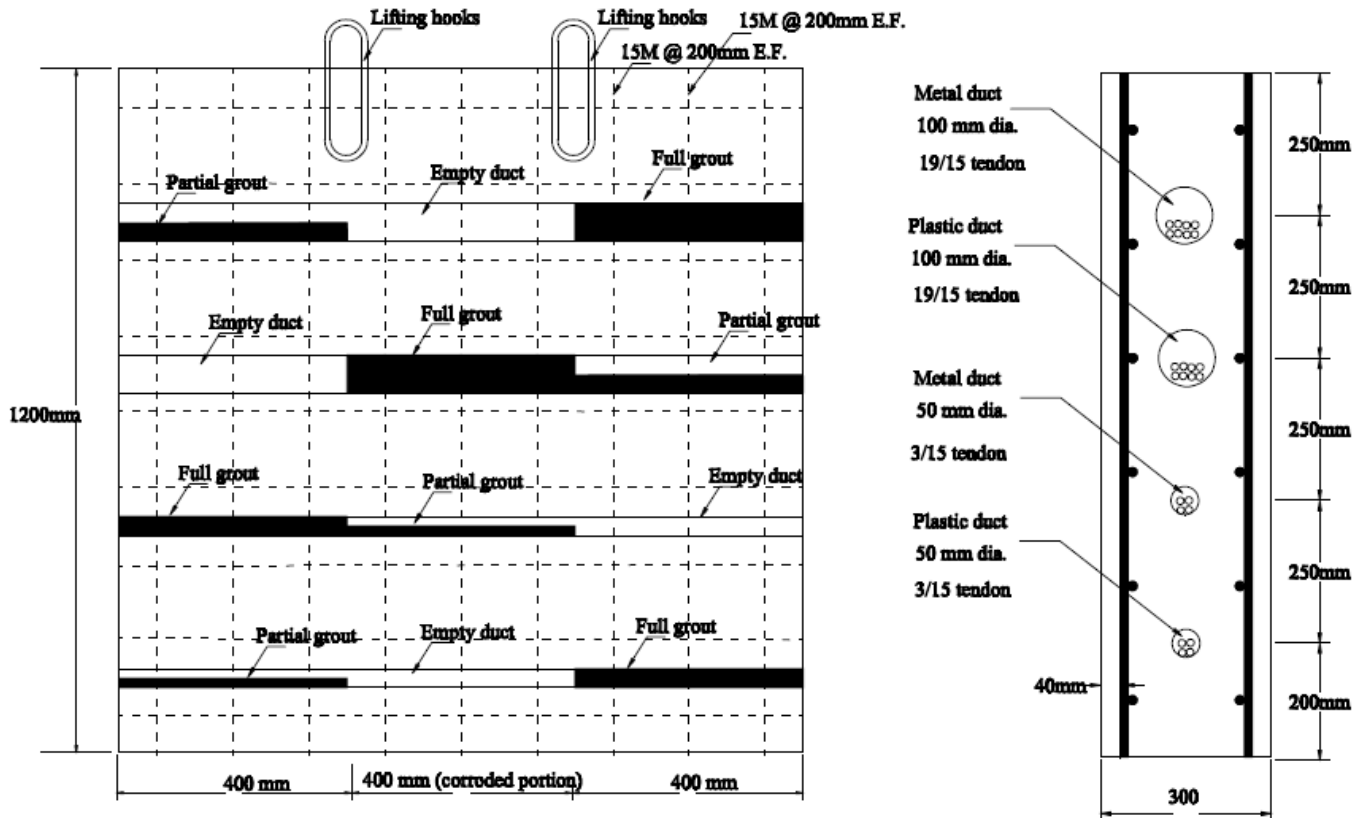
Fig. 3.32 Cross-Section (right) and layout of specimen No. 5 (left) showing duct, reinforcement details and the corroded portion of both the tendon and the reinforcement within its middle third

Fig. 3.33 View of the corroded 3/15 prestressing cable at its middle third portion along with partial grouting

Fig. 3.34 View of the corroded 19/15 prestressing cable with the corroded portion and fully grouted duct at its bottom portion

Fig. 3.35 View of how voids are introduced in plastic duct using Styrofoam infill

Fig. 3.36 View of specimen No. 5 before casting

Fig. 3.37 view of specimen No. 5 after concrete concrete casting

3.2.6 Specimen No. 6

This specimen was constructed to investigate the characteristic of mono-strand compared to bundled strands using NDT methodologies. Specimens No. 6 represents a case of pre-tensioned beam in bridge superstructure including fracture and notch in the wire strands. The specimen was of 1200 mm length, 350 mm depth and 160 mm width. It had one seven-wire strands of 15 mm (0.6 inch) diameter and 140mm² effective area with artificial fracture and notch located 300 mm apart along each side of the specimen as shown in Fig. 3.38. The wire strands were equally placed at 50 mm vertical spacing and 100 mm concrete cover to the top or the bottom of the specimen. The specimen was reinforced with mesh reinforcement of 15M at 200mm c/c placed at each side of the strands, simulating shear reinforcement in pretensioned girder. To create 20 mm fracture in the strand, the strand was cut and taped by placing styrofoam between the two strand segments. Figure 3.39 shows view of the strand after introducing the artificial break and notch. While Fig. 3.40 shows view of specimens No. 6 before concrete casting.
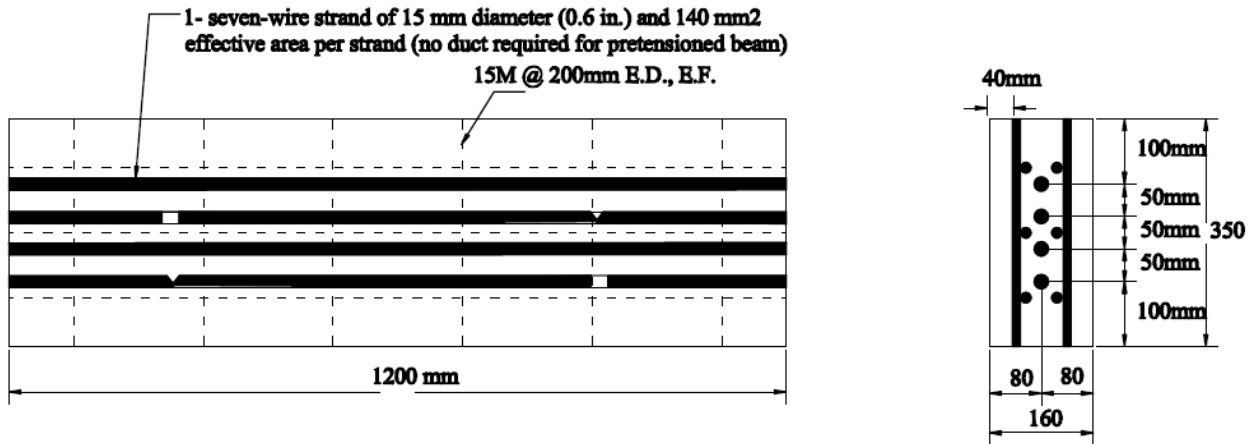
Fig. 3.38 Cross-section (right) and layout (left) of specimen No. 6

Fig. 3.39 View of the strand after introducing
the artificial break and notch

Fig. 3.40 View of specimen No. 6
before concrete casting

3.2.7 Specimen No. 7

Specimen No. 7 was similar to specimen No. 6 with respect to overall cross section, dimension, and rebar and strand arrangements. Unlike specimen No. 6, specimen No. 7 contained artificial corrosion over 300 mm length of selected strands at selected locations in the strand as shown in Fig. 3.41. The selected strands were corroded over either 300 mm length at its middle part or 300 mm length at its end. Figure 3.41 shows the layout and the cross-section of the specimen. While Fig. 3.42 and 3.43 show views of the specimen before and after concrete casting.
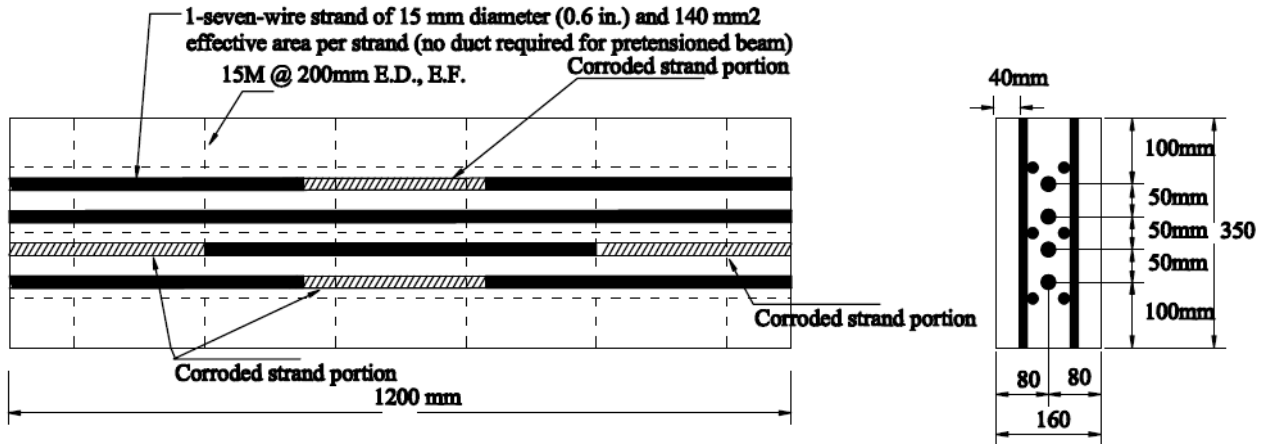
Fig. 3.41 Cross-section (right), and layout of specimen No.7 with limited

corrosion in the strands

Fig. 3.42 View of specimens No. 7 before concrete casting   Fig. 3.43 View of Specimen

No. 6&7 after casting concrete

3.2.8 Specimen No. 8

Specimen No. 8 was constructed in larger dimensions, 4000x4000x400 mm, to allow for using NDT technologies that are affected by the length of the specimen and conditions. This specimen was built with the intention to apply the infrared as well as the MR technologies in bridge deck inspection. However, this plan did not go through. However, this specimen was used to demonstrate the use of vacuum grouting in filling the existing duct voids after locating the ducts using GPR. This specimen included all the deficiencies

introduced in the first 5 laboratory specimens mentioned earlier, such as artificial voids, wire fracture and simulated corrosion at selected portions of the straight bundled strands. The specimen was constructed at Ministry of Transportation of Ontario (MTO) site in Arrow Road, Toronto, Ontario. The specimen had four straight tendons containing 100 mm and 50 mm metal ducts with 19/15 strands and 3/15 strands, respectively, with nominal diameter of 15 mm (0.6 inch) and 140 mm² effective areas per strand, as shown in Fig. 3.44. Two tendons were placed close to the surface with a concrete cover of 76 mm containing fractures and notch in strands in addition to simulated corrosion, as shown in Fig. 3.45. The two other tendons with diameters of 100 mm and 50 mm, respectively, were placed at the mid-depth of the specimen, containing artificial voids in addition to wire fracture, notch and corrosion, as shown in Figs. 3.47 and 3.48. In addition, limited mesh reinforcement was placed in half of the slab width in addition to bottom reinforcing steel mesh over the entire slab area. Figure 3.49 and 3.50 show views of the ducts with air void and wire breaks. While Figs. 3.51 and 3.52 show views of the specimen before and after concrete casting.
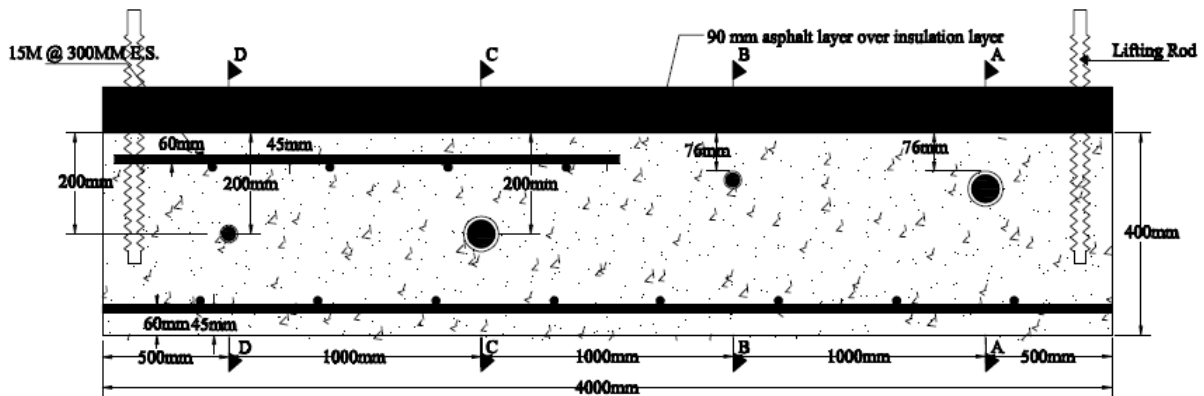
Fig. 3.44 : Cross-section of specimen No.8
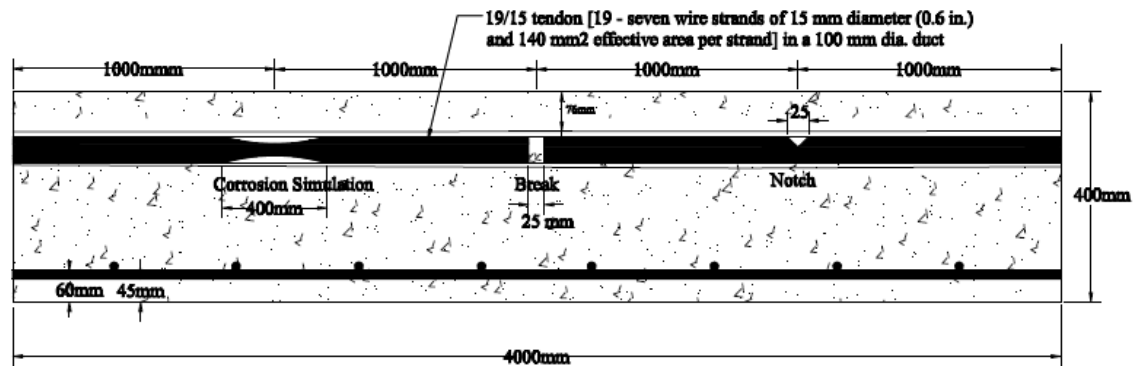
Fig. 3.45 Section A-A of specimen No. 8 showing straight tendon including tendon notch, break and corrosion simulation

87
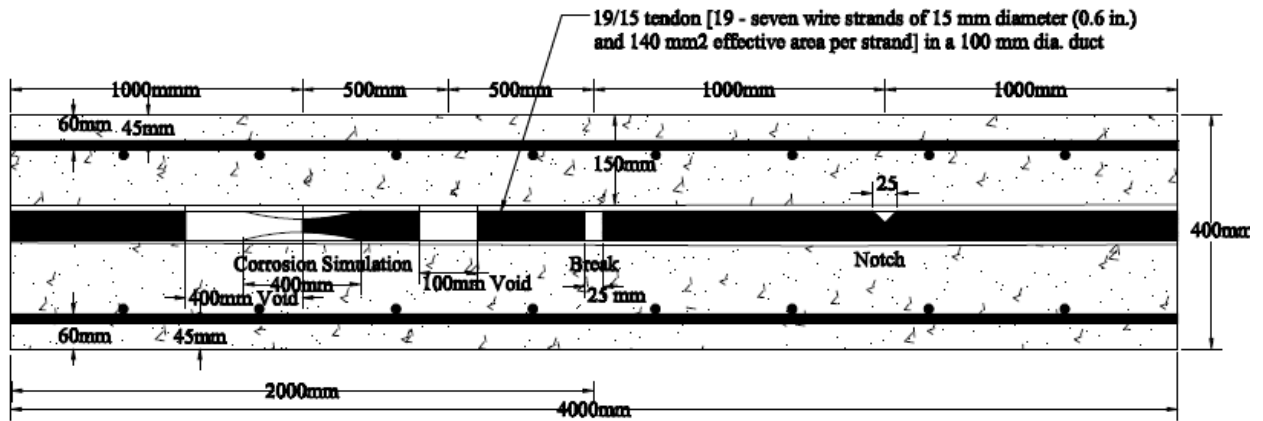
Fig. 3.46 Section B-B of specimen No. 8 showing straight tendon including tendon notch, break and corrosion simulation
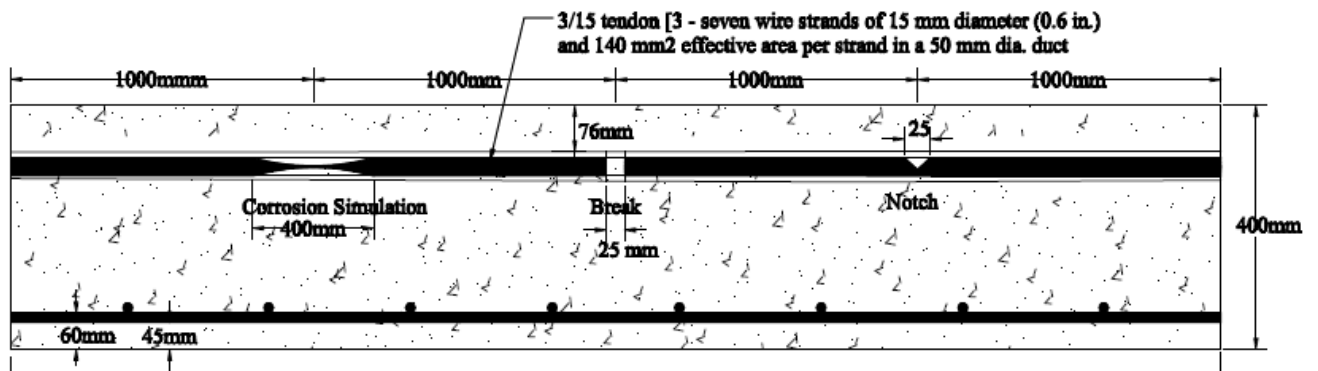
Fig. 3.47 Section C-C of specimen No. 8 showing straight tendon including notch, Break corrosion simulation and limited void
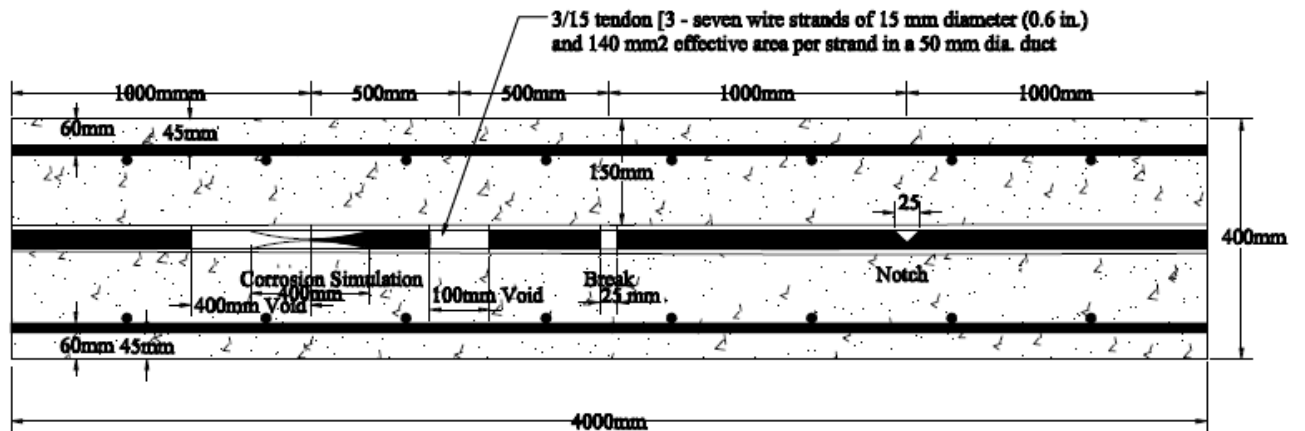
Fig. 3.48 Section D-D of specimen No. 8 showing straight tendon including tendon notch, Break, void and corrosion simulation

88

Fig. 3.49 View of the 100-m duct showing air void and wire breaks (section C-C)

Fig. 3.50 View of complete wire break in the tendon at its mid-length

Fig. 3.51 View of specimen No. 8 before pouring concrete

Fig. 3.52 View of Specimen No.8 after pouring concrete

3.3 Corrosion

3.3.1. General Corrosion (Shivprakash et al., 2005)

To understand the concept of corrosion process in prestressing systems, it is necessary to find out corrosion process of concrete materials. Generally, steel bars embedded into the concrete are maintained against corrosion due to high alkalinity of the concrete. However, if the conditions of concrete change over time by external or internal factors, corrosion of steel bars may increase to a problematic issue. In fact, corrosion of steel bars is an electrochemical reaction between iron ions, H_2O and O_2 as shown in equations (3.1) and (3.2) below:

$$Fe \rightarrow Fe^{2+} + 2e^- \text{ (anodic half-cell reaction)} \qquad (3.1)$$
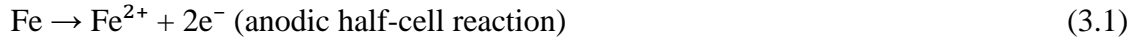
Equation (3.1) which is also called anodic reaction describes that iron atoms release electrons into the concrete to produce ferrous ions (Mehta, 1993).

$$2H_2O + O_2 + 4e^- \rightarrow 4OH^- \text{ (cathodic half-cell reaction)} \qquad (3.2)$$
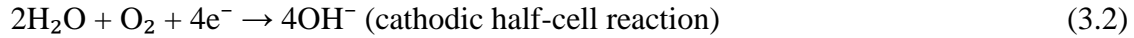
Electrons released from anodic side move to the cathodic region to react with excess H_2O and O_2 in the concrete. This process is called reduction reaction.

$$2Fe + 2H_2O + O_2 \rightarrow 2Fe^{2+} + 4OH^- \rightarrow 2Fe\,(OH)_2 \qquad (3.3)$$
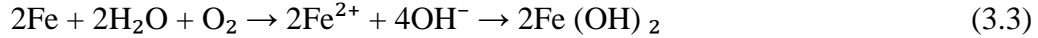
Hydroxyl ions at cathode region combine with Fe^{2+} at anode to produce a solution of ferrous hydroxide (Eq. 3.3).

$$2Fe\,(OH)_2 + 2H_2O + 1/2O_2 \rightarrow 2Fe\,(OH)_3 \qquad (3.4)$$
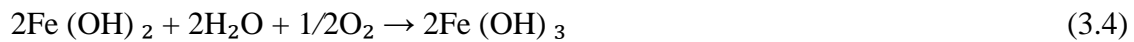
Ferrous hydroxide reacts further with available water and oxygen to form water insoluble red rust (Fe (OH) $_3$).

Anode and cathode are electrochemically different areas. This is because of existing two different metals or single metal with different surface characteristics (Rosenberg et al., 1989). Corrosion of reinforced concrete can be uniform if the location of anode and cathode change over the steel surface or it may be localized if anode and cathode location remain the same along the length of the steel bar. Figure 3.53 illustrates a basic corrosion process in the reinforced concrete. Usually, high alkalinity (high PH) of concrete (grout) develop a passive film on the steel protecting it from corrosion. Once chloride ions attack the concrete, it breaks down the passive film in a concentrated location causing to have pitting corrosion. If the passive film on the steel is lost, the steel is then susceptible to corrosion.
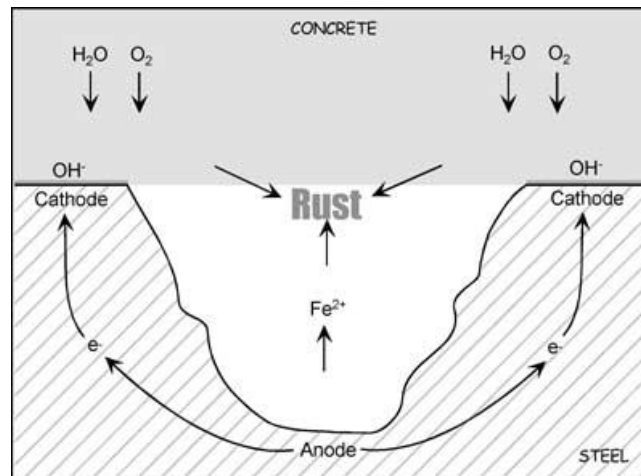
Fig. 3.53 Corrosion of steel in concrete (Rosenberg et al., 1989)

3.3.2 Corrosion of Prestressing Steel (Shivprakash et al., 2005)

In the same way, prestressing steel wires are susceptible to chloride- induced corrosion either by stress corrosion cracking (SCC) or hydrogen embrittlement (HE). Chloride- induced corrosion is the most common corrosion pattern in concrete. Due to series of reactions mentioned above, this type of corrosion pattern produces rust at concrete surface following by spalling and cracking of the concrete. The same uniform corrosion process may be established on an expanded concrete area in prestressing system similar to that of reinforced concrete. Pitting corrosion also occurs in high alkalinity environment due to chloride attack on a small concentrated region depassivating wire strands to cause corrosion. Pitting corrosion is severely catastrophic due to large reduction of cross sectional area with a small amount of overall metal loss (Fontana 1986).

3.3.3 Corrosion of Strands and Rebar at Laboratory Scale

In case of corrosion detection in this report, it was supposed to locate corrosion in some portions of wire strands along the length of the tendon ducts in post-tensioning system. As mentioned above, the strands are susceptible to corrosion due to chloride attack by ingress of water into duct either at seams or end anchors. To simulate corrosion of strands and rebars in laboratory, they were corroded outside of concrete by placing them into the salt solution.

3.3.3.1 Corrosion Process

Models 3, 5 and 7 contain corroded strands and rebars. In these models, only some portion of strands and rebars are subjected to corrosion. To maintain non-corroded parts, the strands and rebars were coated using Candle wax and taped with electrical tape as shown in Figure 3.45. Both candle wax and electrical tape are non-conductive in transferring electrons. A plastic tank ($65'' \times 30'' \times 30''$), steel mesh, water, salt and power suppliers were used to run the corrosion process of strands and rebars. First, the steel mesh was placed into the plastic tank. Strands and rebars are then located on top of the steel mesh with a gap of 5cm. The strands and rebars were connected to positive terminal of power suppliers using electrical wire as anodic side. The negative terminal of power suppliers were connected to steel mesh as cathodic side. Next, the plastic tank was filled with water up to a 5cm distance above the

strands or rebar. Five percent salt per weight of water was added to water.

Power suppliers were run to a maximum current of 3 Ampere applying electrical current to the system. The current causes to transfer electron from iron atoms (anodic side) to the steel mesh (cathodic side). The less distance between strands and steel mesh produce the more corrosion product on the strands' surface. Therefore, the bottom face of strands which is closer to the steel mesh will be more susceptible to corrosion. As a result, the strands should be turned over periodically in order to have a uniform corrosion of strands. To evaluate the required time for corroding of rebars and bundled strands, Faraday's equation has been used. Single strands, single rebars and 3/15 strands were corroded within three to six days. However, this time for 19/15 strands was not adequate to reach a specific degree of corrosion. Thus, after 11 days submerging these bundled strands into the salt solution, the current has been increased to 6 Ampere to accelerate the corrosion process. Figures 3.54 to 3.57 show photos of the laboratory setups for corrosion process.

Fig. 3.54 Coating strands with candle wax (top); taping strands with electrical tape (bottom)
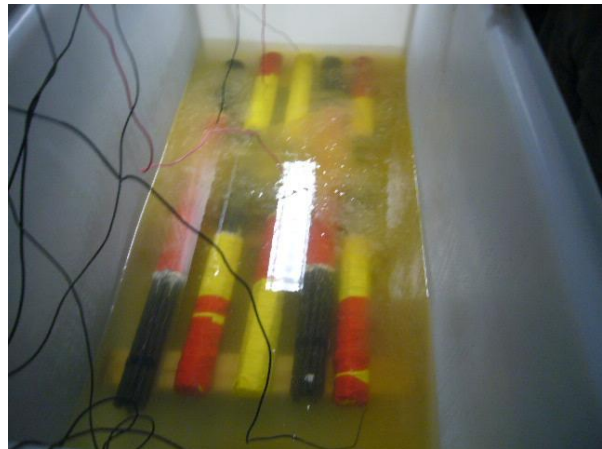
Fig. 3.55 Submerging strands in the salt solution

Fig. 3.56 Corrosion product of strands

Fig. 3.57 Connecting anodic side of power suppliers to the strands and cathodic side to the steel mesh with a maximum current of 3 Ampere

3.3.3.2 Calculation of Degree of Corrosion (DOC)

To calculate mass loss in the wire strands and rebar submerged into the corrosion solution, Faraday's equation has been used as follow:

$$\text{Mass Loss} = \frac{t \times i \times M}{z \times F} \tag{3.5}$$

Where;

t= the time passed (s)

i= the current passed (Ampere)

M= atomic weight (for iron M= 55.847 g/mol)

z= ion charge (2 moles of electrons)

F= Faraday's constant, which is the amount of electrical charge in one mole of electron (F= 96487).

3.3.3.2.1 DOC of 19/15M wire strands (400 mm middle-third corroded part)

Weight of 1.20 meters 19-15M bundled wire strands is being determined as 26000 g. for the length of 400mm corroded part , the weight of the strands is equal to 26000÷3= 8700g. For 10% mass loss, the time required for this amount of mass loss has been calculated using Faraday's equation (Eq. 3.5) as follow:

$$8700 \times 0.10 = 870 \text{ g}$$

$$870 = \frac{\text{time} \times 3 \times 55.847}{2 \times 96487} = 1002067.4 \text{ sec} = 11.5 \text{ days}$$

After 11 days, the current increased from 3 Ampere to 6 Ampere for three more days to accelerate corrosion process. The mass loss for this length of time is determined as 450 g. Thus, the total mass loss after 14 days submerging bundled strands into corrosive agents is determined as 870+ 450= 1320g. This was confirmed by weighing the corroded strands out of solution as 24650g and the total mass loss of 26000- 24650= 1350g.

Accordingly, the degree of corrosion has been calculated as follow:

$$\text{Degree of Corrosion} = \frac{1320}{8700} = 15.17\%$$

3.3.3.2.2 DOC of 19/15M wire strands (300 mm corroded ends, Specimen No. 3)

For the length of 600mm (300+300mm both ends) corroded part, the weight is equal to 26000 ÷2= 13000g. During 11 days submerging the bundled strands in the corrosive solution, the mass loss of 825g has been reached.

$$\text{Mass Loss} = \frac{11 \times 86400 \times 3 \times 55.847}{2 \times 96487} = 825g$$

The current then increased for seven more days to yield the mass loss of 1050g. The total mass loss has been calculated as 1050+825= 1875g and the related degree of corrosion is determined as 14.4% (1875÷13000 = 14.4%). Table 3.2 summarizes the degree of corrosion for the corroded wire strands and rebars.

Table 3.2 Degree of Corrosion of wire strands and rebar

Materials	Length (mm)	Nominal Diameter (mm)	Weight (gr)	Corroded Part (mm)	Time (days)	Weight Loss (gr)	Degree of Corrosion
Rebar	1200	16	1850	Middle Third (400mm)	3	240	39
					4	300	48.6
					6	450	73
				Each End (300mm)	6	450	48.6
Single Strands	1200	15	1100	300mm Middle	3	225	81.8
				300mm Each End	3	225	41
3/15M Strands	1200		3430	Middle Third (400mm)	6	450	39.4
19/15M Strands	1200		26000	Middle Third (400mm)	14	1320	15.17
					17	1770	20.3
				300mm Middle	14	1275	19.6
				300 mm Each End	18	1875	14.4

3.4 Materials

Materials required for the research were delivered from available local industry to Ryerson Structural Laboratory.

3.4.1 Concrete Grout for the Ducts

High Tolerance Cable Grout named as "Euco Cable Grout PTX" was ordered from Euclid Chemical Company and delivered to the lab in order to fill the ducts. Some of the features and benefits of the grout are:

- Easy to pump or pour.

- Non-shrink performance provides excellent bearing.

- High strength.

- Pumping continuously will aid in grout uniformity and ease of placement.

This grout contains specific rate of chemical compositions and should not add aggregate, cement, admixtures or fluidifiers in which it will change the precision of grouting characteristics. All exposed grout should also be cured for 24 hours either by wet curing or with a high solids curing compound.

3.4.2 Concrete

Ready-mix concrete was supplied for the research to cast the concrete forms. The mix concrete was 72 hours High-early strength with 35 MPa minimum compressive strength and air-entrainment inclusion. It had a slump of 3 inches (76.2mm). The cement used in the mix was High- Early strength Portland cement (HE), CSA type 30, manufactured by Canadian Cement Company. The aggregates used in the mix concrete had a maximum aggregate size of 20mm. Generally, concrete is a mix of paste and aggregates. Paste composes of cement and water and aggregates contain both fine (sand) and coarse (gravel) components (Portland Cement Association). The paste coats the aggregate in a way that by a chemical reaction called hydration, it will be hardened to gain strength and form concrete. A proper mix concrete maintains desired workability for the fresh concrete and required durability and strength for the hardened concrete. Typically, a mix concrete compose of 15-20 percent water, 60-75 percent aggregate and 10-15 percent cement. In some concrete mix a 5-8 percent Air-entrainment might be added to the mix. Figure 3.58 shows a basic concrete mix composition (Portland Cement Association).
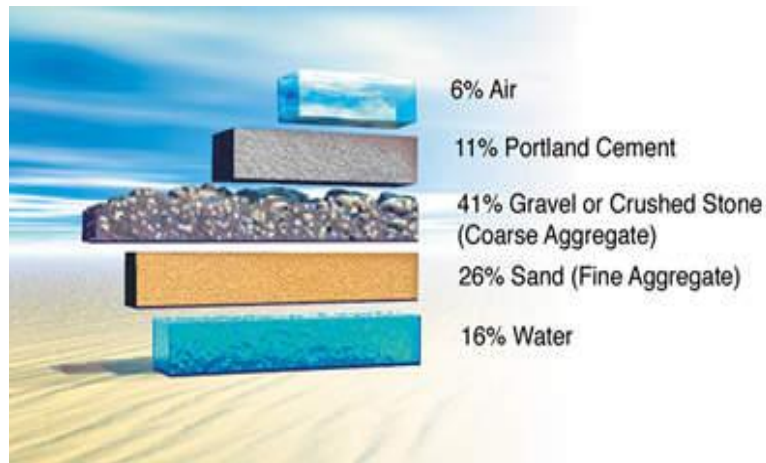
Fig. 3.58 Bar graph showing percent of different components in concrete mix (Adapted by Portland Cement Association)

Six standard 100x200 mm cylinders were cast simultaneously with casting of bridge deck models. The cylinders were cured besides the models to maintain the same curing characteristics as the models. The concrete cylinders were tested within 3 and 7 days to ensure the concrete compressive strength. An average value of three tested cylinders was taken as the compressive strength of the concrete. Table 3.3 shows the peak compressive strength and its relative peak load for each cylinder.

Table 3.3 Compressive strength of standard cylinders

Cylinder #	Peak Compressive Strength (MPa)	Peak Load (KN)	Remark
C1	34.3	270.75	After 3 days
C2	33.72	261.3	After 3 days
C3	34.9	274.4	After 3 days
C4	38.3	293.5	After 7 days
C5	35.6	279.2	After 7 days
C6	37.7	287.5	After 7 days

3.4.2.1 Cement

Cement used for the concrete mix was type 30 (HE) according to Cement Association of Canada (CSA). High Early strength Portland Cement (HE) is applicable to the structures

97

that must be quickly in service or in case the forms required to be removed as soon as possible. In accordance with ASTM C 150, Type IIIA cement representing type 30 with air-entraining inclusion has been used.

3.4.2.2 Water

Natural tap water is being used for the concrete mix. For a normal strength used in concrete structures, compressive strength of concrete inversely related to the water-cement ratio. Water- Cement (W/C) ratio is the weight of water divided by the weight of cement. Thus, lower W/C ratio produces higher concrete strength. However, workability of concrete should be taken into account by lowering W/C ratio. Generally, high quality concrete can be produced by using less amount of water in a way that the concrete is properly placed, consolidated and cured. The water-cement ratio used for the proposed concrete mix was 0.40 with air-entrainment inclusion in accordance with CSA A23.2-3C (ASTM C 31) provision.

3.4.2.3 Aggregates:

Aggregate particle size distribution and nature (such as shape and porosity) are the two significant factors on proportioning of concrete mix. These factors importantly affect workability of the fresh concrete. Aggregates compose of fine (sand) and coarse (gravel or crushed stone) materials. The fine and coarse aggregates generally occupy 60% to 75% of the concrete volume (70% to 85% by mass) and strongly influence the concrete's freshly mixed and hardened properties, mixture proportions and economy (Steven H.K et. al 2002). The most desirable fine aggregate size depends mainly on the type of work and maximum size of coarse aggregates. The maximum size of coarse aggregate is a key factor in determination of the required cementing paste materials. Usually, for small size aggregates more paste (water and cement) is required compared to large size aggregates. Fine and coarse aggregates should meet the requirements of CSA A23.1 (ASTM C 33). Maximum normal aggregate size used for the proposed concrete mix was 20mm.

3.4.2.4: Air-Entrainment

Air entrainment is the creation of air cells in the concrete by adding air entraining agent into the mix concrete. The air cells are introduced during mixing of the concrete (plastic

mode) and most of them remain as part of the concrete after the concrete get hardened. Air entrainment increases durability of hardened concrete especially in case when the concrete structure is subjected to freezing and thawing. It also increases workability of mix concrete once being plastic. Figure 3.59 shows micrograph air cells in concrete structure and figure 3.60 shows the available air entraining admixtures.
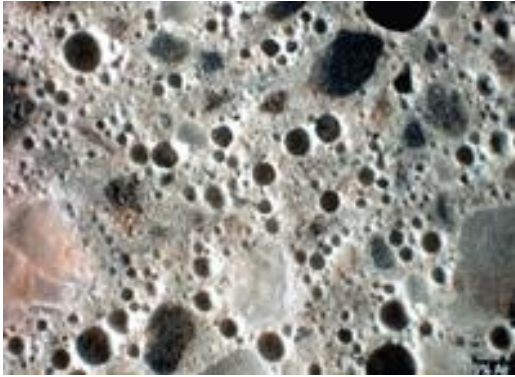
Fig. 3.59 Micrograph air-entrained concrete showing air cells (Portland Cement Association)

Fig. 3.60 Air-entraining admixture

3.4.3 Concrete Transport Truck

To transport the ready mix concrete to construction site, there are special cylindrical trucks named as "Cement Mixer" that deliver and mix concrete from plant to the site. The material was already been prepared in the plant and loaded into the truck for delivering to the Ryerson Laboratory in plastic condition. The truck maintains material in its original state once delivering or turning of the drum. In the structural lab, a pump provides the mean to move the concrete mix to the pre-assigned locations. Figure 3.61 shows photo of a cement mixer truck when discharging concrete ready mix. Ready mix concrete is often remixed on the jobsite so that the suitable slump is obtained. However, the remixed concrete has tendency to set rapid than the concrete mixed only once.

3.4.4 Reinforcing Steel

The deck slabs and beams in all bridge deck and beam models were reinforced with steel rebars. 15M rebars @200mm c/c were used in all models and placed into the models in

accordance with Canadian Highway Bridge Design Code (CHBDC) requirements except for the first three specimens that are reinforced in some portion of the models in order to examine the deck slab under non-congested rebar arrangement.

Fig. 3.61 Concrete transport truck

Table 3.4 technical properties of Grade 270 wire strands

Code Specification	13mm (0.5″)	15mm (0.6″)
	ASTM A 416 Grade 270	ASTM A 416 Grade 270
Yield Strength (MPa)	1670	1670
Ultimate Strength (MPa)	1860	1860
Nominal Dia. (mm)	12.7	15.24
Cross-Sectional Area (mm²)	98.71	140
Weight (Kg/m)	0.775	1.102
Ultimate Load (KN)	183.7	260.7
Modulus of Elasticity (MPa)	195000	
Relaxation After 1000h at 0.7 x Ultimate Strength (%)	Max. 2.5	

3.4.5 Wire Strands

Strands are composed of seven single wires in which six of them wounded helically around the center wire (king wire). These strands in post tensioning system maintain high tensile strength. Strands can be manufactured either bare galvanized or epoxy coated

100

maintaining the same strength characteristics. All strands should meet requirements of ASTM A 416 ("Standard Specification for Steel Strand, Uncoated Seven Wire Strand for Prestressed Concrete"). Strands are usually available in 13mm and 15mm nominal size diameters with 99 and 140mm² cross sectional areas respectively. In accordance with ASTM A 416 the strands used were grade 270 (Ksi) or 1860 (MPa) as of ultimate strength with 15mm (0.6″) nominal diameter and 140mm² (0.217 square inches) cross sectional areas per strand. Table 3.4 provides more information on Grade 270 wire strands.

3.4.6 Ducts

Primarily ducts are used in post-tensioning system as a means of providing void to fill the tendon strands. It is also considered as a secondary means of protecting tendon strands against corrosive agents. Therefore, particular attention should be taken for quality, integrity and continuity assurance of the ducts as a corrosive barrier. Alkalinity of the grout and concrete plays the primary role of corrosion protection. The main characteristic of duct in post-tensioning system is bonding grouted tendons to the surrounding concrete. Usually, ducts are available in different materials for various applications and types of tendons. The most common types of ducts available in the market are; corrugated galvanized metal duct and polyethylene or polypropylene corrugated plastic ducts.

3.4.6.1 Duct Size

In accordance with Post-Tensioning Tendon Installation and Grouting Manual adopted on May 2004, the nominal internal cross sectional area of the circular ducts should be minimum 2.25 times the cross sectional area of the tendon strands or 2.5 times for tendons installed by pull through method. In the proposed research, the net area of 19/15 strands was being determined as 5985 mm² and the required internal duct diameter was calculated as 87.3 mm. However, the internal nominal diameter of 100mm had been considered for 19/15 tendon strands.

3.4.6.2 Corrugated Galvanized Metal Duct

Corrugated metal ducts are the most economical type for the means of providing tendon strands void. These ducts are wounded spirally either by welding or interlocking seams

with proper rigidity to the required diameter from bare steel strand and a wall thickness of 0.45mm for ducts diameter of 66mm (2-5/8 in) or less or 0.6mm for ducts diameters greater than 66mm. Metal ducts are available in 2″, 3″ and 4″ diameters. The ducts should be galvanized and meet the requirements of ASTM A653. In this research, metal duct diameters of 2 and 4 inches have been used. Figure 3.62 shows a view of the metal duct available in the market.

Fig. 3.62 Corrugated metal duct interlocking at seams

3.4.6.3 Polyethylene/ Polypropylene (PE/PP) Corrugated Plastic Duct

Once long-term secondary corrosion protection is the matter of concern, corrugated plastic ducts composed of polyethylene (PE) or polypropylene (PP) materials are the most suitable ducts especially in the region of high corrosion attack. Both PE and PP ducts are fabricated from resins with minimum wall thickness of (2 ± 0.25 mm) or (0.079 ± 0.010 inches). PE ducts should meet requirements of ASTM D3350, while, PP ducts should meet requirements of ASTM D4104. PP ducts are available in 2-3/8″ internal diameters and PE ducts are made of 2″, 3″ and 4″ diameters. In this research, PE ducts with nominal internal diameters of 2″ and 4″ have been used. Figure 3.63 shows a view of high-density polyethylene duct.
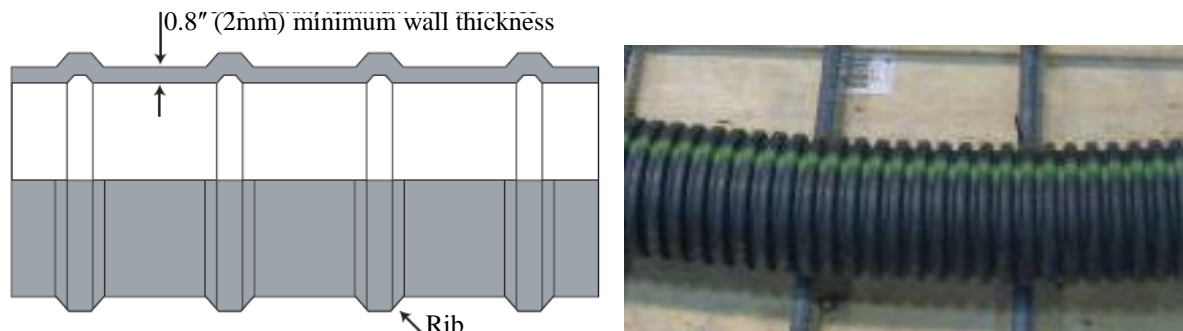
Fig. 3.63 High density polyethylene plastic duct

3.4.7 Styrofoam

To develop void and break simulations in the tendon strands, Styrofoam insulation sheets were used. Figure 3.64 shows view of the Styrofoam sheet creating empty and partial voided ducts. Styrofoam was cut in pieces in specified void length and joined together using tape to form the required void shape along the length of tendon strands.

Fig. 3.64 Use of Styrofoam to form voids   Fig. 3.65 Formwork of specimen No. 4

3.5 Formwork:

Plywood sheets with the thickness of 3/4″ (19mm) were used to support concrete in the proposed bridge deck models. Wood stud 2″×2″ size was also used as the main members to support the formwork frames. Plywood sheets were cut in specified dimensions as per models using an electrical wood saw available at Ryerson Laboratory. The woods were then put side by side to make a framework. A plank wood was placed underneath the framework as shown in Figure 3.65. Circular openings with net diameters of 4-1/4″ (108mm) were made in the plywood sheets as a means of supporting tendon ducts. In addition, the small holes with the diameters of 3/4″ (19mm) were made to support reinforcing bars in the formwork. The duct including tendon strands and reinforcing bars were then placed into the formwork. Figure 3.66 shows a view of bridge model No. 2 after setup.

Fig. 3.66 view of tendon strands and rebar   Fig. 3.67 vibrating concrete of specimen No.3

Placement in specimen No.2

3.6 Placement of Reinforcing Steel Bars

Pre-cut steel bars were ordered and delivered to the Ryerson Structural Laboratory. The reabrs were again cut for adjustment using electrical rebar cutter available at Ryerson Laboratory. The reinforcing steel mesh were made inside the formwork by placing the longitudinal rebars into the prepared circular holes in the formwork and holding the transverse rebars by Standard Ties. The 15M bars were placed 200mm c/c in each directions. Figure 3.66 shows the placement of steel bars in model No. 2.

3.7 Lifting Hooks

After placing tendon strands and rebars in the formwork, the sides lifting hooks were embedded into the forms and tied with tendon ducts. Rebar size of 15M was used to make the hooks. The hooks were used to lift the samples and carry to the proposed location for testing.

3.8 Casting of Concrete

High Early Strength concrete with specified seven days compressive strength of 35 MPa was used to cast the bridge deck models. Ready-mix concrete was delivered to the Ryerson Structural Laboratory and poured into the forms using available concrete bucket. The concrete was poured in the middle as well as each corner of the models and then vibrated using high frequency poker vibrator. A long smooth wood stud was used to level the concrete

surface. The concrete top surface was then smoothened using hand trowel. Figure 3.67 shows view of concrete casting and vibrating specimen No. 3.

3.9 Curing of Concrete

After casting of concrete, the models were cured for seven days. Once the concrete was set after casting which is usually 6-8 hours, the concrete models and cylinders were sprayed with water to minimize evaporation. Generally, high early strength concrete releases a considerable amount of heat for the first few days. Within this period of time the concrete must be cured periodically in order to reach the maximum specified compressive strength. Thus, the samples were sprayed with water two times a day in a period of 12 hours for the total of seven days.

3.10 Removing the Formwork

After seven days curing of the concrete samples, the wooden formworks were removed using crook bar and hammer. The cured cylinders beside the samples were also tested on the same day to confirm the maximum seven days strength of 35 MPa corresponds to the strength of concrete samples.

3.11 Test Equipments

3.11.1 Ground Penetration Radar Equipment

Terra SIRch system, model SIR-3000 was used for the test. The system is property of Geophysical Survey System Inc. (GSSI). The SIR-3000 is a digital Subsurface Interface Radar (SIR) system designed for a wide range of environmental, geotechnical, geological and engineering applications. Some of the advantages of the equipment include;

- High-resolution screen, easily readable in daylight.
- Rugged, lightweight, flexible, handheld and very portable
- Internal battery
- USB, Ethernet, RS-232 ports for greater system flexibility.
- Operates in the temperature range of -10˚C to 40˚C
- The system is environmentally water resistant

The system is applicable for concrete and rebar inspection, utility detection and mapping,

geological and archaeology investigations.

SIR 3000 contains the following items: (i) digital control unit (DC-3000) with preloaded operating system; (ii) antenna; (iii) two Batteries; (iv) AC Adaptor; (v) cable; (vi) transit Case and, (vii) post-processing software. The field operation of the system employs two main modes of structrescan; ConcreteScan and StructureScan.

Fig. 3.68 GPR instrument (Geophysical Survey System Inc.)

3.11.1.1 ConcreteScan:

ConcreteScan works with either 1.5GHz or 900 MHz antennas. It is a proper means of interest for "quick linescan" into a concrete slab. This mode can be used to locate shallow structure features in concrete such as rebar, conduit, PT cables in real time so that their locations on the slab can be marked prior to any cutting, coring or drilling.

3.11.1.2 StructureScan:

StructureScan works only with 1.5 GHz antenna and a black scan pad that collects very high-resolution 3D data over concrete slab or wall. This will produce a 3D cube of data that can be viewed in plan at different depths for clear locations of coring and cutting.

For the proposed test specimens, the ConcereteScan mode with 1.5 GHz antenna has been selected. After the antenna initialized, the screen shown in Figure 3.69 is split into three

windows; menu tree at left, a linescan (main) display in the center and a single scan in the O-scope display on the right. O-scope window shows a single radar scan in an oscilloscope- style (O-scope) depiction. This will show successive single scans as the antenna moves across an area while in setup mode. The main display window in the center shows a radar profile in linescan format. In this window, successive single scans are assigned color or black and white values and stacked next to each other in sequence to form a continuous image. The vertical scale on the left of this display window shows depth, time, or sample number. The menu tree window is used to navigate through the various commands, set system parameters, and enter file name information.
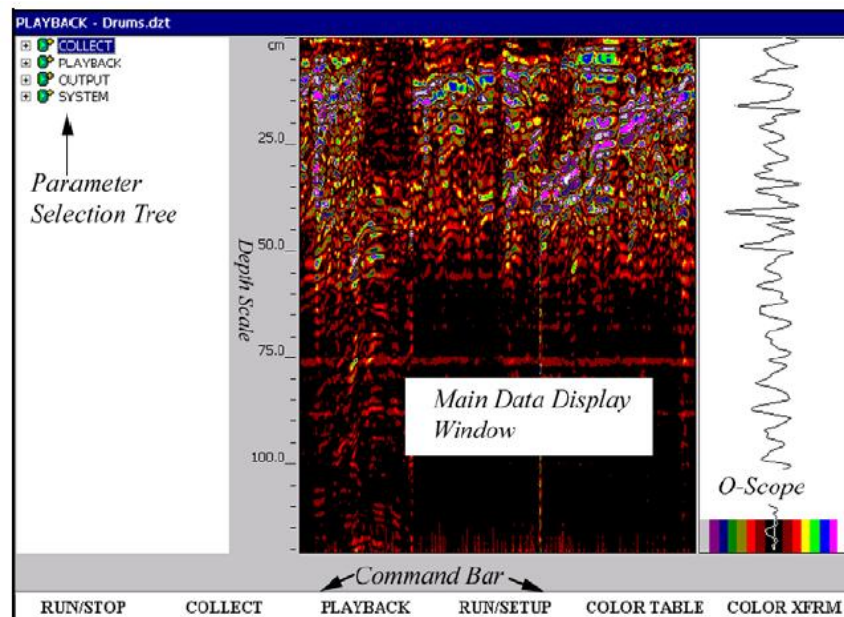
Fig. 3.69 Data Display Windows (Geophysical Survey System Inc.)

Each specimen was scanned in vertical direction so that the location of rebar and tendon duct could be verified. The horizontal scan along the length of tendon ducts as well as the locations that no tendon duct or rebars are presented was carried out.

3.11.2 Portable Impact-Echo System (PIES)

The application of PIES for simple thickness measurements on large components may be readily learned. However, for other complicated applications an in-depth knowledge of the technology and its limitation is required. There are many variables such as geometrical shape,

107

wave speed calibration, speed and length of sampling and impactor selection that significantly affect the test results. Figure 3.70 shows a typical view of the PIES instrument. To maximize the benefits of this technology, the operators should be aware of the complexity of the device and be precisely trained. The field kit of the PIES instrument consists of the following items: (i) digitizer; (ii) iPaq computer; (iii) battery; (iv) two transducers; (v) cable: digitizer- ipaq; and (vi) power cable: battery- digitizer.

Fig. 3.70 Field Kit of impact-echo PIES instrument (Qualitest International Inc.)

3.11.2.1 Digitizer

PIES digitizer consists of two identical channels; single channel (channel 1 or 2) and both channels. Each channel has the following sampling rates which are user selectable: 10 KHz, 20 KHz, 50 KHz, 100 KHz, 200 KHz, 500 KHz, 1 MHz, and 2 MHz. The sampling rate determines the resolution of the signals as well as sensitivity of the instrument to high or low frequency signals.

3.11.2.2 iPaq Computer and Cables

The PIES system uses Microsoft Pocket PC 2002 as its operating system. This operating system is standard based on the handheld computer models. The cabling system is sold by Compaq based on iPaq handheld computer.

3.11.2.3 Battery

The battery is a sealed gel 12V. The charger can be plugged into any AC source powering 90- 240 volts. A fully discharged battery takes 8 hours to recharge and can power approximately 12 hours.

3.11.2.4 Transducers

The surface movements caused by arrival of P-waves are determined by piezoelectric transducers. These movements are then transformed into electrical voltages that can by captured by digitizers. The transducers are very sensitive precision instruments and should be handled with great caution.

3.11.2.5 Impactors

The PIES impactors are stainless steel balls set into stylus pens. The PIES instrument consists of four different sizes of impactor. However, other types of impact-echo instruments may include more sizes. The approximate diameter of each impactor for PIES instrument is as follow: 3.2 mm (1/8″); 6.4 mm (1/4″); 9.4 mm (3/8″); and 12.7 mm (1/2″). Based on the frequency to be generated, the size of the impactor can be selected. The selection of impactor is very important since it determines the contact time (duration of impact). The contact time of the impact is critical in determining the depth and size of the internal defects since it determines the frequency (wavelength) of the stress waves. The stress waves created by impactors generate a wide range of frequencies. However, a small ball will generate a higher range of frequencies than larger ball sizes.

3.11.3 Half-Cell Potential Device, Cor- Map II

Cor-Map II is a product of JAMES Instruments Inc. that conforms to ASTM C-876 standard method of Half- Cell Potential of uncoated reinforcing steel in concrete. The electrode used is designed to perform the test in all vertical, horizontal and inverted positions. The system can be used to locate corroding steel reinforcement inside concrete structures. The nature of corrosion is the transmission of energy in different sections of the steel

reinforcement which can be measured by half-cell potential. Corrosion occurs at anodic side and ions are released into the electrolyte. A reference electrode named as copper-copper sulphate solution (Cu/CuSo4 Half-Cell) with a stable electrochemical potential can determine the relative energy level. An integrated high impedance voltmeter is connected between the reinforcing steel and concrete surface. The potential measurement displayed on the grid of the Cor-Map II is the indication of electrical energy level and corrosion activity of reinforcing steel adjacent to the reference half-cell (Cu/CuSo4). The precise measurement of corrosion activity depends on the direct electrical connection to the exposed reinforcing steel. The Cor-Map II is designed to break down the readings into seven categories from highest level of corrosion, A, to the lowest level, G. The seven categories provided in the Table 3.5 can be used for a detailed analysis of the voltage.

Table 3.5 Categories and their voltages for possible corrosion in Cor-Map II

Category	Voltage	Remark
A	-0.420	A&B= 90% chance corrosion is occurring in this area
B	-0.350	
C	-0.280	C&D= corrosion activity over this area is uncertain
D	-0.210	
E	-0.140	E-G= 90% chance that no corrosion activity occurs over this area
F	-0.070	
G	-0.000	

CHAPTER IV

EXPERIMENTAL FINDINGS

4.1 General

The main purpose of this research was to find out the anomalies inside the post-tensioning bridge deck elements. Recently, the problem with deterioration of post-tensioning wire strands due to corrosion-induced chloride, wire breaks and voids, especially at negative bending moment region in which the tendons are close to the top surface, has been of significant concern. In such cases, due to fracture occurrence on the top surface at bridge deck support locations (Piers), water resulting from rain or snow intrudes inside the concrete surface crack, cracked ducts and voids. If water contains chloride ions, it generates a passive film around the wire strands, leading to corrosion. Correspondingly, wire fractures are resulted from corrosion itself. Voids are mainly generated due to (i) insufficient grouting process, (ii) inaccessibility of duct to be grouted, or (iii) settlement of grouting materials down from the high points of curved ducts at the negative moment region. Therefore, to ease the inspection process, attention has recently been paid to the use of non-destructive testing methods without concrete invasion to find out such deficiencies inside the post-tensioning tendon ducts. In order to contribute to the above-mentioned objective, eight full-scale bridge deck segments were constructed as stated in Chapter III. This chapter presents the experimental findings using GPR, Impact-echo and Half-cell potential technologies. This research went further to demonstrate the use of vacuum grouting in filling the detected voids at high point of curved ducts.

4.2 Ground Penetration Radar Test

Ground Penetrating Radar (GPR) is a non-destructive geophysical method that produces a continuous cross-sectional profile or record of subsurface features, without drilling, probing, or digging. GPR profiles are used for evaluating the location and depth of metals placed into the concrete elements. In post-tensioning systems, the tendon strand paths are determined using ground penetration instrument. The method found to be successful and reliable to quickly locate metal ducts and reinforcing steel bars. In case of post-tensioning system using plastic ducts, the ducts can be located by experienced operators looking for

characteristics of the bundled strands inside the ducts rather than the duct itself.

4.2.1 GPR Principle

The principle of GPR is based on using electromagnetic short-pulse radar transmitted into the surveyed materials. The pulse for concrete investigations usually ranges from 1 to 3 nanoseconds in duration and often contains reflected peaks at surface, internal interfaces and bottom surface. The theory of electromagnetic wave propagation into concrete structures found to be complex because the transmitted and reflected waves are affected by (relative) dielectric constant and conductivity of the materials (ACI 228.2R). A material dielectric constant is the amount of electrostatic energy stored per unit volume for a unit potential gradient. Typical values of relative dielectric constant (ε_r) of materials are given in Table 4.1.

Table 4.1 Range of relative dielectric constant (Carino, 1994)

Material	Relative dielectric constant (ε_r)
Air	1
Portland Cement Concrete*	6 to 11
Bituminous Concrete*	3 to 5
Gravel*	5 to 9
Sand*	2 to 6
Rock*	6 to 12
Water	80

*ASTM D 4748

As shown in the table, relative dielectric constant of water is much higher than other materials. This shows that the dielectric constant of concrete is significantly affected by moisture in concrete. Once the relative dielectric constant of materials is known, the speed of electromagnetic waves C for low loss materials can be calculated by the following equation:

$$C = \frac{C_0}{\sqrt{\varepsilon r}}$$
(4.1)

Where: C_0 = speed of light in air (3×10^8 m/s), and ε_r = relative dielectic constant.

The depth of the reflecting interface (D) can then be evaluated by measuring the round

trip travel time (t) between surface and interface boundaries.

$$D = \frac{C.t}{2}$$
(4.2)

The difference in dielectric constant of dissimilar materials at interface determines the reflected energy. Reflection coefficient which is the ratio of the reflected to incident amplitudes of the electromagnetic field at an interface is given by the following formulas (Clemena, 1991; Bungey and Millard, 1993).

$$\rho_{1,2} = \frac{\sqrt{\varepsilon r1} - \sqrt{\varepsilon r2}}{\sqrt{\varepsilon r1} + \sqrt{\varepsilon r2}}$$
(4.3)

Where;

$\rho_{1,2}$ = reflection coefficient

$\sqrt{\varepsilon r1}$ = relative dielectric constant of Material 1

$\sqrt{\varepsilon r2}$ = relative dielectric constant of Material 2

When the dielectric constant of material 2 is greater than material 1 such as concrete/steel interface, there would be a phase reversal (change in polarity) of the reflected waves that means the positive part of the wave reflected as a negative part.

4.2.2 GPR Test Results for Specimens No. 1, 2 and 3

GPR test was performed on the bridge deck specimens No. 1, 2 and 3. The three specimens have similar configurations with respect to overall dimensions, rebar and tendon arrangements. The GPR test was carried out on each of the model in both vertical and horizontal directions. In each direction, specific characteristics of rebar and tendon ducts were imaged by the device. It should also be noted that because the images were processed with enhanced gain for clear visibility, in most figures, the entire image was shifted down for a depth of 40-50 mm from point of scan. Specimen No. 1 was scanned vertically in the direction of arrow V (hereafter V is referred to vertical direction) as shown in the Fig. 4.1. Figure 4.2 shows the resulting image from GPR vertical scan. The location of rebar and metal ducts are clearly shown in the image. While passing the antenna, the first longitudinal rebar (Rebar 1) was scanned at a distance of 100 mm and a depth of 50 mm from the point of scan. The rebar shows a bright hyperbolic shape in the image. The second scan corresponds to the metal duct (duct 1) located at 150 mm depth and 200 mm length from the scan point. It should be noted

that the 100-mm diameter duct 1, shown in Fig. 4.1, is located at mid-depth of the deck, 200 mm to the top face. However, the signals from antenna were reflected at the exterior side of the duct as reflected in the GPR image in Fig. 4.2. The second longitudinal rebar and other metal ducts are located in the image at depths of 50 and 150 mm, respectively, showing hyperbola shapes as pointed out in the Fig. 4.2.
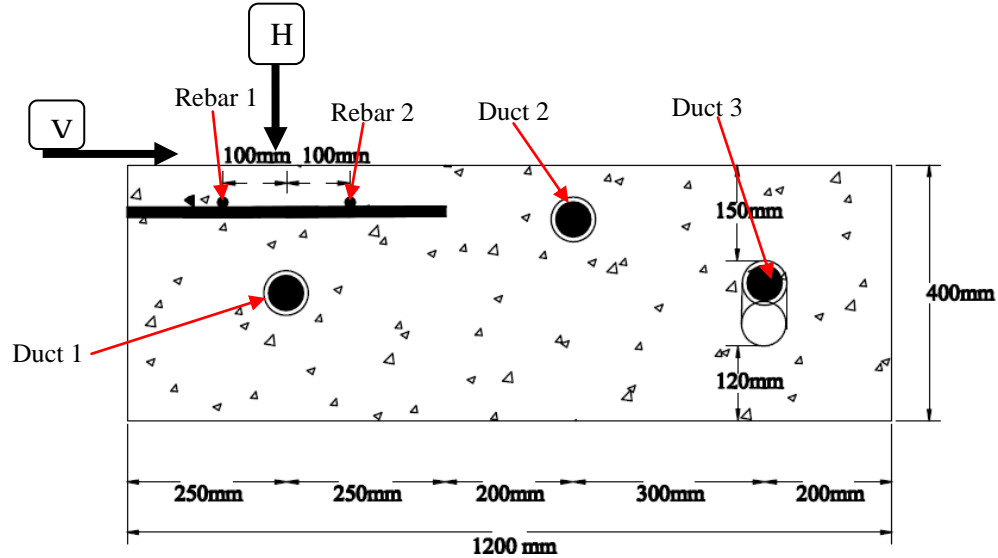
Fig. 4.1 Specimens No. 1, 2 and 3 showing the direction of GPR scan
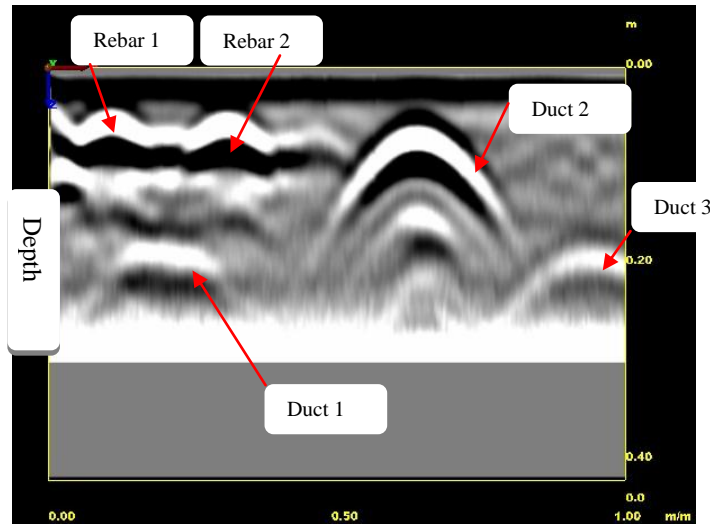
Fig. 4.2 GPR vertical scanning of specimen No. 1

(the entire image was shifted down 40mm due to enhanced gain)

Figure 4.3 shows horizontal scan (H1) taken from the GPR device, with the linescan

path shown in Fig. 4.1 (H corresponds to horizontal direction). In this image, the six transverse rebar along the 1200 mm length of the specimen are shown in bright hyperbolic shapes. At 200 mm depth, a continuous bright line is observed showing the scan along the length of tendon duct 1. However, the longitudinal rebar 1 could not be clearly shown in the image since the electromagnetic signals from antenna pass conically through the concrete element and may not intersect the small size rebar located close to the surface.
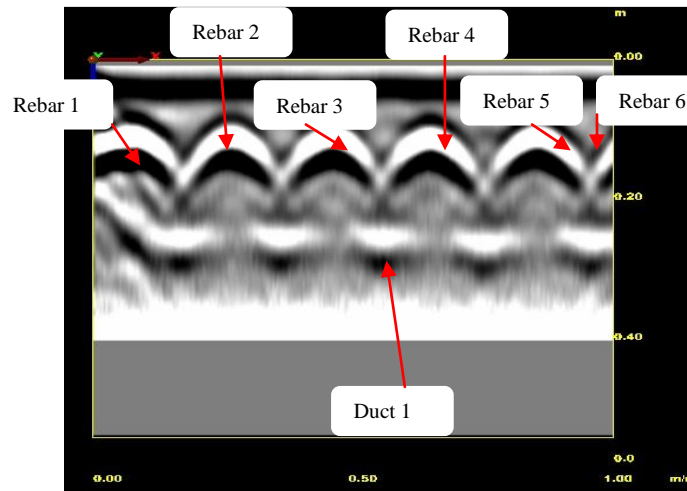
Fig. 4.3 GPR horizontal scanning (H1) of specimen No. 1

4.2.3 GPR Test Results for Specimens No.4 and 5

GPR test was performed on specimens No. 4 and 5 in both vertical and horizontal directions as shown in Fig. 4.4. These specimens are identical with respect to overall dimensions, rebar and tendon/duct arrangements. These specimens are characterised by the presence of metal and plastic ducts of different sizes (50 and 110 mm diameters) in addition to two layers of mesh reinforcement placed near each face of the specimen as shown in Fig. 4.4. In each vertical and horizontal direction, the rebar and metal ducts were clearly identified and located by the device. However, due to penetration of radar into plastic duct, it was uncertain to differentiate between the metal and plastic ducts. Consequently, it was understood that radars are reflected by steel strands rather than plastic duct itself.

Specimen No. 5 was scanned vertically in the direction of arrow V as shown in the Fig. 4.4. Figure 4.5 shows the resulting GPR image, on which the steel rebar and metal ducts

115

are clearly shown. While passing the antenna, the first longitudinal rebar was scanned at a distance of 100 mm and a depth of 50 mm from the point of scan. Steel rebar, metal ducts and prestressing cables show a bright hyperbolic shape in the image. The second scan from left to right corresponds to the reflection of radar from the prestressing cable inside the plastic duct (Duct P1) located at 150 mm) depth and 180 mm length from the scan point. The schematic diagram in Fig. 4.4 shows that the metal duct "duct M1" is placed at the same line as the plastic "Duct P1". However, the GPR scan of Duct M1 shows that concrete depth to the metal duct is 130 mm which is slightly smaller than concrete depth of Duct P1. In addition, the distance of Duct M1 to the scan point is measured at 430 mm, proving that the signals are reflected from metal ducts. Similar differences in the concrete depth to the metal and plastic ducts were observed for Duct P2 (the plastic duct) and Duct M2 (the metal duct) of 100 mm diameters. Specimen No. 5 was also scanned horizontally in the direction H shown in Fig. 4.4. The GPR scan was performed along the length of the metal Duct M2 in a distance near to the edge of the duct. In this scan, all vertical rebar were identified at a depth of 40 mm. Figure 4.6 shows view of the horizontal scan, on which the longitudinal duct M2 was identified as a continuous bright line in the image showing the length of the duct at 100 mm concrete cover (depth) to the scan surface.
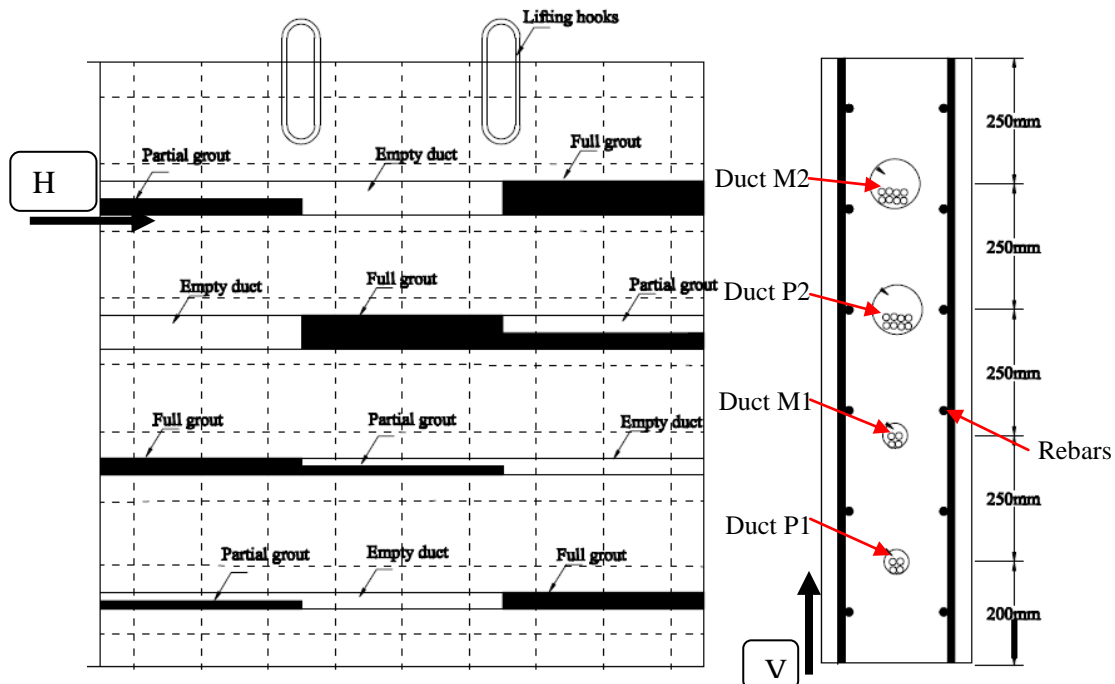
Fig. 4.4 Specimens No. 4 and 5 showing GPR scanning directions

116
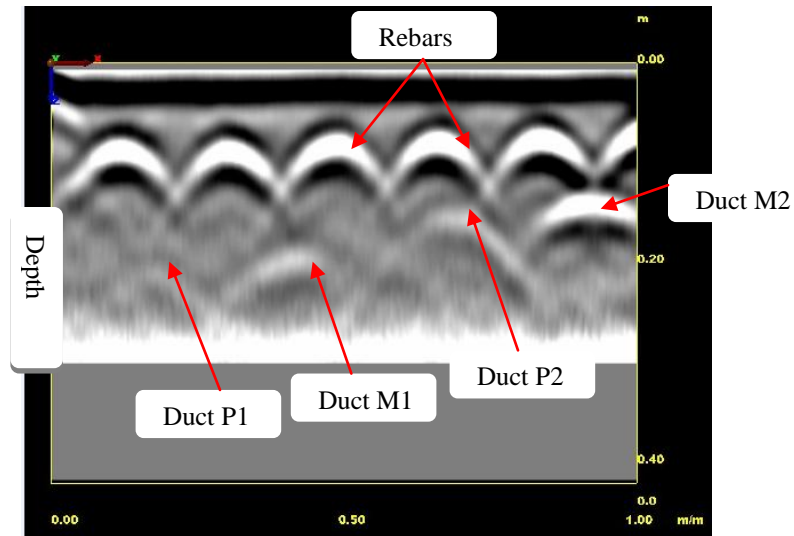
Fig. 4.5 Vertical scan of specimen No. 5 showing the rebar, metal and plastic ducts
(The entire image was shifted down 40 mm due to enhanced gain)
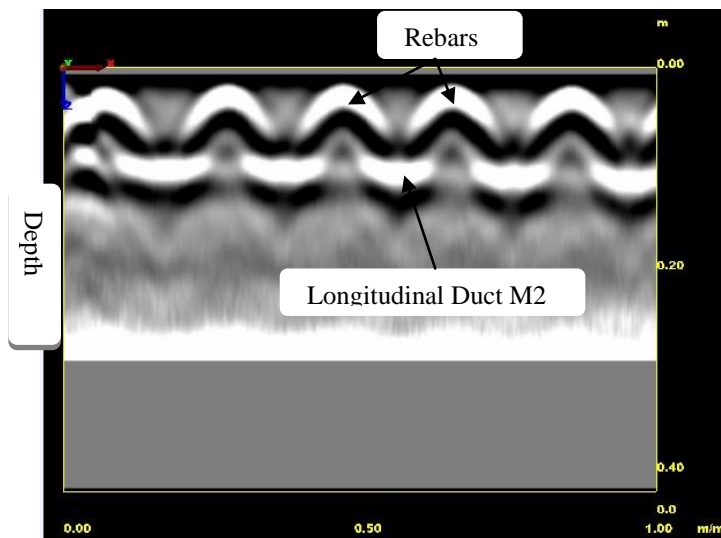
Fig. 4.6 Horizontal scan of specimens No. 5 showing vertical rebar
and longitudinal metal duct M2

In addition, the GPR test was carried out on specimen No. 5 in grid lines to obtain a 3D image of the specimen. Figure 4.7 shows a photo of the specimen during performing the GPR test along the gird lines. The test has been conducted for the argument that GPR is not sensitive to plastic duct and can penetrate beyond the duct, therefore voids inside the plastic duct might be visible. However, the 3D-image obtained indicated that there is strong reflection from steel mesh reinforcement obscuring the reflections from metal and plastic ducts. As a

result, due to masking effect of mesh reinforcement, prestressing cables and hence voids inside the plastic ducts could not be detected.

Fig. 4.7 performing GPR test in gird line of specimen No. 5 to obtain 3D-image
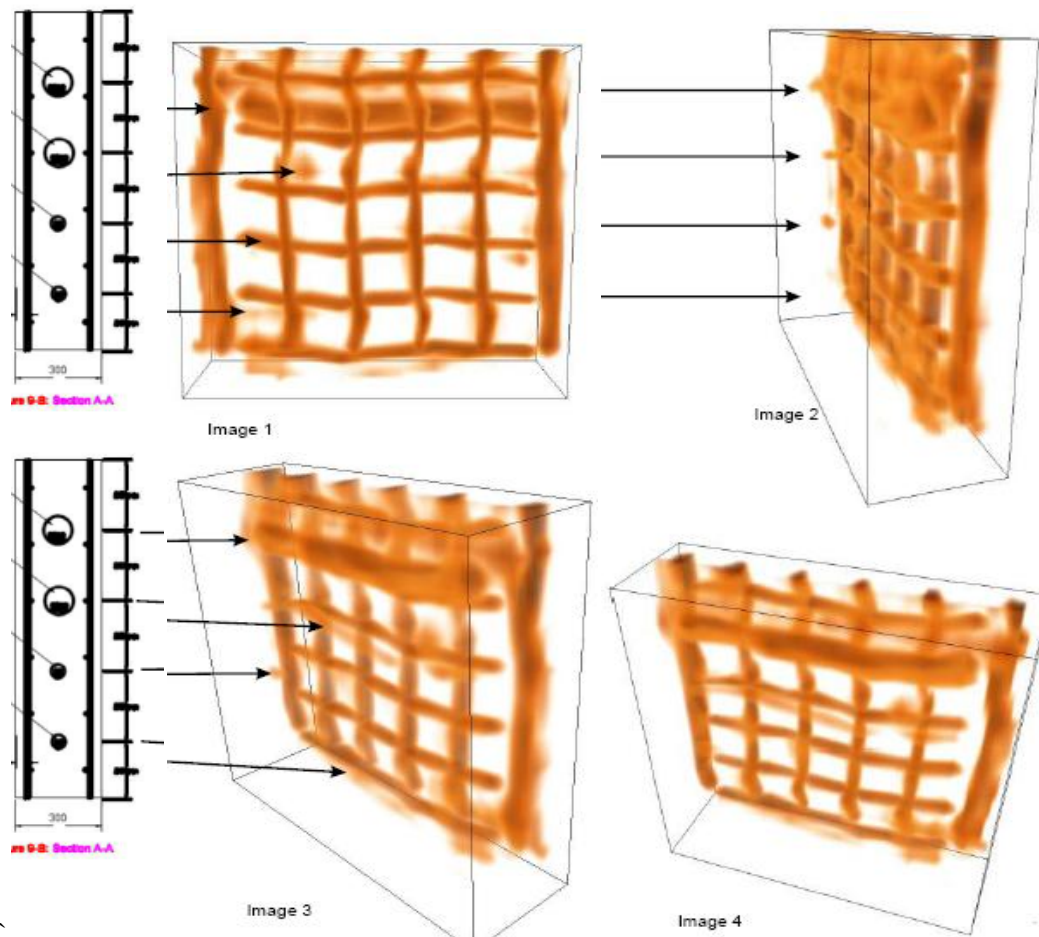
Fig. 4.8 GPR 3D-image showing strong reflection from mesh reinforcement obscuring reflections from metal and plastic ducts (Provided by Tekron Company Inc.)

Figure 4.8 shows a 3D-image of the specimen presenting the location of steel mesh reinforcement and ducts in different positions. It can be observed that the 100 mm diameter metal duct was clearly visible in the 3d image, however, other 50 mm metal duct and the two plastic ducts could not be observed irrespective of the traces that were shown to lead to their locations. Nevertheless, the duct voids could not be detected at all using GPR based per the procedure used in this test. It is worth mentioning that the reinforcing steel mesh at the other side of the specimen did not appear in the 3D image since the GPR was adjusted to scan the specimen up to 150 mm depth.

4.2.4 GPR Test Results for Specimens No. 6 and 7:

Ground penetrating radar was carried out on specimens No. 6 and 7 in both vertical (V) and horizontal (H) directions shown in Fig. 4.9. These specimens represent pre-tensioned concrete beam containing congested steel rebar and prestrssing wire strands, which are commonly used in bridge girders. Vertical scan along depth of the beam showed the two longitudinal rebar (rebar 1 and 2) located at top of the beam with 50 mm concrete cover, as well as the top longitudinal prestressing strand (strand 1) with 75 mm concrete cover and 100mm distance from the scan point. However, the group of rebar and strands (two rebar and two strands) located at mid-depth of the beam were scanned as a single hyperbolic shape as a result of being very close to each other (i.e. congested metal objects in considerably small area. As a result, as the bar spacing decreases, the arch patterns overlap. Also below certain spacing, the individual bars can no longer be distinguished and reflection patterns are analogous to a solid steel plate.
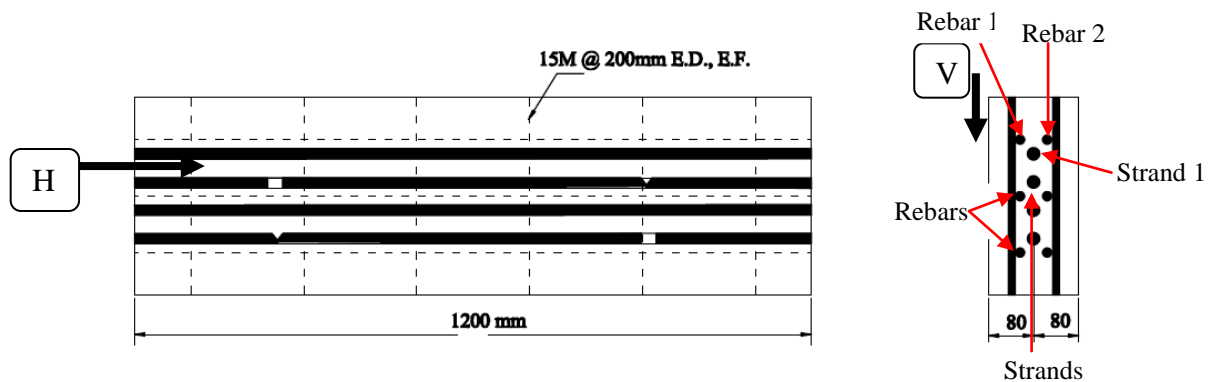
Fig. 4.9 Specimens No.6 and 7 showing GPR scanning direction

119
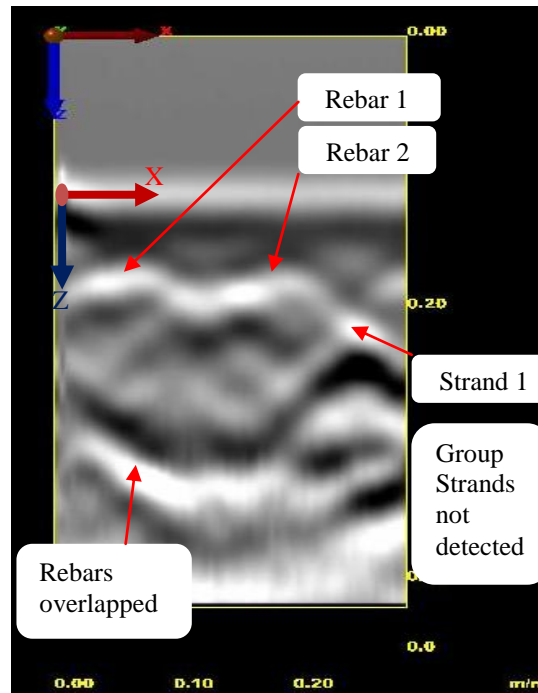
Fig. 4.10 Vertical scan of specimen No. 7 showing rebar and prestressing strands

(the entire image shifted down a distance of about 130 mm)
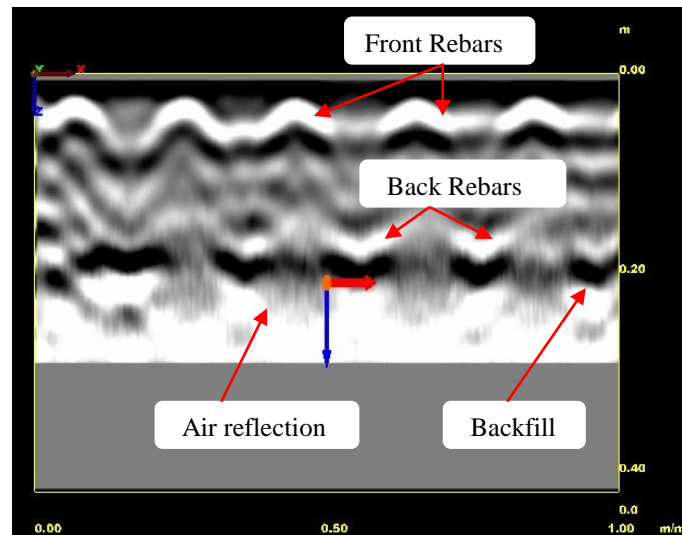
Fig. 4.11 Horizontal scan of specimen No. 7 showing vertical reinforcements on each side

Figure 4.10 shows clear image of the vertical scan along the depth of the beam that reflects this observation. Figure 4.11 provides information about horizontal scan (H) along the length of the beam. In this figure, the vertical rebar placed on each side of the beam are clearly shown. It was observed that the rebar that are closer to the antenna are in brighter stand

compared to the rebar located farther to the antenna.

Generally, at concrete/steel interface because the dielectric constant of steel is significantly higher compared to that of concrete there is a complete reflection and the polarity of the reflected waves are reversed. For this reason, GPR is very effective in locating the metal ducts, steel strands inside the plastic ducts and reinforcing bars in concrete structures. However, because of the strong reflections from metals, the reflections from weaker interfaces beyond the metals may be obscured. In addition, the ability to discern individual bars depends on bar size, bar spacing, cover depth, and the configuration of the antenna (Bungey et al., 1994). Figure 4.12 shows the relationship between minimum individual bar spacing with concrete cover. It is observed that bar spacing in which the individual bar can be detected increases up to concrete cover of about 150 mm. For cover depth of greater than 150 mm, the bar spacing is not significant and bar detection depends mainly on the size of the bar (Bungey et al., 1994).
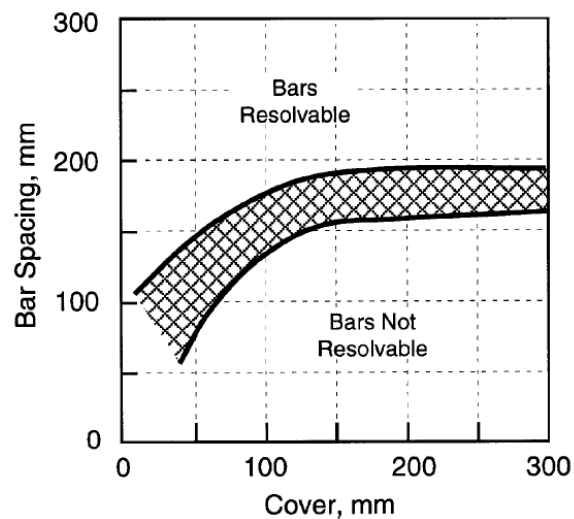
Fig. 4.8 Minimum spacing at which individual reinforcing steel bars can be resolved (adapted from Bungey et al., 1994)

From Fig. 4.12 minimum bar spacing of about 140 mm is required for the bars to be clearly detected for a concrete cover of 40 mm as for specimens No. 6 and 7. Fig. 4.10 shows that the two rebar No. 1 and 2 and strand 1, shown in Fig. 4.9, were first scanned by GPR device. However, due to insufficient bar spacing between rebar 1 and 2 and strand 1 to the adjacent rebar and strand, the scan taken for the rebar shown in Fig. 4.9 was found to be

overlapped, while the scan from strands was undetected.

4.3 Impact-echo Test

Impact-echo is a method of non-destructive test of concrete structures based on the use of stress waves or echoes that propagate through the structure and are reflected by internal flaws such as voids, honeycombing, cracks, metal or external surface which are different in acoustic impedance. Impact-echo can be used to make accurate, non-destructive, ASTM-approved measurements of thickness in concrete slabs and plates, (ASTM C 1383-98a). It can also be used to detect voids in grouted tendon ducts in many, but not all, situations (Sansalone and Street, 1997). The accuracy of method depends on some factors including locations and arrangement of the tendon ducts and the geometry of structure. The principle of impact-echo is based on introduction of a short-duration mechanical impact produced by a small steel sphere into the concrete structure, producing low frequency stress waves, which are reflected by flaws or external surface. Multiple reflections of such stress waves within the structure produce local modes of vibration, and the resulting surface displacements are recorded by a piezoelectric transducer located adjacent to the impact point. The piezoelectric transducer then produces voltage-time signal (called a waveform) that is digitized and transferred to a computer, where it is transformed mathematically (Fast Fourier Transform, FFT) into a spectrum of amplitude vs. frequency. Both the waveform and spectrum are plotted on the computer screen. The dominated frequencies, which appear as peak frequencies in the spectrum are resulted from multiple reflections of stress waves within the structure.

4.3.1 Reflection at Interface

For a concrete structure with dissimilar boundaries, when stress waves travel through material 1 and reach the boundary, some portions of incident waves are reflected at interface between dissimilar materials 1 and 2 and some portions are refracted (transmitted) beyond the interface. For normal incidence (angle of incident stress waves at 90˚), the reflection coefficient, R, is given by the following equation (Krautkrämer, 1990).

$$R = \frac{Z_2 - Z1}{Z_2 + Z1}$$
(4.4)

Where Z1 is the acoustic impedance of material 1 in which the wave approaching the interface

and Z_2 is the acoustic impedance of material 2 beyond the interface. Reflection at interface is due to the change in acoustic impedance (Z) of the material which is a product of wave speed and density of the material. Generally, acoustic impedance is interfered with the passage of sound waves by objects in the path of those waves. It equals the velocity of sound (Cp) in a medium multiplied by the density of the medium (ρ) and given by equation 4.5. The following are approximate Z- values for some materials (Sansalone and Carino, 1991).

$$Z = Cp \times \rho \tag{4.5}$$

Table 4.2 Acoustic impedance of materials

Material	Specific Acoustic Impedance (Kg/ m²s)
Air	0.4
Water	0.5×10^6
Soil	0.3 to 4×10^6
Concrete	7 to 10×10^6
Steel	47×10^6
Polyethylene	1.76×10^6

As given in the table above, acoustic impedance of air is significantly smaller than concrete. Therefore, at concrete/air interface, there would be almost complete reflection of stress waves. This is the main advantage of impact-echo in locating internal defects within solids. The reflection coefficient given in Eq. (4.4) can be positive or negative depending on the acoustic impedance of the materials 1 and 2. When acoustic impedance of material 1 is relatively higher than material 2 ($Z1 > Z_2$) such as concrete-air interface, the reflection coefficient approaches a negative value. The change in the sign means that the stress waves undergo a phase change upon reflection. Thus, the incident P-waves with compressive stress reflects as tensile stress at interface. Figure 4.13 shows schematic of a layered plate where $Z1 > Z_2$ and its corresponding waveform and spectrum produced by reflection at interface. As shown in the figure, the tensile stress arrived at surface produces a downward displacement of the surface (2P). This tensile stress is then converted into compressive stress at concrete/air interface and cycle repeats again. The frequency of P-wave reflection can be determined using the following equation (Sansalone and Streett, 1997).

$$f = \frac{\beta \, Cp}{2 \, A} \tag{4.6}$$

Where Cp is the P-wave speed in concrete and A is the characteristic dimension and β is a shape factor determined by geometry of the concrete element.
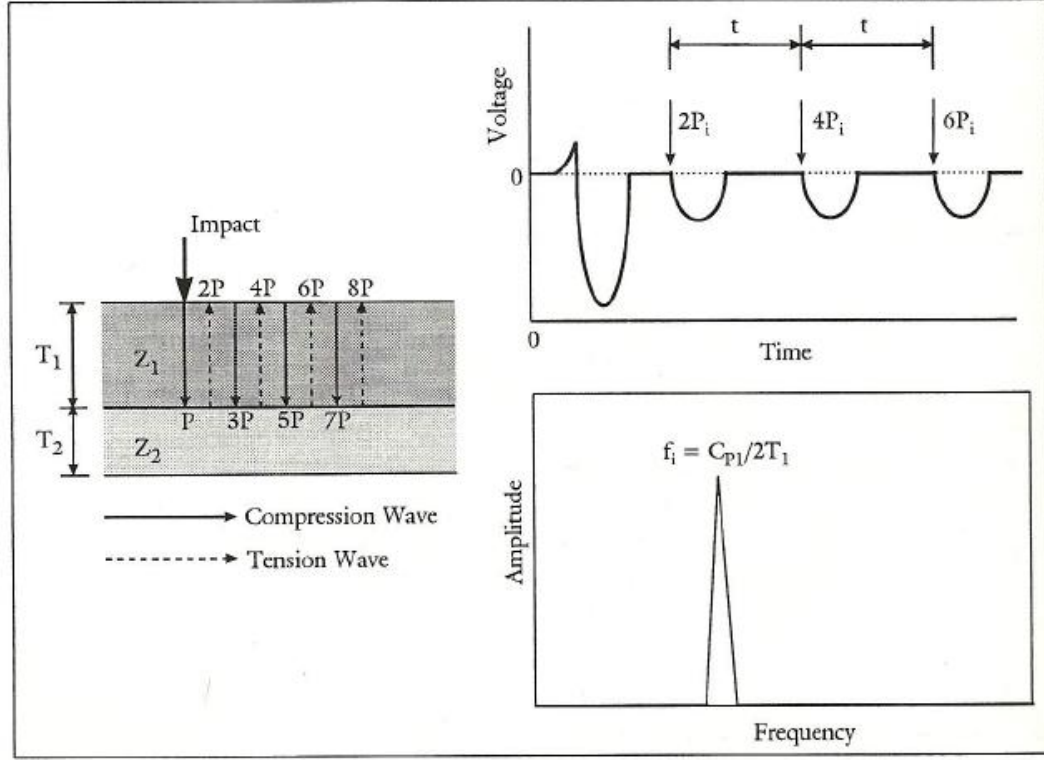
Fig. 4.9 Waveform and spectrum patterns where Z1 > Z_2

(Sansalone and Streett, 1997)

For a solid plate, the characteristic dimension is the thickness of the solid, T, and the shape factor, β, is 0.96. Therefore, Eq. (4.6) can be written as:

$$f = \frac{0.96 \, Cp}{2 \, T} \tag{4.7}$$

The reflection coefficient given in Eq. (4.4) is positive when acoustic impedance of material 2 is relatively higher than acoustic impedance of material 1 (Z_2 > Z1), therefore, there is no change in the sign of the stress waves. This mainly occurs at concrete-steel interface. In this case, the compressive P-wave stress reflects back as a compressive stress again until

reaches a boundary with $Z_2 < Z1$ such as concrete-air interface. When the compressive stress reaches concrete-air at surface, it produces an upward displacement of the surface (2P). At concrete-air interface a change phase occurs and the compressive stress reflects as a tensile stress. This tension wave propagates down through the concrete to be reflected back again as a tensile stress which produces a downward displacement upon reaching concrete surface (4P). Figure 4.14 shows a schematic diagram where $Z_2 > Z1$ with corresponding waveform and spectrum showing that the lower layer has higher acoustic impedance than the upper layer.
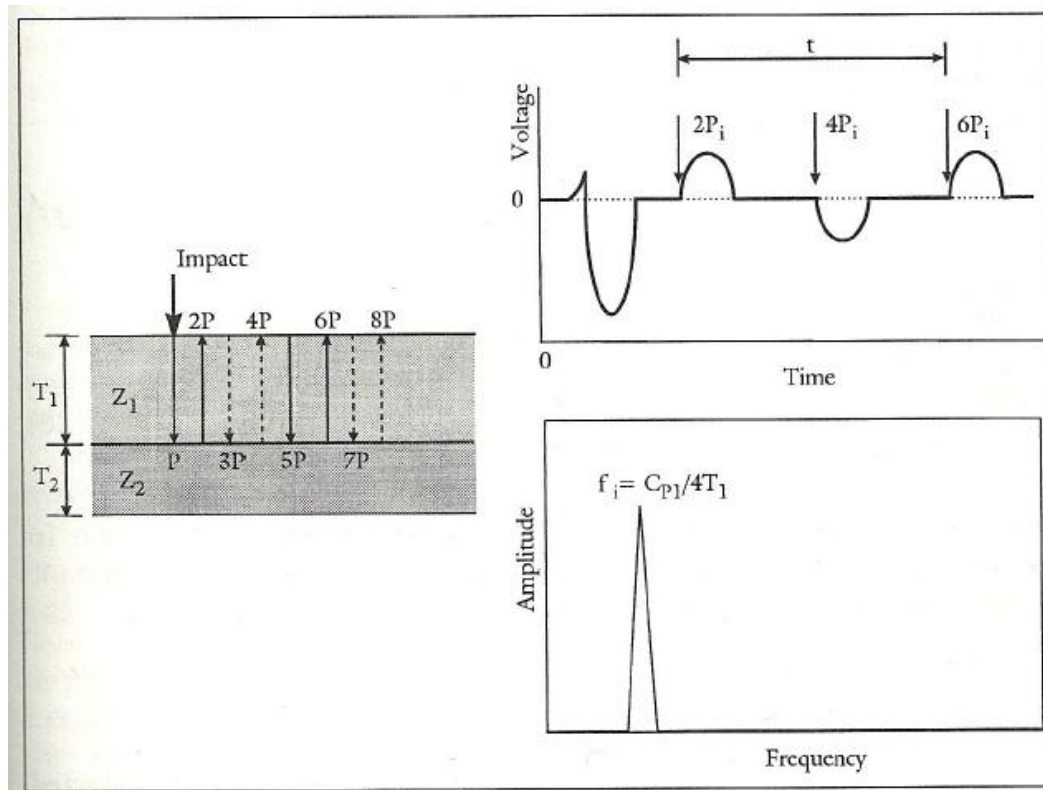
Fig. 4.10 waveform and spectrum patterns where $Z1 < Z_2$

(Sansalone and Streett, 1997)

In this case $(Z_2 > Z1)$ such as concrete- steel interface, the frequency of P-wave reflection can be determined using the following equation (Sansalone and Streett, 1997).

$$f = \frac{Cp}{4\,T} \tag{4.8}$$

In equation (4.8), the factor $\beta = 0.96$ disappeared because in this case, the concrete above the interface is not free to vibrate as a simple plate.

125

4.3.2 Bonded Post-Tensioning (PT) Duct

The reflection coefficient in bonded post-tensioning duct is similar to the case where $Z_2 > Z1$. Thus, the frequency of the multiple reflections of P-waves at grout-strand interface is similar to the equation (4.8), $f = (Cp)/(4d)$. The response from bonded steel strands inside the duct can be predicted using the distance, d, to the nearest strand. Figure 4.15 illustrates the three basic responses that can be possible for a plate containing a single post-tensioning duct in any particular- cross section (Sansalone and Streett, 1997). These are the basic responses that help interpreting the results obtained from post-tensioning systems using impact-echo.
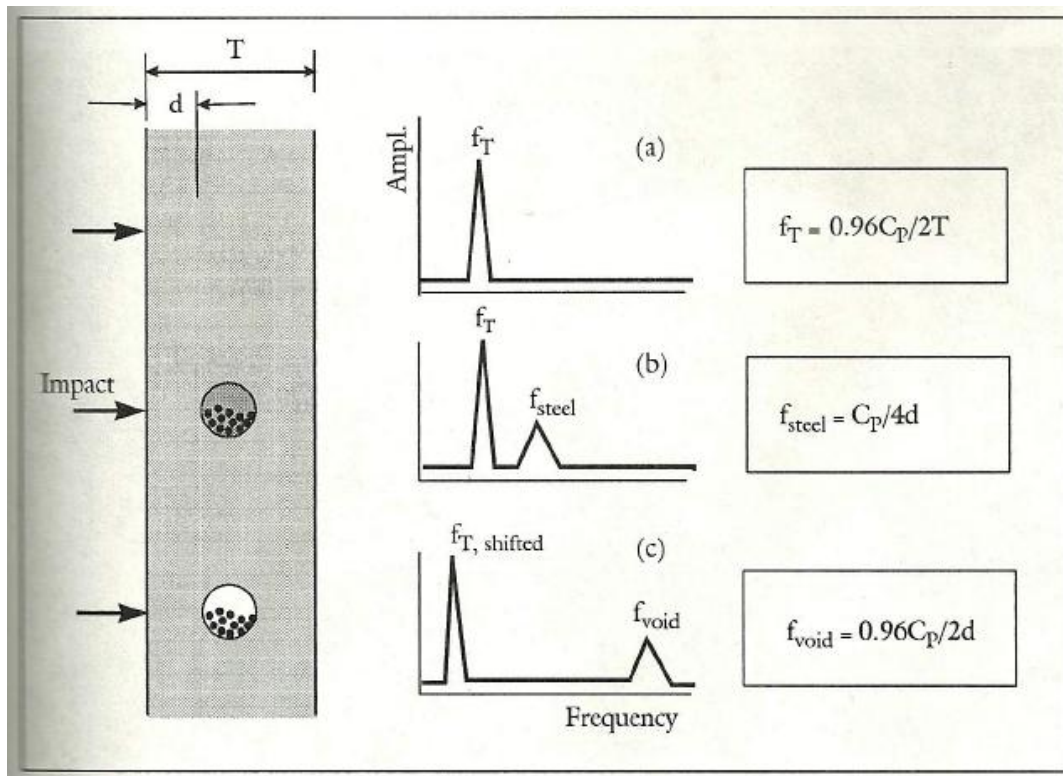
Fig. 4.11 schematic diagram of plate containing PT system; (a) solid plate (b) grouted duct and (c) duct containing a void (Sansalone and Streett, 1997)

4.3.3 Test Procedure

Impact-echo test was carried out on each specimen using the following procedure. First, by using Ultrasonic tool, the round trip travel time within a solid portion of the specimens was determined. The corresponding frequency and consequently the P-wave speed

126

in concrete were determined for each specimen as provided in Table 4.3. Second, the effective use of impact-echo in locating voids inside the ducts requires locating the centerline of tendon duct. This was performed using Ground Penetration Radar. Figure 4.16 shows a photograph of GPR investigating the centerline of tendon duct. Then, the rough expected frequencies of reflected waves from tendon strands and voids inside the duct were calculated for the approximate range of concrete cover to strands or voids. Table 4.4 provides the expected peak thickness frequencies and Tables 4.5 to 4.8 provide the approximate expected frequencies of fully grouted tendon ducts or voids inside the ducts in each sample.

Table 4.3 P-wave speed determination in concrete using Ultrasonic tool

Specimen No.	Round-trip Travel Time (t), μs	$f_p= 1/t$ (KHz)	Thickness (T), (m)	$Cp= \dfrac{2T.fp}{0.96}$ (m/s)
1	181	5.52	0.4	4600
2	180.4	5.54	0.4	4617
3	182.2	5.5	0.4	4583
4	142.6	7	0.3	4375
5	129	7.75	0.3	4844
6	72.2	13.85	0.16	4617
7	71.6	13.96	0.16	4653
Average P-wave Speed, Cp = 4600 m/s				

Fig. 4.12 Use of GPR to locate tendon duct centerline

Table 4.4 Approximated peak thickness frequencies in each specimen

Specimen No.	Cp (m/s)	Thickness (T), (m)	$f_p = \dfrac{0.96\,Cp}{2T}$ (KHz)
1,2,3	4600	0.4	5.52
4,5	4600	0.3	7.36
6,7	4600	0.16	13.8

Table 4.5 Expected fully grouted metal duct peak frequencies, f_p

Specimen No.	Line of impact	Cp (m/s)	Thickness (T), (m)	$fp = \dfrac{Cp}{4T}$ (KHz)
1,2,3	A	4600	0.15	7.67
1,2,3	B	4600	0.05	23
			0.25	4.6
1,2,3	C	4600	0.15	7.67

Table 4.6 Expected ungrouted (voided) duct peak frequencies, f_p

Specimen No.	Line of impact	Cp (m/s)	Thickness (T), (m)	$f_p = \dfrac{0.96Cp}{2T}$ (KHz)
1,2,3	A	4600	0.15	14.72
1,2,3	B	4600	0.05	44.16
			0.25	8.83
1,2,3	C	4600	0.15	14.72

Table 4.7 Expected voided duct and fully grouted tendon duct peak frequencies

Specimen No.	Line of impact	Cp (m/s)	Thickness (T), (m)	$f_p, \text{void} = \dfrac{0.96Cp}{2T}$ (KHz)	$f_p, \text{steel} = \dfrac{Cp}{4T}$ (KHz)
4,5	A	4600	0.125	17.66	9.2
4,5	B	4600	0.125	17.66	9.2
4,5	C	4600	0.100	22.08	11.5
4,5	D	4600	0.100	22.08	11.5

Table 4.8 Expected steel peak frequencies in specimens No. 6 and 7

	Cp (m/s)	Thickness (T), (m)	$f_p = \dfrac{Cp}{4T}$ (KHz)
Rebars	4600	0.055	20.91
Strands	4600	0.075	15.33

Impact-echo test were then carried out along the length of each tendon duct in 100 mm increments. The results of impact-echo test were analyzed to confirm the presence of simulated voids or wire fractures in tendon ducts. After completing the impact echo test and confirmation of voids with the device, one of the voided regions in specimen No. 8 was repaired using vacuum grouting method (refer to section 4.5 for vacuum grouting of voided duct).

4.3.4 Impact-echo Test Results
4.3.4.1 Impact-echo Test for Specimen No. 1

Specimen No.1 contains wire fracture and notch in some portion of each tendon duct (see Fig. 3.1 to 3.4). Impact-echo test results on this specimen showed no sign of wire fracture or notch in all cases. Figure 4.17 shows peak thickness frequency that was taken from a solid portion of the sample. A frequency of 5.56 KHz was taken as peak thickness frequency which was close to the approximated peak frequency given in Table 4.4 (5.52 KHz). Figure 4.18

also shows the spectrum taken from impact echo result where the tendon duct is close to the top surface (section B-B in Fig. 3.1). However, impact-echo test was performed from opposite side where the concrete cover to the tendon duct was 250 mm. At this depth, no sign of wire fracture was found, and peak thickness frequency was also remained as 5.56 KHz.
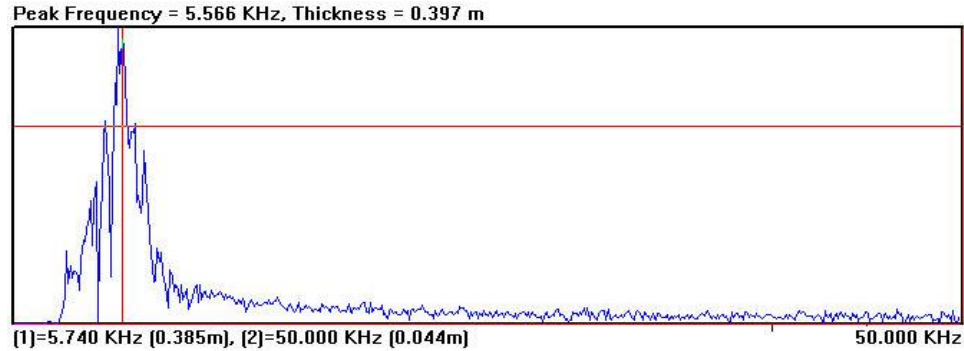
Fig. 4.13 Peak thickness frequency obtained from a solid portion of specimen No. 1
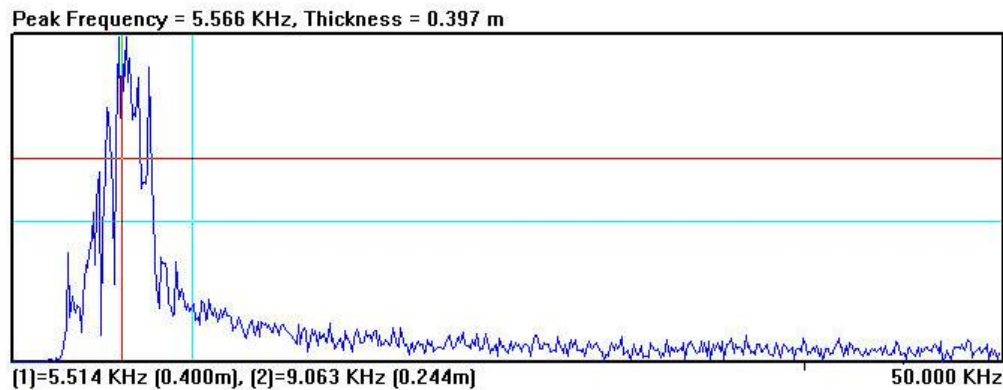
Fig. 4.14 Spectrum obtained from Specimen No. 1, section B-B in Fig. 3.1 at break location, where concrete cover is 250 mm

4.3.4.1 Impact-echo Test for Specimen No.2

Specimen No. 2 contains voids of 20, 60 and 100 mm length, along the length of tendon ducts. Impact-echo test was performed along the length of each duct. The test also conducted on a solid portion of the sample showed a peak thickness frequency of 5.664 KHz as shown in Fig. 4.19, which was very close to expected value (5.52 KHz given in Table 4.4). Results not shown here revealed that void of 20 mm length could not be found in all tendon ducts with variable concrete cover. This might be due to the use of greater size of wavelength of impact compared to the tiny size the void. On the other hand, the void of 60 mm length was

130

found only in section B-B of the sample (Fig. 3.12) where the concrete cover to the tendon was 250 mm. Figure 4.20 shows spectrum obtained from the test on this part. In the spectrum, at the depth of 250 mm, there is a peak frequency of 8.837 KHz corresponding to the P-wave reflection at concrete/air-void interface. The expected peak frequency given in Table 4.6 showed the same peak frequency of 8.83 KHz at void location. In addition, the peak thickness frequency shifted down from 5.52 KHz to 5.176 KHz that confirms the presence of void. Cluster of peaks at the location of dominant peak corresponding to void can be also an indication of void size, since the waves travel around the void to be reflected from bottom face. Void size of 100 mm was found in tendons located in Sections A-A and C-C of Fig. 3.10 where the concrete cover to the tendons was 150 mm. Figure 4.21 shows spectrum obtained from section A-A of the sample where the 100 mm simulated void is located (see also Fig. 3.11). In the spectrum at depth of 153 mm, a small rise in the reflected waves with a peak frequency of 14.426 KHz corresponding to the void was observed, which was close to the expected value of 14.72 KHz given in Table 4.6. The peak thickness frequency also shifted down to 4.98 KHz that confirms the presence of void. The impact-echo test was also carried out at surface where concrete cover to the tendon was 50 mm (Fig. 3.12). The spectrum obtained from this part showed many peaks that are not indication of void inside the duct. Figure 4.22 shows a spectrum obtained in the region where the 60 mm void exists.

Peak Frequency = 5.664 KHz, Thickness = 0.390 m

50.000 KHz
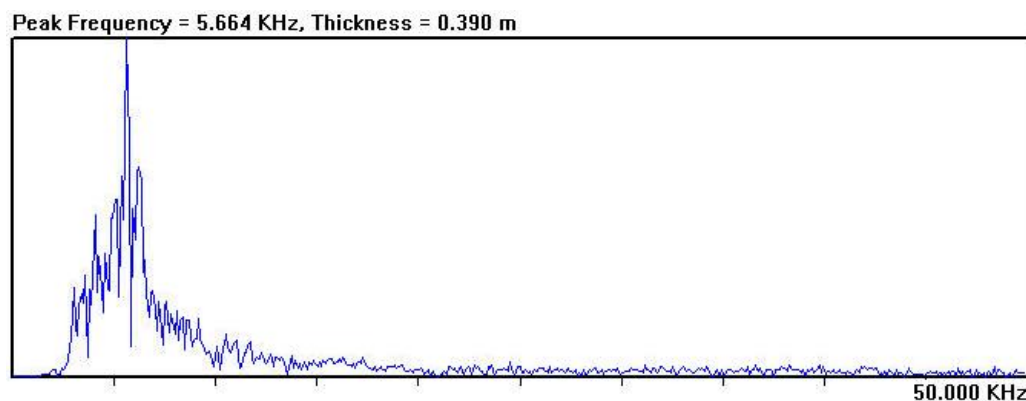
Fig 4.15 Peak thickness frequency obtained from Specimen No. 2 at a solid portion of the specimen

131

Peak Frequency = 5.176 KHz, Thickness = 0.427 m

[1]=5.514 KHz (0.400m), [2]=8.837 KHz (0.250m)   50.000 KHz
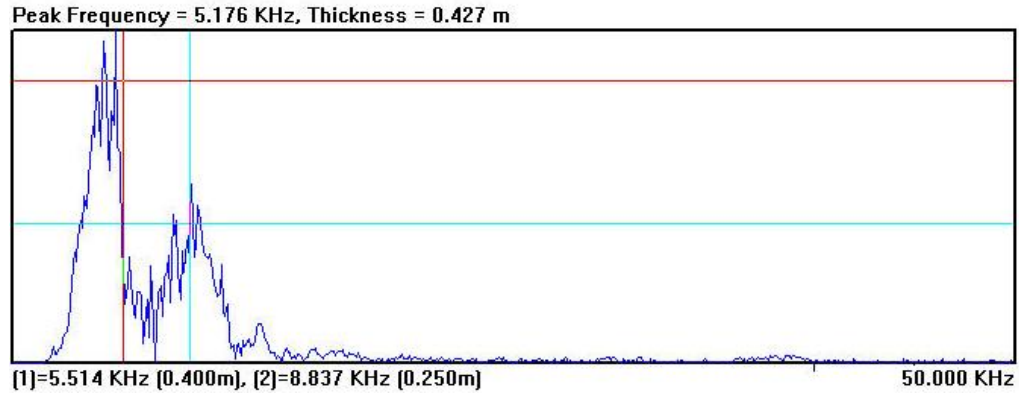
Fig. 4.16 Spectrum obtained at the location of 60 mm void in section B-B (Fig. 3.12) of sample No. 2 with concrete cover of 250 mm to the tendon

Peak Frequency = 4.980 KHz, Thickness = 0.443 m

[1]=5.514 KHz (0.400m), [2]=14.426 KHz (0.153m)   50.000 KHz
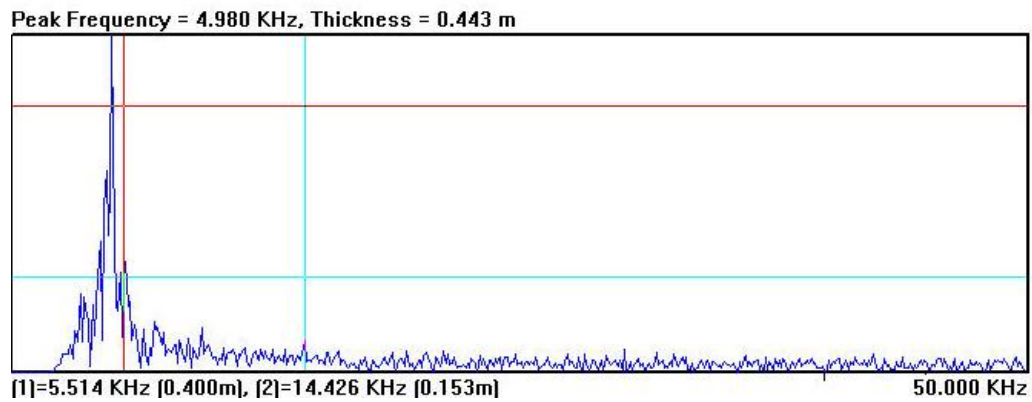
Fig 4.17 Spectrum obtained in the location of the 100 mm length void in section A-A (Fig. 3.11) of specimen No. 2 with concrete cover of 150 mm to the tendon

Peak Frequency = 5.469 KHz, Thickness = 0.404 m

[1]=5.438 KHz (0.406m), [2]=43.882 KHz (0.050m)   50.000 KHz
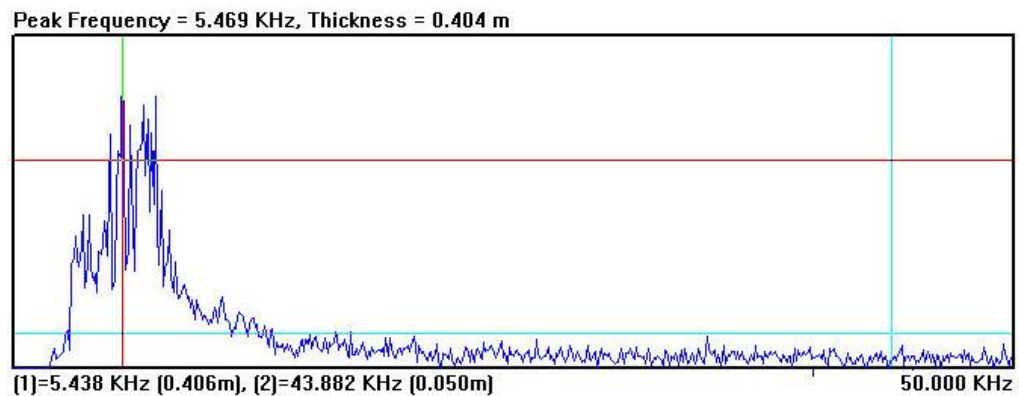
Fig. 4.18 Spectrum obtained at location where concrete cover to the tendon is 50 mm (Fig. 3.12, the test was performed to evaluate the existence of the 60 mm length void in the duct)

132

4.3.4.1 Impact-echo Test Results for Specimen No. 3

Specimen No. 3 contains a limited void size of 60 mm length within the length of each tendon duct. Impact-echo test was conducted on the sample along the length of each duct. The peak thickness frequency, shown in Fig. 4.23, was obtained on a solid portion of the specimen showing a frequency of 5.664 KHz, which is close to the expected peak thickness frequency of 5.52 KHz given in Table 4.4.

Peak Frequency = 5.664 KHz, Thickness = 0.390 m

(1)=5.514 KHz [0.400m], (2)=49.622 KHz [0.044m]   50.000 KHz
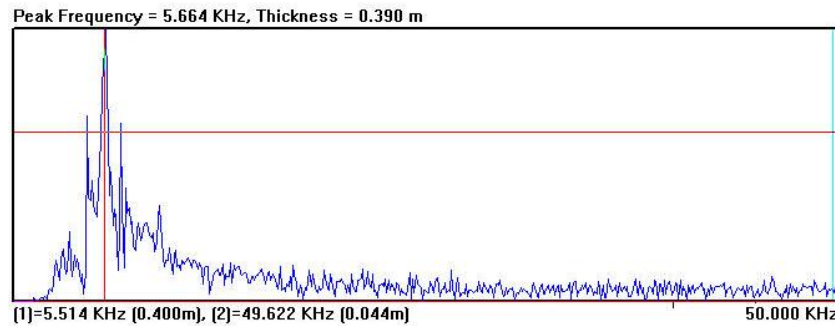
Fig. 4.19 Peak thickness frequency obtained from a solid portion of specimen No. 3

Peak Frequency = 5.176 KHz, Thickness = 0.427 m

[1]=5.514 KHz [0.400m], [2]=14.728 KHz [0.150m]   50.000 KHz
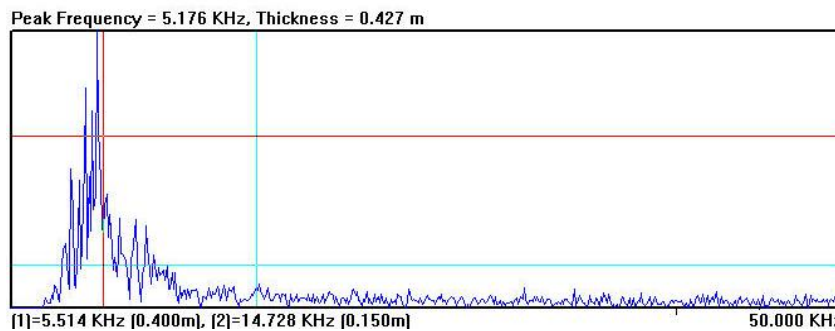
Fig. 4.20 Spectrum obtained at 60 mm length void location in Fig. 3.18 in specimen No. 3

Peak Frequency = 4.980 KHz, Thickness = 0.434 m

[1]=5.514 KHz [0.392m], (2)=9.063 KHz [0.238m]   50.000 KHz
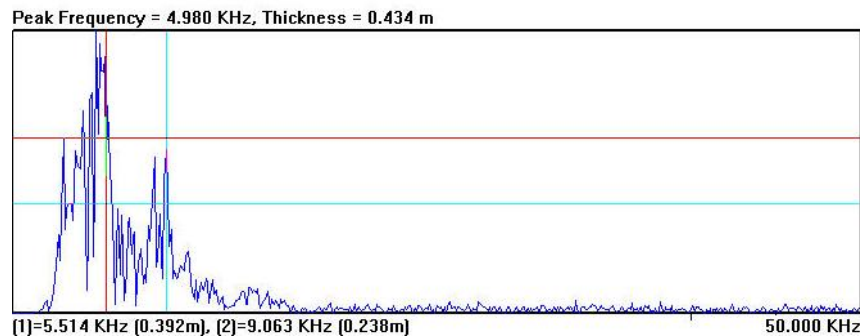
Fig. 4.21 Spectrum obtained at the 60 mm length void (Fig. 3.19) in specimen No. 3, where concrete cover to the tendon was 250 mm

133

Peak Frequency = 5.273 KHz, Thickness = 0.410 m

[1]=5.514 KHz (0.392m), [2]=13.973 KHz (0.155m)   50.000 KHz
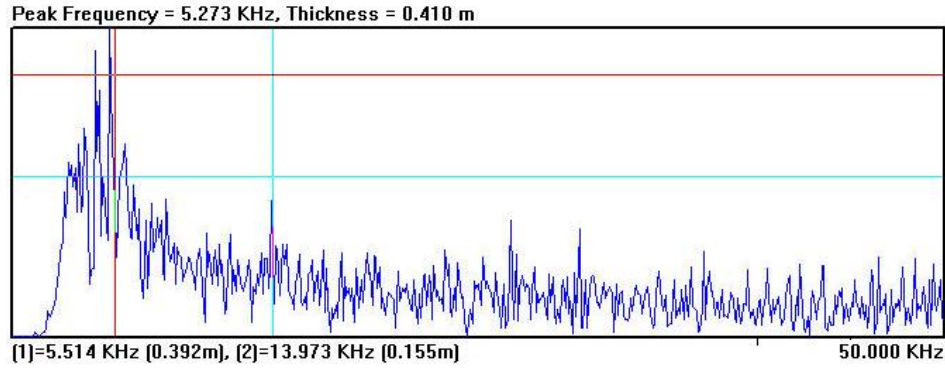
Fig. 4.22 Spectrum obtained at 60 mm length void location (Fig. 3.20) in specimen No. 3

Peak Frequency = 5.469 KHz, Thickness = 0.404 m

[1]=5.514 KHz (0.392m), [2]=43.278 KHz (0.050m)   50.000 KHz
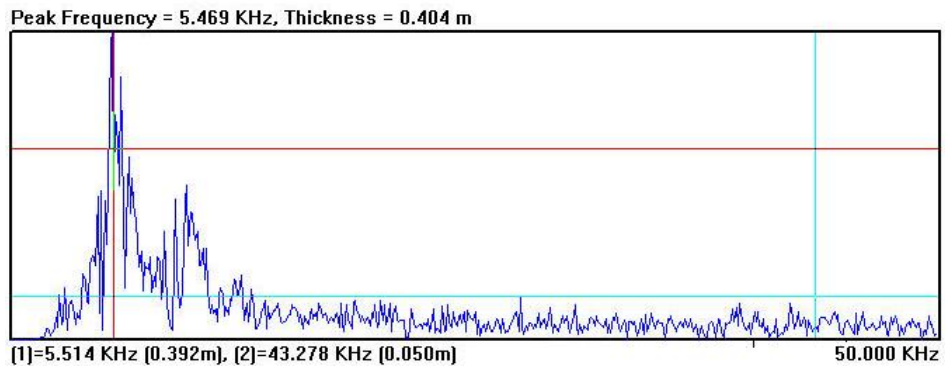
Fig. 4.23 Spectrum obtained at 60 mm length void location (Fig. 3.19) in specimen No. 3, where the concrete cover to the tendon was 50 mm

The 60 mm void size in each tendon was located using impact-echo device at concrete cover of 150 mm and 250 mm. However, conducting impact-echo test in the region where the tendon duct has a concrete cover of 50 mm showed no sign of void in the duct. In this region, the impact-echo was carried out on the opposite side of the tendon where the concrete cover to the tendon was 250 mm, and the presence of void was confirmed. Figures 4.24 to 4.27 show the spectrum obtained at the location of 60 mm simulated void in each duct. The spectrum in Figs. 4.24 and 4.26 show higher frequencies of 14.728 KHz and 13.973 KHz corresponding to the presence of void at 150 mm depth to the tendon (see Figs. 3.18 and 3.20). These frequencies are close to the expected peak frequency of 14.72 given in Table 4.6. The shifted peak frequencies of 5.176 KHz and 5.273 KHz also confirm the existence of void. Figure 4.25 show the spectrum obtained at the location where the void exists in the tendon duct in which the concrete cover to the tendon is 250 mm (see Fig. 3.19). The frequency obtained at this concrete depth is 9.06 KHz that confirms the presence of the void, similar to the expected

peak frequency of 8.83 KHz at 250 mm depth. Also, at the location of dominant peak corresponding to void, there are cluster of peaks showing that the wave is reflected along its path while turning around the void location. Therefore, if the length of this cluster of peaks is large, it can be assumed there is a large void size at that location. However, the spectrum shown in Figure 4.27 was obtained at a location with 50 mm concrete cover to the tendon. There was no indication of void in the spectrum compared to the expected frequency of 44.16 KHz given in Table 4.6.

4.3.4.1 Impact-echo Test Results on Specimen No. 4

Impact-echo test was carried out on specimen No. 4. This specimen contained partially-grouted and empty voids along 50 and 100 mm lengths in the plastic and metal ducts. The spectrum in Fig. 4.28 showed a peak thickness frequency of 7.32 KHz obtained from a solid portion of the specimen. Concrete cover to the 50 mm diameter plastic and metal ducts was 125 mm with an expected peak frequency corresponding to void of 17.66 KHz (Table 4.7). However, because plastic is of lower acoustic impedance than surrounding concrete or grout, stress waves could not propagate easily into plastic, complicating the attempt to detect void inside the plastic ducts. Impact-echo results on 50 mm diameter plastic duct indicated that stress waves were reflected at concrete/plastic interface and the presence of void in the duct is uncertain. Figure 4.29 shows the spectrum obtained from 50 mm diameter plastic duct in specimen No. 4. The spectrum showed a frequency of 17.67 KHz at concrete depth of 122 mm which rather supposed to be reflected from plastic duct than the void inside the duct. The uncertainty is due to slightly lower acoustic impedance of plastic duct compared to concrete, resulting in absorption of energy by plastic duct. The test performed on the 50 mm diameter metal duct showed no sign of void inside the duct. This might be due to the use of improper impactor size. The spectrum obtained at this location showed a peak frequency of 23.4 KHz at a depth of 94 mm, which may confirm the presence of defect such as honeycombing or delimitation in the concrete deck. The frequency obtained was considerably greater than the expected frequency showing that anomaly occurred within the concrete cover depth to the 50 mm diameter metal duct. Therefore, a larger impactor producing larger wavelength must have been used to detect void inside the 50 mm diameter metal duct. Figure 4.30 showed the spectrum obtained from the duct showing anomaly in concrete rather than void inside the duct.

Impact-echo test performed on the 100 mm dia. plastic duct showed uncertainty of existing void inside the duct. The expected peak frequency corresponding to void inside the plastic duct was calculated to be 22.08 KHz at 100 mm concrete cover to the plastic duct. Figure 4.31 shows the spectrum obtained in the region of the specimen where the ungrouted duct exists. In the spectrum, a frequency of 22.28 KHz at 100 mm depth was obtained. This frequency was slightly larger than expected frequency representing the waves that were reflected at interface rather than from the void. Figure 4.32 also shows the spectrum obtained in the region of partially-grouted duct. Peak frequency of 23.79 KHz at a depth of 93 mm showed that waves were reflected from plastic duct rather than from the void. The test performed on the 100 mm dia. metal duct showed the presence of void only in the partially-grouted region. The expected peak frequency corresponding to the void was calculated as 22.08 KHz (Table 4.7). Figure 4.33 is the spectrum obtained from partially-grouted duct showing a peak frequency of 21.9 KHz at 100 mm depth which was close to the expected value and confirmed the presence of void. However, the impact-echo resulted from ungrouted duct region went unnoticed. The test performed on fully-grouted tendon showed peak frequency corresponding to the peak thickness frequency of 7.32 KHz as shown in Fig. 4.34.
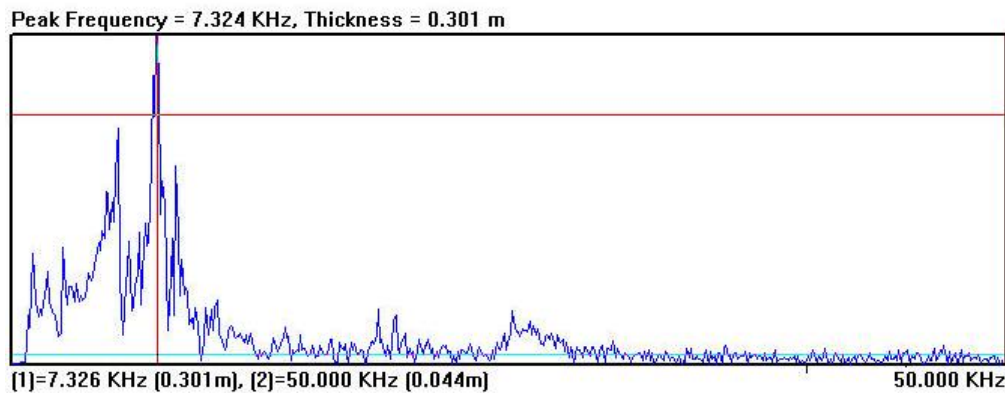
Fig. 4.24 Spectrum of a solid portion of specimen No. 4 showing peak thickness frequency
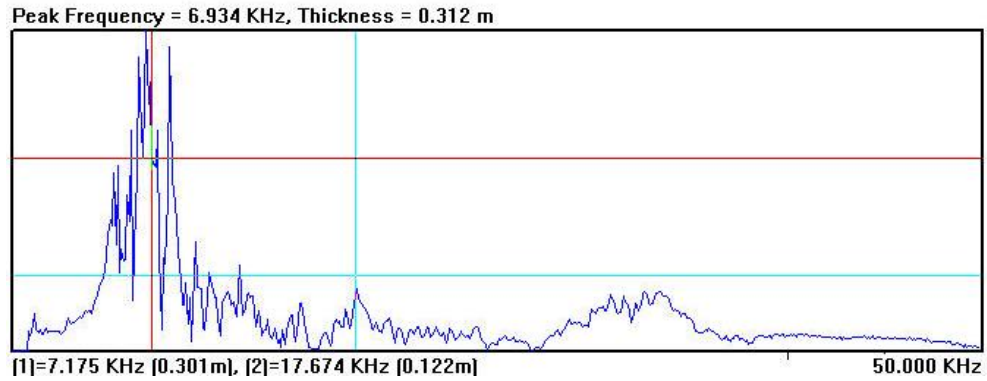
Fig. 4.25 Spectrum obtained from the 50 mm diameter plastic duct in specimen No. 4 in the region of partially grouted duct
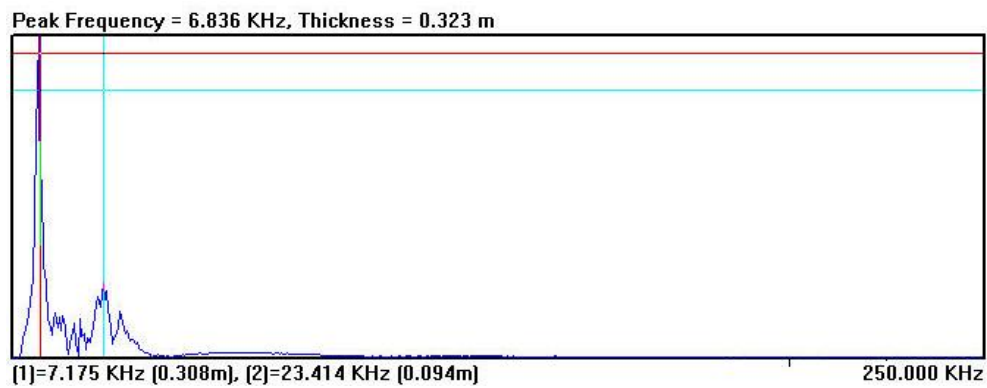
Fig 4.26 Spectrum obtained from 50 mm diameter metal duct in specimen No. 4 showing anomaly in concrete rather than inside the duct
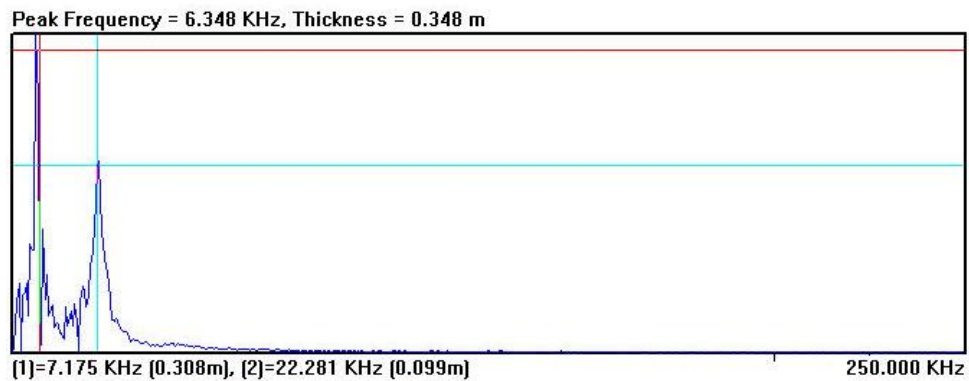
Fig. 4.27 Spectrum obtained from the 100 mm diameter plastic duct in specimen No. 4 in the region of fully-voided duct

137
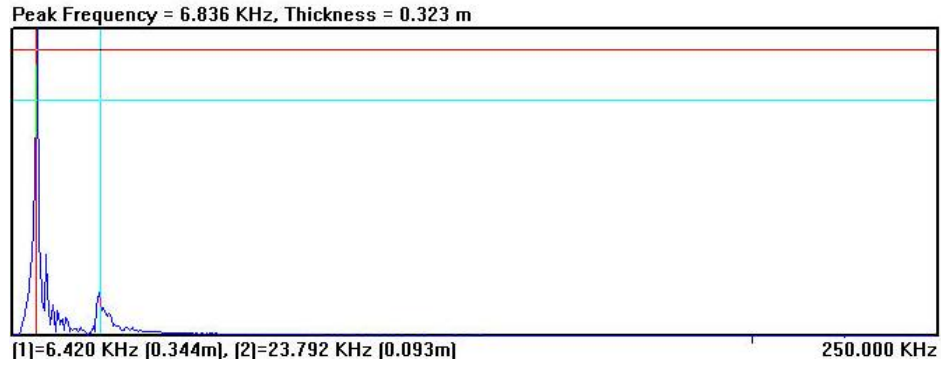
Fig. 4.28 Spectrum obtained from the 100 mm diameter plastic in specimen No. 4 in the region of partially-grouted tendon duct
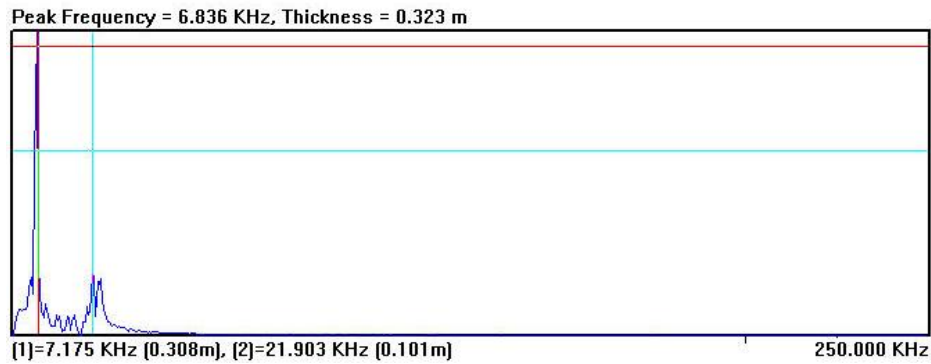
Fig. 4.29 Spectrum obtained from the 100 mm diameter metal duct in specimen No. 4 in the region of partially-grouted duct
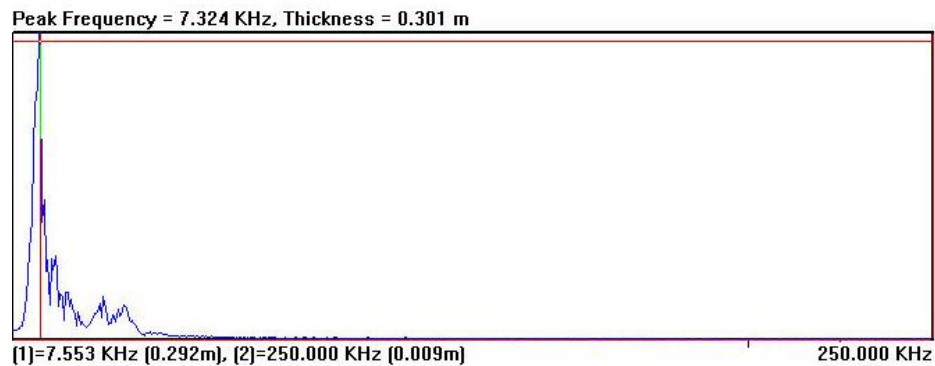
Fig. 4.30 Spectrum obtained from specimen No. 4 in the region of fully-grouted tendon duct

4.3.4.1 Impact-echo Test Results on Specimen No. 5

Specimen No. 5 was similar to specimen No. 4 with respect to overall void arrangement inside the 50 and 100 mm diameter plastic and metal ducts. The impact-test performed on a solid portion of the specimen showed a high amplitude peak thickness

138

frequency of 7.32 KHz as shown in Fig. 4.35. The test performed on the 50 mm diameter plastic duct showed no sign of void in the duct and consequently, reflection at concrete/ plastic interface went unnoticed. The impact-echo test result on the 50 mm diameter metal duct showed the existence of the void inside the duct. In the spectrum obtained from partially-grouted and un-grouted regions of the duct, shown in Figs. 4.36 and 4.37, respectively, there were low amplitude of frequencies of 17.75 KHz and 17.34 KHz corresponding to the reflection from the void inside the duct. These frequencies were close to the expected frequency of 17.66 KHz given in Table 4.7 and were taken at concrete depths of 124 and 127 mm to the metal duct.

Peak Frequency = 7.324 KHz, Thickness = 0.301 m

[1]=7.175 KHz (0.308m), [2]=248.867 KHz (0.009m)   250.000 KHz
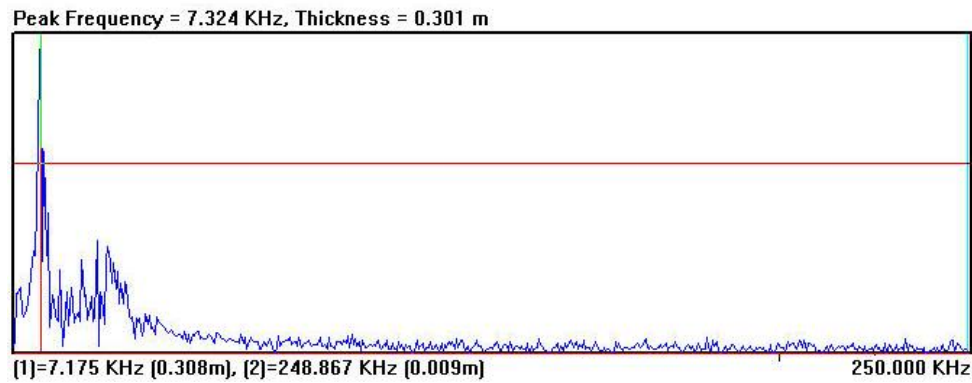
Fig. 4.31 Spectrum of a solid portion of specimen No. 5 showing peak thickness frequency

Peak Frequency = 6.836 KHz, Thickness = 0.323 m

[1]=7.553 KHz (0.292m), [2]=17.749 KHz (0.124m)   250.000 KHz
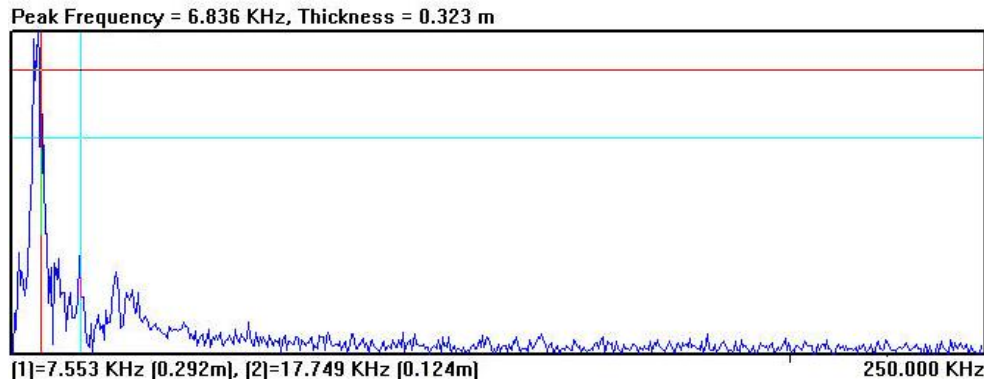
Fig. 4.32 Spectrum for the 50 mm dia. metal duct at the partially-grouted region

of specimen No. 5

139
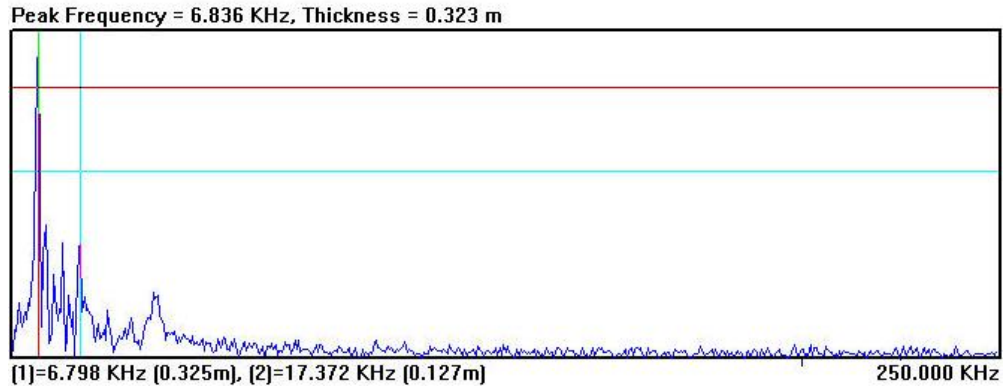
Fig. 4.33 Spectrum obtained from the 50 mm diameter metal duct in specimen No. 5 at the fully-voided region
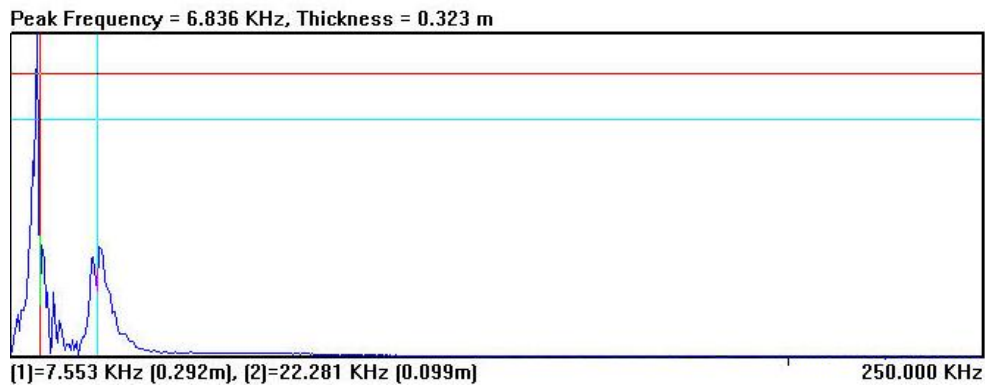
Fig. 4.34 Spectrum obtained from the 100 mm diameter plastic duct in specimen No. 5 at the partially-grouted region

Fig. 4.35 Spectrum obtained from the 100 mm diameter plastic duct in specimen No. 5 at the fully-voided region

140

Peak Frequency = 6.836 KHz, Thickness = 0.323 m

[1]=7.553 KHz (0.292m), (2)=21.148 KHz (0.104m)   250.000 KHz

Fig. 4.36 Spectrum obtained from the 100 mm diameter metal duct in specimen No. 5 at the fully-voided region

Peak Frequency = 6.348 KHz, Thickness = 0.348 m

[1]=7.553 KHz (0.292m), (2)=19.260 KHz (0.115m)   250.000 KHz
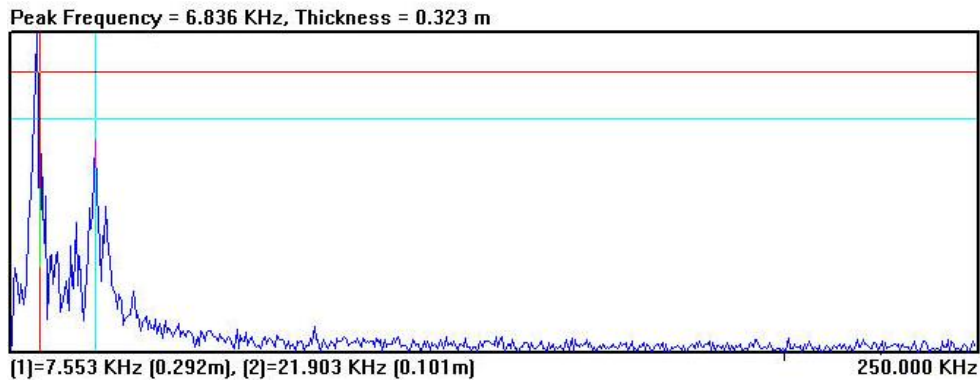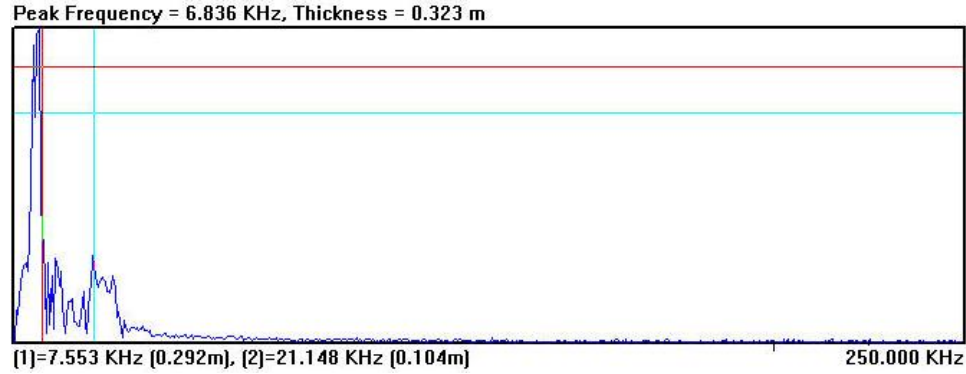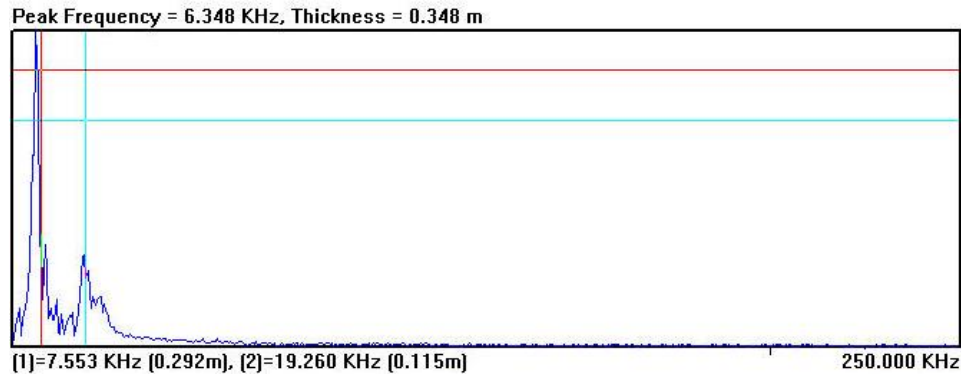
Fig. 4.37 Spectrum obtained from the 100 mm diameter metal duct in specimen No. 5 at the partially-grouted region

The impact-echo test along the length of 100 mm diameter plastic duct showed the reflection of waves at concrete/plastic interface and therefore, presence of void was uncertain. Figures 4.38 and 4.39 show the spectrum obtained at the partially-grouted and ungrouted regions of the duct presenting that the reflection occurred at 100 mm concrete depth, which is equal to the concrete cover to the plastic duct. Since the acoustic impedance of plastic is slightly lower than surrounding concrete, reflection/refraction occurred at interface. This makes complexity in interpretation of impact-echo result on plastic ducts. The spectrum obtained from testing the 100 mm diameter metal duct showed the existence of the void in both the partially-grouted and ungrouted region of the duct. Figures 4.40 and 4.41 show the spectrum obtained from partially-grouted and ungrouted duct, respectively, presenting high frequencies of 21.15 KHz and 19.26 KHz corresponding to the reflection from air void inside the duct. These frequencies were close to the expected frequency of 22.08 KHz and were

141

taken at concrete depths of 104 and 115 mm. At concrete/steel interface, because of relatively high difference in acoustic impedance of steel compared to concrete, stress waves propagates into the metal duct and are reflected from air-void in the duct. Limited invasion test was also confirmed the location of void in the region of partially grouted tendon in 100 mm metal duct as shown in Fig. 4.56.

4.3.4.1 Impact-echo Test Results for Specimen No. 6

Specimen No. 6 contained wire strands with break and notch at selected locations along the strands. The spectrum obtained from this specimen showed unrealistic results due to the use of improper size of impactor. Figure 4.42 shows the spectrum obtained at the location of break in one the strands. Specimen No. 6 had a thickness of 160 mm. However, due to improper use of impactor, the spectrum showed a peak thickness frequency of 6.445 KHz corresponding to the thickness of 343 mm. This means that a larger size impactor has been used generating a wavelength larger than the specimen thickness.
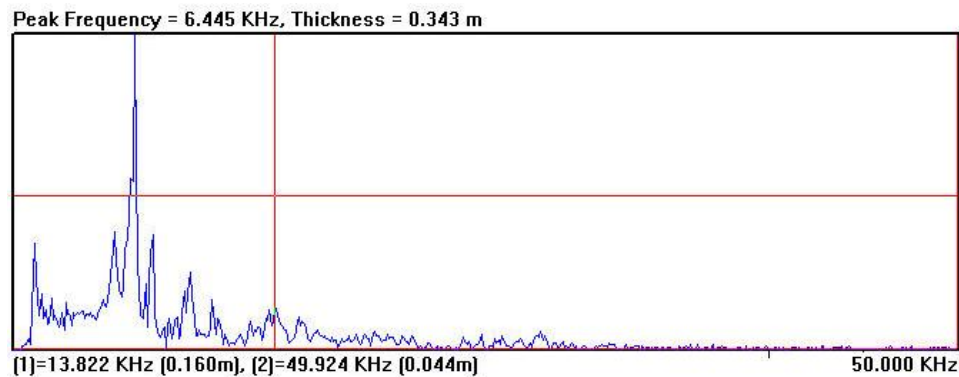
Fig. 4.38 Spectrum obtained from specimen No. 6

__In summary, it can be concluded that the following impact-echo procedure leads to a meaningful result:__

- As GPR is sensitive to metals, it can be reliably used to locate the centerline of metal ducts as well as concrete cover to the tendons.
- P-wave speed in concrete must be determined by using indirect method through measuring round-trip travel time in the solid portion of concrete or by using direct method through performing impact-echo test on solid portion of concrete with known thickness.

142

- The approximate expected frequencies corresponding to peak thickness frequency, reflection from strands and voids in duct must be calculated. Using these values and approximated depth to the void in the duct, a proper size impactor should be used to produce a wavelength of equal or less than depth to the void. The following equations (adapted from Sansalone and Streett, 1997) *can be further used to determine a proper size impactor as follows:*

Knowing P-wave speed in concrete (C_p) and two times the distance to the duct corresponding to the approximated depth to the void (λ), the frequency of stress waves can be determined using equation (4.9).

$$C_p = f \times \lambda \tag{4.9}$$

Considering the frequency calculated above as the maximum frequency of useful energy, $fmax$, the maximum required diameter of spherical impactor, D, can be determined using equation (4.10).

$$fmax = \frac{291}{D} \tag{4.10}$$

Impact-echo test can then be performed along the length of each tendon duct in closely spaced locations using calculated sizes of impactors. In performing each test, the spectrum and peak frequencies obtained must be compared with expected frequencies corresponding to the thickness frequencies, metal reflections and reflection from voids. In cases where there is mismatch of frequencies to that of expected, different sizes of impactos may be used to end up with a meaningful result.

4.4 Half-Cell Potential Test

Concrete is usually known as an excellent corrosion protection for reinforcing steel due to the high PH-value of hydrated cement. This produces a high alkaline environment around the reinforcing bars protecting them from corrosion. However, depending on concrete quality, casting process and environmental conditions passivation effect (alkalinity) of concrete against corrosion of steel can be neutralized. Additionally, penetration of chloride ions into concrete resulting in carbonation of concrete causes destroying the passive layer of reinforcements. Thus, if the alkalinity of concrete is removed, corrosion of steel begins if moisture and oxygen is present. The corrosion reactions develop cathodic and anodic activities

along the reinforcing bars in such a way that ions transfer from steel to the concrete producing rust (Fe (OH) $_3$). This produces an area in concrete where there are a large concentration of negative ions as a result of corrosion of steel compared to areas where there are no corrosion. This concentration of ions creates a small electric voltage potential. By measuring and mapping voltage potential found in the concrete we are able to rapidly determine the presence of corroded steel reinforcement without costly and time consuming demolition of the concrete.

The half- cell potential method can be used to determine the area where there is possibility of active corrosion. This method employs the use of a voltmeter to measure the potential difference (voltage) between the steel strands and a half-cell, which is mapped across the surface of the concrete. The analysis of potential difference indicates the area where active corrosion is taking place along the length of steel strands. Areas with high corrosion activity produce lower voltage (more negative voltage) than areas without corrosion; therefore, the corroded steel strands can be rapidly located. However, the method requires the connection to an exposed steel strands and because the concrete is being tested, any material on the surface should be removed.

As shown in Figure 4.43, a direct electrical connection was made to connect the positive terminal of the device to an exposed wire strand from outside. The wire strand was cleaned using a chisel down to a bright metal. The negative terminal is connected to half-cell device which is placed on the concrete surface by means of a porous plug and sponge that is moistened with a liquid detergent. To perform the test efficiently, the concrete surface was moistened with regular tap water and left for some times to have a damp surface. Since the test can only detect corrosion directly under the half-cell device, a systematic grid of test points should be created to map the potential readings throughout the concrete surface. The grid lines were created directly along the length of tendon ducts in 100 mm spacing to observe the corrosion characteristic of wire strands. The map can then be analyzed to determine the possible areas of active corrosion. Figures 4.44 to 4.47 provide some photos of test performance. Using ASTM C 876 guidelines, the potential measurements can be interpreted as follows:

- Potentials more negative than -0.35 volts indicates greater than 90 percent possibility

that corrosion is occurring.

- -0.2 to -0.35 volts potential indicates that corrosion is uncertain.

- 0 to -0.20 volts indicates greater than 90 percent possibility of no corrosion at the time of measurement.

- Positive voltage indicates that the moisture content of the concrete is insufficient or the wire connections are poor and, therefore, the test is invalid.
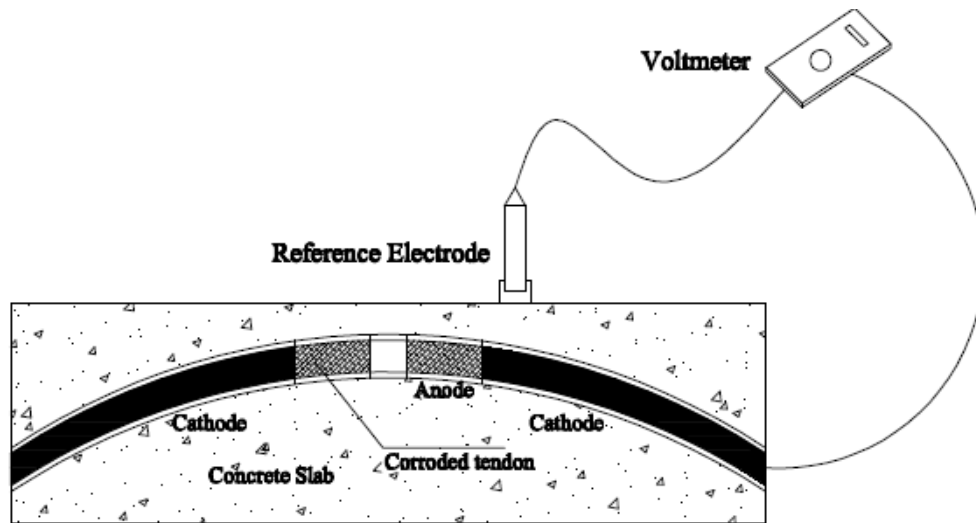
Fig. 4.39 Schematic illustration of half-cell potential measurement setup that is simulated in the present study

Fig.4.40 Cleaning strand using chisel   Fig. 4.41 Watering the concrete surface prior to testing

| Fig.4.42 Electrical connection to | Fig. 4.43 Half-cell potential measurement of |
| an exposed wire strand | corroded region |
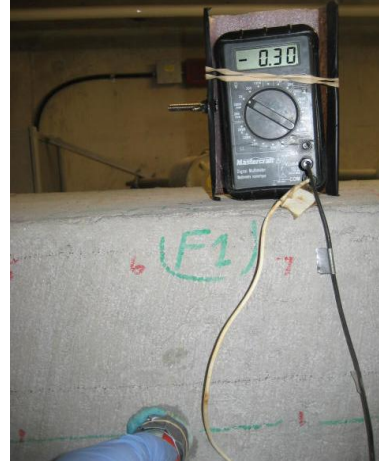
4.4.1 Half-Cell Potential Test Results

4.4.1.1 Half-Cell Test Results for Specimens No. 3, 5 and 7

Samples 3, 5 and 7 contain corrosion in portions of both the prestressing cables and the reinforcing bars as presented in Chapter III. Half- Cell Potential test was performed on these specimens and the results provided a good indication of corrosion in the artificially corroded prestresssing cables and rebar. Figures 4.48 to 4.51 show the potential differences (maps) of typical area surrounding the tendon ducts. In each test, a grid line was created along the length of tendon ducts with a distance of 100 mm spacing. The red color in the figures indicates the areas of active corrosion. Data obtained to plot the contour maps for each test results are presented in Appendix A. Figure 4.48 shows the contour map taken from specimen No. 3 in which the tendon ducts located at 25, 70 and 100 cm from left edge. As shown in the figure, at depths of 25 and 70 cm, the prestressing cables were shown corroded at both ends which conform to the artificially corroded arrangement presented in Chapter III. In the same manner at depth of 100 cm from edge, corrosion at middle part of the tendon (40-80 cm distance from edge) was clear showing the corrosion of the curved tendon in this part. However, at the distance between 10 and 40 cm, it has been deemed to have a passive area, while showing the active corrosion was occurring. This is believed to be resulted from the interference of electrical conduit in the concrete slab structure.

Figure 4.49 shows the contour map within the area surrounding the ducts in specimen

No. 5 in which the tendons located at 20, 45, 70 and 95 cm from bottom face of the slab. It was assumed to have limited corrosion in the middle third part of the panel as indicated in the artificially corroded tendon arrangements presented in Chapter III. However, the map displayed showed the sign of corrosion (red color) on entire surface. This was found to be resulted from either improper connection to the exposed prestressing cable, which was not completely cleaned or excessive moisture content of concrete. The test was repeated some more times after wetting the surface and using the connection to a cleaned prestressing cable. The map resulted from half-cell potential cell (Fig. 4.50) clearly confirmed the proposed corrosion at middle part except at a depth of 70 cm within the distance of 45-65 cm as unexpected.

In a similar manner, the test was performed on specimen No. 7 which contained prestressing strands with limited corrosion in selected portions of the strands as presented in Chapter III. The contour map was taken within the area surrounding the strands in which the strands are located at 10, 15, 20 and 25 cm from top face of the specimen (Fig. 51). At depths of 10 and 25 cm, corrosion was confirmed at the middle part of the specimen. Similarly at a depth of 20 cm, corrosion at both ends of the strand was confirmed per the artificially corroded strand arrangement presented in Chapter III. However, at a depth of 15 cm, it was assumed passive area along the length of the strand, while it showed that active corrosion was occurring. This could result from the strands being very close to each other causing the electrical voltage from corroded strands to be captured by the half-cell device.
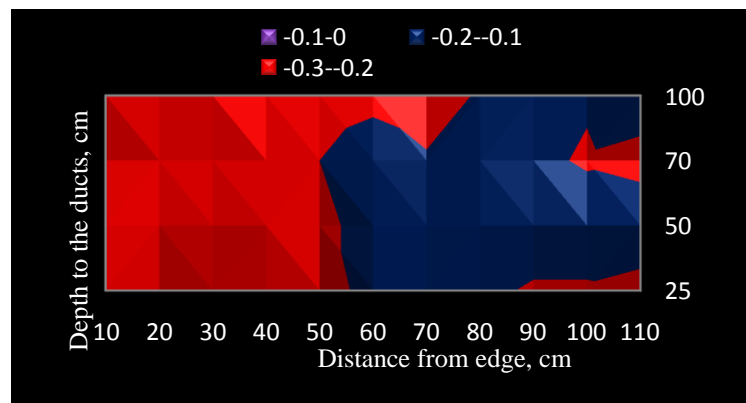
Fig. 4.44 Contour map of specimen No. 3 within the area surrounding the tendon ducts (red color showing area of active corrosion)

147
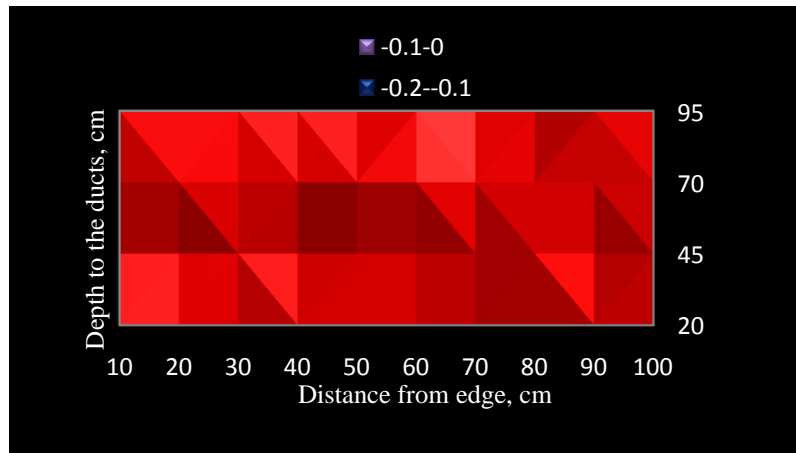
Fig. 4.45 Contour map of specimen No. 5 showing corrosion in red color over entire surface
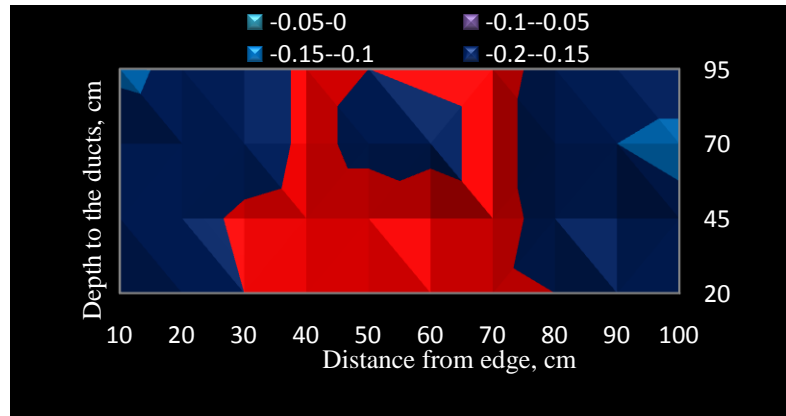
Fig. 4.46 Contour map of specimen No. 5 (repeated) showing corrosion within the area

that has artificially-induced corrosion
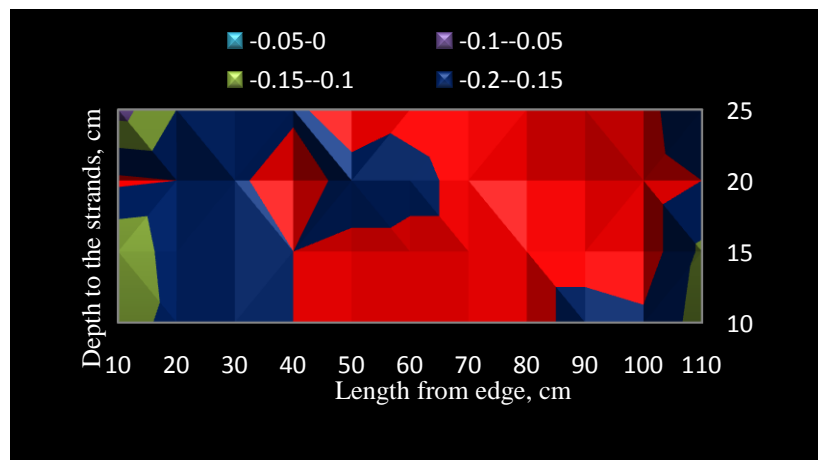
Fig. 4.47 Contour map of specimen No. 7 showing corrosion within the area that has

artificially induced corrosion

4.4.1.2 Half-Cell Test Results for Specimens 1, 2, 4 and 6

Half-cell potential test was carried out on specimens No. 1, 2, 4 and 6. These specimens contained voided duct and wire fractures in the tendon and strands. Therefore, it was predicted that there would be no sign of corrosion in these specimens after testing. The results from half-cell potential confirmed no corrosion on contour maps. Figures 4.52 to 4.55 show the contour map results taken on these specimens.
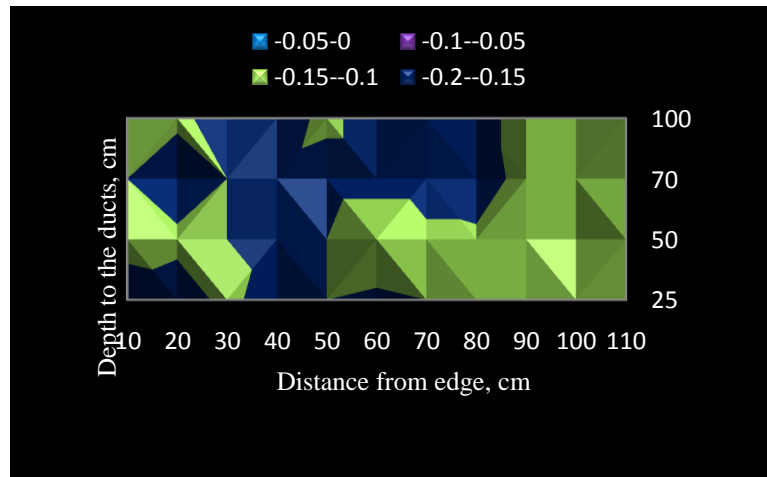
Fig. 4.48 Contour map of specimen No. 1 showing no corrosion in areas surrounding the ducts
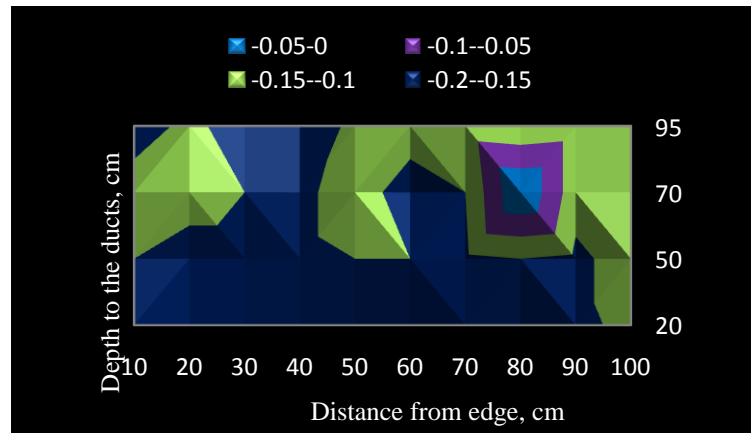
Fig. 4.49 Contour map of specimen No. 2 showing no corrosion
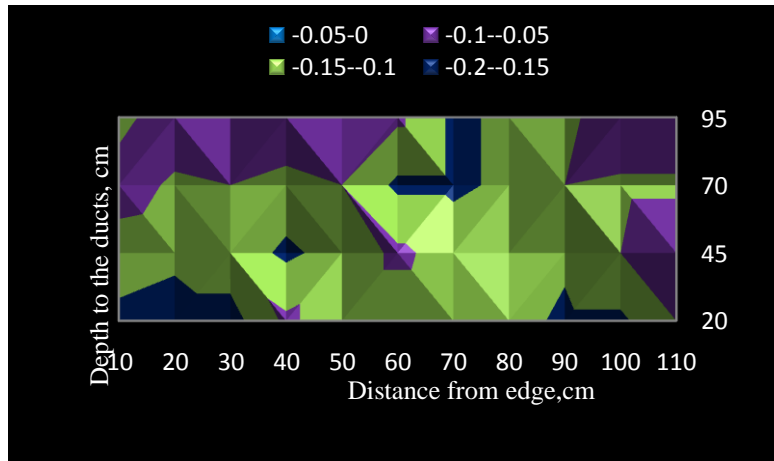
Fig. 4.50 Contour map of specimen No. 4 showing no corrosion
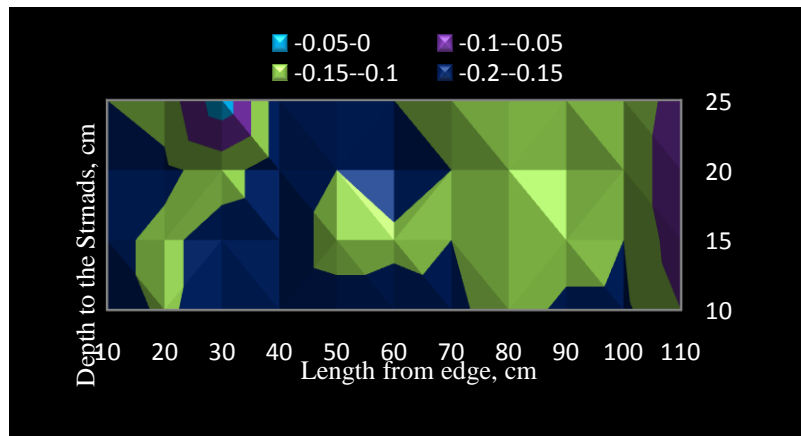
Fig. 4.51 Contour map of specimen No. 6 showing no corrosion

4.4.1.3 Half-Cell Potential Test Results for Specimens No. 4, 5 and 7 using Drilled Holes (i.e. limited invasion)

Since the laboratory specimens were of length 1200 mm, it was easy to connect the wiring of the Half-Cell Potential devise to the exposed end of the prestressing cable that is projecting from the side of the specimen. However, thus may not be the case in practice, especially over the negative moment region of a bridge superstructure. As such, it is proposed herein to drill a hole at one location close to the area under investigation. This hole will be deep enough to reach the surface of the strand or the prestressing cable. A stick was a magnetic base can be used to make sure that the cable or the strand is reached.

The half-cell potential test was repeated on specimens No. 4, 5 and 7 using limited

150

invasion on concrete by drilling holes (see Fig. 4.56). A hole was drilled into concrete along the length of each tendon to reach the strands in each of the tested specimens, because the tendon strands were not electrically continued. Using vacuum and chisel, the strands were cleaned as much as possible. Performing the half-cell potential test on specimen No. 4 shows no sign of active corrosion on this specimen, which also was confirmed when the half-cell test was performed using electrical connection to an exposed strands from the side of the specimen. Figure 4.57 shows contour map of specimen No. 4 within the area surrounding the tendon strands. Comparison of Figs. 4.54 and 4.57 shows electrical voltage differences of higher values in the range of -0.15 to -0.20V in most of the area. This must be due to poor electrical connection to strands or insufficient wetting of concrete surface compared to the Fig. 4.54. Similarly, the test was carried out on specimen No. 5 using drilled holes to the strands. In this specimen, the hole was provided in the ungrouted region of the duct, therefore a clean connection to the strands could be reached much easier. The obtained contour map shown in Fig. 4.58 showed a good indication of active corrosion in the middle third part of the specimen was imposed. Specimen No. 7 was also tested using drilled hole to the strand location. A clean access to the strand was made. As shown in Fig. 4.59, the contour map taken from the tested specimen showed the corrosion region of the strands.
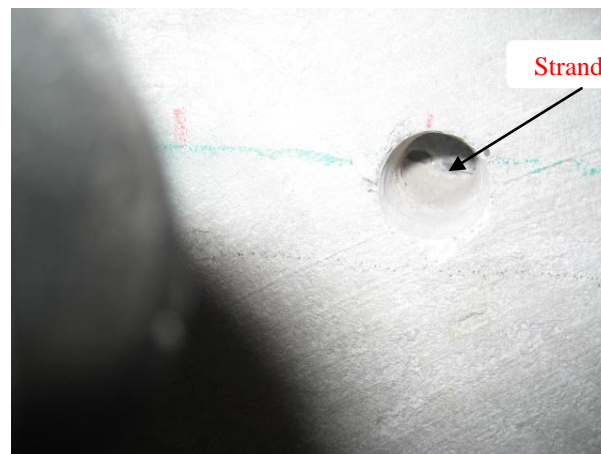
Fig. 4.52 Drilling hole to reach the prestressing cable surface (limited invasion confirmed the presence of void in partially grouted tendon in Specimen No.5 by impact-echo test).
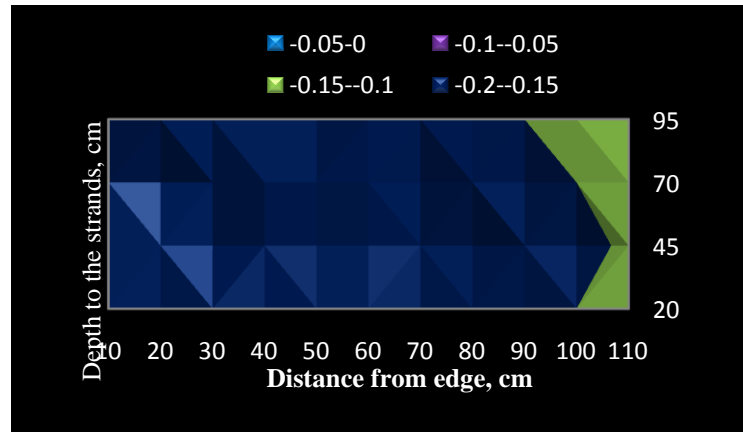
Fig. 4.53 Contour map of specimen No. 4 showing no sign of corrosion (using limited invasion)
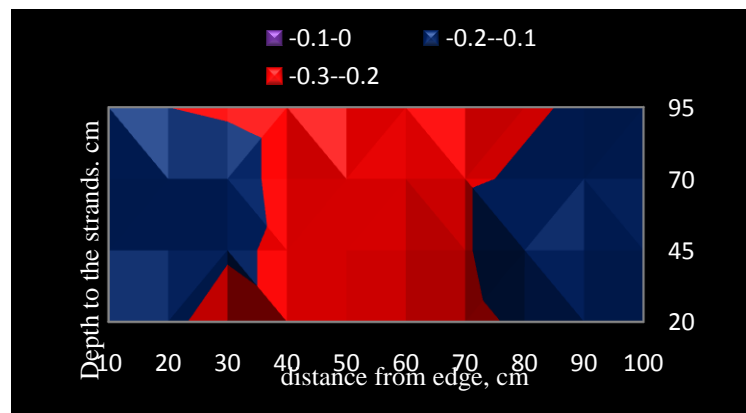
Fig. 4.54 Contour map of specimen No. 5 showing corrosion region (red color) in the middle third part of the specimen (using limited invasion)
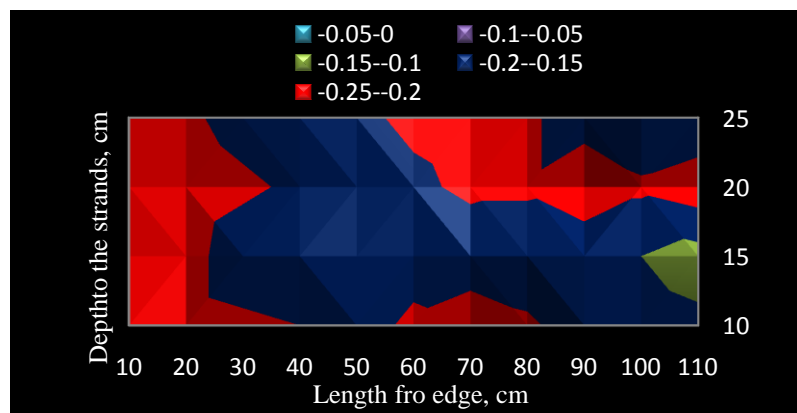
Fig. 4.55 Contour map of specimen No. 7 showing the corrosion region (using limited invasion)

In addition, half-cell potential test was carried out on specimens No. 3 in the region where concrete cover to the tendon duct was 250 mm (Fig. 3.19). Potential readings obtained indicated that due to large concrete cover, potential values at concrete surface changed to more positive values showing no sign of corrosion allover actively corroded steel strands. As a result, with increasing concrete cover, the potential values of active corroded strands become similar to that of passive strands and this makes it difficult to interpret the data. Figure 4.60 shows contour map obtained from testing specimen No. 3, where concrete cover to the tendon is 250 mm at level 70 cm. In this tendon, it was assumed to have active corrosion of strands at both ends of the tendon at distances of 10-40 cm and 70-100 cm. However, as it is evident in the figure, corrosion zone was shown only at distance of 25-40cm but not at the other end. Figures 4.61 and 4.62 also show differences in potential readings once half-cell potential tests were performed on opposite sides of the concrete deck, where concrete covers to the tendon were 50 and 250 mm (see Fig. 3.19).
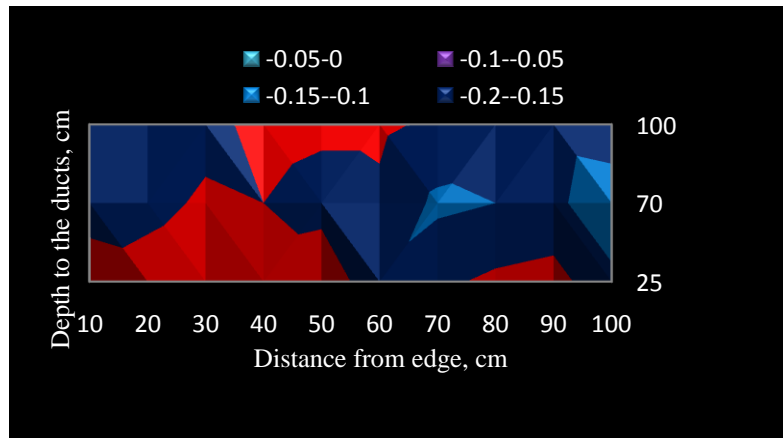
Fig. 4.56 Contour map obtained from specimen No. 3 where concrete cover to the tendon was 250 mm at level of 70 cm

Fig. 4.57 Half-cell potential reading obtained from specimen No. 3 in corroded region where concrete cover to tendon is 50 mm

Fig. 4.58 Half-cell potential reading obtained from specimen No. 3 in corroded region where concrete cover to tendon is 250 mm (on the other side of the tendon)

Generally, half-cell potential is a method of ease and be used to locate corrosion in steel strands in short period of time. However, some considerations should be taken into account to end up with a meaningful result. Some of the most important limitations of half-cell potential device include:

- The method requires a clean connection with steel strands, so holes may need to be drilled into concrete to connect with a strand in order to provide an electrical contact with steel strands in the member under examination. If the tendon strands in the structure are not electrically connected, more drilling holes are required so that the continuity of electrical resistance of the strands being tested is maintained. False readings may also be encountered if the electrical connection to strands or half-cell is poor. Figure 4.63 shows poor connection to an exposed strand which is not adequately cleaned. Figure 4.64 shows a photo when the wires were oppositely connected to strand and the half-cell. In this figure, the positive side of voltmeter was connected to half-cell and negative side to steel strand. The voltmeter shows a positive voltage that

means there is an open-circuit with no electrical current in the system.

Fig. 4.59 Poor connection to steel strand in which the strand was not properly cleaned
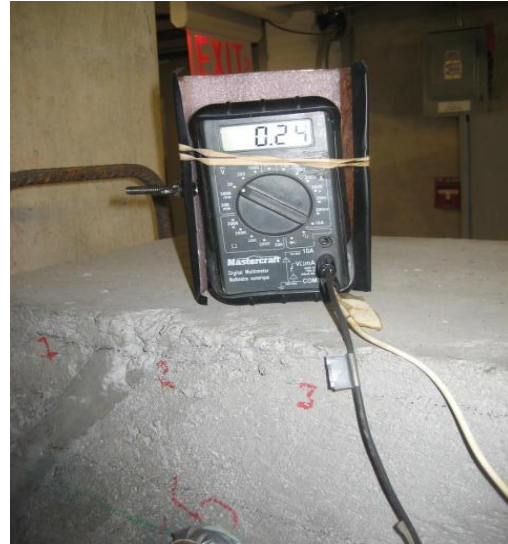
Fig. 4.60 Improper (opposite) connection of wires to steel strands and half-cell showing positive voltage in voltmeter

- The method also indicates the possibility of corrosion at the time of testing and does not provide information regarding the extent or rate of corrosion. Moreover, the half-cell potential readings indicate the possibility of corrosion activities directly beneath the reference cell. Figures 4.65 and 4.66 show fluctuation in half-cell potential readings once point of testing changed. The readings were obtained at location of active corrosion and a point just underneath the corroded strands.

Fig. 4.61 half-cell potential reading obtained from specimen No. 3 (Fig. 3.18) in the region of active corrosion in strands

Fig. 4.62 Half-cell potential obtained from specimen No. 3 (Fig 3.18) at a point located below the region of active corrosion

- It should be assured that concrete surface is sufficiently moist. ASTM C 876 recommends if the measured potential at a test point does not change by more than $\pm$ 20 mV within a 5 min period, the concrete is sufficiently moist. Figures 4.67 and 4.68 shows the differences in half-cell readings on a wetted and a damp concrete surface.

Fig. 4.63 Half-cell potential test on a wet concrete surface showing more negative voltage
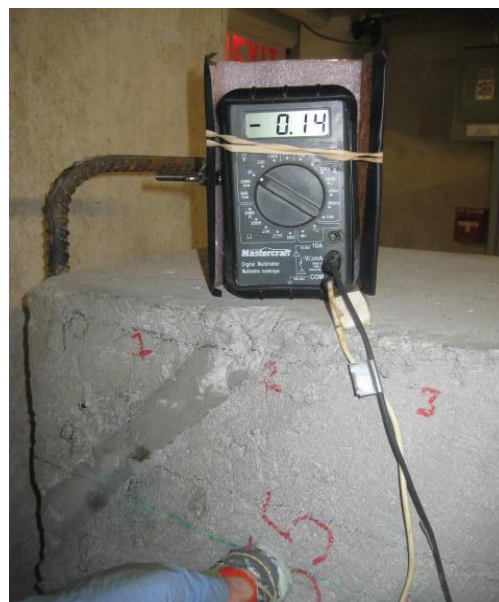
Fig. 4.64 Half-cell potential test on a damp concrete showing more positive voltage

- To perform the test accurately and provide a contour map, the test should be carried out at points arranged in grid. However, the required spacing between test points depends on the particular structure (ACI 228.2R). ASTM C 876 recommends a spacing of 1.2 m for bridge decks if the difference in voltages between adjacent points does not exceed 150mV. Otherwise, a closer spacing is required. However, others suggested a spacing of 60-70 cm for the test points (Clemena et al., 1992).

- The method has proved to locate the existence of an active corrosion, however, there might be areas where assumed to be passive while active corrosion has been occurred. Therefore, false readings have also been encountered while testing due to improper testing performance or wire connections and because the concrete surface may was dried.

- Practically, concrete structures are at risk of chloride and carbonation attack and this leads the half cell potential to more negative readings, which may not be associated with active corrosion of the rebar or strands. Therefore, half-cell potential test should be performed in conjunction with other concrete test methods such as water soluble chloride content, carbonation content and rebar electrical resistance measurements.

In addition to above-mentioned limitation and precautions of the use of this test method, more limitations are available which are summarized in Table 4.9 (Adapted from Ping Gu et. al.1998):

Table 4.9 Effect of various factors on half-cell potential shift and corrosion probability

Situation	Half-Cell Potential Shift	Corrosion of Steel Reinforcement	Applicable to ASTM C 876
Decrease in Oxygen concentration	to negative	May not increase	No
Carbonation/ decrease in PH	to negative	Increase	Yes
Increase in chloride concentration	to negative	Increase	Yes
Anodic corrosion inhibitor	to positive	Decrease	Yes
Cathodic corrosion inhibitor	to negative	Decrease	No
Mixed corrosion inhibitor	to negative or positive	Decrease	No
Epoxy- coat rebar	to positive	Not related	No
Galvanized rebar	to negative	Not related	No
Dense concrete cover	to negative	Not related	No
Concrete resistance	to positive	Not related	No
Dry Concrete	to positive	Not related	No
Reference electrode position	to positive	Not related	No
Coatings and Sealers	to positive	Not related	No
Concrete repair patch	to negative or positive	Not related	No
Cathodic protection	to negative	Not related	No
Stray current	Fluctuation between positive and negative	Not related	No

Table Note: The first column presents the situation and the second column shows how the half-cell potential responds to such a condition. The shift may be towards more positive or more negative directions. The third column shows how such a half-cell potential shift relates to the severity of the steel reinforcement corrosion. For example, the half-cell potential shift may be associated with corrosion activity that is high or low or a particular situation may not relate to the reinforcement corrosion probability. The fourth column indicates whether the ASTM corrosion probability guideline can be applied directly.

4.5 Vacuum Grouting of Voided Ducts

Vacuum grouting of voids in existing ducts is proposed in lieu of conventional grouting methods in bridge restoration. It has been used before in bridge construction in USA. Corven and Moreton (2004) prepared a manual entitled "Post-tensioned tendon installation and grouting manual" for the US Department of Transportation, Federal Highway Administration, that includes procedure for vacuum grouting for the installation of the post-

tensioned tendons. The use of such technology in rehabilitation of existing bridges that have detected voids in the ducts is somewhat new in North America. No applications of vacuum grouting were recorded in the literature in Canada. It can be carried out by qualified technicians who are skilled to adequately perform the grouting. The fundamental basis of vacuum grouting relies mainly on eliminating air in the voids and injecting grout into the voided regions. What makes vacuum grouting so unique is that only one hole is necessary to grout the voids, without the need for vents. This hole is often 12.5 to 25 mm in diameter. The objective of this testing is to demonstrate the use of such technology in the remedy of detected voids at the high points of curved ducts in existing post-tensioned bridge decks in Ontario.

Vacuum grouting was carried out on specimens No. 8 built at Ministry of Transportation of Ontario site. To perform the test, the concrete was scanned from top surface, perpendicular to the direction of tendon duct using Ground Penetration Radar to locate the tendon duct. Once passing the antenna on top of the duct, a peak point in hyperbola GPR image was observed, and then this location was marked for drilling a hole for inspection. Figures 4.69 and 4.70 show location of the duct marked on the top concrete surface and GPR image of the tendon duct and steel rebar, respectively. An artificial air-void with a length of 400 mm was originally placed in the specimen before casting as presented in Chapter III. This void was located at a distance of 1000 mm from the side of the specimen, representing the location of the high point in a curved duct at the centerline of an interior support line (pier) in an existing bridge deck. Figure 4.71 shows a photo of such artificial air-void in the duct before joining the two halves of the duct and casting concrete in specimen No. 8. To prepare the drilled hole at the location of the void in specimen No. 8, special tools such as metal sensitive drills, borescope, digital volumeter and grout injection device were then employed to re-grout the simulated voided region.

Fig. 4.65 GPR used to locate
the tendon duct
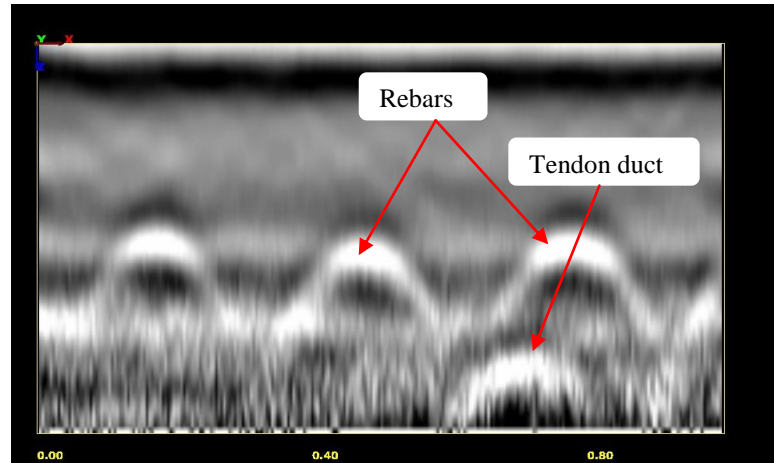
Fig. 4.66 GPR image showing locations of tendon duct
and steel rebar
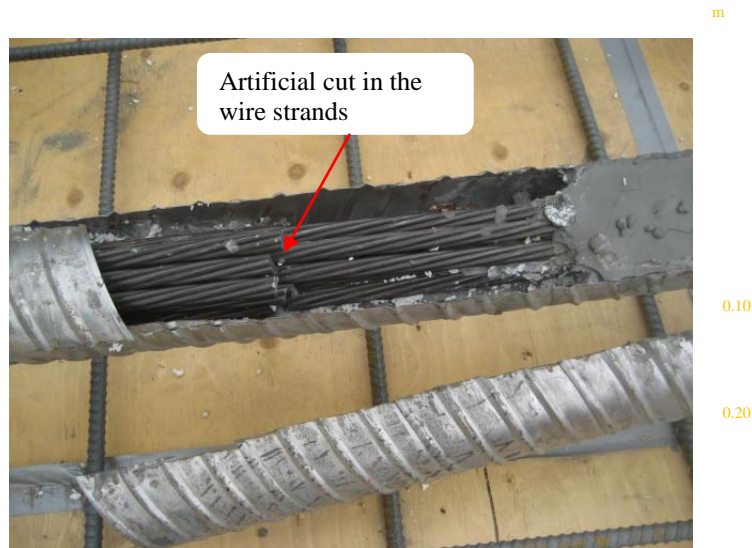
Fig. 4.67 Artificial air-void provided in the 100 mm diameter metal duct

Upon locating the tendon duct, vacuum grouting of the voided area was performed. Generally, vacuum grouting is a specified means for filling voids subsequent to preliminary grouting. It can also be used for initial grouting of the tendon ducts but the problem raise to seal the entire tendon rather than a small void. The vacuum grouting, however, requires sealing the duct system. As it is shown in Fig. 4.72, the tendon duct was sealed at both ends using plastic cap and epoxy injection to avoid air leakage while pressurizing or evacuating air from the system.

Fig. 4.68 Sealing the tendon duct from ends
to prevent air leakage

Fig. 4.69 Drilling a small diameter hole
to verify presence of void

The concrete was then drilled using metal sensitive drill to verify presence of void. Drilling equipment employed the use of an automated shut-off system when steel is encountered so that the tendon duct is not damaged. A small drilled hole, 12.5 mm diameter, was provided until the drilling equipment touched the metal duct. All dusts and crunched concrete were vacuumed out. The hole was made larger using 25 mm diameter drill. Figures 4.73 to 4.75 show photos of performing drilled hole in the concrete. A stick with magnetic base (shown in Fig. 4.76a) was used to detect the presence of the prestressing cable at bottom of the drilled hole.

Fig. 4.70 Vacuuming out the crunched
concrete from the hole

Fig. 4.71 Making larger diameter hole to
the void using 25 mm diameter drill bit

The small hole drilled for limited invasion inspection of inside condition of the tendon

can be used to insert a flexible cable of borescope to investigate the extent of the void and possibly corrosion of the wire strands. The cable was inserted into the hole and pictures and video clips showing the air-void in the duct were recorded. However, measurement of void size by borescope alone cannot be achieved as small gaps or bottlenecks may be neglected by the device. Figure 4.76b depicts a photo of borescope to examine the condition of voided duct.

Fig. 4.76a Views of the stick with magnetic base to detect the presence of the prestressing cable at bottom of the drilled hole

Fig. 4.72b Borescope recording the inside condition of the tendon duct

The final step was vacuum grouting or filling void with grout. Vacuum grouting is a method of withdrawing air from void to create vacuum and using this vacuum to inject grout into the duct. When the presence of void is confirmed by borescope, all leaks including the tendon end caps should be sealed to prevent air-leakage in order to measure the volume of

void (see Figures 4.72 and 4.77). The efficiency of vacuum grouting method is mainly dependent upon the degree to which the leaks are sealed. A digital volumeter was employed to estimate the volume of the void (Figure 4.78). A pressure-tight connection to the drilled hole is required to vacuum the duct to the lowest vacuum pressure that can be reached. The air is then drawn out of the void and a digital volumeter measures the volume of air drawn back into the void after the vacuum was released. If vacuum cannot be achieved due to air-leakage, checks were required at leak locations to ensure prevention of air-leakage. The void volume was essential to be estimated to ensure the amount of grout injected in the duct is sufficient.

Fig. 4.73 Closing pre-drilled hole (right), tight-connection to drilled hole for grouting (left)

Fig. 4.74 Digital volumeter to measure void volume

When the void volume is measured, the last step is to re-establish the vacuum and inject the same volume of grout into the void. Vacuum grouting required only one port to completely fill the void with grout, as negative pressure created by vacuum inside the void. In case where an acceptable level of vacuum inside the void cannot be reached, a combination of vacuum and positive pressure can be used to fill the void. A flow meter can then be used to determine the volume of grout injected into the voided ducts. Comparing void volume size with the volume of grout injected ensures if the void is completely filled with grout or further grouting is required. Figure 4.79 shows a photo performing vacuum grouting of the voided duct. Figure 4.80 shows grout leakage as the tendon anchorage was not adequately sealed.

Fig. 4.75 Vacuum grouting of voided duct   Fig. 4.76 Grout-leakage showing insufficient

sealing of the tendon ends

Generally, vacuum grouting needs ideal conditions where there is no air leak as vacuum can be held when there is no air leakage. Therefore, the method employs the use of either negative or positive pressures to fill the voids. In case when a complete vacuum can be achieved, the negative pressure is what sucks the grout into the void. In many conditions, however, there may be leaks and a desired vacuum cannot be achieved as the rate of leaks may be more than the rate at which the vacuum is pulled. In this case, vacuum-assisted pressure or positive pressure with vacuum may be desirable. This means it first attempts to pull vacuum inside the void as much as possible. Once a complete vacuum cannot be achieved, the grout is left to be sucked by vacuum inside the void. The remaining volume of grout is then pushed into the void using positive pressure. In normal operation without vacuum, the normal grouting operation is done with positive pressure.

In brief, vacuum grouting involves the following activities:
- Pressurize void and check for leaks.
- Seal leaks (tighten all caps and seal leaks with epoxy or epoxy injection).
- Measure the volume of the void to determine the necessary quantity of grout.
- Mix sufficient grout for use and for testing, record quantity of mixed grout.
- Test the grout using the flow-cone or modified flow-cone method.
- Evacuate air from the voids.
- Switch valve and inject grout into voids under pressure.

164

- Record quantity of grout remaining and calculate the amount injected.

- Seal grout injection inlets.

- Clean equipment, area of operations on structure and properly discard unused grout.

- Record and report vacuum grouting operations.

CHAPTER V
CONCLUSIONS AND RECOMMENDATIONS
FOR FUTURE RESEARCH

5.1 Summary

Post-tensioned concrete bridge decks have been in service in Ontario for more than 30 years. Many of them have been operating without any waterproofing/asphalt protection from their initial construction. Concerns currently exist as to the condition of the prestressing cables in the grouted ducts, particularly in the negative moment regions where the cables are closest to the deck surface. Deterioration of post-tensioned bridge decks due to prestress cable corrosion is matter of considerable concern since the repair or replacement is proved to be a costly process. As Ontario bridge infrastructure enters the era of maintenance, rehabilitation and replacement, there is an urgent need for investigating non-destructive inspection methodologies or procedure to assess the conditions of the grouted ducts and cables inside without invasive concrete work involving major concrete removal to expose the ducts for visual inspection. As such, the main objectives of this research were to (i) conduct state-of-the-art and state-of-practice review on the available non-destructive testing (NDT) techniques; (ii) conduct laboratory testing on simulated bridge deck segments with grout-encased prestressing cables to evaluate promising candidate method identified from the literature review that may be applicable to detect voids in the ducts, cable fracture or corrosion in post-tensioned decks; and (iii) propose a remedial procedure to fill the detected voids with grouting materials. Eight concrete specimens were cast to investigate the applicability of selected NDT methods on locating the reinforcing steel bars, ducts, corrosion in cables and voids. These methods were (i) Ground Penetration Radar; (ii) Impact-Echo; and (iii) Half-cell Potential. Also, Remedial procedure using vacuum grouting was experienced to fill the detected voids. This chapter summarizes the experimental findings and recommendations for further research.

5.2 Conclusions

5.2.1 Ground Penetration Radar Testing

Specific conclusions on the use of GRP in NDT testing of post-tensioned decks can be drawn as follows:

1- Ground Penetration Radar has proved to be very effective and successful in locating tendon ducts in PT structures and reinforcing steel bars as well as concrete depth in a short period of time.

2- The method found to be very sensitive to the presence of metals in the concrete. Due to large difference in dielectric of concrete materials compared to that of steel, the scan obtained from GPR device clearly showed the location of metal ducts in a bright hyperbolic shape. However, because of the characteristics of plastic ducts, the device was unable to locate plastic duct itself, while the reflection occurred from the prestressing cables inside the plastic ducts. Therefore, in case of plastic duct detection, an experienced person is required to locate the duct by looking for the characteristics of strands inside the duct rather than plastic duct itself.

3- GPR is able to detect the location of reinforcing steel bars or strands up to certain spacing. The GPR results were conformed to the findings of Bungey et al. (1994) in this regard. In addition, there is not much difference between relative dielectric constant of air to that of concrete materials. Therefore, there is not a complete reflection at concrete/air interface, and electromagnetic energy can penetrate beyond the interface to see the condition below the interface.

4- The drawbacks of the GPR method include (i) only the conic zone irradiated by the antenna provide information on the GPR scan, and (ii) the congested reinforcing bars or tendon strands prevent penetration of radar beyond them. Therefore, information beyond these materials goes unnoticed.

5.2.2 Impact-echo Testing

Specific conclusions on the use of Impact-Echo in NDT testing of post-tensioned decks can be drawn as follows:

1- Impact-echo has confirmed the ASTM standard C 1383-98a for measurement of thickness in concrete slab. The slab thickness in each specimen was determined by

impact-echo device. This was due to the large difference in acoustic impedance of air compared to that of concrete resulting in almost 100% stress wave reflection at concrete/ air interface. The spectrum obtained from each specimen showed a peak frequency corresponding to the thickness frequency, representing low frequency of higher amplitude. This characteristic of impact-echo has been used to locate internal voids in the post-tensioning system based on the principle that impact-echo shows a complete reflection at concrete/air interface.

2- Impact-echo test was unable to locate break and notch in post-tensioning cables. This was due to the fact that stress waves produce cluster of reflected peaks at concrete/ steel interface, which make difficulty in interpretation of the results. Wave characteristics are not defined to locate cross sectional loss in cables due to fracture. As previously mentioned, acoustic impedance differences of dissimilar materials at boundaries is the key factor in reflection of waves.

3- Impact-echo results on plastic ducts found to be complicated and therefore, impact-echo is not a suitable means in case of voids detection in plastic ducts. This is owing to the fact that plastic has lower acoustic impedance compared to surrounding concrete resulting in reflection of waves at interface. In other word, plastic is not transparent in propagating stress waves and difficulty rises in refraction of waves beyond the interface.

4- Impact echo was capable to locate voids inside the metal duct but not in all cases as the wavelengths are significantly dependent upon the size of impactors. Therefore, special attention should be taken into account to successfully locate voids in metal ducts. Existing equations were extended in this research to calculate the proper impactor size to obtain more accurate and reliable results.

5- An important difference between GPR and impact-echo is the amplitude characteristic of reflected waves at concrete/ air interface. For Impact-echo, the reflection is almost 100% at interface because the acoustic impedance of air is considerably small compared with concrete. While, because of small difference between dielectric constant of air and concrete, GPR can penetrate beyond the air/concrete interface. As a result, GPR is not sensitive to the air/concrete interface and cannot be used to clearly detect the voids in concrete structures. However, because the electromagnetic energy

penetrates beyond the interface, GPR is capable of evaluating the condition beyond the interface.

5.2.3 Half-Cell Potential Testing

Specific conclusions on the use of Half-Cell Potential devise in NDT testing of post-tensioned decks can be drawn as follows:

1- Typically, half- cell potential method is found to be simple to use. This allows the user to carry out an almost a non-destructive testing method to create isopotential contour maps of the surface of the concrete member being tested. Regions of high-likelihood of corrosion possibilities show a high negative voltage and can be identified from maps.

2- Half-cell potential is also found to be a fast method in locating corrosion activities of steel strands; however, there are some limitations involved that the method employs the use of an experienced operator to interpret the results in real situations. The successful test performance is significantly depend upon; proper connection to a clean strand, temperature, wetness of concrete surface and concrete resistance to electrical current.

5.2.4 Vacuum grouting of Voided Ducts

It is demonstrated that vacuum grouting can successfully be used to remedy the detected voids in post-tensioned decks. Ground Penetration Radar can be used to locate the tendon duct and marke the tendon on the concrete surface. After successful investigation of voids in metal ducts using impact-echo, the location of tendon ducts containing voids should be marked. As the final step, vacuum grouting can be used as a proper means of re-grouting the voided region in the duct. The method has proved to be very successful in filling continuous voids in the ducts. In cases where voids are not continuous, drilling holes in other locations are required for similar operations. The main advantages of this method are allowing the users to utilize a borescope capable of recording the inside conditions of voids as well as measuring void volume using volumeter to compare with the amount of grout injected.

Vacuum grouting method requires some considerations so that the grouting operation can be performed properly. The tendon end anchorages and any leaks along the length of tendon duct must be adequately sealed using tendon caps and epoxy injection. The continuity of tiny voids along the length of tendon duct should be checked out, and in case if the continuity is interrupted from one side of the tendon, another drilling hole should be made to fill the entire void from the opposite side.

5.3 Recommendations for Future Studies

It is recommended the following considerations to be directed for future study:

1. To be more precise with practical cases, bridge deck specimens containing post-tensioned systems in both directions to be developed to examine the power of above-mentioned promising NDT methods under this situation.

2. Ground Penetration Radar investigation on plastic ducts especially in void detection using 3D-image should be developed. In this study, the effect of plastic on electromagnetic wave propagation could be examined in both cases of congested and non-congested steel reinforcements.

3. GPR investigation on crossed metal tendon ducts can be performed.

4. GPR investigation on closely spaced steel strands or bundled tendon strands should be developed.

5. Characteristics of impact-echo stress waves on concrete component should be of more interest to examine the multiple reflections of waves from concrete itself.

6. Temperature effects on propagation of stress waves into concrete can be investigated.

7. The effects of multiple boundaries with dissimilar acoustic impedance on reflection of impact-echo stress waves can be examined. In this study, it is recommended to examine stress wave reflections on crossed tendon ducts located at different depth of concrete deck.

8. The effects of temperature changes and freezing and thawing on half-cell potential readings can be done.

9. Other NDT methods, such as the RM method, Infrared and Ultrasonic Share Wave, can be investigated to stand on their capabilities and limitations on detecting voids in ducts, as well as defects in the prestresssing cables due to corrosion.

REFERENCES

ACI 228.2R-98. 2004. Nondestructive Test Methods for Evaluation of Concrete in Structures. Reported by ACI Committee 228. Pp. 62.

ASTM C 876. 2009. Standard Test Method for Corrosion Potentials of Uncoated Reinforcing Steel in Concrete. ASTM International. American Society for Testing of Materials.

ASTM C 215-02. 2002. Standard Test Method for Fundamental Transverse, Longitudinal, and Torsional Frequencies of Concrete Specimens. American Society for Testing of Materials.

ASTM C 1383-98a. Test Method for Measuring P-Wave Speed and the Thickness of Concrete Plates Using the Impact-Echo Method. American Society for Testing of Materials.

ASTM D 4788. 2007. Standard Test Method for Detecting Delaminations in Bridge Decks Using Infrared Thermography. American Society for Testing of Materials.

ASTM G 15. 2008. Standard Terminology Relating to Corrosion and Corrosion Testing. American Society for Testing of Materials.

Bungey, J. H. 1989. Testing of Concrete in Structures. 2nd ed., Chapman and Hall, New York.

Bungey, J. H., and Millard, S. G. 1993. Radar Inspection of Structures. *Proceedings, Institute of Civil Engineers, Structures and Buildings Journal* (London), V. 99, May, pp. 173-186.

Bungey, J. H.; Millard, S. G.; and Shaw, M. R. 1994. The Influence of Reinforcing Steel on Radar Surveys of Structural Concrete. *Construction and Building Materials*, V. 8, No. 2, pp. 119-126.

Bungey, J. H., Millard, S. G. and Shaw, M. R. 1997. Radar assessment of post-tensioned concrete, In Proceedings of the 7 International Conference on Structural Faults and Repair-97, Edinburgh, , Vol. 1, Engineering Techniques Press, Edinburgh, pp. 331-339.

Cady, P. D., and Gannon, E. J. 1992. Condition Evaluation of Concrete Bridges Relative to Reinforcement Corrosion. *Volume 8: Procedure Manual*, SHRP-S/FR-92-110, Strategic Highway Research Program, National Research Council, Washington, D.C., 124 pp.

Cantor, T. R. 1984. "Review of Penetrating Radar as Applied to Nondestructive Evaluation of Concrete," *In Situ/Nondestructive Testing of Concrete*, V. M. Malhotra, ed., ACI SP-82, American Concrete Institute, Farmington Hills, Mich., pp. 581-601.

Carino, N. J. 1992. Performance of Electromagnetic Covermeters for Nondestructive Assessment of Steel Reinforcement. NISTIR 4988, National Institute of Standards and Technology, Sept., 130 pp.

Carino, N. J. 1994. Recent Developments in Nondestructive Testing of Concrete. *Advances in Concrete Technology*, 2nd ed., V. M. Malhotra, ed., MSL 94-1(R), CANMET, Natural Resources Canada, Ottawa, pp. 281-337.

Cartz, L. 1995. Nondestructive Testing, Materials Park. Ohio, ASM International.

Chefdeville, J. 1953. Application of the Method toward Estimating the Quality of Concrete, RILEM Bull. (Paris), No.15, August, special Issue- Vibrating testing of Concrete, 2nd part,61.

Ciolko, A., and Tabatabai, H. 1999. Nondestructive methods for condition evaluation of prestressing steel strands in concrete bridges, phase I: Technology Review. NCHRP project 10-53.Transportation Research Board of the National Research Council.

Clear, K. C. 1989. Measuring Rate of Corrosion of Steel in Field Concrete Structures. *Transportation Research Record* No. 1211, Transportation Research Board, Washington, D.C., pp. 28-37.

Clemeña, G. G. 1991. Short-Pulse Radar Methods. *Handbook on Nondestructive Testing of Concrete*, Chapter 3, V. M. Malhotra and N. J. Carino, eds., CRC Press, Boca Raton, Fla., pp. 253-274.

Clemeña, G. G.; Jackson, D. R.; and Crawford, G. C. 1992a. Benefits of Using Half-Cell Potential Measurements in Condition Surveys of Concrete Bridge Decks. *Transportation Research Record* No. 1347, Transportation Research Board, Washington, D.C., pp. 46-55.

Clemeña, G. G.; Jackson, D. R.; and Crawford, G. C. 1992b. Inclusion of Rebar Corrosion Rate Measurements in Condition Surveys of Concrete Bridge Decks. *Transportation Research Record* No. 1347,Transportation Research Board, Washington, D.C., pp. 37-45.

Corven, J, and Moreton, J. 2004. Post-tensioned tendon installation and grouting manual. US Department of Transportation, Federal Highway Adminstration, Washington, DC. 172 pages.

Cullington, D., Bradbury, T., and Paulson, P. 2000. Continuous acoustic monitoring of steel tendons and cables in bridges. Pure technologies Canada Ltd, Calgary, pp. 1-8.

Cullington, D., Hill, M., Woodward, R., and Storrar, D. 1996. Special inspections of post-tensioned bridges in England: Report on progress. FIP Symposium 1996: Post-tensioned concrete structures. The Concrete Society, pp. 482-491.

Cullington, D., MacNeil D., Paulson, P., and Elliot. 1999. Continuous Acoustic Monitoring of grouted post-tensioned concrete bridges. Proceedings of the 8th International Structural Faults & Repair Conference, London, UK.

Cullington, D. W., MacNeil, D., Paulson, P., and Elliot, J. 2001. Continuous Acoustic Monitoring of Grouted post-tensioned concrete bridges, Non-Destructive Testing Evaluation Int. 34: 95-106.

Cullington, D. W, M. E. Hill, R. J. Woodward and D. B. Storrar. 1996. Special inspections on post-tensioned bridges in England: Roprt on Progress. FIP Symposium 1996; Post-tensioned concrete structures. The Concrete Society pp. 482-491.

Daniels, D. J., Gunton, D. J., and Scott, H. F. 1988. Introduction to Subsurface Radar. *Proceedings* Institution of Electrical Engineers, V. 135, Part F, No. 4, Aug., pp. 278-320.

Edward, G., Nawy. 1989. Prestressed Concrete. Prentice Hall. ISBN 0136983758

Elliot, J. F. 1996. Monitoring prestressed structures. Journal of Civil Engineering, 66:7: 61-63.

Fallis, G., Peeler, M. 2008. Non Destructive Detection of Fractures in Prestressed and Post-tensioned Cables. Vector Corrosion Technologies, pp. 1-9.

Feliu, S., González, J. A., Andrade, C., and Feliu, V. 1989. Polarization Resistance Measurements in Large Concrete Specimens: Mathematical Solution for Unidirectional Current Distribution. *Materials and Structures: Research and Testing (RILEM),* V. 22, No. 129, May, pp. 199-205.

Feliu, S., González, J. A., Feliu, S., Jr., and Andrade, M. C. 1990. Confinement of the Electrical Signal for In Situ Measurement of Polarization Resistance in Reinforced Concrete. *ACI Materials Journal,* V. 87, No. 5, Sept.-Oct., pp. 457-460.

Feliu, S.; González J. A.; Escudero, M. L.; Feliu, S., Jr.; and Andrade, M. C. 1990. Possibilities of the Guard Ring for Electrical Signal Confinement in the Polarization Measurements of Reinforcements. *Journal of Science and Engineering Corrosion*, V. 46, No. 12, pp. 1015-1020.

Fisk, P., Holt, R., Sargent, D., El Beck, A. 2004. Detection and Evaluation of Voids in Tendon Ducts by Sonic Resonance and Tomography Techniques. NDT Coportation, pp. 1-13.

Fitzgerald, A. E.; Higginbotham, D. E.; and Grabel, A. 1967. *Basic Electrical Engineering*, McGraw-Hill Book Co., New York.

Flis, J., Sehgal, A., Li, D., Kho, Y. T., Sabol, S., Pickering, H., Osseao- Asare, K., and Cady, P. D. 1992. Condition Evaluation of Concrete Bridges Relative to Reinforcement Corrosion. *Volume 2: Method for Measuring the Corrosion Rate of Reinforcing Steel*, SHRP-S/FR-92-104, Strategic Highway Research Program, National Research Council, Washington, D.C., 105 pp.

Fricker, S., and Vogel, T. 2006. Detecting wire breaks in a prestressed concrete road bridge with continuous acoustic monitoring, Proceedings of the 3rd International Conference on Bridge Maintenance, Safety and Management. Porto, Portugal, pp. 847-849.

Garth, F., Matt, P. 2008. Non Destructive Detection of Fractures in Prestressed and Post-tensioned Cables. Vector Corrosion Technologies, pp 1-9.

Giannopoulos, A. 1997. The investigation of transmission-line matrix and finite-difference time-domain methods for the forward problem of ground probing radar. DPhil Thesis, University of York, Department of Electronics, York, UK.

Giannopoulos, A., Macintyre, P., Rodgers, S., and Forde, M.C. 2002. GPR Detection of Voids in Post-Tensioned Concrete Bridge Beams. Ninth International Conference on Ground Penetrating Radar. Steven K. Koppenjan, Hua Lee, Editors, 376 Proceedings of SPIE Vol. 4758. 6 pp.

Gu, P., Beaudoin, J.J. 1998. Obtaining Effective Half-Cell Potential Measurements in Reinforced Concrete Structures. National Research Council of Canada July, ISSN 1206-1220. P. 1-4.

Halabe, U. B., Sotoodehnia, A., Maser, K. R., and Kausel, E. A. 1993. Modeling the Electromagnetic Properties of Concrete. *ACI Materials Journal*, V. 90, No. 6, Nov.-Dec., pp. 552-563.

Halabe, U. B.; Maser, K. R.; and Kausel, E. A. 1995. Condition Assessment of Reinforced Concrete Structures Using Electromagnetic Waves. *ACI Materials Journal*, V. 92, No. 5, Sept.-Oct., pp. 511-523.

Halsall, A., Wlech, W., and Trepanier, S. 1996. Acoustic monitoring technology for post-tensioned structures. FIP Symposium 1996: Post-tensioned concrete structures. The Concrete Society, pp. 521-527.

Hillemeier, B. 1995. Assessment of Structural Stability of Prestressed Concrete by Non-Destructive Detection of Steel Fractures in the Proceedings Vol. 1 of the International Symposium Non-Destructive Testing in Civil Engineering (NDT-CE). Ed. by G. Schickert, H. Wiggenhauser, Deutsche Gesellschaft für zerstörungsfreie Prüfung e. V., p. 23 – 29.

Hillemeier, B., and Scheel, H. 1998. Magnetic detection of prestressing steel fractures in prestressed concrete, Mater, Corros. 11: 799-804.

Hillemeier, B., and Walther, A. 2008. Fast non-destructive localization of prestressing steel fractures in post-tensioned concrete bridges. Proceedings of the 2008 Accelerated Bridge Construction – Highway for Life Conference, organized by University of Nebraska, USA.

Hillemeier, B. K., Scheel, H. 2002. Non-destructive location of prestressed steel fractures in post-tensioned and prestressed concrete, Transportation research board Committee. A2C03-Concrete Bridges, Washington (DC).

Hillemeier, B. K., Scheel, H. 2003. Fast Location of Prestressing Steel Fractures in Bridge Decks and Parking Lots. International Symposium (NDT-CE 2003)

Hellier, C. 2001. Handbook of Nondestructive Evaluation. McGraw-Hill Professional.

Hornibrook, F.B. 1939. Application of sonic Method to Freezing and Thawing Studies of Concrete. *ASTM Bulletin,* No. 101, December, pp.5-8.

Jaeger, B., Sansalonc, M., and Poston, R. 1996. Detecting voids is Grouted Tendon Ducts of Post- Tensioned Concrete Structures Using the Impact echo Method. ACI Structural Journal, 462-473.

Jaeger, B.J., Sansalone, M.J., and Poston, R.W. 1997. Using Impact-Echo to Assess Tendon Ducts. *Concrete International,* Vol. 19, No.2, pp. 42-46.

Krause, H. et al. 2000. SQUID system for magnetic inspection of prestressed tendons on concrete bridges. Proceedings of the 15th World Conf. NDT, Paper IDN 320.

Krause, H., Wolf, W., Glaas, W., Zimmermann, E., Faley, M., Sawade, G., Mattheus, R., Neudert, G., Gampe, U., and Krieger, J. 2002. SQUID array for magnetic inspection of prestressed concrete bridges. Physica C, www.Elsevier.com/locate/physc. 368: 91-95.

Krause, M., Milmann, B. Schickert, M, Mayer, K. 2006. Investigation f Tendon Ducts by Means of Ultrasonic Echo Methods; A comparative study, In: Proceedings of the 9th

European Conference on NDT, September 2006. BB 103- CD, Vol. Tu.3.2.1. DGZfp, Berlin.

Krause, M., Milmann, B., Mielentz, F., Streicher, D., Redmer, B., Mayer, K., Langenberg, K., and Schickert. 2008. Ultrasonic imaging methods for investigation of post-tensioned concrete structures: A study of interfaces at artificial grouting faults and its verification. Journal of Non-Destructive Evaluation, 27: 67-82.

Krautkrämer, J., and Krautkrämer, H. 1990. Ultrasonic Testing of Materials. 4th Edition, Springer-Verlag, New York.

Lanza di Scalea, F., Rizzo, P. and Seible, F. 2003. Stress measurement and defect detection in steel strands by guided stress waves ASCE J. Mater. Civil. Eng. 15: 219-227.

Lauer, K. R. 1991. Magnetic/Electrical Methods, Handbook on Nondestructive Testing of Concrete. Chapter 9, V. M. Malhotra and N. J. Carino, eds., CRC Press, Boca Raton, Fla., pp. 203-225.

Maierhifer, C., Arndt, R., RÖllig, M., Rieck, C., Walther, A., Scheel, H., and Hillemeier, B. 2006. Application of impulsive-thermography for non-destructive assessment of concrete structures. Journal of Cement & Concrete Composites, 28: 393-401.

Maierhifer, C., Krause, M., Mielentz, F., Streicher, D., Milmann, B., Gardei, A., Kohl, C., and Wiggenhauser, H. 2004. Complementary application of radar, impact echo and ultrasonics for testing concrete structures and metallic tendon ducts. Transport Research Record, Journal of Transportation Research Board. TRB, National Research Council, Washington D.C., Paper No. 04-2651, pp. 170-177.

Malhotra, V.M., Caino, N.J. 2004. Handbook on Nondestructive Testing of Concrete. 384 Pp.

Malhotra, V.M., Caino, N.J. 1991. Handbook on Nondestructive Testing of Concrete. 343 Pp.

Malhotra, V.M., Sivasundaram, V. 1991. Resonant Frequency Methods. Handbook on non-destructive testing of concrete. Chapter 6. Malhotra, V.M., Caino, N.J Pp. 147-168.

Malhotra, V. M. 1976. Testing Hardened Concrete: Nondestructive Methods. American Concrete Institute Monograph No. 9, ACI/Iowa State University Press, 204 pp.

Martin, J., Broughton, K., Giannopolous, A., Hardy, M., and Forde, M. 2001. Ultrasonic tomography of grouted duct post-tensioned reinforced concrete bridge beams. NDT & E International, 34(2).

Maser, K. R. 1986. Detection of Progressive Deterioration in Bridge Decks Using Ground

Penetrating Radar, Experimental Assessment of the Performance of Bridges. *Proceedings* ASCE/EM Division Specialty Conference, Boston, Mass., pp. 42-57.

Mitchell, T. W. 1991. Radioactive/Nuclear Methods, Handbook on Nondestructive Testing of Concrete. Chapter 10, V. M. Malhotra and N. J. Carino, eds., CRC Press, Boca Raton, Fla., pp. 227-252.

Muszynski, L., Chini, A., and Andary, E. 2003. Evaluating nondestructive testing techniques to detect voids in bonded post-tensioned ducts. Report No. DOT HS 809 412, Florida Department of Transportation, 135 pages.

Nawy, Edward G. 1989. Prestressed Concrete. Prentice Hall. ISBN 0136983758.

Nawy, E. G. 1996. Fundamentals of High Strength High Performance concrete. Longman Grout. U.K.

NCHRP Report 621. 2008. Acceptance Tests for Surface Characteristics of steel strands in prestressed concrete. National Cooperative Highway Research Program.

Nour, S. 2006. Testing/Evaluation and grout remediation of post-tensioned tendons for bridges. PCI Journal, July 2006, p. 57-58.

Paulson, P. 1999. Practical continuous acoustic monitoring of suspension bridge cables. Transportation Research Board 78th Annual Meeting, January 10-14, 1999. Washington, D.C. TRB.

Perenchio, W. F. 1989. The Condition Survey, Concrete International. V. 11, No. 1, Jan., pp. 59-62.

Poston, R., and Sandsalone, M. 1997. Detecting cracks in the beams and columns of a post-tensioned parking garage using the impact-echo method. Paper taken from "Innovations in Nondestructive Testing of Concrete", SP-168, American Concrete Institute, Michigan, Pp. 199-219.

Powers, T.C. 1938. Measuring Young's Modulus of Elasticity by Means of Sonic Vibrations. Proc, *ASTM, 38, Part II, 460.*

Raj, B., Jayakumar, T. 1997. NDE methodologies for characterisation of defects, stresses and microstructures in pressure vessels and pipes. International Journal of Pressure vessels and Piping, Volume 73, Issue 2, September. Pp 133-146.

Rodríguez, P., Ramírez, E., and González, J. A. 1994. Methods for Studying Corrosion in Reinforced Concrete, *Magazine of Concrete Research.* V. 46, No. 167, June, pp. 81-90.

Sansalone, M. 1993. Detecting delaminations in concrete bridge decks with and without asphalt overlays using an automated impact-echo field system. Proceedings of the British Institute of Non-Destructive Testing International Conference NDT in Civil Engineering, Liverpool, UK, pp. 807-820.

Sansalone, M., and Carino, N. J. 1991. Stress Wave Propagation Methods, *Handbook on Nondestructive Testing of Concrete.* Chapter 12, V. M. Malhotra and N. J. Carino, eds., CRC Press, Boca Raton, Fla., pp. 275-304.

Sansalone, M., Street, W. 1995. Use of Impact-echo method and field instrument for non-destructive testing of concrete structures, Proc, Int. Symp, on Non- Destructive Testing in Civil Engineering Berlin, 1: 495-502.

Sansalone, M., and Streett, W. 1997. Impact-Echo: Nondestructive evaluation of concrete and masonry.. Bullbier Press, Jersey Shore, PA, USA.

Sansalone, M., and Streett, W. 1997. Impact-Echo: Nondestructive evaluation of concrete and masonry. Chapter 18: Bonded Post-tensioning tendons p.181-200. Bullbier Press, Jersey Shore, PA, USA.

Scheel, H., and Hillemeier, B. 1997. Capacity of the remanent magnetism methods to detect fractures of steel in tendons embedded in prestressed concrete. NDT & E International, 30(4): 211-216.

Scheel, H., and Hillemeier, B. 2008. Fast location of prestressing steel fractures in bridge decks and parking lots. Transportation Research Record, Journal of the Transportation Research Board, Special Volume CD 11-S: 253-256.

Scheel, H., and Hillemeier, B. 1995. The capacity of the remanent magnetic methods to detect fractures of steel in tendons embedded in prestressed concrete, proc. Int. Symp. on Non-Destructive Testing in Civil Engineering Berlin, 1: 211-218.

Scheel, H., and Hillemeier, B. 1998. Magnetic detection of prestressing steel fractures in prestressed concrete. Journal of Materials and Corrosion, 49: 799-804.

Shivprakash, R., Iyer, Sunil K. Sinha & Andrea, J., Schokker. 2005. Ultrasonic C-Scan Imaging of Post-Tensioned Concrete Bridge Structures for Detection of Corrosion and Voids. *Computer-Aided Civil and Infrastructure Engineering* **20.** pp.79-94.

Serway, R. A. 1983. Physics for Scientists and Engineers/ with Modern Physics. Saunders College Publishing, Philadelphia, Pa.

Streicher, D., Algernon, D., Wöstmann, J., Behrens, M., and Wiggenhauser, H. 2006. Automated NDE of post-tensioned concrete bridges using imaging echo methods. Proceedings of the 9th European Conference on NDT: ECNDT Berlin 2006 (DGZfP-Proceedings BB 103-CD), pp. 985-992.

Swamy, R. N., Al-Asali, M. M. 1988. Engineering properties of concrete affected by alkali-silica reaction, *ACI Mater. J., 85 (5), 367.*

Tabatabai, H. 1995. Self-Monitoring Surveillance System for Prestressing Tendons. *NUREG/CR- 6420,* U.S. Nuclear Regulatory Commission 62 pp.

Taveira, L. V., Sagues, A.A., Lopez- Sabando, J. 2008. Detection of Corrosion of Post-Tensioned Strands in Grouted Assemblies. NACE International corrosion Conference and Expo. Pp. 1-19.

Ulriksen, C. P. F. 1983. Application of Impulse Radar to Civil Engineering. PhD thesis, Lund University, Dept. of Engineering Geology, Sweden. Published by Geophysical Survey Systems, Inc., Salem, N.H.

Whiting, D. 1987. Permeability of Selected Concrete, *Permeability of Concrete.* D. Whiting and A. Walit, eds., ACI SP-108, American Concrete Institute, Farmington Hills, Mich., pp. 195-222.

Bibliography

Abraham, O. and Côte, P. 2002. Impact echo thickness frequency profile for void detection and masonry in post-tensioned duct. ACI Structures Journal, 99(3): 239-247.

Algernon, D., and Hiltunen, D. 2009. Real-time imaging of NDT data in combination with scanning techniques. TRB 2009 Annual Meeting CD-ROM, p. 1-11.

Ata, N., Mihara, S., Ohtsu, M. 2006. Imaging of ungrouted tendon ducts in prestressed concrete by improved SIBIE. NDT&E International pp. 258-264.

Azizinamini A., Koeler, B., Rohde, J. and Mehrabi, B. 1996. Application of a New Nondestructive Evaluation Technique to a 25 years old Prestressed Concrete Girder. PCI Journal, vol.41, No.3, pp. 82-85.

Bartels, K.A., Kwun, H., and Hanley, J.J. 1996. Magnetostrictive Sensors for the Characterization of Corrosion in Rebars and Prestressing Strands. SPIE Proceedings, Vol. 2946 pp. 40-50

Beard, M. D., Lowe, M., and Cawley, P. 2003. Ultrasonic guided waves for inspection of grouted tendons and bolts ASCE J. Mater. Civil Eng., 15: 212-218.

Bligh, R. 2001. NDE techniques for detecting grout defects in cable stays. Ph.D. thesis, Texas A&M University, Texas.

Bligh, R.P., Nakirekanti, S., Bray, D. E. and James, R. W. 1994. Evaluation of NDT techniques for detecting grout defects in cables stays, *Materials Evaluation*, 52(4): 508-514.

Butt, S. D., Limaye, V., Mufti, A. A., Bakht, B. 2004. Acoustic Transmission Technique for Evaluating Fatigue Damage in Concrete Bridge Deck Slabs. ACI Structural Journal, Vol 101. Issue, 1. Pp. 3-10.

Chaki, S., and Bourse, G. 2009. Non-destructive evaluation of the stress levels in prestressed steel strands using acoustoelastic effect. Non-Destructive Testing in Civil Engineering, NDTCE'09, Nantes, France, July, 108.

Chaki, S., and Bourse, G. 2009. Guided ultrasonic waves for nondestructive monitoring of the stress levels in prestressed steel strands. Ultrasonics, 49(2): 162-171.

Center for Civil Engineering Research, Codes and Specifications (CUR), *CUR Report 124. 1986. Acoustic Inspection and Monitoring of Prestressing Tendons and Bars in Concrete Structures,*Balkema Publishers, Holland, Netherlands (1986) 31 pp.

Chen, H.M. and Wissawapaisalm, K. 2002. Application of Wigner-Ville transform to evaluate tensile forces in seven- wire prestressing strands ASCE J. Eng. Mech., 128: 1206-1214.

Chotickai, P. 2001. Acoustic emission monitoring of prestressed bridge girders with premature concrete deterioration. Mater's thesis, University of Texas, Austin, TX, USA.

Conner, J.M., Pollock, D.G., and Khaleghi, B. 2006. "Detection of simulated voids in grouted ducts using ground-penetrating radar," Proceedings of the Concrete Bridge Conference, Reno, NV.

Dean, A. 1998. Using Board- Band Radar Focused Array for the Assessment of Pre-stressed Members in Concrete Bridges, Confidential Report to CTL, Geo- Centers, Inc. Fairfax, VA.

DeSitter, W.R. 1989. Acoustic Inspection and Monitoring of Prestressing Tendons and Bars, CUR-VB Committee B30 Report No. 124, Centre for Civil Engineering Research, Codes and Specifications for Concrete, Gouda, Netherlands, 31 pp.

Devalapura, R. K., Kamel, M. R., and Arumugasaamy, P. 1994. Non-Destructive techniques for corrosion evaluation of steel in concrete. Proceedings of the International Conference held at the University of Sheffield, vol. 1, pp. 300-309.

Di- Scalea, F.L., Rizzo, P., Seiblem F., Ascem, M. 2003. Stress measurement and defect detection in steel strands by guided stress waves. J Mater Civil Eng. 15(3): 219-227.

Duncan, P. J., Gaydecki, P.A., and Burdekin, F. M. 1996. Ultrasonic NDT prototype for the inspection of ducted post stressing tendons in concrete beams. Review of Progress in Quantitative Nondestructive Evaluation, 15: 1799-1806.

Dérobert, X., Aubagnac, C., and Abraham, O. 2002. Comparison of NDT techniques on a post-tensioned beam before its autopsy. Journal of NDT & E International, 35: 541-548.

Elsener, B., Nava, G., and Seifert, N. 1992. "Nondestructive Examination of Prestressing Tendons with Reflectometric Impulse Technique." Swiss Federal Department of Transportation, Zurich 98 pp. (In German).

Elsener, B., Bohni, H., Braunlich, R., and Markees, A. 1997. "Evaluation of Integrity and Extent of Corrosion in Prestressing Strand in Bridge Structures." Swiss Federal Department of Transportation, Zurich 98 pp. (In German).

Florida Department of Transportation Central Structures Office. 2003. Test and Assessment of NDT Methods for Post Tensioning Systems in Segmental Balanced Cantilever Concrete Bridges. DMJM & HARRIS, 283 pages.

Ghorbanpoor, A. 1993. Evaluation of post-tensioned concrete bridge structures by the impact echo technique. Publication No. FHWA-RD-92-096, Federal Highway Administration, U.S.A.

Ghorbanpoor, A. 1998. Magnetic-based NDE of steel in prestressed and post-tensioned concrete bridges. Proceedings of the Structural Materials Technology III: An NDT conference, San Antonio, USA. pp. 343-349.

Ghorbanpoor, A. 1996. Magnetic-based system for NDE of prestressed steel in pre-tensioned and post-tensioned concrete bridges. Prepared by University of Wisconsin-Milwaukee under FHWA Contract No. DTFH61-95-C-00101, Milwaukee, WI., pp. 77.

Ghorbanpoor, A. 2000. Condition assessment of external P-T tendons in the Mid Bay Bridge. Technical report, University of Wisconsin-Milwaukee, 16 pages.

Ghorbanpoor, A., Borchelt, R., Edwards, M., and Abdel-salam, E. S. 2000. Magnetic based NDE of prestressed and post- tensioned concrete members: the MFL system. Publication FHWA-RD-00-026. Federal Highway Administration, U.S. Department of Transportation, Mclean.

Gostatuas, R., and Tamutus, T. 2007. Condition assessment of prestressed concrete girders from the Lake View Drive bridge (I-70) using acoustic emission. Western Pennsylvania Transportation Research Forum, pp. 1-4.

Griess, J. C., and Naus, D. J. 1978. Corrosion of Steel Tendons Used in Prestressed Concrete Pressure Vessels. A Symposium of the American Society for Testing and Materials, Committee G-1 on Corrosion of Metals, *Special Technical Publications 713* (December 1978) pp. 32-50.

Gucunski, N., Rascoe, C., Parrillo, R., and Roberts, R. 2009. Complementary condition assessment of bridge decks by high frequency GPR and Impact Echo. TRB 2009 Annual Meeting CD-ROM, pp. 1-14.

Gucunski, N., Consolazio, G., and Maher, A. 2006. Concrete bridge deck delamination detection by integrated ultrasonic methods. International Journal of Materials and Product Technology, Special Issue on Non-destructive Testing and Failure Preventive

Technology, 26(1/2): 19-34.

Hamilton. H. 2002. Post-tensioning grout bleed, duct and anchorage protection test. Report prepared by University of Florida to Florida Department of Transportation, 8 pages.

Harries, K., Gostatuas, R., Earls, C., and Stull, C. 2006. Full-scale testing program on de-commissioned girders from the Lake View Drive Bridge. Report to The Pennsylvania Department of Transportation FHWA-PA-2006-EMG001, 147p.

Hariri, K., Holst, A., Wichmann, H.-J., Budelmann, H. 2002. Assessment of the state of condition of prestressed concrete structures with innovative measurement techniques and first applications, in Proceedings of the 1st European Workshop on Structural Health Monitoring 2002. July 10-12, 2002, Paris, 1278-1285.

Hartt, W. H., Venugopalan, S. 2002. Corrosion Evaluation of Post-tensioned Tendons on the Mid Bay Bridge in Destin, Florida, Final Report. Florida Department of Transportation, Tallahassee.

Henriksen, C. F., Knudsen, A., Braestrup., M. W. 1998. Cable Corrosion: Undetected. Concrete. International, 20(10), 50-54.

Holst, A., Hariri, K., Wichmann, H. J., Budelmann, H. 2004. Innovative Non-Destructive Techniques for the Monitoring of Prestressed Concrete Structures. *2nd Int. Workshop on SHM of Innovative Civil Eng. Struct.*, 22-23 September 2004, Winnipeg, Manitoba, Canada, pp. 513-523.

Hsuan, G. 2004. Evaluation of high density polyethylene ducts of the Sunshine Skyway bridge. Report prepared by Drexel University to Florida State of Department of Transportation, 39 pages.

Hunspperger, R.G., and Chajes, M. J. 2000. Detection of Corrosion of Steel Strands Using Time Domain Reflectometry. Report No. DT1 119. Delaware Department of Transportation, Dover.

Iyer, S.R. 2002. Evaluation of ultrasonic C-scan Imaging to detect corrosion and voids in post-tensioning tendons. M.S. thesis, The Pennsylvania State University.

Iyer, S., Schokker, A., and Sinha, S. 2003. Ultrasonic C-Scan imaging: Preliminary evaluation for corrosion and void detection in posttensioned tendons. Transportation Research Record 1827, paper No. 03-2667, 44-52.

Iyer, S., Schokker, A., and Sinha, S. 2002. Ultrasonic imaging – A novel way to investigate corrosion status in post-tensioned concrete members. Journal of Indian Institute of Science, 82: 197-217.

Iyer, S. R., Sinha, S. K., and Schokker, A. J. 2005. Ultrasonic C-Scan imaging of post-tensioned concrete bridge structures for detection of corrosion and voids. Journal of Computer-Aided Civil and Infrastructure Engineering, 20: 79-94.

Hunsperger, R. G., Chajes M. J. 2005. Void Detestion in Post-Tensioning Ducts Using Time-Domain Refleotometry, Proceedings of National Academy of Sciences, Transportation Researoh Board, 6th Intenrational Bridge Engineering Conferenoe, Boston, M. 27pp.

Kovac, C., Leban, M., and Legat, A. 2007. Detection of SCC on prestressing steel wire by the simultaneous use of electrochemical noise and acoustic emission measurements. Electrochim. Acta, 52: 7607.

Kukay, B. Bridge instrumentation and the development of non-destructive and destructive techniques used to estimate residual tendon stress in prestressed girders. Ph.D. thesis, Utah State University.

Kwun, H. and Teller, C. M. 1994. Detection of fractured wires in steel cables using magnetostrictive Sensors Mater. Eval., 51: 503-507.

Lohrer, C., and Poepel, M. 1996. Combination of a covermeter with a GPR system: a tool for detecting prestressed bars in concrete structures. Proceedings of the 5th GPR'96 Congress, Sendai, Japan, p. 273-278.

Mietz, J., and Isecke, B. 2002. Assessment of test methods for evaluation of stress corrosion cracking susceptibility of prestressing steel. Materials Corrosion, 53: 373-375.

Makar, J., and Desnoyers, R. 2001. Magnetic field techniques for the inspection of steel under concrete cover. NRCC Report No. 3699, National Research Council Canada, Ottawa, pp. 1-28.

Manning, D. G., and Holt, F. B. 1980. Detecting Deterioration in Concrete Bridge Decks. *Concrete International*, V. 2, No. 11, pp. 34-41.

Matt, P. 2001. Non- Destructive Evaluation and Monitoring of Post-tensioning Tendons. Technical Report, fib, Bulletin 15: Durability of post-tensioning tendons EPFL, 103-108, pp. 1003-1012. http://fib.epfl.ch/publications/fib/15/.

Matt. P., et al. 2000. Durabilty of Prestressed Concrete Bridges in Switzerland. In Congress Report, 16th Congress of IABSE. International Association for Bridge and Structural Engineering, Zurich, Switzerland.

May, A. 2004. Nondestructive eddy current testing of embedded steel components in prestressed concrete cylinder pipe. Ph.D. Thesis, Queen's University, Canada.

McHugh, J. 1999. Aspects of the impact-echo method for the detection of voids within metal ducted post-tensioned bridge beams. Ph.D. thesis, University of Southampton, United Kingdon.

Muldoon, R., Chalker, A., Forde, M., Ohtsu, M., and Kunisue, F. 2007. Identifying voids in plastic ducst in post-tensioning prestressed concrete members by resonant frequency of impact-echo, SIBIE and tomography. Journal of Construction and Building Materials, 21(3): 527-537.

Nair, A., and Cai, C. 2007. Acoustic emission monitoring of field bridges in Louisiana. TRB 2007 Annual Meeting CD-ROM, p.1-21.

Nanni, A., Huang, P.C., & Tumialan, G. 2001. Strengthening of Impact- Damaged Bridge Girder Using FRP Laminates, 9th Int. Conf, Structural Faults and Repair, London, UK, M.C. Forde, Ed, Engineering Techniques Press, CD-ROM version 7.

Nu¨rnberger, U. 1992. Special corrosion problems in post-tensioned Structures. *Otto Graf J. (FMPA Baden Wu¨rttemberg),* 3, 148–163.

Okanala, E., Gaydecki, P., and Burdekin, F. 1997. Detecting Faults in post-tensioning ducts by electrical time-domain reflectometry. Journal of Structural Engineering, ASCE, 567-574.

Olson Engineering, Inc., Internal Report, Phase II. 2002. Nondestructive Testing Investigation Internal Grout Concrete Inside Steel and Plastic Post-tensioning Ducts, University of Florida, Olson Engineering Job No. 1211B.

Olson Engineering, Inc., Internal Report, Phase III. 2003. Nondestructive Evaluation Research Internal Grout Conditions Inside Steel and Plastic Post-tensioning Ducts, University of Florida, Olson Engineering Job No. 1211B.

Pavlakovic, B. N., Lowe, M., and Cawley, P. 1999. The inspection of Tendons in Post-tensioned concrete using guided ultrasonic waves. Insights, 41: 446-452.

Parretti, R., Nanni, A. 2004. Strengthening of RC Members Using Near Surface Mounted FRP Composites; Design Overview, Advances in Structural Engineering. An International Journal.

Parretti, R., Nanni, A., Cox, J., Jones, C. and Mayo, R. 2003. Flexural Strengthening of Impacted PC Girder with FRP Composite, Field Application of FRP reinforcement. Case Studies, ACI Convention, Boston, Sep. 27-Oct.1, 2003. Rizkalla, S & Nanni A, Editors, ACI Special Publication No. 215, American Concrete Institute, Farmington Hills, MI, pp.249-261.

Perrin, M., Ramadan, S., Gaillet, L., Tessier, C., and Idrissi, H. 2008. Detection and monitoring by acoustic emission of hydrogen embrittlement of prestressing tendon. COFREND Proceedings (Toulouse, France, 20-23, May).

Podolny, W. 1992. Corrosion of Prestressing Steels and Its Mitigation. *Journal of thePrecast/Prestressed Concrete Institute,* Vol. 37, No. 5 pp. 34-54.

Poston, R. W., Wouter, J. P. 1998. NCHRP Web Document 15: Durability of precast Segmental Bridges. Final Report. TRB, National Research Council, Washington D.C.

Psiachos, D. 2001. An analytical tool for the eddy current inspection of broken prestressing windings in prestressed concrete pressure pipe. M.Sc. Thesis, Queen's University, Canada.

Puri, S., and Moser, D. 2007. Condition assessment of unbonded post-tensioning strands. Concrete International,???.

Ramadan, S., Gaillet, L., Tessier, C., and Idrissi, H. 2008. Detection of stress corrosion cracking of high-strength steel used in prestressed concrete structures by acoustic emission technique. Journal of Applied Surface Science, 254: 2255-2262.

Ramadan, S., Gaillet, L., Tessier, C., and Idrissi, H. 2008. Assessment of the stress corrosion cracking in a chloride medium of cables used in prestressed concrete structures by the acoustic emission technique. Journal of Measurement Science and Technology, 19: 1-9.

Ramadan, S., Perrin, M., Gaillet, L., Tessier, C., and Idrissi, H. 2008. Interest of acoustic emission technique for real-time health monitoring of stress corrosion cracking of cables used in prestressed concrete structures. COFREND Proceedings (Toulouse, France, 20-23, May).

Rizzo, P., and Lanza di Scalea, F. 2004. Dispersive wave propagation in multi- wire strands by laser ultrasonic and wavelet transform. Exp. Mech. 44: 407-415.

Rizzo, P., and Lanza di Scalea, F. 2005. Ulterasonic inspection of multi-wire steel strands with the aid of the wavelet transform. Smart Materials and Structures, 14: 685-695.

Rizzo, P., and Lanza di Scalea, F. 2005. Wavelet coefficient analysis for the quantitative determination of damage in tendons and cables SPIE and Smart Structures Technologies for Civil, Mechanical, and Aerospace Systems vol. 5765, (Bellingham WA: SPIE optical Engineering Press) pp. 863-872.

Sagues, A. 1999. Acoustic and Electrical Evaluation of Post-tensioned Tendons of the Niles Channel Bridge: Preliminary Findings. Memorandum to Rod Powers, Assistant State Corrosion Engineer. Florida Department of Transportation, Tallahassee, July.

Sagues, A. A., kraric, S. C. 2000. Initial Development of Methods of Assessing Condition of Post-tensioned Tendons of Segmental Bridges. Final Report, Contract # BC374. Department of Civil and Environmental Engineering, University of South Florida.

Sawade, G. et. Al. 1995. Signal analysis method for remote magnetic examination of prestressed element in: Proc. Int. Symp. NDT Civil Engng. (NDT-CE). Vol 2, DGZfP, Berlin, pp. 1077-1084.

Sawade, G., Gampe, U., and Krause, H. 1998. Non destructive field method. Proceedings of the 4th Conf. Eng. Struct. Integrity Ass, Cambridge UK. pp. 353-363.

Schiebel, S., Parretti, R. & Nanni, A. 2001. Repair and Strengthening of Impacted PC girders on Bridge A4845, Final Report RDT01- 017éRI01-016, Mission DOT, Jefferson City, Missouri, 21pp.

Schiebel, S., Parretti, R., Nanni, A. and Huck, M. 2002. Strengthening and Load Testing of Three Bridges in Boone County Missouri, ASCE Practice Periodical on Structural Design and construction, vol.7, No. 4, pp. 156-163.

Schokker, A. J., Hamilton, H. R., and Schupack, M. 2002. Estimating post-tensioning grout bleed resistance using a prestress- filter test, *Precast Concrete Institute Journal,* 47(2), pp. 32-39.

Schupack, M. 1994. Studies of Bissell Bridge Post-tensioning tendons after 35 years. *Concrete International,* 16(3): 50-54.

Schupack, M., and Suarez, M. G. 1982. Some recent corrosion embrittlement failures of prestressing systems in the United States. *Journal of the prestressed concrete institute,* 27(2): 38-55.

Schupack, M. 1978. A Survey of the Durability Performance of Posttensioning Tendons. *Journal of American Concrete Institute,* Vol. 75, No. 10, pp. 501-510.

Spencer, F. W. 1996. Visual inspection research project report on benchmark inspections. DOT/FAA/AR-96-65, FAA Office of Aviation Research, Washington.

Streincher, D., Algernon, D., Kohl, C., Krause, M., Maierhofer, C., and Wiggenhauser, H. 2006. Development and combined applications of NDT echo-methods for the investigation of post-tensioned concrete bridges. Proceedings of the 3rd International Conference on Bridge Maintenance, Safety and Management, Porto, Portugal, pp. 941-942.

Suzuki, N., Takamatsu, H., Kawashima, S., Sugii, K., and Iwasaki, M. 1998. Ultrasonic Detection Method for Wire Breakage. *Kobelco Technology Review,* No. 4 pp. 23-26.

Tinkey, Y., Olson, L., and Wiggenhauser, H. 2005. Impact-Echo scanning for discontinuity detection and imaging in post-tensioned concrete bridges and other structures. Journal of Materials Evaluation, 63(1): 64-69.

Washer, G., Fenwick, R., Bolleni, N., and Harper, J. 2009. Effects of environmental variables on the Infrared Imaging of substructure features in concrete bridges. TRB 2009 Annual Meeting CD-ROM, p. 1-15.

Washer, G. A., Green, A. E., and Pond, R. B. 2002. Velocity constants for ultrasonic stress measurements in prestressing tendons Res. Non destruct. Eval., 14: 81-94.

Watanabe, T., Morita, T., Hashimoto, T., and Ohtsu. 2004. Detecting voids in reinforced concrete slab by SIBIE. Journal of Construction and Building Materials, 18(3): 225-231.

Watanabe, T., Ohtsu, M. 2000. Spectral imaging of impact-echo technique for grouted duct in post-tensioning prestressed concrete beam. In: Uomoto T, editor. Nondestructive testing in civil engineering. Amstredam: Elsevier; p. 453–61.

Wichmann, H.-J., Holst, A., Hariri, K., Budelmann, H. 2003. Detection and localization of fractures in tendons by means of electromagnetic resonance measurement. *Proc. of the 5th Int. Symp. on NDT in Civil Engineering*, 16-19 September 2003, Berlin, Germany, Session 23/104 (CD-Rom), Amazeum Conference Centre at Deutsches Museum.

Wiggenhauser, H., Streicher, D., Algernon, D., Wöstmann, J., and Behrens, M. 2007. Automated application and combination of non-destructive echo methods for the investigation of post-tensioned concrete bridges. Proceedings of Concrete Platform, Queen's University of Belfast, pp. 261-269.

Wissawapaisal, K. 2001. Nondestructive testing of reinforced and prestressed concrete structures using acoustic waveguides. Ph.D. thesis, West Virginia University.

Xu, J. 2008. Nondestructive evaluation of prestressed concrete structures by means of acoustic emissions monitoring. Ph.D. Thesis, Auburn University.

Yuyama, S., Yokoyama, K., Niitani, K., Ohtsu, M., and Uomoto, T. 2007. Detection and evaluation of failures in high-strength tendon of prestressed concrete bridges by acoustic emission. Journal of Construction and Building Materials, 21: 491-500.

Yuyama, S., Li, Z., Yoshizawa, M., Tomokiyo, T., and Uomoto, T. 2001. Evaluation of fatigue damage in reinforced concrete slab by acoustic emission. Journal of NDT & E International, 1(34): 381-407.

Appendix A- Half-Cell Data

Half-cell data for Fig. 4.48

Sample 1				
	25	**50**	**70**	**100**
10	-0.18	-0.13	-0.15	-0.15
20	-0.17	-0.14	-0.18	-0.14
30	-0.14	-0.15	-0.15	-0.17
40	-0.17	-0.16	-0.16	-0.17
50	-0.15	-0.15	-0.17	-0.14
60	-0.16	-0.11	-0.17	-0.17
70	-0.15	-0.14	-0.17	-0.15
80	-0.14	-0.14	-0.18	-0.17
90	-0.14	-0.14	-0.13	-0.13
100	-0.13	-0.15	-0.14	-0.13
110	-0.11	-0.12	-0.13	-0.11

Half-Cell data for Fig. 4.49

Sample 2				
	20	**50**	**70**	**95**
10	-0.15	-0.15	-0.13	-0.17
20	-0.18	-0.17	-0.13	-0.14
30	-0.18	-0.17	-0.15	-0.17
40	-0.18	-0.16	-0.16	-0.18
50	-0.19	-0.15	-0.13	-0.14
60	-0.19	-0.15	-0.17	-0.13
70	-0.18	-0.16	-0.15	-0.13
80	-0.18	-0.15	-0.15	-0.14
90	-0.16	-0.16	-0.13	-0.13
100	-0.14	-0.13	-0.14	-0.14

Half-Cell data for Fig. 4.44

Sample 3				
	25	**50**	**70**	**100**
10	-0.23	-0.21	-0.23	-0.2
20	-0.27	-0.23	-0.22	-0.21
30	-0.25	-0.22	-0.22	-0.2
40	-0.24	-0.2	-0.21	-0.22
50	-0.24	-0.22	-0.2	-0.22
60	-0.17	-0.17	-0.18	-0.21
70	-0.17	-0.17	-0.19	-0.25
80	-0.18	-0.15	-0.17	-0.19
90	-0.21	-0.15	-0.18	-0.19
100	-0.21	-0.15	-0.21	-0.19

Half-Cell data for Fig. 4.56

Sample 3			
	25	**70**	**100**
10	-0.25	-0.16	-0.17
20	-0.23	-0.18	-0.19
30	-0.25	-0.21	-0.18
40	-0.23	-0.2	-0.22
50	-0.24	-0.18	-0.21
60	-0.16	-0.19	-0.21
70	-0.19	-0.14	-0.19
80	-0.21	-0.15	-0.18
90	-0.22	-0.16	-0.17
100	-0.16	-0.12	-0.18

Half-Cell data for Fig. 4.50

Sample 4				
	20	**45**	**70**	**95**
10	-0.16	-0.13	-0.07	-0.12
20	-0.17	-0.14	-0.11	-0.06
30	-0.17	-0.12	-0.1	-0.09
40	-0.09	-0.16	-0.12	-0.05
50	-0.13	-0.13	-0.1	-0.09
60	-0.13	-0.09	-0.16	-0.09
70	-0.13	-0.12	-0.16	-0.16
80	-0.13	-0.14	-0.14	-0.14
90	-0.16	-0.14	-0.1	-0.12
100	-0.16	-0.1	-0.11	-0.05
110	-0.1	-0.06	-0.11	-0.05

Half-Cell data for Fig. 4.53

Sample 4				
	20	**45**	**70**	**95**
10	-0.15	-0.16	-0.17	-0.18
20	-0.16	-0.16	-0.19	-0.15
30	-0.15	-0.19	-0.18	-0.17
40	-0.17	-0.17	-0.16	-0.17
50	-0.17	-0.18	-0.16	-0.17
60	-0.17	-0.18	-0.16	-0.15
70	-0.19	-0.19	-0.18	-0.16
80	-0.18	-0.19	-0.16	-0.16
90	-0.17	-0.17	-0.17	-0.15
100	-0.15	-0.17	-0.15	-0.14
110	-0.15	-0.14	-0.14	-0.14

Half-Cell data for Fig. 4.45

Sample 5				
	20	**45**	**70**	**95**
10	-0.23	-0.27	-0.23	-0.23
20	-0.26	-0.29	-0.21	-0.24
30	-0.31	-0.28	-0.25	-0.25
40	-0.3	-0.32	-0.25	-0.28
50	-0.3	-0.3	-0.23	-0.3
60	-0.32	-0.3	-0.23	-0.27
70	-0.31	-0.29	-0.27	-0.32
80	-0.29	-0.25	-0.26	-0.3
90	-0.27	-0.28	-0.25	-0.24
100	-0.27	-0.24	-0.24	-0.25

Half-Cell data for Fig. 4.46

Sample 5				
	20	**45**	**70**	**95**
10	-0.2	-0.17	-0.18	-0.14
20	-0.19	-0.18	-0.17	-0.16
30	-0.2	-0.21	-0.17	-0.17
40	-0.22	-0.22	-0.21	-0.21
50	-0.23	-0.22	-0.19	-0.2
60	-0.23	-0.24	-0.18	-0.21
70	-0.21	-0.22	-0.22	-0.22
80	-0.2	-0.18	-0.17	-0.18
90	-0.17	-0.19	-0.15	-0.17
100	-0.17	-0.16	-0.14	-0.17

Half-cell data for Fig. 4.54

Sample 5				
	20	**45**	**70**	**95**
10	-0.12	-0.16	-0.16	-0.17
20	-0.16	-0.17	-0.15	-0.2
30	-0.28	-0.18	-0.16	-0.21
40	-0.22	-0.22	-0.23	-0.23
50	-0.24	-0.22	-0.22	-0.26
60	-0.25	-0.23	-0.22	-0.24
70	-0.23	-0.21	-0.21	-0.25
80	-0.18	-0.13	-0.19	-0.21
90	-0.17	-0.16	-0.17	-0.19
100	-0.16	-0.15	-0.17	-0.16

Half-cell data for Fig. 4.51

Sample 6				
	10	**15**	**20**	**25**
10	-0.18	-0.16	-0.18	-0.15
20	-0.14	-0.14	-0.16	-0.13
30	-0.18	-0.17	-0.13	-0.017
40	-0.18	-0.18	-0.18	-0.18
50	-0.17	-0.13	-0.15	-0.16
60	-0.17	-0.14	-0.18	-0.15
70	-0.16	-0.15	-0.15	-0.12
80	-0.13	-0.13	-0.13	-0.12
90	-0.16	-0.13	-0.15	-0.13
100	-0.16	-0.15	-0.13	-0.13

Half-Cell data for Fig. 4.47

Sample 7				
	10	**15**	**20**	**25**
10	-0.12	-0.1	-0.21	-0.08
20	-0.17	-0.18	-0.2	-0.15
30	-0.17	-0.18	-0.19	-0.18
40	-0.2	-0.2	-0.23	-0.19
50	-0.21	-0.21	-0.18	-0.23
60	-0.21	-0.21	-0.19	-0.21
70	-0.21	-0.21	-0.21	-0.22
80	-0.22	-0.22	-0.25	-0.23
90	-0.18	-0.22	-0.25	-0.23
100	-0.19	-0.23	-0.23	-0.22

Half-cell data for Fig. 4.55

Sample 7				
	10	**15**	**20**	**25**
10	-0.2	-0.23	-0.23	-0.21
20	-0.22	-0.22	-0.23	-0.21
30	-0.21	-0.13	-0.21	-0.18
40	-0.2	-0.16	-0.19	-0.17
50	-0.18	-0.17	-0.19	-0.17
60	-0.19	-0.18	-0.19	-0.18
70	-0.19	-0.17	-0.19	-0.15
80	-0.19	-0.16	-0.18	-0.13
90	-0.17	-0.15	-0.17	-0.13
100	-0.17	-0.15	-0.17	-0.14
110	-0.16	-0.13	-0.15	-0.12